Government of Western Australia

Department of
Mines and Petroleum

REPORT 134

MAFIC-ULTRAMAFIC INTRUSIONS OF THE GILES EVENT, WESTERN AUSTRALIA: PETROGENESIS AND PROSPECTIVITY FOR MAGMATIC ORE DEPOSITS

by WD Maier, HM Howard, RH Smithies, S Yang, S-J Barnes, H O'Brien, H Huhma, and S Gardoll

Geological Survey of Western Australia

Government of **Western Australia**
Department of **Mines and Petroleum**

REPORT 134

MAFIC–ULTRAMAFIC INTRUSIONS OF THE GILES EVENT, WESTERN AUSTRALIA: PETROGENESIS AND PROSPECTIVITY FOR MAGMATIC ORE DEPOSITS

by
WD Maier[1], HM Howard, RH Smithies, S Yang[2], S-J Barnes[3], H O'Brien[4], H Huhma[4], and S Gardoll[5]

1 School of Earth and Ocean Sciences, Cardiff University, Cardiff, Wales, UK
2 Department of Geology, Oulu University, Oulu 90014, Finland
3 Sciences de la Terre, Université du Quebec á Chicoutimi, Chicoutimi G7H 2B1, Canada
4 Geological Survey of Finland (GTK), FI-02151 Espoo, Finland
5 Department of Applied Geology, Curtin University, GPO Box U1987, Perth WA 6845, Australia

Perth 2014

Geological Survey of Western Australia

MINISTER FOR MINES AND PETROLEUM
Hon. Bill Marmion MLA

DIRECTOR GENERAL, DEPARTMENT OF MINES AND PETROLEUM
Richard Sellers

EXECUTIVE DIRECTOR, GEOLOGICAL SURVEY OF WESTERN AUSTRALIA
Rick Rogerson

REFERENCE
The recommended reference for this publication is:
Maier, WD, Howard, HM, Smithies, RH, Yang, S, Barnes, S-J, O'Brien, H, Huhma, H and Gardoll, S 2014, Mafic–ultramafic intrusions of the Giles Event, Western Australia: petrogenesis and prospectivity for magmatic ore deposits: Geological Survey of Western Australia, Report 134, 82p.

National Library of Australia Cataloguing-in-Publication entry:

Author:	Maier, W.D., author.
Title:	Mafic–ultramafic intrusions of the Giles Event, Western Australia: petrogenesis and prospectivity for magmatic ore deposits. Report 134 / W.D. Maier, H.M. Howard, R.H. Smithies, S.Yang and S-J. Barnes, H. Huhma and S. Gardoll
ISBN:	9781741685497 (ebook)
Subjects:	Ultrabasic rocks--Western Australia--Musgrave region. Petrogenesis--Western Australia--Musgrave region. Geology--Western Australia--Musgrave region.
Other Authors/Contributors:	Howard, H.M., author. Smithies, R.H., author. Yang, S., author. Barnes, S-J., author. Geological Survey of Western Australia.
Dewey Decimal Classification:	552.26099416

ISSN 1834–2280

Grid references in this publication refer to the Geocentric Datum of Australia 1994 (GDA94). Locations mentioned in the text are referenced using Map Grid Australia (MGA) coordinates, Zone 50. All locations are quoted to at least the nearest 100 m.

Copy editor: K Hawkins
Cartography: M Prause
Desktop publishing: RL Hitchings
Printed by Images on Paper, Perth, Western Australia

Published 2014 by Geological Survey of Western Australia
This Report is published in digital format (PDF) and is available online at <www.dmp.wa.gov.au/GSWApublications>.

Further details of geological publications and maps produced by the Geological Survey of Western Australia are available from:
Information Centre
Department of Mines and Petroleum | 100 Plain Street | EAST PERTH | WESTERN AUSTRALIA 6004
Telephone: +61 8 9222 3459 Facsimile: +61 8 9222 3444 **www.dmp.wa.gov.au/GSWApublications**

Cover image: Contact between medium-grained leucotroctolite and coarse-grained gabbronorite; note the melanocratic layer within the troctolite shows normal modal grading to the right, possibly indicating younging direction

Contents

Appendices

Figures

Tables*

---

* Tables 1, 5, 6, 7, 8, and 9 are provided separately on a USB. The Report may be accessed directly on our website independent of the USB.

Mafic–ultramafic intrusions of the Giles Event, Western Australia: petrogenesis and prospectivity for magmatic ore deposits

by

WD Maier[1], HM Howard, RH Smithies, S Yang[2], S-J Barnes[3], H O'Brien[4], H Huhma[4], and S Gardoll[5]

Abstract

More than a dozen mafic–ultramafic layered intrusions were emplaced across >100 000 km^2 in the Musgrave region of central Australia at c. 1075 Ma as part of the c. 1090–1040 Ma Giles Event. The intrusions crystallized from tholeiitic magma of variable composition (<7–12.5 wt% MgO) emplaced at mid- to upper crustal levels (at pressures of up to ~6.5 kbar). As a result, individual intrusions show distinctive compositions. Intrusions such as Wingellina Hills, Pirntirri Mulari, The Wart, Ewarara, Kalka, Claude Hills, and Gosse Pile contain significant ultramafic portions of wehrlite, harzburgite, and websterite. Others, including Hinckley Range, Michael Hills, and Murray Range, are of predominantly olivine-gabbronoritic composition. Mafic intrusions containing substantial troctolitic portions include Morgan Range, Cavenagh, Bell Rock, Blackstone, and Jameson–Finlayson. The latter three are tectonically dismembered portions of an originally contiguous body, here named the Mantamaru intrusion that had a strike length of >170 km and a width of at least 20 km, making it one of the world's largest layered intrusions.

The Giles Event intrusions were emplaced into the Musgrave Province, a complex Proterozoic terrane at the intersection between the West Australian, North Australian, and South Australian Cratons. The region underwent several episodes of orogeny and rifting over a time span of >200 Ma. The oldest event that clearly affected the entire province was the 1220–1150 Ma Musgrave Orogeny. It arose either in an intracratonic setting or as a distal back-arc and featured early, rapid, and substantial lithospheric thinning. These events allowed convecting mantle to be channelled upward along the contacts with surrounding craton keels to the newly exposed base of the Musgrave lithosphere. The result was large-degree mantle melting and subsequent ponding of basalt at (and intrusion into) the base of the lithosphere, lower-crustal melting, voluminous granite magmatism, and widespread mid-crustal ultra-high-temperature (UHT) metamorphism. The ductile (UHT) nature of the lower crust, and the development of substantial crystal-rich magma storage chambers — or melt, assimilation, storage, and homogenization (MASH) zones — prevented ascent of basic magmas into the upper crust. This resulted in the predominantly felsic character of magmatism during the Musgrave Orogeny. The c. 100 Ma (1220–1120 Ma) duration of UHT mid-crustal conditions suggests that re-establishment of lithospheric mantle was significantly retarded.

Magmatism largely ceased between c. 1150 and 1090 Ma, possibly because the lower crust became too refractory, or because a buoyant lithospheric mantle began to form. Therefore, the MASH zone may have solidified; however, mid-crustal temperatures remained anomalously high, as suggested by the continued growth of migmatite-related zircon for more than another c. 80 Ma.

Renewed mantle melting from c. 1090 Ma onwards led to the magmatism-dominated Giles Event (c. 1090 to 1040 Ma), comprising voluminous basic and felsic volcanic and intrusive rocks grouped into the Warakurna Supersuite. One particularly notable component of the Giles Event was the Warakurna Large Igneous Province, represented by doleritic intrusions that outcrop across ~1.5 million km^2 of central and western Australia (Wingate et al., 2004). The source to the Giles basic magmas was largely asthenospheric, reflected by their relatively minor crustal component (low large ion lithophile elements [LILE], ε_{Nd} up to +2), and low Pt/Pd ratios.

The long-lasting magmatism and UHT metamorphism in the Musgrave Province suggests that magmatism was plate driven rather than plume driven. In many regards, the Giles Event can be viewed as an extension of the anomalous thermal regime established during the Musgrave Orogeny. Although initial extension and rifting, emplacement of the layered G1 Giles intrusions, and then significant uplift all happened between 1078 and 1075 Ma, mantle-derived magmatism lasted for >50 Ma and is unrelated to a deep mantle plume. Periods of deformation (both extension and compression) during both the Musgrave Orogeny and the Giles Event may be related to far-field compressive influences that allowed the formation of thick sill complexes, ultimately resulting in some of the world's largest layered intrusions.

1 School of Earth and Ocean Sciences, Cardiff University, Cardiff, Wales, UK

2 Department of Geology, Oulu University, Oulu 90014, Finland

3 Sciences de la Terre, Université du Quebec á Chicoutimi, Chicoutimi G7H 2B1, Canada

4 Geological Survey of Finland (GTK), FI-02151 Espoo, Finland

5 Department of Applied Geology, Curtin University, GPO Box U1987, Perth WA 6845, Australia

A comparison of current models of ore formation with the geology generated by the Giles Event indicates that the region has potential prospectivity for the following types of mineral occurrences:

- platinum group element (PGE) reefs in the ultramafic–mafic transition zones of layered intrusions, and in magnetite layers in the differentiated portions of the intrusions. Potential PGE reefs are more likely in the early (G1) intrusions, whose parental magmas failed to interact with abundant juvenile sulfur of relatively late-stage felsic volcanic rocks
- Cu–Ni sulfide deposits within magma feeder conduits of late basaltic pulses that could assimilate sulfur-rich felsic volcanic rocks
- vanadium in the lowermost magnetite layers within the most fractionated intrusions
- apatite in the unexposed uppermost magnetite layers of the fractionated intrusions
- ilmenite as granular disseminated grains in magnetite layers within the upper portions of the intrusions
- iron, particularly in tectonically thickened magnetite layers or magnetite pipes of the upper portions of intrusions
- gold and copper in the roof rocks and contact aureoles of the large intrusions, and in associated granites and felsic volcanic rocks
- lateritic nickel in weathered portions of the olivine-rich ultramafic portions of intrusions.

KEYWORDS: layered intrusions, magma chamber, magmatic differentiation, mineral chemistry, orebodies, platinum group elements

Introduction

The Musgrave Province of central Australia contains one of the largest concentrations of mafic–ultramafic layered intrusions on Earth (Fig. 1, Appendices 1–5). These are called the Giles Complex (Daniels, 1974) or the Giles intrusions (Smithies et al., 2009). In some intrusions (notably the Kalka intrusion in South Australia), a thick stratigraphy and wide range of lithologies is preserved from ultramafic rocks at the base to anorthosite and magnetite gabbro at the top, providing ideal opportunities for investigating a variety of petrogenetic questions. The intrusions were emplaced at variable crustal depths (Goode and Moore, 1975; Ballhaus and Glikson, 1995; Glikson, 1995) from c. 1078 to 1075 Ma (Howard et al., 2011b). These intrusions, together with earlier and later bimodal magmatism of the Bentley Supergroup and the basic magmas of the Warakurna Large Igneous Province (including the Alcurra Dolerite suite), form the components of the Warakurna Supersuite, formed during the c. 1090 to 1040 Ma Giles Event.

Many aspects of the Giles intrusions remain poorly understood, notably their potential to host magmatic ore deposits. This is partly due to poor exposure, although is also because much of the region forms part of the Ngaanyatjarra – Anangu Pitjantjatjara – Yankunytjatjara Central Reserve, established in the late 1970s, into which access is strictly regulated. Much of the work documented here arose through a regional-scale geological mapping project jointly coordinated through the Ngaanyatjarra Council and the Geological Survey of Western Australia (GSWA), and guided by the local Indigenous people in the region between the communities of Wingellina and Warburton.

During the regional mapping program, the Giles intrusions were remapped on a scale of 1:100 000, and are portrayed on the Bell Rock, Holt, Blackstone, Finlayson, and Cooper 1:100 000-scale map sheets, covering a total area of 120 000 km^2 (Howard et al. 2006a, 2007, 2011b; Evins et al. 2009, 2010a; Smithies et al. 2009). More than 450 geochemical samples of the Giles intrusions were analysed and most of the data are available from the WACHEM database at <http://geochem.dmp.wa.gov.au./geochem/>.

The large volume of mafic igneous rocks and the enormous size of some of the intrusions (up to several 1000 km^2) reflect a significant flux of mantle magma and heat into the crust. Such events tend to be favorable for the formation of a range of ore deposits, including magmatic Cu–Ni–PGE, Cr, Fe, V, Ti, apatite, lateritic Ni, and hydrothermal deposits. As yet, two world-class deposits have been discovered, the Nebo–Babel magmatic Ni–Cu deposit (Seat et al., 2007, 2009) and the Wingellina Ni laterite deposit (Metals X Ltd, 2013), in addition to several smaller deposits. In this Report, we attempt to further constrain the petrogenesis of the Giles intrusions and their magmatic ore deposits in Western Australia, and evaluate the mineral prospectivity of the Giles intrusions and related mafic intrusions of the Warakurna Supersuite in general.

Past work

Early geologic research of the west Musgrave Province began with a GSWA mapping program (at 1:250 000 scale) in the 1960s (reported in Daniels, 1974), during which the Blackstone, Murray, and Morgan Ranges, and parts of the Cavenagh and Jameson Ranges, were mapped (Figs 1 and 2), and their petrology was evaluated. Nesbitt and Talbot (1966) were the first to propose that some of the intrusions could be tectonized remnants of an originally contiguous larger body. These authors studied the petrology of the intrusions and compiled Landsat 5 and airborne total magnetic intensity (TMI) data flown at 1500-m intervals. More highly detailed petrogenetic studies of some of the Giles intrusions were subsequently conducted by Goode and Krieg (1967), Goode (1970, 1976a,b, 1977a,b,c, 1978), and Goode and Moore (1975).

In the late 1980s, the Australian Geological Survey Organisation (AGSO, now Geoscience Australia) conducted a multidisciplinary study of the Musgrave Province (Glikson, 1995; Glikson et al., 1996), concentrating on the Giles intrusions. The project comprised mapping, structural, petrologic, and pressure–temperature studies; U–Pb and Sm–Nd isotope analyses; and remote sensing using Landsat 5 and Geoscan MK I

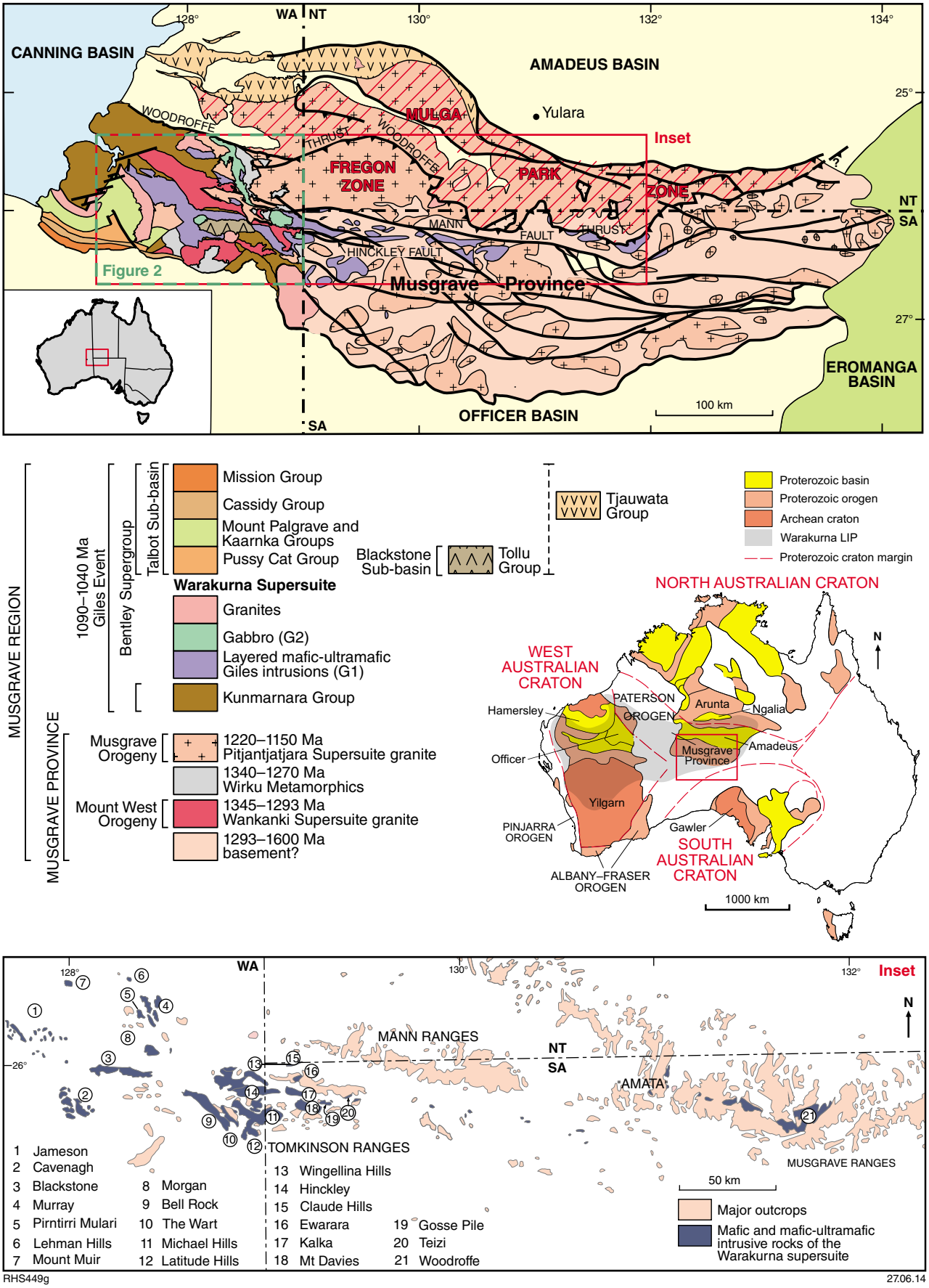

Figure 1. **a) Simplified geological map of the Musgrave Province, highlighting mafic–ultramafic intrusions; for detailed geology of several Giles intrusions within the west Musgrave Province and locations of geochemical sample sites, see Appendices 1–5 and Figure 5; b) inset adapted from Nesbitt et al. (1970).**

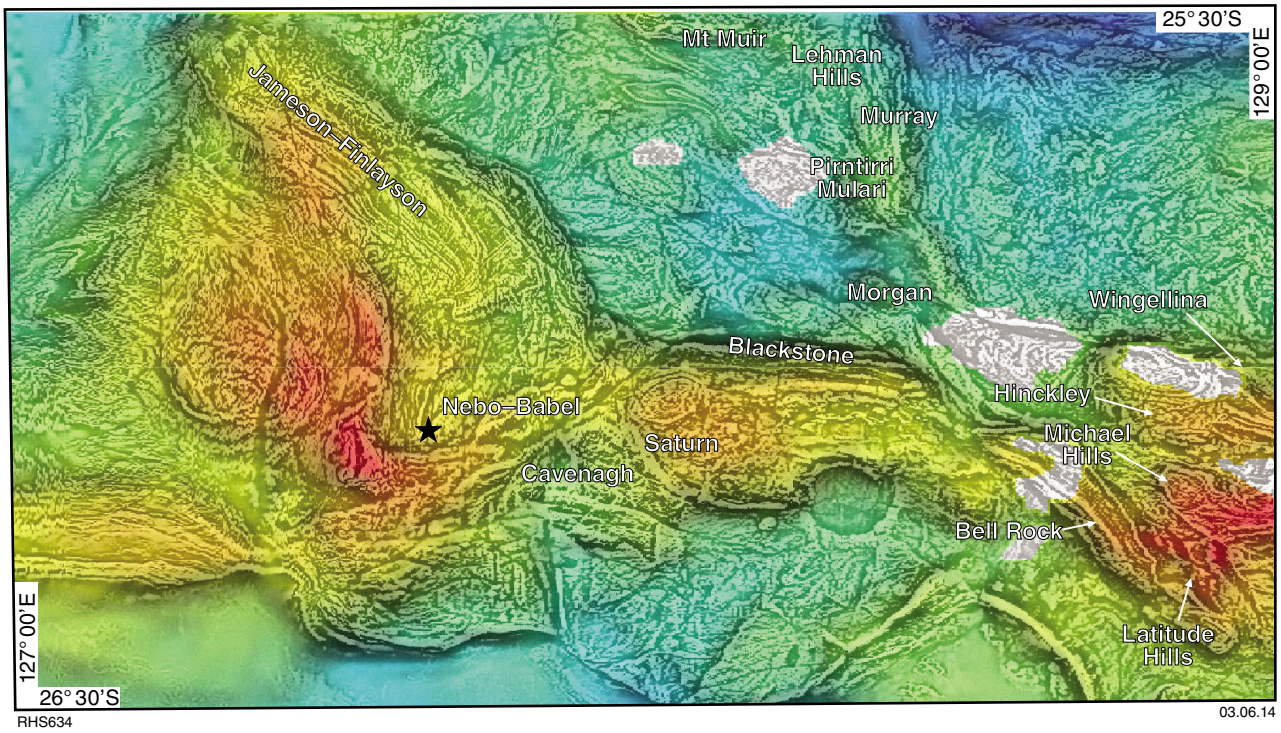

Figure 2. **Combined gravity and total magnetic intensity (TMI) (grey scale) image of the west Musgrave Province. Grey scales range from high (red) to low (blue). White areas indicate regions where gravity data could not be collected. Labels refer to selected mafic–ultramafic intrusions. Black star shows location of Nebo–Babel Ni–Cu deposit.**

(Ballhaus and Glikson, 1989, 1995; Ballhaus and Berry, 1991; Clarke et al., 1995a,b; Glikson, 1995; Sheraton and Sun, 1995; Stewart, 1995). These authors suggested that the Giles intrusions were emplaced at variable crustal depth, although these authors also reiterated earlier proposals that the Blackstone and Bell Rock intrusions are fragments of an initially contiguous intrusion. More recent contributions on the Giles intrusions and related mafic bodies of the Warakurna Supersuite include by Seat et al. (2007, 2009), who studied the Nebo–Babel intrusion and its Ni–Cu ore deposit; Evins et al. (2010a,b), who investigated the structural evolution of the area during the Giles Event; Godel et al. (2011), who conducted a petrologic study of dyke suites in the Nebo–Babel area; and Aitken et al. (2012), who published geophysical modelling constraints on intrusion geometry and evolution.

Regional geology

The Musgrave Province is a Mesoproterozoic belt tectonically bound by the Neoproterozoic to Paleozoic sedimentary rocks of the Amadeus Basin in the north and the Officer Basin in the south (Edgoose et al., 2004). The province is expressed on geophysical images as a series of east-trending anomalies covering an area up to 800 km long and 350 km wide that straddles the borders between the Northern Territory, Western Australia, and South Australia (Fig. 1). The term 'Musgrave Province' is used here to refer to all the high-grade metamorphic rocks affected by the Mesoproterozoic Musgrave Orogeny. That component of the Musgrave Province within the State of Western Australia is called the 'west Musgrave Province'. A comprehensive account of the geologic evolution of the province is given in Howard et al. (2011b), and is summarized here.

Main tectono-magmatic events

The basement to the west Musgrave Province remains poorly known. With the exception of the recent discovery of c. 1575 Ma rocks in the Wannarn area, the basement can only be studied through isotopic data on the detrital components in paragneisses, and on zircon xenocrysts. A recent study of Hf isotopes in zircons from magmatic and sedimentary rocks throughout the Musgrave Province (Kirkland et al., 2013) indicates that the unexposed basement is dominated by two major juvenile crust formation events, one at 1600–1550 Ma, and a possibly more important event at 1950–1900 Ma.

Outcrop in the west Musgrave Province consists largely of granites formed during several Mesoproterozoic events. The oldest of these is a recently identified, although unnamed, event that involved intrusion and possible extrusion of felsic calc-alkaline magmas of the Papulankutja Supersuite and contemporaneous redistribution of this material into local sedimentary

basins at c. 1400 Ma (Howard et al., 2011b; Kirkland et al., 2013). The oldest clearly recognizable event in the west Musgrave Province is the Mount West Orogeny. During this period, calc-alkaline granites of the Wankanki Supersuite were emplaced mainly within the central and southeastern part of the province (Evins et al., 2009; Smithies et al., 2009). Crystallization dates range from c. 1345 Ma to c. 1293 Ma (Gray, 1971; Sun et al., 1996; White et al., 1999; Bodorkos et al., 2008a–e; Kirkland et al., 2008a–f; Smithies et al., 2009), although ages cluster between c. 1326 and 1312 Ma. Rocks of the Wankanki Supersuite are typically metaluminous, calcic to calc-alkaline granodiorites and monzogranites with strong compositional similarities to the Phanerozoic granites of the Andean continental arc (Smithies et al., 2010). The Mount West Orogeny may reflect final subduction and accretion during the amalgamation of the North, West, and South Australian Cratons (Giles et al., 2004; Betts and Giles, 2006; Smithies et al., 2009, 2010; Kirkland et al., 2013).

The 1220–1150 Ma Musgrave Orogeny involved mylonitic deformation and widespread granulite-facies crustal reworking. It is typically regarded as essentially intracratonic (Wade et al., 2008; Smithies et al., 2009, 2010), although Smithies et al. (2013) suggest that it may alternatively reflect an ultra-hot orogen initiated on the back-arc region of the Mount West Orogeny. Orthopyroxene-bearing (charnockitic) and locally rapakivi granites of the Pitjantjatjara Supersuite intruded the mid-crust more-or-less continuously throughout the Musgrave Orogeny. They are ferroan and typically alkali-calcic granites with significant enrichment of rare earth elements (REE) and high field strength elements (HFSE). In all areas, the earliest Pitjantjatjara intrusions are strongly ytterbium-depleted granites formed through deep crustal melting under garnet-present conditions. A transition from these to ytterbium-undepleted granites formed at lower melting pressures is diachronous, migrating from the northeast to the southwest of the province from c. 1220 to c. 1200 Ma. This transition has been attributed to progressive removal of the lower crust and lithosphere, previously thickened during the Mount West Orogeny (Smithies et al., 2010, 2011).

The Pitjantjatjara granites were emplaced at temperatures up to 1000°C (Smithies et al., 2010, 2011) and intrusion coincided with a 100–70 Ma period of regional ultra-high-temperature (UHT) metamorphism (King, 2008; Kelsey et al., 2009, 2010; Smithies et al., 2010, 2011), characterized by temperatures in the lower to mid-crust of >1000°C, along a geothermal gradient of ≥35–40°C/km (King, 2008; Kelsey et al., 2009, 2010). These thermal conditions are consistent with complete removal of the lithospheric mantle during the early Musgrave Orogeny.

Voluminous mafic to felsic magmas were intruded into and extruded onto the west Musgrave Province during the c. 1090 to 1040 Ma Giles Event (Fig. 3). All igneous rocks that formed during the Giles Event are grouped into the Warakurna Supersuite. These include the giant layered mafic–ultramafic 'Giles intrusions' (G1), massive gabbro (G2) locally mixed and mingled with granite, various dyke suites including the Alcurra Dolerite suite, granite plutons, and mafic and felsic lavas. The latter are grouped into the Bentley Supergroup, which also includes volcaniclastic and sedimentary rocks.

The outcrop extent of the Bentley Supergroup defines the preserved extent of the Bentley Basin (Fig. 4). This basin can be subdivided into several sub-basins in Western Australia, including the Talbot Sub-basin in the area west of Jameson Community, and the smaller Blackstone Sub-basin (Tollu Group) in the area south of Blackstone Community. The lithological range, lithological associations, and distribution of the Warakurna Supersuite and the Bentley Supergroup, and their geologic history, are consistent with a long-lived intracontinental

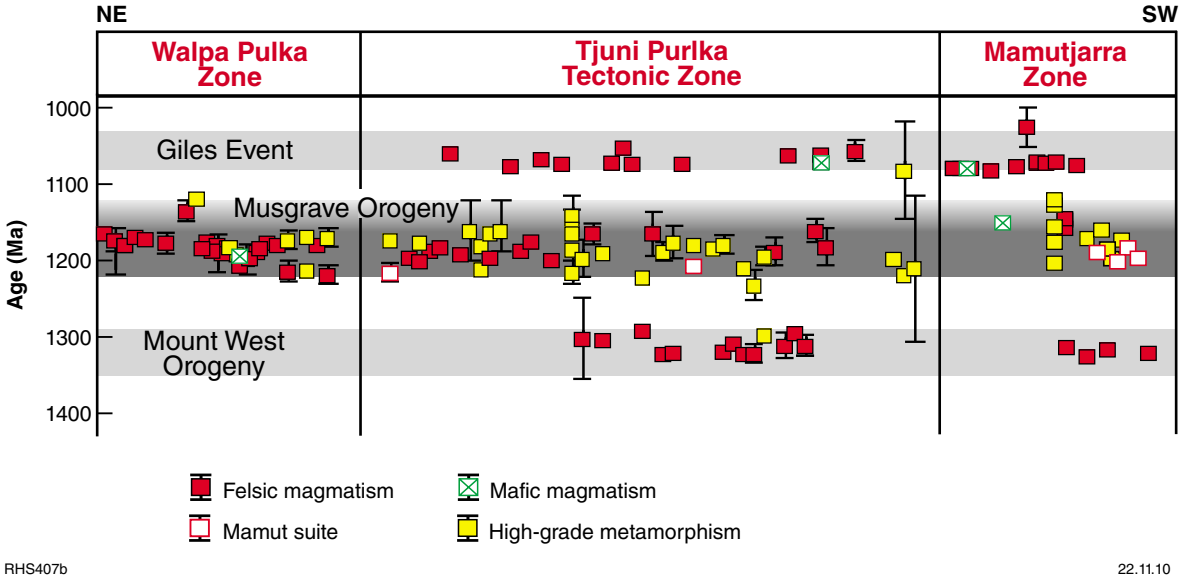

Figure 3. Time–space plot showing GSWA sensitive high-resolution ion microprobe (SHRIMP) U–Pb zircon ages from the west Musgrave Province (after Smithies et al., 2010). Error bars show standard errors.

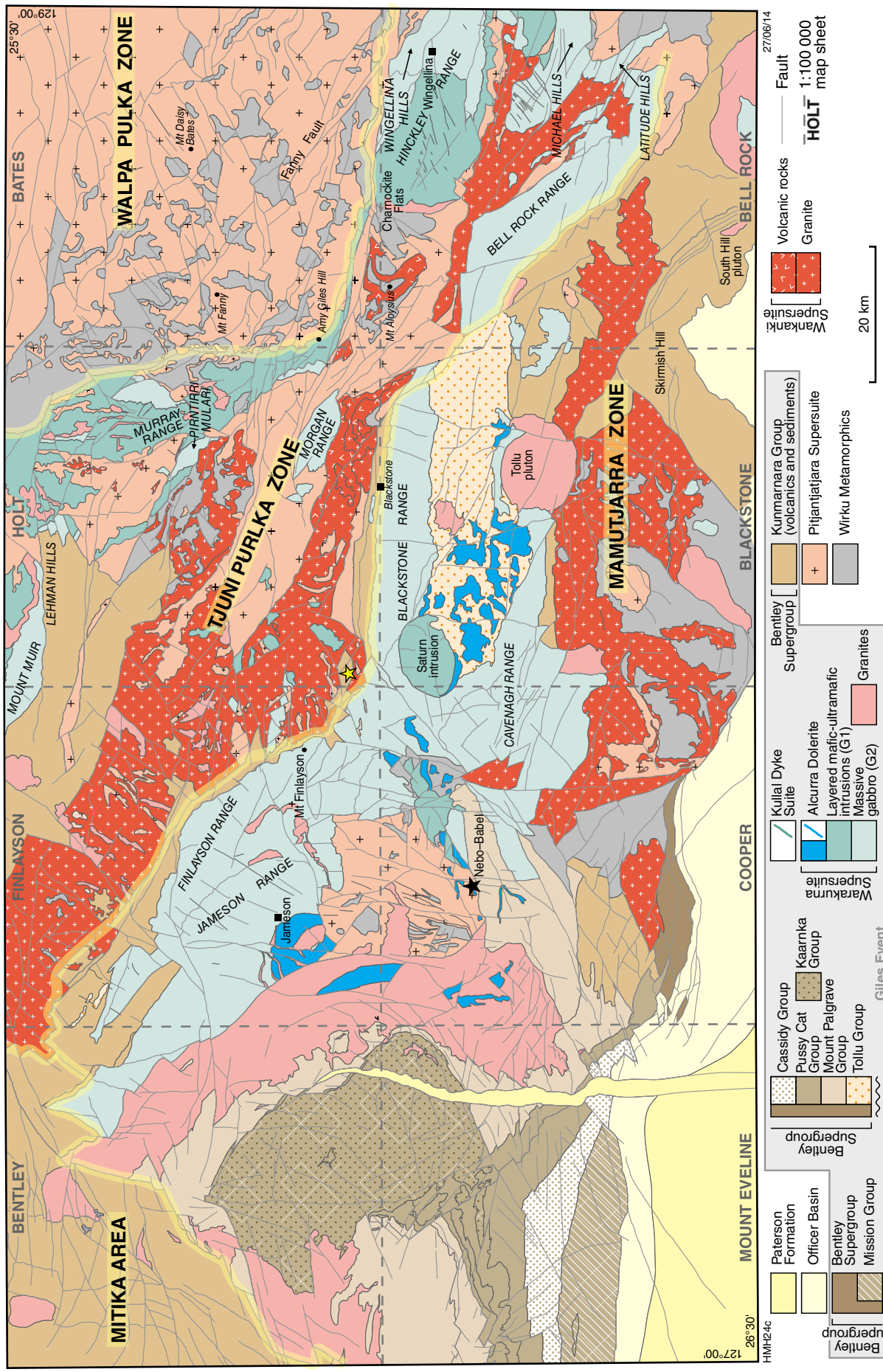

Figure 4. Interpreted bedrock geology map of the west Musgrave Province. Black star shows location of Nebo–Babel Ni–Cu deposit.

rift setting called the Ngaanyatjarra Rift (Evins et al., 2010b; Aitken et al., 2013). Intrusive rocks of the Warakurna Supersuite are particularly abundant within the Mamutjarra and Tjuni Purlka Zones, where they typically occur as tectonically dismembered bodies of layered mafic–ultramafic 'Giles intrusions (G1)', 'massive gabbro (G2)', and granite.

The Giles Event has been interpreted as the result of a mantle plume, based on the observation that mafic rocks of the Warakurna Supersuite outcrop across approximately 1.5 million km^2 of central and western Australia, forming the Warakurna Large Igneous Province (Wingate et al., 2004; Morris and Pirajno, 2005). However, mantle-derived magmatism lasted more-or-less continuously for at least 50 Ma, suggesting that the Giles Event reflects a more protracted and complex geodynamic setting inconsistent with a simple plume model (Smithies et al., 2009, 2013; Evins et al., 2010a,b), as discussed in more detail in a later section.

Younger events include the 580–530 Ma intracratonic Petermann Orogeny, which coincides with the global Pan-African Plate reorganization that marks the assembly of Gondwana. Granulites and high-grade gneisses of the Musgrave Province were thrust northwards, over or into (interleaved with) rocks of the Neoproterozoic basins (Camacho, 1997; Flöttmann and Hand, 1999; Edgoose et al., 2004), and many of the Giles intrusions were fragmented. The Alice Springs Orogeny was a further major intraplate event, or series of events, which affected much of central Australia from c. 450 to 300 Ma (Collins and Teyssier, 1989; Haines et al., 2001), although there is no firm evidence that the orogeny had any significant effect on the Musgrave region. Additional younger events are indicated through the presence of regional dolerite dyke suites (at c. 1000, c. 825, and c. 750 Ma) and low-volume felsic magmatism (at c. 995 Ma and c. 625 Ma).

Tectonic subdivisions of the west Musgrave Province

The Musgrave Province has been subdivided into several distinct zones with different structural and metamorphic characteristics separated by major west- and west-northwesterly trending faults that were last active during the Petermann Orogeny (Camacho, 1989). These faults include the south-dipping Woodroffe Thrust (Fig. 1) which separates the amphibolite-facies Mulga Park Zone in the north from the granulite-facies Fregon Zone in the south, the latter comprising most of the west Musgrave Province. In the eastern part of the west Musgrave Province, the Fregon Domain shows a marked north-to-south change in the pressure of granulite-facies metamorphism. To the north, high-pressure (10–14 kbar) metamorphism during the Petermann Orogeny has masked the effects of Mesoproterozoic metamorphism (Scrimgeour and Close, 1999). To the south, where metamorphic overprints of Petermann Orogeny age are not as marked, evidence for Mesoproterozoic high-temperature metamorphism, at much lower pressures, is preserved (Clarke et al., 1995b). In the west Musgrave Province, the boundary separating these two metamorphic styles lies close to the west-trending and near vertical Mann Fault (Fig. 1).

The western part of the Fregon Domain is subdivided into the Walpa Pulka, Tjuni Purlka, and Mamutjarra Zones (from northeast to southwest; Smithies, et al., 2009, 2010; Fig. 4). The Tjuni Purlka Zone is a broad northwest-trending zone of multi-generational (c. 1220, 1075, and 550 Ma) shearing. The extent and intensity of northwest-trending shearing in this zone exceeds that of neighbouring zones. The margins of the Tjuni Purlka Zone, in particular, have formed the focus for felsic and mafic magmas of the Warakurna Supersuite (Fig. 4). These tectonic boundaries were synmagmatic shear zones throughout much of the Giles Event. The effects of the Petermann Orogeny in this zone are most intense to the northeast, near the contact with the Walpa Pulka Zone, and decrease to the southwest. Further to the north, the Walpa Pulka Zone (Fig. 4) is a deep crustal domain dominated by c. 1220–1150 Ma high-K granite plutons of the Pitjantjatjara Supersuite emplaced during the Musgrave Orogeny. The zone contains high-pressure metamorphic assemblages preserved by rapid exhumation along east- and northwest-trending mylonitic and migmatitic shear zones related to the Petermann Orogeny (Camacho et al., 1997; Scrimgeour and Close, 1999; Raimondo et al., 2009, 2010). The Mamutjarra Zone, south of the Tjuni Purlka Zone (Fig. 4), is dominated by Giles intrusions and the c. 1345–1293 Ma calc-alkaline granites of the Wankanki Supersuite, formed during the Mount West Orogeny. The effects of the Petermann Orogeny in this zone are minimal.

Geology and petrology of mafic and mafic–ultramafic intrusions of the Giles Event

Introduction

The Giles intrusions include three lithologies: (i) predominantly ultramafic; (ii) interlayered mafic–ultramafic; and (iii) predominantly mafic bodies. Intrusions with important ultramafic segments include Wingellina Hills, Pirntirri Mulari, The Wart (Fig. 1) and, in South Australia, Ewarara, Claude Hills, Gosse Pile, and Kalka. The ultramafic rocks contain mainly wehrlite, harzburgite, websterite, and (olivine) orthopyroxenite, with less-abundant dunite.

Predominantly mafic intrusions in the west Musgrave Province include Hinckley Range, Michael Hills, Latitude Hill, Murray Range, Morgan Range, Cavenagh, Saturn, Blackstone, Jameson, Finlayson, Bell Rock, and several smaller intrusions or fragments of intrusions to the north of the Tjuni Purlka Zone; these include the Mt Muir and Lehmann Hills intrusions (note that the Jameson, Finlayson, Blackstone, and Bell Rock intrusions are now believed to be tectonically segmented portions of an originally single body, hereafter called the Mantamaru

intrusion). These mafic intrusions are predominantly of leucogabbronoritic composition, with >50 vol.% plagioclase and variable proportions (commonly clustering around unity) of orthopyroxene to clinopyroxene.

Several intrusions contain thick troctolitic successions where olivine and plagioclase are the main cumulus phases and pyroxenes are either interstitial or form minor cumulus minerals. These intrusions include Cavenagh, Morgan Range, and Mantamaru. Anorthosites form relatively thin layers (centimetres to several tens of centimetres) in the 'troctolitic' intrusions and in many gabbronoritic intrusions. The layers may attain thicknesses of several tens of metres at Kalka in South Australia. Massif-type anorthosite intrusions do not occur in the west Musgrave Province, although one such body has been delineated in South Australia (Teizi; Gray, 1967). Ballhaus and Glikson (1995) proposed that the ultramafic intrusions occur predominantly in the northern portion of the west Musgrave Province, whereas mafic intrusions occur mainly in the central parts, and troctolites in the south. However, our work suggests that the ultramafic bodies are concentrated mainly in a narrow, 150 km-long, northwest–southeast-trending belt bound by the Hinckley and Mann Fault Zones. In the following section, we provide details of the geology and petrography of each of the intrusions studied.

Mafic–ultramafic layered intrusions

Pirntirri Mulari intrusion

This intrusion is 30 km north of Blackstone Community (Fig. 4). It was previously studied by Ballhaus and Glikson (1995), who grouped it with the gabbronoritic Murray Range intrusion, although the distinct lithologies and composition of the Pirntirri Mulari intrusion render this interpretation questionable. The exposed portion of the body is wedge-shaped, so that the upper mafic portions are markedly wider than the ultramafic portions (Fig. 5), analogous to, for example, the Bushveld (Kruger, 2005) or Uitkomst Complexes (Gauert et al., 1995). The layers strike about 150° and have steep dips (60–90°), mostly to the southwest, although in some cases to the northeast. The width of the body is about 5 km, and its stratigraphic thickness is about 3 km.

The rocks consist mostly of medium-grained (olivine) websterite, peridotite, (olivine) orthopyroxenite, and (olivine) gabbronorite. Dunite is rare, although this may partly reflect poor preservation and exposure of these commonly highly altered rocks. The websterites are concentrated at the base and top of the intrusion where they are interlayered with gabbronorites. Peridotites and orthopyroxenites are concentrated in the centre. The basal ultramafic rocks are predominantly orthocumulates, whereas the rocks in the centre of the intrusion are adcumulates or mesocumulates. Based on compositional variations such as a trend from fertile to PGE-depleted rocks toward the northeast, and field evidence such as the presence of pegmatoids directly to the southwest of ultramafic layers, we propose that the succession youngs to the northeast, contrary to the interpretation of Ballhaus and Glikson (1995). This model implies that much of the intrusion is slightly overturned.

The rocks consist largely of olivine, clinopyroxene, orthopyroxene, and plagioclase. Phlogopite and chromite are accessory phases, the latter mainly existing in wehrlite (sample GSWA 189354). The basal contact of the intrusion is not exposed, although because the proportion of intercumulus minerals increases progressively towards its southwestern edge, this is interpreted to reflect a higher cooling rate. Thus, we argue that the basal contact is under cover and not far beyond the exposed southwestern edge. The top contact of the intrusion is likely of a tectonic nature, as suggested by the mylonitization of the uppermost rocks and by their relatively unevolved chemical composition, where Mg# (= molecular ratio Mg/[Mg+Fe] with all Fe as Fe^{2+}) of 0.7, and Cr/V > 1 (Table 1).

Contacts between layers tend to be sharp or, in some cases, gradational (Fig. 6b). At the top of the main ridge in the centre of the intrusion (sample GSWA 189374; Fig. 5), coarse-grained unaltered websterite underlies gabbronorite with an undulose, sharp contact, and has locally intruded the gabbronorite (Fig. 6e,f). The gabbronorite is markedly more deformed than the pyroxenite, and has an altered endo-contact zone, suggesting intrusion of pyroxenite into, and stratigraphically below, older gabbronorite. A few hundreds of metres to the southwest (sample GSWA 189368), fine-grained lherzolite overlies a coarse-grained peridotite with an undulose, sharp contact (Fig. 6c). Inclusions of coarse-grained material exist within the fine-grained rock. These observations could suggest that the fine-grained peridotite crystallized from a new magma influx that underwent intra-plutonic quenching. Elsewhere, pyroxenite is underlain by pegmatoidal gabbronoritic orthocumulate layers tens of centimetres wide (sample GSWA 189360; Fig. 6d), consisting of 40% plagioclase, 30% orthopyroxene, 20% clinopyroxene, and accessory phlogopite and chromite. The pegmatoid has relatively high trace element concentrations (e.g. P, light REE [LREE], Nb, Rb) and shows relative enrichment in the most incompatible elements, suggesting it may have formed through a combination of supercooling (Ballhaus and Glikson, 1989) and upward percolation of evolved melt or fluid.

In the lower portion of the intrusion, textural evidence suggests a complex intrusive history and substantial synmagmatic cumulate mobility. Gabbroic layers contain abundant ultramafic and anorthositic schlieren (Fig. 6a,g,h). The schlieren horizons are concentrated both below and above pyroxenite layers, with the latter also containing gabbroic schlieren. The Wingellina Hills intrusion shows similar textures (Ballhaus and Glikson, 1989). A model of synmagmatic tectonism would be consistent with the varying degree of deformation in the rocks; pyroxenites and gabbronorites tend to show abundant subgrain formation and bent twin lamellae, whereas some wehrlites (notably sample GSWA 189354) are relatively unaltered and undeformed.

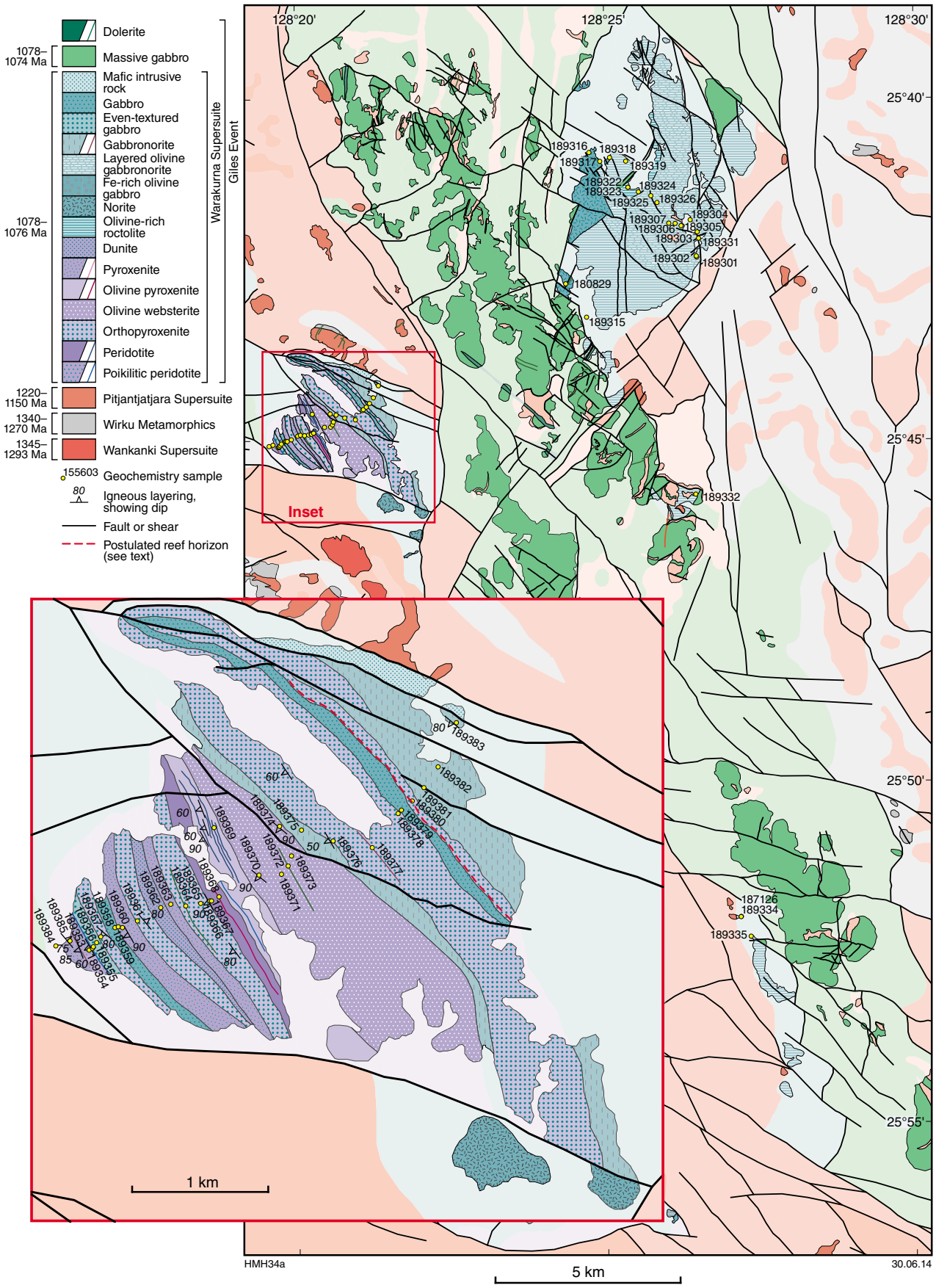

Figure 5. Interpreted bedrock geological map of the Pirntirri Mulari intrusion, showing sample localities (yellow circles). Light shaded areas indicate regions of regolith cover.

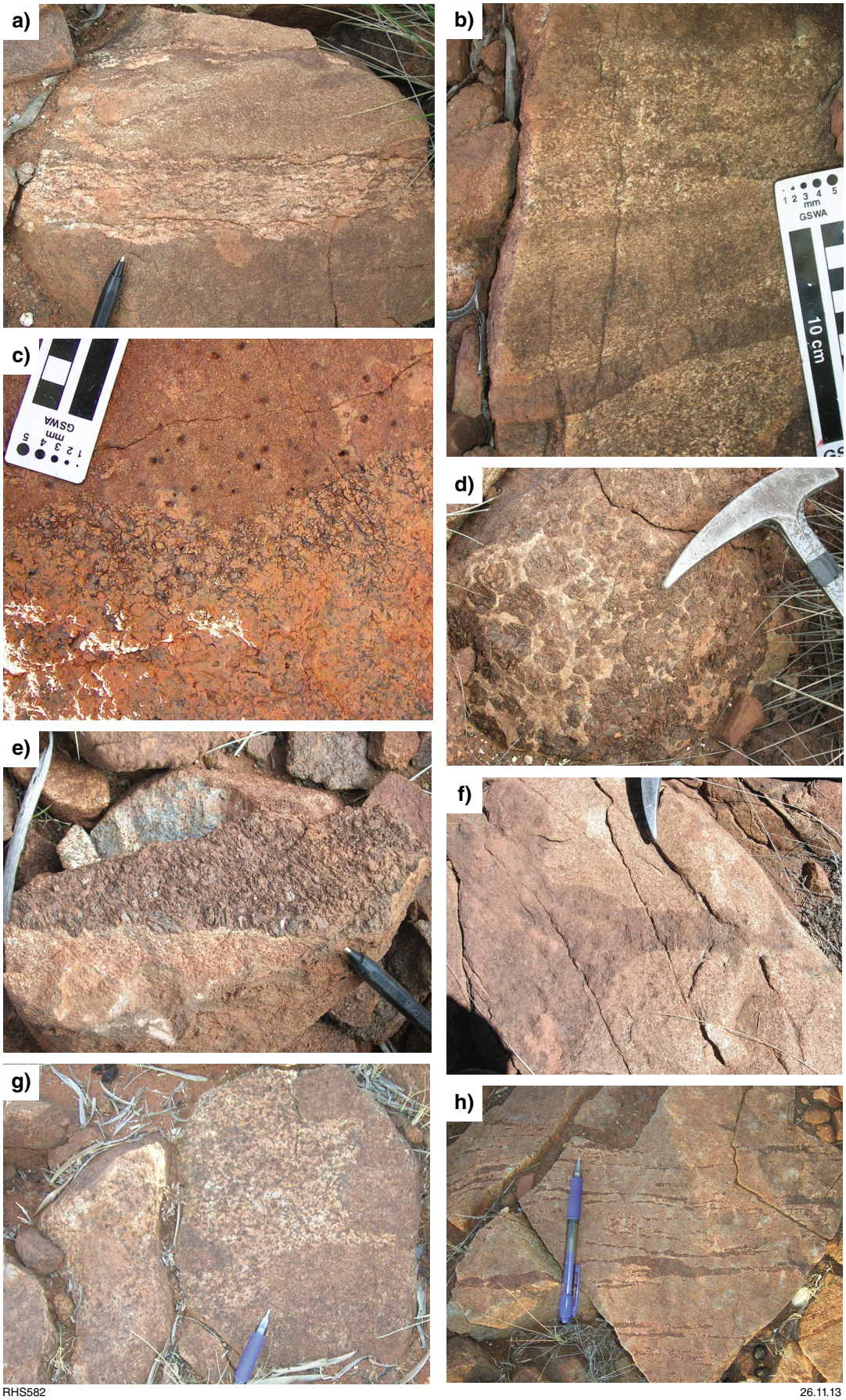

RHS582 26.11.13

Figure 6. (facing) Textures of rocks in the Pirntirri Mulari intrusion: a) interval containing abundant schlieren of anorthosite, gabbronorite, and pyroxenite near contact between units of gabbronorite and overlying pyroxenite, within lower portion of intrusion (near sample GSWA 189359, see Fig. 5); b) centimetre-scale interlayering of pyroxenite and gabbronorite showing sharp bottom contact and upward grading; note small lenses and schlieren of pyroxenite within gabbronorite (near GSWA 189359); c) contact between fine-grained lherzolite overlying coarse-grained peridotite with an undulose, sharp contact (central portion of intrusion, GSWA 189368); d) pegmatoidal layer within medium-grained pyroxenite (GSWA 189360); e) contact between coarse-grained pyroxenite and overlying altered, medium-grained gabbronorite; note undulose, sharp contact (near GSWA 189374); f) contact between pyroxenite and overlying gabbronorite; finger-like structure of pyroxenite is interpreted as injection of pyroxenite mush into gabbronorite (near GSWA 189374); g) irregular lenses of gabbronorite and melagabbronorite within websterite; note sharp, undulating contact (lower portion of intrusion, near GSWA 189355); h) schlieren of pyroxenite within leucogabbronorite (near GSWA 189358)

Many of the rocks at Pirntirri Mulari and in many other Giles intrusions show well-developed textural equilibration as expressed, for example, by 120° grain boundaries, abundant bronzite and spinel exsolution in clinopyroxene, recrystallization of plagioclase to small granoblastic grains with spinel inclusions, and orthoclase exsolution blebs. Where in contact with olivine, plagioclase has recrystallized to a two-pyroxene spinel symplectite. These features were interpreted to indicate high crystallization pressures and temperatures (Ballhaus and Glikson, 1989).

Figure 7 presents the lithostratigraphy and chemostratigraphy of the Pirntirri Mulari intrusion, based on our sampling traverse (see Table 1 for data). The concentrations of incompatible elements are lowest in the centre (for example, <10 ppm Zr and Cu), reflecting the adcumulate nature of these rocks. Platinum group element concentrations are mostly <10 ppb, and the Cu/Pd ratio is mostly around primitive mantle levels (4000–7000), suggesting that the magma was sulfur undersaturated. With the exception of a few samples, PGE patterns of the rocks are flat or show depletion in Pt and Pd relative to the IPGE (i.e. Pt and Pd relative to Os, Ir, and Ru; Fig. 8). However, at about 2600 m above the base of the intrusion, Cu/Pd ratios increase markedly, suggesting that the magma reached sulfide saturation at this stage. A sample analysed from this level has low PGE concentrations, although almost 500 ppm Cu. The stratigraphic position of this sample in the mafic–ultramafic transition interval is analogous to the stratigraphic position of PGE reefs in the Bushveld Complex and in many other PGE-mineralized intrusions.

Redstone Resources Ltd assayed a sulfide-bearing pyroxenite at an equivalent stratigraphic level, although at the southeastern edge of the intrusion (Fig. 5). This sample has similar chromium, copper, and nickel concentrations to the equivalent internal horizon, although much higher Pt+Pd (172 ppb) and gold (17 ppb) concentrations. Niton assay results yielded elevated Ni and Cu over a stratigraphic interval of 5–10 m, with peak values of 0.43% Cu and 0.7% Ni in weathered rock (Redstone Resources Ltd, 2008a). Whether this interval contains further horizons of elevated PGE concentrations is unknown as no detailed sampling or PGE assaying has yet been conducted.

Wingellina Hills intrusion

This intrusion extends for about 12 km along a strike of 110–120° and is up to 3 km wide (Fig. 9, Appendix 3). Originally, the dip of the layering was assumed to be to the northeast (Ballhaus and Glikson, 1989), although drilling programs by Acclaim Minerals and Metals X Ltd, and mapping by GSWA, established dips of about 65–75° to the southwest. Based on these data, the exposed stratigraphic thickness amounts to 2.5 km, barring tectonic duplications of stratigraphy. The base of weathering varies considerably depending on rock type and degree of shearing. The outcropping gabbros and pyroxenites tend to be unaltered at the surface, although in the peridotites the depth of weathering varies from about 60 m to >200 m in shear zones.

The petrography of the central portion of the intrusion was studied by Ballhaus and Glikson (1989). They identified numerous cyclic units consisting of basal pegmatoidal (ortho) pyroxenite, overlain by clinopyroxenite and then peridotite (olivine–spinel cumulate), wehrlite, and gabbronorite.

The pegmatoidal orthopyroxenite contains up to 30% intercumulus plagioclase and occasional sulfide. It overlies gabbronorite with sharp but undulating contacts, and locally erodes the gabbronorite. The gabbronorite contains fragments and schlieren of ultramafic rock, and may show convoluted and folded layering and 1–2-cm layering, analogous to the Pirntirri Mulari intrusion (Fig. 6). The orthopyroxenite was interpreted to have formed due to mixing of replenishing (primitive) magma with silica-rich resident magma, whereas the overlying clinopyroxenite and peridotite would represent progressively less-hybridized replenishing magma.

The gradation of peridotite to wehrlite would reflect fractionation. The peridotite contains amoeboidal olivine crystals and abundant chromite locally forming centimetre-thick schlieren. The overlying wehrlites contain large poikilitic clinopyroxene oikocrysts, minor intercumulus plagioclase, orthopyroxene, and trace sulfide. Notably, the olivine and pyroxene in the wehrlite have lower forsterite (Fo) contents and Mg# than in the basal, chromite-poor pyroxenites. Ballhaus and Glikson (1989) suggested that the peridotites and wehrlites would have formed from replenishments of the chamber with primitive

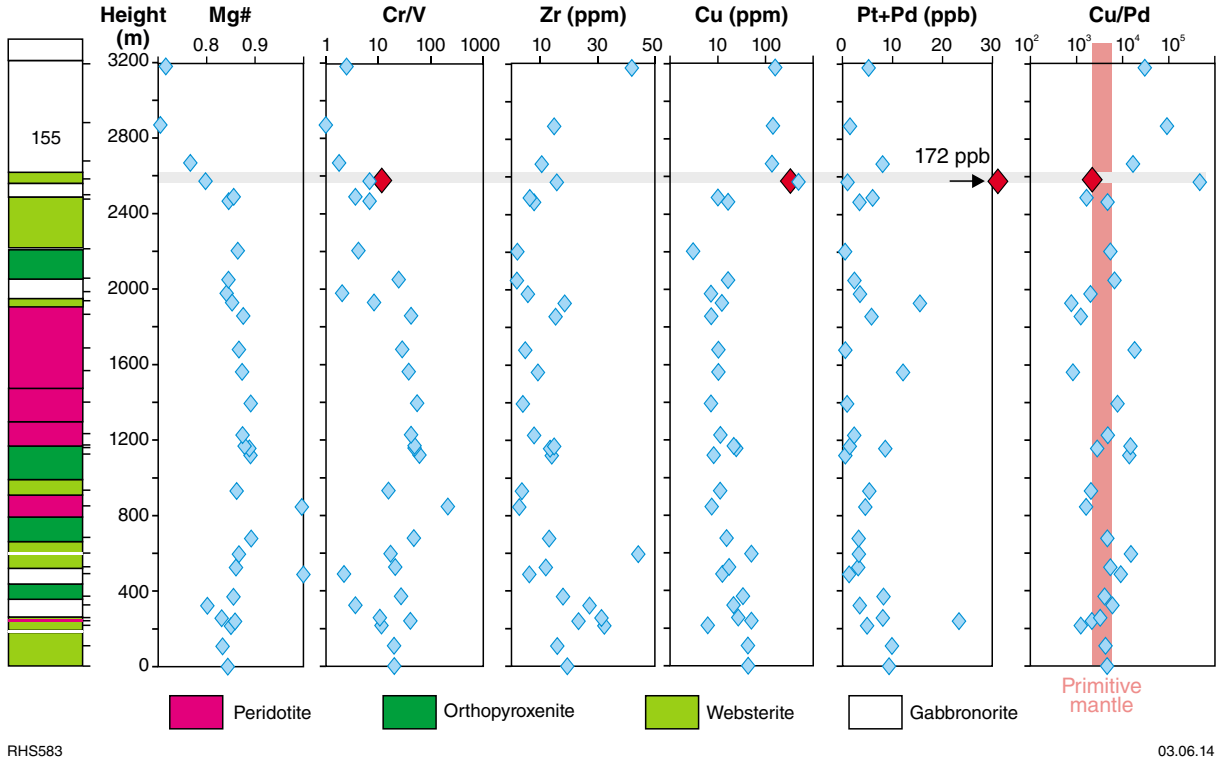

Figure 7. **Compositional variation with stratigraphic height in the Pirntirri Mulari intrusion. Red diamonds indicate the platinum group element (PGE) – rich sample analysed by Redstone Resources Ltd, and horizontal shaded bar indicates postulated position of PGE reef. Range of primitive mantle composition (for Cu/Pd) is based on Barnes and Maier (1999) and Becker et al. (2006).**

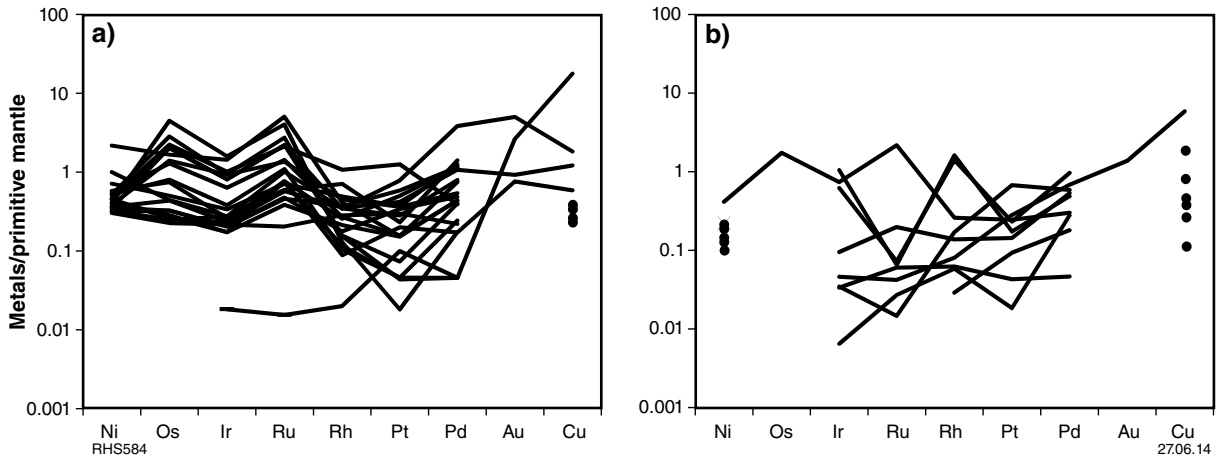

Figure 8. **Mantle-normalized multi-element diagrams of chalcophile elements for Pirntirri Mulari: a) ultramafic rocks; and b) gabbronorites. Normalization factors from Barnes and Maier (1999). Black circles indicate Cu and Ni contents of samples that have Au and/or Os below the detection limit.**

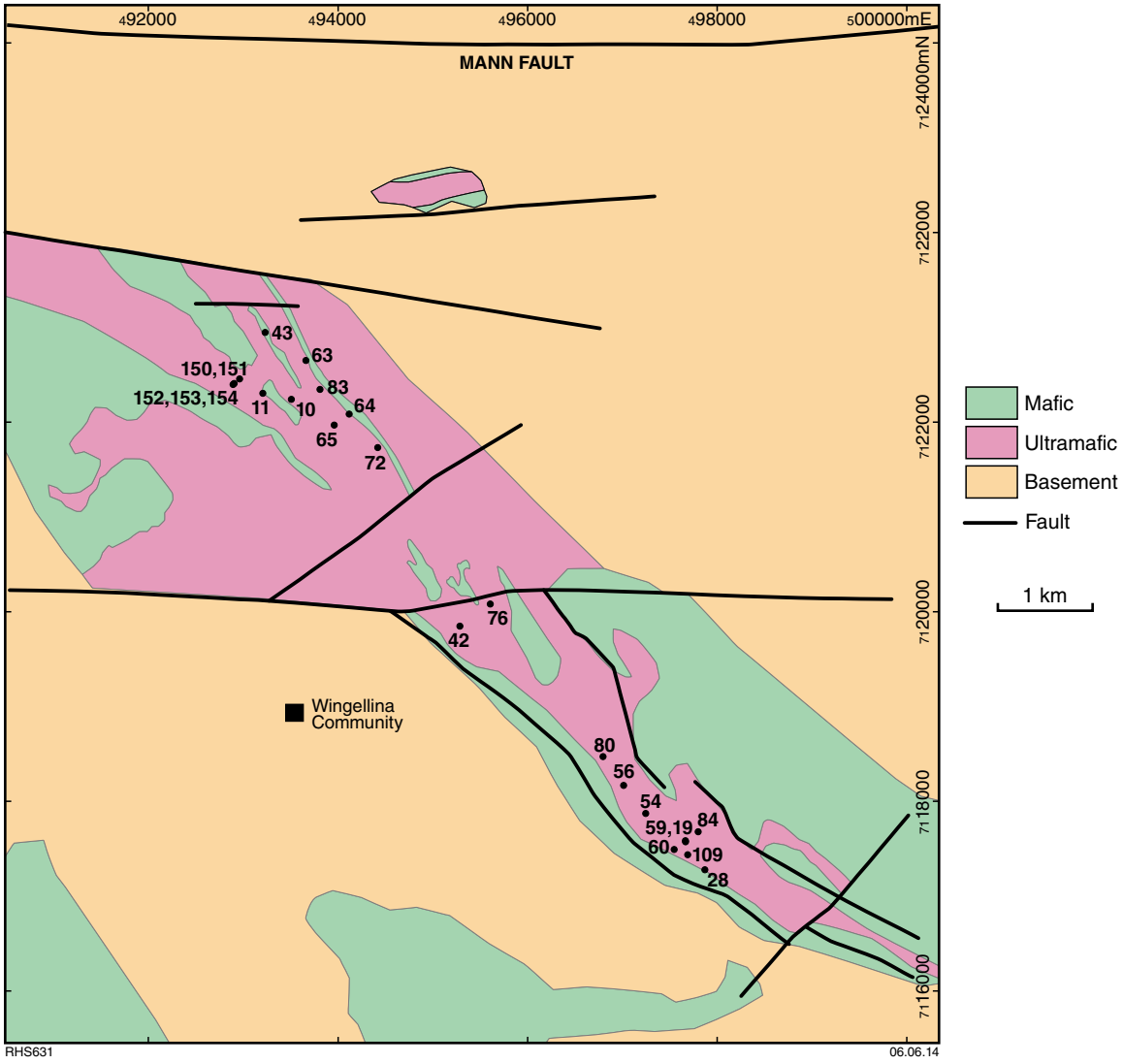

Figure 9. Simplified geological map of Wingellina Hills intrusion, showing location of boreholes where platinum group element mineralization has been intersected. Figure provided by Metals X Ltd, reproduced with permission.

magma, although that supercooling led to metastable crystallization of chromite and relatively low Fo contents of co-crystallizing olivine. Subsequently, the magma would have reverted to the olivine–clinopyroxene cotectic precipitating relatively more magnesian clinopyroxenite without chromite. Based on these interpretations and observations, Ballhaus and Glikson (1989) proposed that the magma had a crystallization sequence of olivine(+spinel)–olivine+clinopyroxene+orthopyroxene+plagioclase.

The compositional variation of the basal to central portion of the intrusion has been reassessed based on several stratigraphic boreholes (Fig. 10). The basal contact is exposed in a reverse circulation (RC) borehole WPRC0-023 (Fig. 11). It is likely intrusive, because the basal pyroxenite shows a well-defined basal compositional reversal that is typical of the basal contacts of layered intrusions (e.g. Latypov, 2003). Whole-rock data further suggest that there is a hybrid contaminated contact zone 1–2 m thick, although few details are available. Petrographic study of a rock chip from about 2 m above the contact revealed a medium-grained, moderately deformed olivine gabbronorite, inconsistent with the presence of a major fault (R Coles, 2013, written comm., 27 May).

Through the next 300 m of the borehole, the basal olivine gabbronorite and pyroxenite are overlain by progressively more magnesian harzburgite and then peridotite and wehrlite. Because the basal reversal has a similar thickness to that in the Bushveld Complex (Teigler and Eales, 1996), we infer that the rocks are the stratigraphic base of the intrusion, and that the crystallization sequence of the magma in the basal portion of the Wingellina Hills intrusion was olivine+orthopyroxene–

olivine+clinopyroxene+orthopyroxene–olivine+clinopyroxene+orthopyroxene+plagioclase, possibly reflecting contamination of the initial magma pulses. The data also indicate that the Wingellina Hills intrusion has a significantly larger proportion of olivine-rich rocks than, for example, the Pirntirri Mulari or The Wart intrusions.

The wehrlite is overlain by about 20 m of pyroxenite and >40 m of olivine gabbronorite forming the upper portion of the first cyclic unit of the intrusion. The contacts between wehrlite and pyroxenite, and between pyroxenite and gabbronorite, can be sharp (for example, in drillcore WPRCD0-083) or gradational over a few metres. Within the pyroxenite occurs a PGE reef (described below), which has been traced along a strike of 2–3 km. The remainder of the intrusion consists of interlayered peridotite, wehrlite, pyroxenite, and olivine gabbronorite. Megarhythmic layering forms on a scale of tens of metres, although centimetre-scale layering may also be present (Ballhaus and Glikson, 1989).

The compositional variation across the PGE reef interval can be studied in three selected boreholes (WPRC0-043 and 064, and WPRCD0-083; Figs 12–14, respectively). The reef is hosted in websterite, which overlies wehrlite with a sharp contact, reflected by a decrease in MgO and an increase in Cr concentration. Platinum group element concentrations show an initial peak of almost 100 ppb at, or just below, the wehrlite–websterite contact, and then increase through the websterite layer to a point about 5–7 m beneath the top of the websterite, where concentrations reach up to 2 ppm Pt+Pd+Au over a 1-m interval, and >1 ppm of PGE over a 3–5-m interval. Above the reef, PGE concentrations fall rapidly across a few metres of stratigraphy. Of note is that Au and Cu concentrations remain relatively low (<5 ppb Au, <10 ppm Cu) throughout much of the PGE-enriched zone. However, Au and Cu peak just above the main Pt+Pd-enriched horizon (up to 330 ppb Au over a 1-m interval, and up to 400 ppm Cu in rocks 2 m above the Au peak). From here, Au and Cu concentrations decrease with stratigraphic height, although at a much slower rate than the PGE concentrations. Analogous metal distribution patterns have been observed in the Great Dyke of Zimbabwe (Wilson et al., 1989), the Munni Munni intrusion of the Pilbara Craton (Barnes, 1993), and the Stella intrusion of South Africa (Maier et al., 2003b), where they were termed ‘offset patterns’ (Barnes, 1993). Compared to the Bushveld reefs (~1–2% S), the Wingellina Hills reefs are relatively sulfur poor, having mostly <500 ppm S. The reefs are thus invisible in hand specimen, posing an added challenge to exploration. It remains unclear whether the paucity of sulfur is a primary magmatic feature or is the result of metamorphic devolatilization.

A comparison of the boreholes indicates that the thickness of the PGE reef changes along strike. Concentrations of >500 ppb PGE occur over a thickness of 8 m in drillcores WPRC0-064 and WPRCD0-083. Total PGE+Au concentrations calculated over a width of 1 m (i.e. concentrated into one metre) are broadly similar in the two cores, at 10.6 ppm in drillcore WPRC0-064 and 9.6 ppm in drillcore WPRCD0-083. WPRC0-043 has >100 ppb platinum group elements over a thickness of 12 m, and a total PGE+Au concentration of 5.5 ppm (normalized to 1 m). The samples were relatively unaltered from those near the surface and thus the relatively low bulk PGE values in this hole cannot be caused by laterization. The data instead suggest some variation in PGE grade along strike. Notably, the total PGE concentrations of the Wingellina Hills reef interval (at least in holes WPRC0-064 and WPRCD0-083) are similar to those in the combined Merensky Reef and UG2 chromitite of the Bushveld Complex, although the Bushveld reefs are much narrower, so the PGE are more concentrated.

At Wingellina Hills, the cyclic units overlying the main reef also show elevated concentrations. Notable enrichments occur, for example, in boreholes WPRC0-060 (157–159 m = 2.18 g/t), and WPRC0-084 (136–138 m = 2.5 g/t). Both holes were drilled at the southeastern end of the intrusion (Fig. 9). They appear to intersect a different stratigraphic level from WPRCD-083 and WPRC0-064; however, the south end of the intrusion is faulted, and thus the exact stratigraphic level is not known. These two holes were collared in a deeply oxidized shear zone and do not intersect unaltered rock until >170 m depth. The zone of elevated PGE concentrations is within lateritic clay in both holes. The weathering may have modified the Pt/Pd ratio because Pt concentrations are about twice those of Pd, whereas in the main reef the Pt/Pd ratio is at unity (R Coles, 2011, written comm., 8 July). Other important intersections were found in hole WPRC0-151 (>1 km to the west of holes WPRCD0-083 and WPRC0-064 (Fig. 9), with concentrations of up to 300 ppb Pt+Pd+Au over up to 35 m), and in WPRC0-152 (8 m at 486 ppm and 4 m at 537 ppm). Oxidized peridotite (now Ni-bearing limonites) of the interpreted fourth cycle of the Wingellina Hills intrusion show elevated PGE concentrations.

In addition to the reef horizons, PGE (and S) concentrations are also slightly enriched at the basal contact of the intrusion (Fig. 11), possibly due to sulfur saturation in response to contamination. This style of contact mineralization is found in many other layered intrusions (see summary in Maier, 2005). However, this mineralization appears economic only where the internal reefs abut floor rocks, as in the Bushveld and Portimo Complexes (Iljina and Lee, 2005). Local PGE enrichment (up to 40 ppb Pt+Pd) also occurs within the 300 m-thick basal harzburgite unit, in marked contrast to the Pirntirri Mulari intrusion, where the basal ultramafic rocks are PGE poor. The PGE enrichments in the Wingellina Hills harzburgite may reflect downward percolation of PGE-rich sulfides from the reefs, although further study is necessary to resolve this question.

The Wingellina Hills laterite comprises yellow-brown to dark brown ochre material composed of goethite, manganese oxides, gibbsite, and kaolinite derived from the weathering of dunite and peridotite. This forms the world-class Wingellina laterite nickel deposit, discovered by INCO in 1956. The laterites formed by selective leaching of SiO_2 and MgO and the resulting residual concentration of alumina, iron oxides, and nickel, which is especially

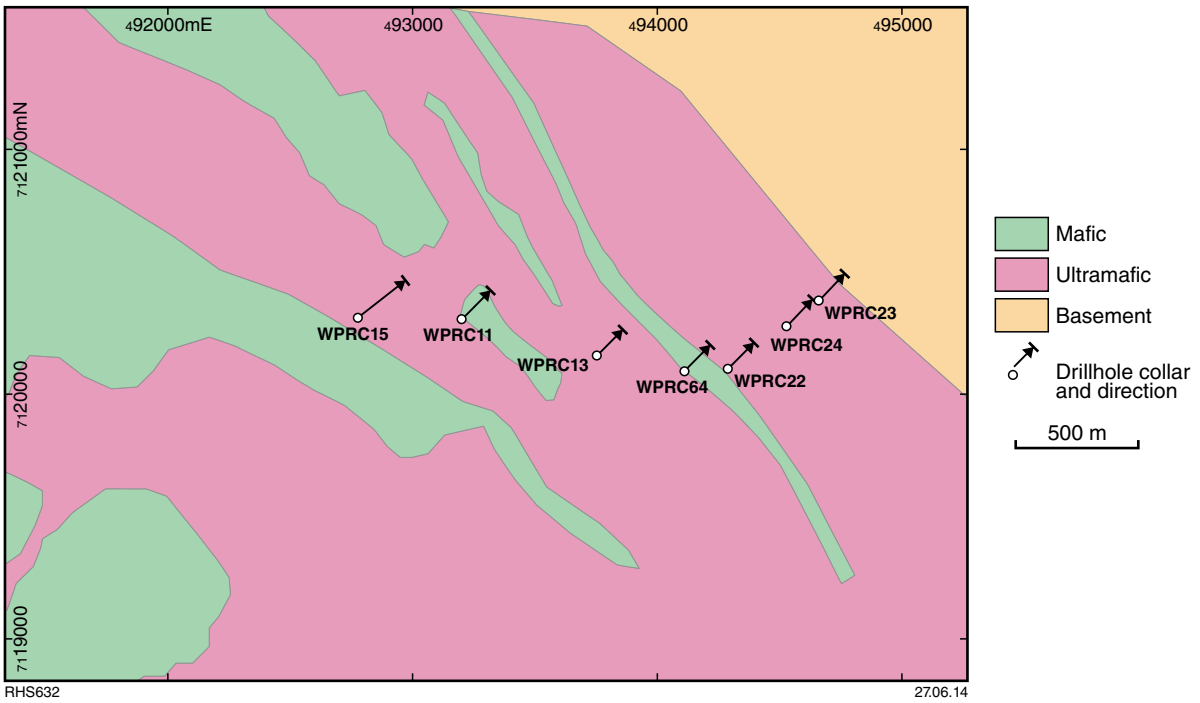

Figure 10. Location of boreholes intersecting the basal portion of the Wingellina Hills intrusion. Figure provided by Metals X Ltd, reproduced with permission. (WPRC15 = WPRC0-015 etc.)

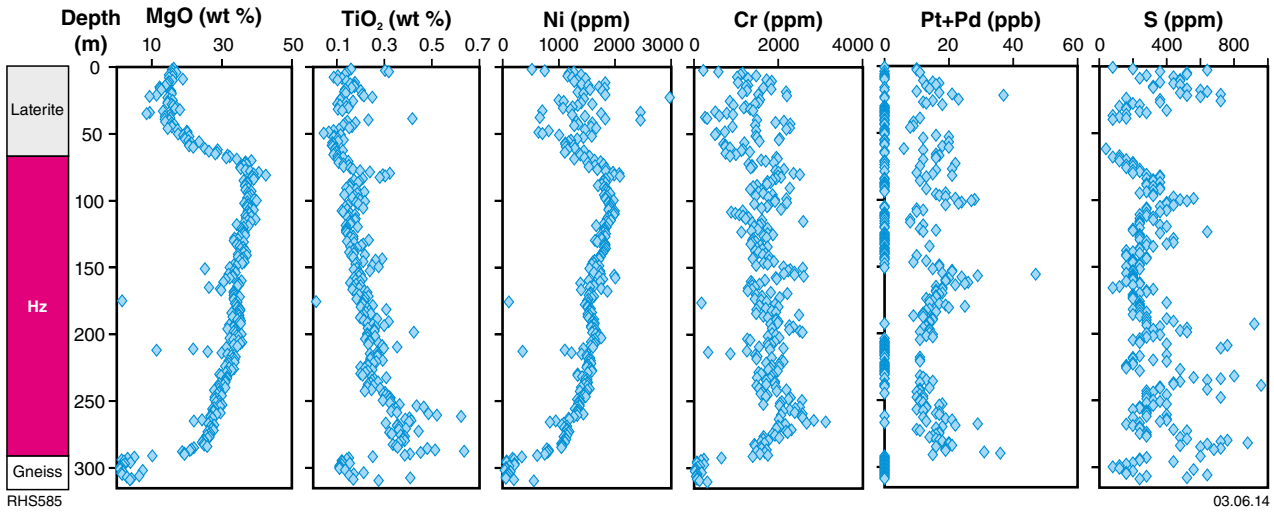

Figure 11. Drillcore WPRC0-023, intersecting contact between Wingellina Hills intrusion (in purple, Hz = harzburgite) and country rock gneiss. Note progressive increase with height in MgO and Ni, but decrease in TiO_2 and Cr, possibly reflecting decreasing trapped liquid component. Figure 10 shows drillcore location.

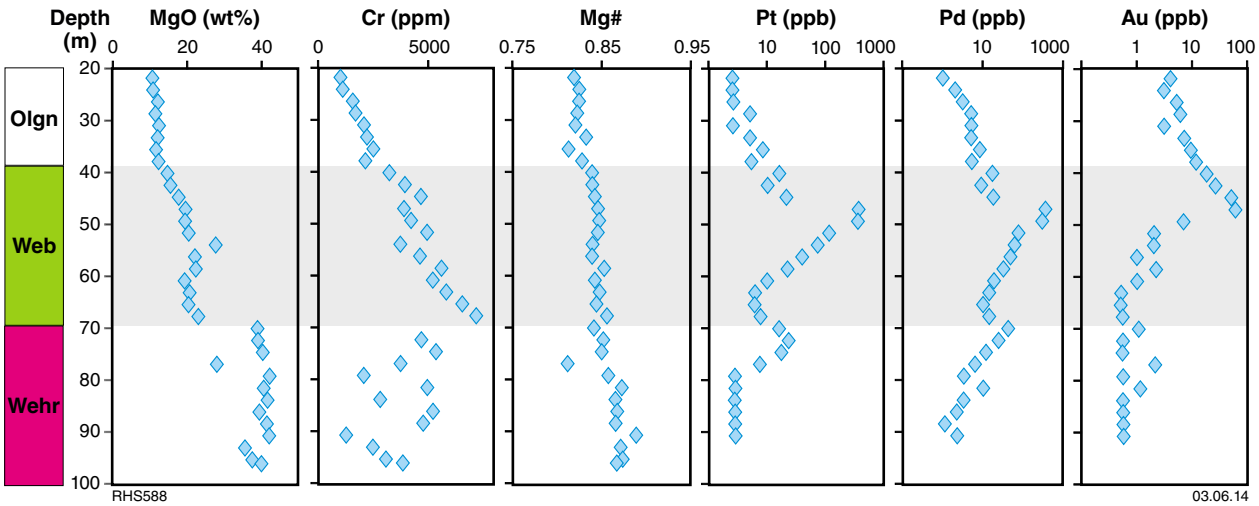

Figure 12. Log of diamond drillcore WPRCD0-083, Wingellina Hills intrusion (Olgn = olivine gabbronorite; Web = websterite, Wehr = wehrlite)

pronounced along shear zones. The lateritic material is locally cut by semiprecious, pale green chrysoprase. The lateritic ore is exposed at the surface, with an average thickness of 80 m and a maximum of 200 m. The deposit also has a high aspect ratio and therefore a very low strip ratio.

The Wart intrusion

This intrusion is a relatively small mafic–ultramafic body, about 20 km south of Wingellina Community. Its main preserved portion measures about 5 x 2 km (Fig. 4, Appendix 3). In addition, there are several smaller mafic slivers to the northwest of the main body. The latter strikes about 130° and dips steeply at 80–90° to the southwest. Ballhaus and Glikson (1995) suggested that it might form the lower portion of the Bell Rock intrusion. At its northeastern margin, The Wart has an intrusive contact with granulite (Ballhaus and Glikson, 1995). The stratigraphic thickness of the intrusion is about 1–2 km.

The Wart shares certain lithological and compositional features with the Pirntirri Mulari intrusion. For example, both contain layers of medium-grained mesocumulate wehrlite–peridotite within clinopyroxenite and melagabbronorite adcumulates and mesocumulates. Many ultramafic units have sharp contacts and may represent sills (Ballhaus and Glikson, 1995). Both intrusions contain microgabbro layers or sills (Ballhaus, 1993). The textures of the rocks are highly equilibrated, resulting from either high-grade metamorphism or slow cooling. We collected only a few gabbroic and ultramafic samples because access to much of the body is culturally sensitive, although more extensive mineral compositional data are reported in Ballhaus and Glikson (1995).

The rocks are relatively unevolved, showing whole-rock Mg# up to 0.88 and Cr/V ratios up to 13. The rocks show relatively high Fo content of olivine (0.86), Mg# of orthopyroxene (0.84) and clinopyroxene (0.87), and anorthite (An) content of plagioclase (87). The mineral compositions mostly overlap with those of the Pirntirri Mulari intrusion, as previously noted (Ballhaus and Glikson, 1995). However, The Wart intrusion appears to lack chromite, and plagioclase is greatly more calcic than in the Pirntirri Mulari intrusion.

Predominantly mafic intrusions

Latitude Hill – Michael Hills intrusions

The Latitude Hill intrusion is 5–10 km east of The Wart and Bell Rock intrusions (Fig. 4, Appendix 3). The body has been interpreted as a folded segment of the Michael Hills gabbro (Ballhaus and Glikson, 1995), forming one of thickest intrusions related to the Giles Event, at about 8000 m. The present work indicates that deformation is broadly synmagmatic, based on observations made on similarly deformed intrusions (e.g. West Hinckley Range) of mingling textures between gabbro and coeval deformed and undeformed granite (Howard et al., 2011b). The body has an intrusive contact with granulite analogous to, for example, the Wingellina Hills and The Wart intrusions (Ballhaus and Glikson, 1995; present work). Pascoe (2012) indicates that Latitude Hill is in faulted contact with the Bell Rock intrusion.

The intrusion contains numerous layers and lenses of olivine gabbronorite, olivine pyroxenite, and rare peridotite, although it is unclear if these all form one body or fragments of several distinct intrusions (Glikson, 1995). It also remains uncertain in which direction the layers dip. Abundant fine-grained gabbros were interpreted as intraplutonic quench zones (Ballhaus and Glikson, 1995). In terms of mineral and whole-rock compositions, the Latitude Hill and Michael Hills intrusions resemble the Hinckley Range intrusion (Ballhaus and Glikson,

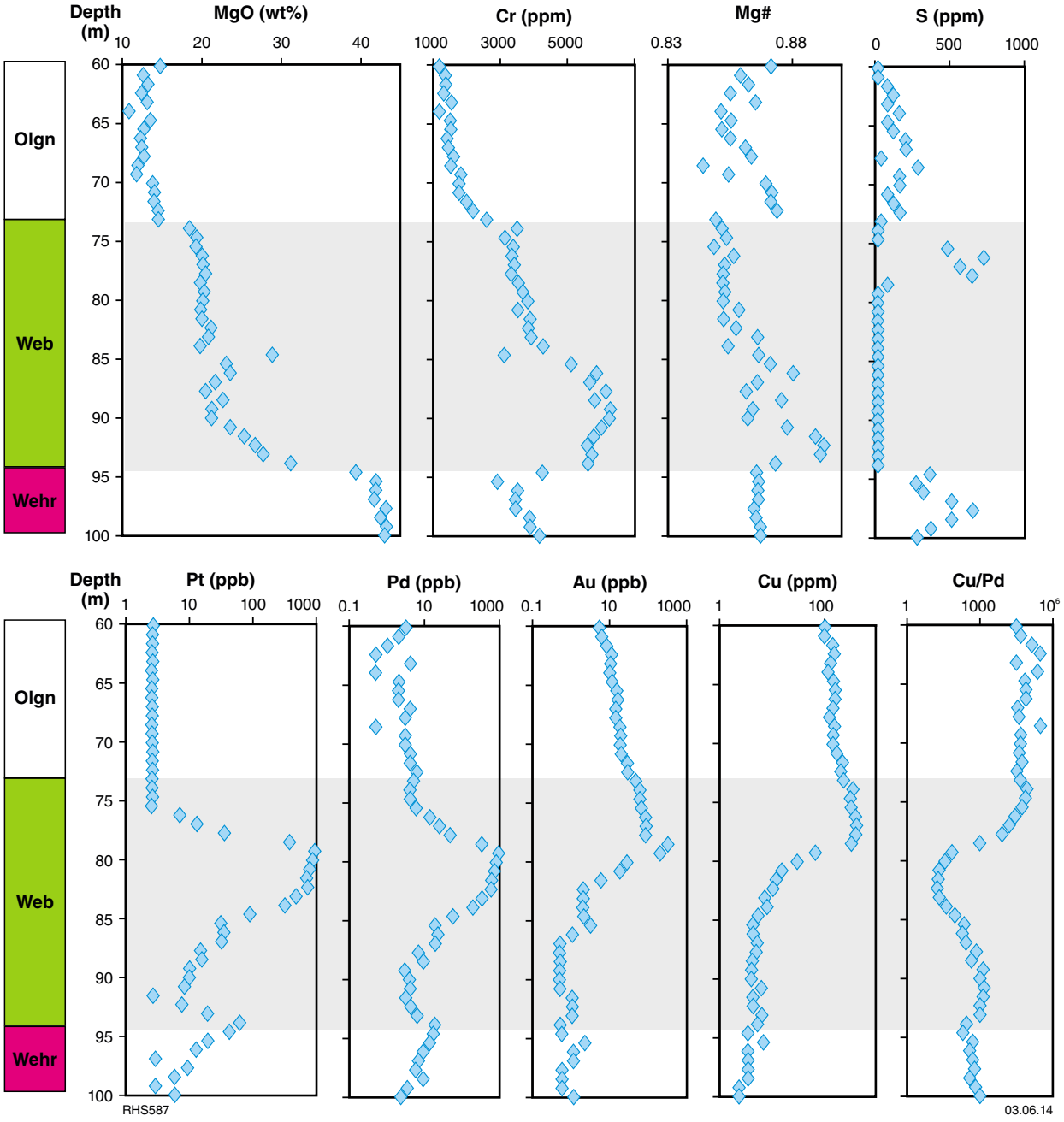

Figure 13. Log of percussion drillhole WPRC0-064, Wingellina Hills intrusion (Olgn = olivine gabbronorite; Web = websterite, Wehr = wehrlite)

1995; present data). Our samples yielded whole-rock Mg# of 0.45 – 0.7, and Cr/V ratios of 0.4 – 1.6. The Mg# of orthopyroxene is 0.7 – 0.73 (Latitude Hill), that of clinopyroxene is 0.72 – 0.74, and the An content of plagioclase is 60–65. The more extensive mineral data of Ballhaus and Glikson (1995) indicate that olivine has Fo contents of 0.7 – 0.8, orthopyroxene has Mg# of 0.6 – 0.8, and plagioclase has An contents of mostly 0.5 – 0.75.

Morgan Range intrusion

The Morgan Range intrusion lies within the Tjuni Purlka Zone, some 10 km north of Blackstone Community (Figs 4 and 5). It is an approximately 10 x 5 km (~50 km^2) body striking broadly 120°. Its stratigraphic thickness is >1 km. Most of the rocks are relatively unaltered olivine gabbronorites and troctolites that show modal layering on a scale of centimetres to metres. The intrusion forms a boat-shaped synclinal structure whose margins dip steeply (up to 80°) to the interior of the massif, whereas in the centre the dip is sub-horizontal. Most samples from the margins of the intrusion are relatively primitive (Cr/V ≤10) and contain some moderately fertile sulfide (Cu/Pd mostly <10 000). By contrast, several samples from the southern edge, defining the structural centre of the intrusion, are more differentiated (Mg# as low as 0.62, Cr/V < 1). These values suggest that the intrusion is not overturned, and that it plunges at a relatively shallow angle to the southeast. Platinum group element concentrations are mostly <10 ppb, although locally reach 40 ppb, with Cu/Pd ratios commonly below primitive mantle values.

At the northeastern tip of the body lies a small (~300 x 300 m) interlayered mafic–ultramafic lens containing dunite, troctolite, and melagabbronorite. The nature of the contact with the main Morgan Range intrusion either is concealed by regolith or highly altered, although is likely a fault. The rocks of the lens strike about 100° and dip steeply (80°) to the north. It is presently unclear whether this segment forms part of the Morgan Range intrusion, or is a fragment of a different intrusion that was tectonically attached to the Morgan Range intrusion. The mafic–ultramafic lens shows some compositional similarities to the Wingellina Hills and Pirntirri Mulari intrusions: MgO concentrations reach 37 wt%, Cr/V ratios are up to 69, PGE concentrations are up to 70 ppb, and Cu/Pd ratios are below primitive mantle values. Chromium concentrations of the rocks are lower than in the Wingellina Hills intrusion, although they are in the range of the Pirntirri Mulari intrusion.

Hinckley Range intrusion

This large (~30 x 10 km), strongly deformed, mostly poorly layered body has a stratigraphic thickness of about 5800 m, strikes about 100°, and dips steeply to the north at 70–80°. The rocks are mostly (olivine) gabbros, troctolites, and microgabbros, with some layers or lenses of anorthosite, and minor pyroxenite. The overprint of the Petermann Orogeny is evident in abundant pseudotachylite veins. In some rocks, particularly those close to bounding shear zones, garnet coronas around pyroxene suggest exhumation from reasonably deep crustal levels. We analysed about 20 samples, which returned slightly more differentiated compositions than those of the Morgan Range intrusion (whole-rock Mg# 0.55 – 0.75, Cr/V ≤ 3.65). Many of the samples have relatively high concentrations of K_2O and incompatible trace elements, indicative of assimilation of, or mixing with, a granitic component. Our most primitive samples come from the southern edge of the intrusion, consistent with the interpretation of Ballhaus and Glikson (1995) that the intrusion faces toward the northeast.

To the west, the Hinckley Range intrusion is in direct contact with the younger West Hinckley Range intrusion (MGA 472843E 7118953N). Here, well-developed mingling textures between gabbro and granite are related to the Giles Event (Howard et al., 2011b). The gabbro belongs to the voluminous, massive, unlayered variety (G2), which, wherever it is seen in contact with the layered Giles intrusions (G1), everywhere crosscuts, engulfs, and post-dates them. The G2 gabbros at this locality can locally be described as agmatite or injection migmatite. The precise relationship between the mafic and felsic rocks varies from place to place and, even at a single locality, a range of relationships might exist that reflect a multi-stage history (Fig. 15).

In some cases, gabbro forms angular blocks engulfed by granite, or brittle fractures in gabbro are infilled by granite veins. Such relationships indicate that the granite has intruded a largely solidified gabbro. In other cases, contacts between the felsic and mafic components are cuspate, indicating that the mafic component was ductile in the presence of the felsic component and that the granitic magmas intruded gabbro that was only partially solidified. Some 20 km to the northwest, at Amy Giles Hill, contacts between the same two mafic and felsic components are typically cuspate, with tear-shaped protrusions of gabbro in granite and of granite in gabbro, reflecting two coexisting liquids. A leucogranite showing well-developed comingling textures with gabbro (Howard et al., 2006a) has been dated at 1074 ± 3 Ma (GSWA 174589; Bodorkos and Wingate, 2008).

In the West Hinckley Range intrusion, locally mingled gabbro forms a kilometre-scale fold with a steep northwest-trending axial plane that has been intruded by syndeformational leucogranite. A strong ‘gneissic’ fabric has locally formed in mixed or agmatitic rocks as the axial planar fabric continued to develop, and this has been again engulfed within subsequent injections of leucogranite. A sample of undeformed leucogranite from within one of these axial planar zones, approximately 2 km south of the mingled gabbro–granite described above, yielded a crystallization date of 1075 ± 7 Ma (GSWA 174761; Kirkland et al., 2008e). Synmylonitic leucogranite has also pooled into boudin necks in a northwest-trending mylonite directly south of Charnockite Flats (~2.5 km northwest of the West Hinckley Range intrusion), and has been dated at 1075 ± 2 Ma (GSWA 185509; Kirkland et al., 2008f). These data effectively define a very narrow period of intrusion of massive G2 gabbro and multi-phase intrusion of leucogranites (1078–1074 Ma), northwest-directed folding, and northwest-trending shearing.

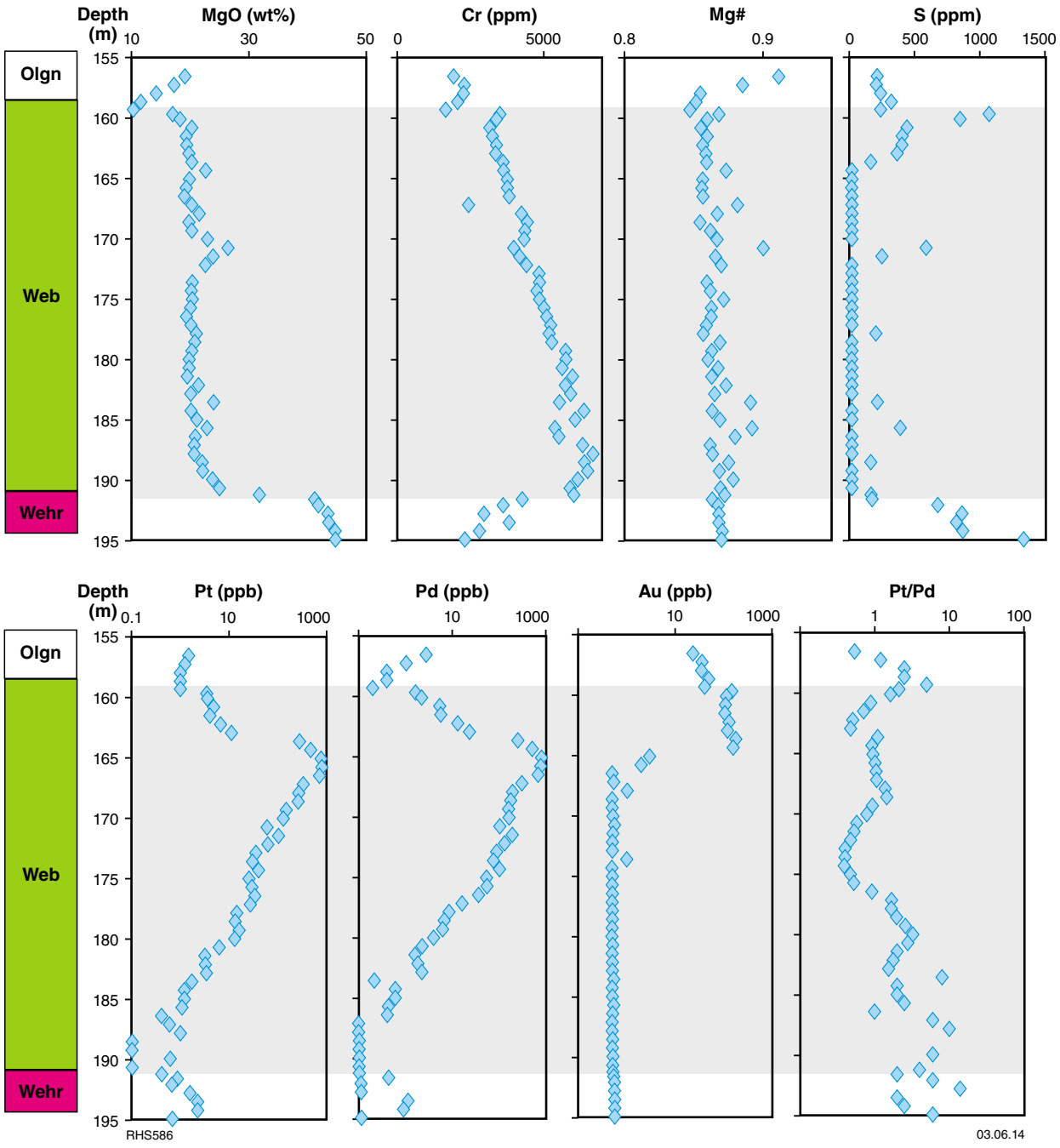

Figure 14. Log of percussion drillhole WPRC0-043, Wingellina Hills intrusion (Olgn = olivine gabbronorite; Web = websterite, Wehr = wehrlite)

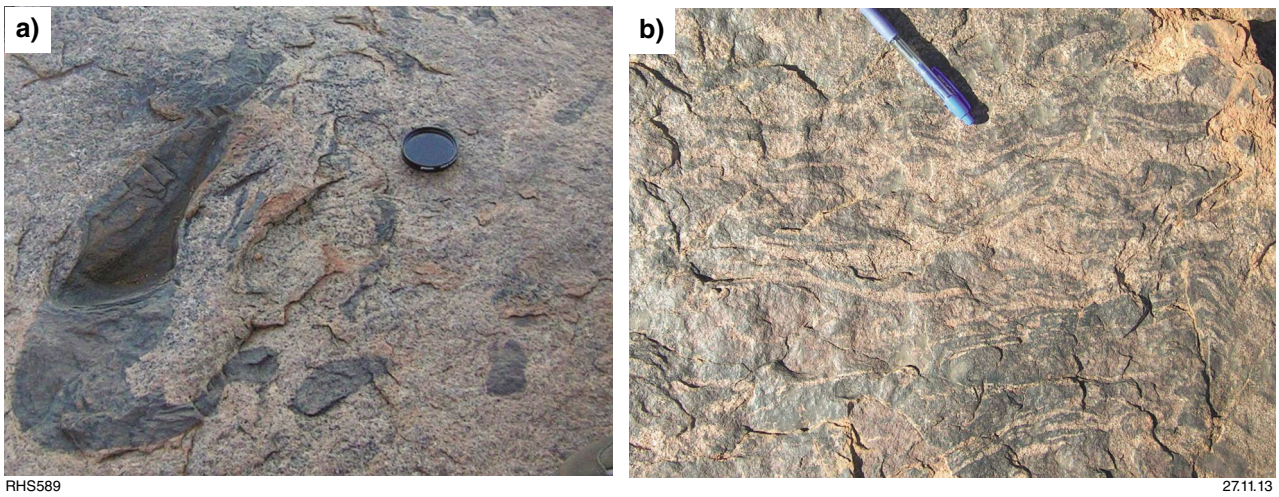

Figure 15. a,b) Examples of mingling textures between G2 gabbro and granite in the West Hinckley Range

The relationships between gabbro and granite in the Hinckley Range intrusion confirm earlier suggestions by Clarke et al. (1995b) that substantial deformation occurred during the Giles Event.

Murray Range intrusion

This is a large gabbroic body comprising a layered portion of >25 km^2 and extensive segments of massive gabbro, to the east and northeast of the Pirntirri Mulari intrusion (Figs 4 and 5). The strike of the commonly prominent, centimetre- to tens of centimetre-scale layering is mostly 50–70°, and the layers dip subvertically to the northwest or southeast. The body underwent significant tectonic dismemberment due to its location at the tectonic contact between the Tjuni Purlka and Walpa Pulka Zones. As a result, the true stratigraphic thickness and structure of the intrusion remain uncertain. The Murray Range intrusion is also one of the G1 bodies that (like the Hinckley Range intrusion) was pervasively intruded by G2 gabbro at its margins, consistent with the idea that at the stage of G2 emplacement, the contact between the Tjuni Purlka and Walpa Pulka Zones was a synmagmatic shear zone (Evins et al., 2010a,b). The intrusion also contains abundant stratiform microgabbro layers and lenses (Fig. 16a), and medium-grained gabbronorites that are commonly cross-bedded (Fig. 16b).

Most of the G1 rocks examined here are gabbronorites or olivine gabbronorites, with 10–20% olivine, 50–70% plagioclase, and orthopyroxene and clinopyroxene in roughly even proportions. Biotite and Fe–Ti oxides are trace phases, as is sulfide, which was observed in just one sample. Deformation and alteration are commonly slightly more pronounced than in the other intrusions. The textures are highly equilibrated, with clinopyroxene showing abundant exsolution of orthopyroxene and spinel.

The most primitive rocks occur in a zone within the centre of the intrusion. Here, the rocks have whole-rock Mg# ≤ 0.81, Cr/V ≤ 12, and Fo contents of olivine of up to 82, in the range of undifferentiated samples of the Morgan Range intrusion. Elsewhere, the rocks are more evolved, with Mg# as low as 0.45 and Cr/V < 0.5. Platinum group element concentrations in seven analysed samples were mostly low (≤ 15 ppb in the most differentiated samples) and at >10 000, Cu/Pd ratios are higher than primitive mantle, indicating that the magma had equilibrated with sulfide before final emplacement.

Cavenagh intrusion

Because access to much of the Cavenagh intrusion is restricted for cultural reasons, this body has remained one of the least studied among the Giles intrusions. Glikson (1995) and Aitken et al. (2013) interpreted the intrusion as a shallow-dipping segment of a large lopolith also including the Bell Rock and Blackstone intrusions.

The Cavenagh intrusion is south of the Blackstone intrusion (Fig. 4, Appendix 4). It is defined by several circular remnant magnetic highs over an area of approximately 22 x 18 km and can be subdivided into two main portions. The southern portion, around Mt Morphett, forms a syncline measuring about 15 km along a strike of about 100°, with a width of about 7 km, and a stratigraphic thickness of about 1 km. The rocks here are predominantly olivine gabbronorites, olivine gabbros, troctolites, and norites. Pyroxenites (mainly websterites), anorthosites, and microgabbros form bands and discontinuous pods, schlieren, and autoliths (Fig. 17d–f). Rare xenoliths of basement gneiss attest to some degree of country rock assimilation. A major east-trending fault separates the Mt Morphett segment from the northern portion of the Cavenagh intrusion. The latter measures about 10 x 20 km

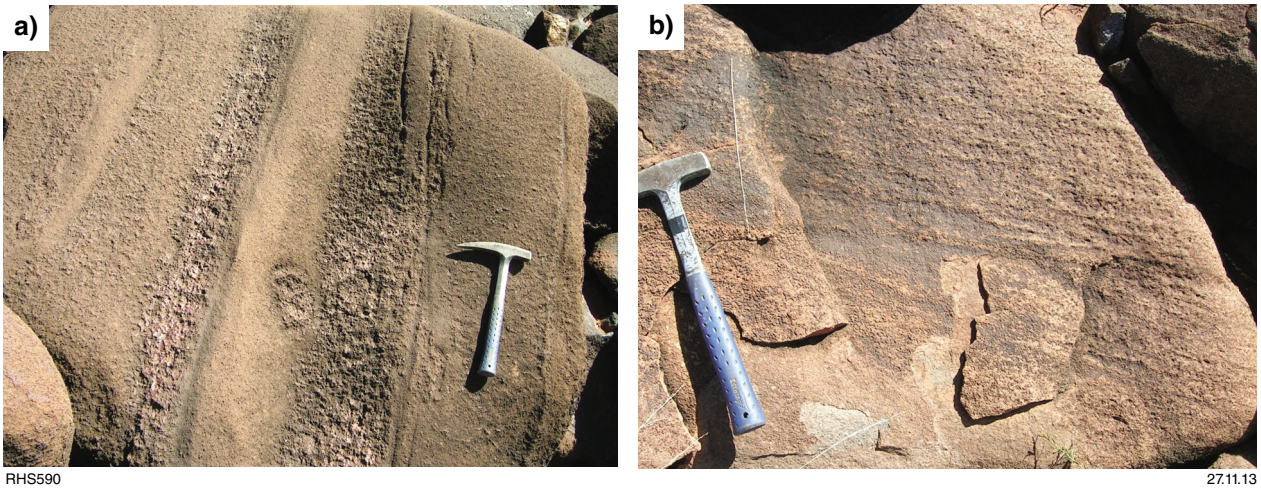

Figure 16. Structures in rocks of the Murray Range intrusion: a) interlayering between medium- to coarse-grained G1 gabbronorite and fine- to medium-grained G2 (micro)gabbronorite; both phases occur as layers, lenses, and fragments, suggesting broadly coeval emplacement (near GSWA 189304); b) cross-bedding in gabbronorite near margin of intrusion (near GSWA 189322)

on the surface, strikes at 100°, and dips at about 15–30° to the northeast. The stratigraphic thickness of this segment is about 2–4 km (assuming no structural duplication). It consists mostly of relatively homogenous olivine gabbronorite, troctolite, and magnetite-bearing olivine gabbronorite, although gabbronorites and microgabbros are also present.

Layering in the Cavenagh intrusion is expressed mainly by modal variation between olivine, pyroxene, and plagioclase. Boundaries between layers are gradational or, in the case of pyroxenites, anorthosites, and many microgabbros, sharp. Pyroxenites and anorthosites tend to form lenses, schlieren, and fragments within gabbronorite and troctolite. Pyroxenes are commonly aligned subparallel to the layering, imposing a distinct foliation to the rocks.

In terms of geochemistry, the southern to central portion of the Cavenagh intrusion is the most primitive, showing the highest Mg# (0.78), Cr/V (12), and Fo content in olivine (75). However, PGE concentrations are mostly low (Staubmann, 2010; present data). In the northern portion of the intrusion there is a subtle trend towards more differentiated compositions with height, expressed, for example, by decreasing Cr/V ratio and olivine Fo content to the northeast. By contrast, PGE concentrations tend to increase toward the stratigraphic top, with two samples containing 80–100 ppb PGE and Cu/Pd ratios about 1000, markedly lower than primitive mantle. Samples GSWA 189632, 189643, 189645, and 189649 contain trace sulfides.

The nature and origin of the microgabbros in the Cavenagh intrusion and in other Giles intrusions are not completely understood. The microgabbros are conspicuously interlayered with medium-grained gabbronorite (Fig. 17d), with sharp or gradational contacts. In places, microgabbro has been injected by medium-grained gabbro (Fig. 17c), although elsewhere the microgabbros may contain autoliths of anorthosite and thin bands, irregular clasts (Fig. 17f), and circular concretions of granular websterite and clinopyroxenite adcumulate (Fig. 17e). These field relationships indicate that the microgabbros and associated medium-grained mafic–ultramafic rocks intruded broadly contemporaneously. In most cases, the textures of the rocks are equigranular and show 120° grain boundaries (Fig. 18a,b). However, olivine and pyroxene grains may form strings, oriented in a radial configuration in places, that are interpreted to have resulted from crystal growth in a flowing, supercooled magma (Fig. 17h). Large olivine oikocrysts may form wispy crystals, surrounded by thin rims of anorthosite (Fig. 17g). Microscopic examination reveals that the olivine oikocrysts contain numerous rounded inclusions of plagioclase (for example, in sample GSWA 155649, Fig. 18c), interpreted as early formed crystals. The plagioclase coronas may have formed when rapid crystallization (e.g. due to supercooling or degassing) led to depletion in the olivine component in a boundary layer around the growing crystals. Some microgabbros contain clinopyroxene oikocrysts hosting abundant rounded and wispy exsolved oxide grains, which are absent in the matrix rock.

The microgabbros have highly variable compositions. Some samples have among the most evolved clinopyroxene compositions in the Cavenagh intrusion, although the composition of other samples broadly overlaps with their medium-grained host rocks. Most samples clearly contain a cumulus component, indicated by, for example, high whole-rock chromium concentrations (up to 1900 ppm Cr), positive strontium anomalies on multi-element variation plots, and extremely low incompatible trace element concentrations (commonly <5 ppm Zr).


a)
b)
c)
d)
e)
10 cm
GSWA
f)
g)
5 cm
h)
RHS591
27.06.14

Figure 17. (facing) Structures in rocks of the Cavenagh Range: a) modal layering in olivine gabbronorite; weathering highlights layers enriched in pyroxene (dark) and plagioclase at Mount Morphett (MGA 399231E 7096712N); b) inclusion of troctolite in gabbronorite (Mount Morphett, sampling locality GSWA 155614); note pitted texture in troctolite, resulting from weathering of olivine; note rounded contact between rocks, suggesting broadly coeval intrusion; c) mingling between fine-grained troctolite and medium-grained gabbronorite (Mount Morphett, sampling locality GSWA 155611); d) lens of microgabbro in olivine gabbronorite; lens is approximately 2 m wide and pinches out at edge, at Mount Morphett (MGA 399355E 7096103N); e) rounded fragments of websterite within gabbronorite at Mount Morphett (MGA 400491E 7094432N); f) irregular fragment of websterite in microgabbro at base of northern Cavenagh segment (MGA 396592E 7100818N); g) wispy olivine oikocrysts in microgabbroic matrix at base of northern Cavenagh segment (MGA 394111E 7103629N); h) oikocrystic microgabbro showing flow textures (sample locality GSWA 155325, northern Cavenagh segment)

Microgabbros in the Wingellina Hills intrusion and other Giles intrusions were previously explained by intraplutonic quenching (Ballhaus and Glikson, 1989). A similar model was applied to microgabbros in the Kap Edvard Holm intrusion of Greenland (Tegner et al., 1993), which shows many textural analogies with the Giles intrusions. For example, Tegner et al. (1993) described interfingering of microgabbro with medium-grained gabbro, skeletal and oikocrystic olivine and clinopyroxene, and reversed and patchy zoning of plagioclase. The coprecipitation of plagioclase with olivine and clinopyroxene was interpreted to result from the overwhelming of nucleation barriers during supercooling, and the equigranular textures by synmagmatic annealing. To explain the absence of skeletal textures in plagioclase, we considered the model of Kouchi et al. (1986) who argued that nucleation rates increase in shear flow.

At Kap Edvard Holm, the model of a comagmatic lineage of microgabbros and medium-grained rocks is consistent with the fact that the average composition of the microgabbroic quench zones is broadly similar to that of the coarser grained rocks (i.e. both have ~9% MgO). However, a major difference between the Kap Edvard Holm and the Cavenagh microgabbros is that the former are flows on top of the cumulate pile, whereas the latter appear to form sills. Other examples of microgabbros with a similar origin may include those in the Klokken (Parsons and Becker, 1987), Insch (Wadsworth, 1988), and Hettasch intrusions (Snowflake troctolite; Berg, 1980). The relative scarcity of intraplutonic quench zones in many other layered intrusions (for example the Bushveld Complex) may be because the replenishing magmas are more differentiated and thus cooler than the resident magma. Quench-textured rocks are only expected in magma chambers that were replenished by magma of unevolved and, likely, uncontaminated composition.

The association of microgabbro with fragments and schlieren of pyroxenite suggests that the emplacement of the microgabbro was associated with, and possibly led to, slumping of semiconsolidated cumulates in the chamber, resulting in sorting of crystals to form pyroxenite and anorthosite (cf. Maier et al., 2013b). The combined observations from the Cavenagh intrusion thus indicate a dynamic, semiconsolidated magma chamber that was frequently replenished by unevolved magma.

Lehmann Hills, Mt Muir, and other small intrusions north of the Blackstone and Wingellina Communities

The Lehman Hills intrusion forms several low hills scattered over about 2 km^2, some 40 km north of Blackstone Community (Fig. 4). The rocks consist mostly of medium-grained olivine gabbronorites, although in places we observed interlayered pyroxenite and anorthosite (Fig. 19a). These rocks may show a distinct flow structure, containing elongated and aligned lenses and schlieren of anorthosite in pyroxenite, and fragments and clots of pyroxenite within anorthosite. The gabbroic rocks contain 60–85% plagioclase, 7–25% clinopyroxene, 5–10% orthopyroxene, 3–5% olivine, and accessory magnetite, biotite, and serpentine. Plagioclase forms euhedral, grey, cloudy phenocrysts, and less commonly, fine-grained rims on olivine. Pyroxene typically shows strong lamellar twinning and orthopyroxene forms rare oikocrysts, and more commonly, rims on clinopyroxene. Trace sulfides (pyrrhotite and chalcopyrite) are relatively abundant, constituting up to about 1% of the rock. The degree of deformation is moderate, largely confined to incipient subgrain formation. The composition of the rocks shows some overlap with the Morgan Range, Murray Range, and Cavenagh intrusions, with Mg# ≤ 0.78, Cr/V ≤ 8, and olivine Fo content up to 73.

The Mt Muir intrusion is a small (3 x 1 km) mafic body, or an isolated tectonic fragment of a larger body, about 15 km northwest of the Lehman Hills (Fig. 4). The rocks are well-layered olivine gabbronorites and troctolites. Layering is spaced at about 1–3 cm, strikes at about 100°, and dips steeply (80–90°) to the north. The body appears slightly more differentiated than the Lehmann Hills intrusion, with Mg# of 0.74 and Cr/V ratios of 1.5.

Several additional small mafic bodies have been mapped and sampled up to 10 km north of Mt Muir (termed 'North' in Table 1). The rocks are mostly gabbronorites and less commonly, olivine gabbronorites. They contain approximately 75% pink cloudy plagioclase, 5% clinopyroxene, 5–15% orthopyroxene, 5% magnetite, and accessory hornblende and chlorite. Pyroxene forms small crystals and oikocrysts of orthopyroxene–clinopyroxene symplectite. Magnetite is typically interstitial although it also commonly forms inclusions along cleavage planes within clinopyroxene crystals. The North bodies are of broadly similar composition to Mt Muir, with Mg# ≤ 0.73 and Cr/V ≤ 3.

We also sampled several small mafic bodies up to 20 km to the north of the Hinckley Range intrusion, in the

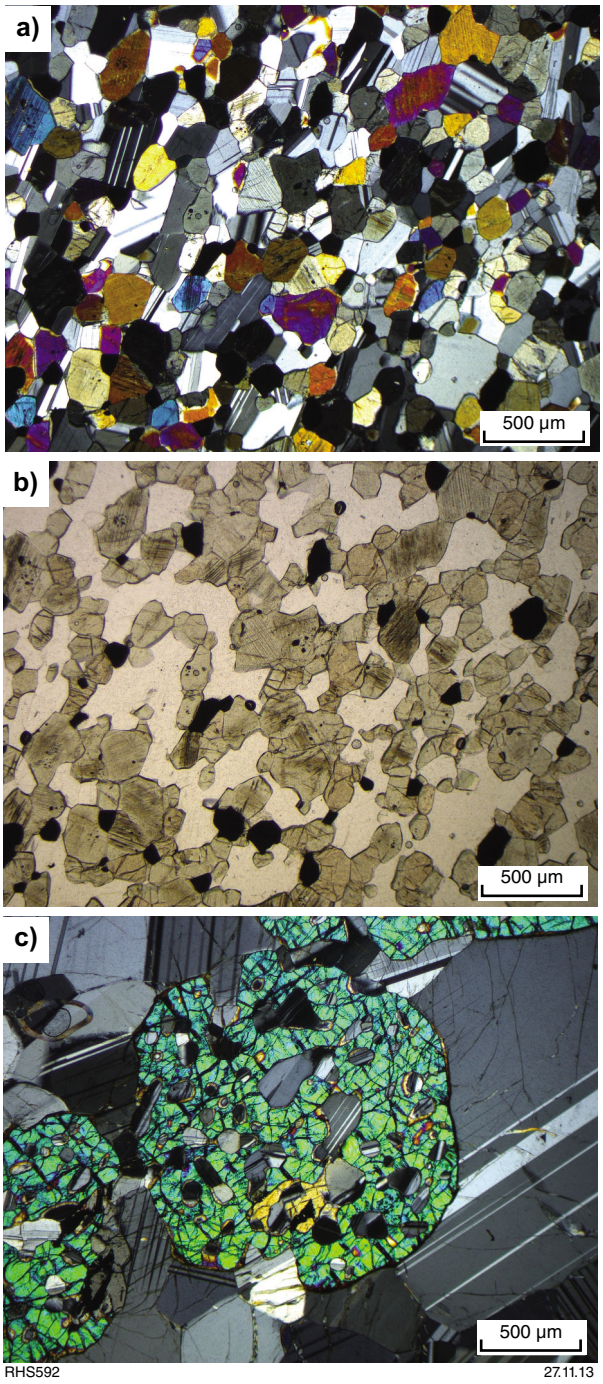

Figure 18. Photomicrographs of microgabbro from Cavenagh intrusion: a) granular textured rock, sample GSWA 185651; b) same sample shown in plane-polarized light; c) olivine oikocryst with rounded plagioclase chadacrysts (sample GSWA 155649)

Mt Gosse – Mt Daisy Bates area (termed 'Northeast' in Table 1). These mafic bodies are metagabbros and metagabbronorites. They commonly have a partial granoblastic texture, and garnet forms fine-grained rims on pyroxene and magnetite grains, or more rarely forms garnet porphyroblasts. Pyroxene is commonly replaced by hornblende, and biotite is also common. Magnetite is interstitial. The rocks contain 50–60% cloudy, euhedral (where primary texture is preserved) feldspar. Fine-grained plagioclase also forms rims on orthopyroxene. Where orthopyroxene is present, it exists in similar proportions (~20%) to clinopyroxene. Most of these Northeast bodies are relatively evolved, with Mg# < 0.7 and Cr/V ≤ 1. They are PGE poor (<10 ppb Pt+Pd), although have markedly elevated Au concentrations compared with most other Giles intrusions, overlapping with the Alcurra Dolerite suite, as discussed below.

Jameson–Finlayson intrusion

The combined Jameson–Finlayson intrusion extends for 66 km along a strike of about 120° and is about 30 km wide (Fig. 4, Appendix 5). Layering is not overturned and dips at about 20° to 30° to the southwest, indicating a stratigraphic thickness of up to about 10 km. Several layer-parallel mylonitic zones near the base of the intrusion allow for a small degree of structural repetition, although this is unlikely to greatly affect the overall thickness estimates. The bottom and top contacts are not exposed.

Daniels (1974) recognized four zones within the intrusion, with a total maximum outcrop width of 19 km and a maximum thickness (with an assumed average dip of 30°) of 11 km. His basal Zone 1, in the northeast of the intrusion, is described as glomeroporphyritic gabbro. Similar gabbro is associated with basalt in the lower stratigraphy of the Bentley Supergroup and it is possible that the gabbros identified by Daniels (1974) belong to that dominantly volcanic package (Mummawarrawarra Basalt of the Kunmarnara Group). Zone 2 comprises well-banded lherzolite and magnetite–ilmenite-bearing lherzolite; the ultramafic layers contain 20–50 vol.% opaques, with the V_2O_5 tenor of the magnetite estimated at about 1.4 wt%. Zone 3 is characterized by rhythmically layered troctolite and olivine gabbronorite (Fig. 19b,d–f). Zone 4, in the southwest, forms a layered succession of troctolite, olivine gabbro, and olivine gabbronorite, with at least 11 major titaniferous magnetite bands (Figs 19c, 20). The thickness and contact relationships of most seams remain uncertain, due to poor outcrop.

Our samples cover the bulk of the intrusion (Appendix 5). The troctolites contain approximately 70–85% plagioclase, 10–20% olivine, 5% orthopyroxene, and accessory clinopyroxene, biotite, and interstitial magnetite. Olivine and magnetite are concentrated into schlieren of a few millimetres in length and oriented subparallel to the plagioclase lineation. The gabbronorites contain approximately 80% plagioclase, 15% pyroxene, 2% subhedral olivine, 2% magnetite, and accessory biotite. Orthopyroxene forms rims on, or commonly replaces, olivine, and clinopyroxene forms oikocrysts. Some small outcrops of gabbro to the northeast of the Jameson Range

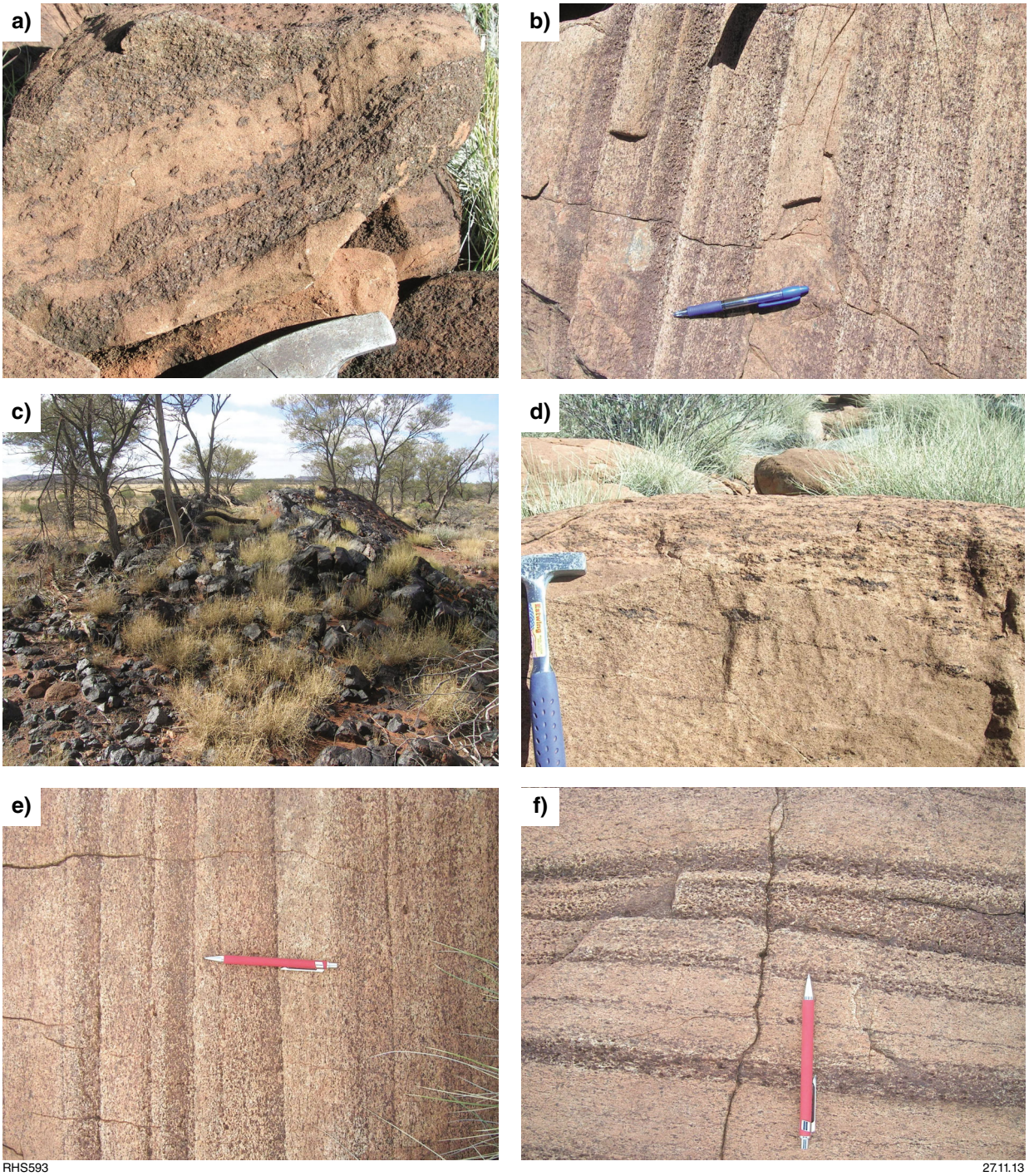

Figure 19. Field photographs of samples from the Lehman Hills and Jameson intrusions: a) banded horizon containing schlieren, lenses and fragments of fine-grained gabbronorite, and medium- to coarse-grained pyroxenite (Lehman Hills, near GSWA 189310); b) layered gabbronorite showing size grading and modal grading toward the left of frame, at Jameson Range (MGA 363619E 7494405N); c) basal magnetite layer, Jameson Range; note shallow dip of layer to the right (locality GSWA 194642); d) contact between medium- and coarse-grained gabbronorite, Jameson Range (MGA 363619E 7494405N); fine-grained rock locally crosscuts coarse-grained phase and contains inclusions and schlieren of the latter; e,f) modally graded layering in olivine gabbronorite at Jameson Range (MGA 363526E 749428N)

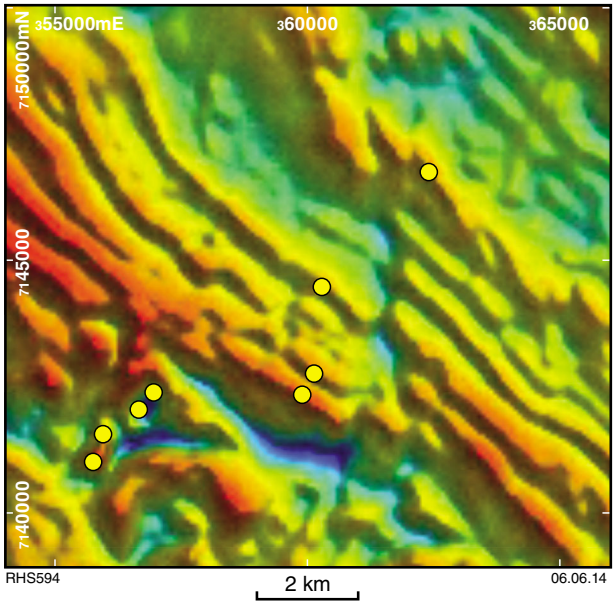

Figure 20. Aeromagnetic total magnetic intensity (TMI) image of the area to the northwest of Jameson, showing interpreted trend of magnetite layers (aeromagnetic highs) within the Jameson intrusion. Yellow circles are GSWA sample sites.

contain abundant hornblende and biotite (≤10% and 5%, respectively). This gabbro has a glomeroporphyritic texture and clinopyroxene oikocrysts enclose plagioclase. The olivine gabbronorites contain approximately 80% plagioclase, 10% pyroxene, 10% subhedral olivine, and accessory (interstitial) magnetite, biotite, and hornblende. Clinopyroxene forms oikocrysts, while orthopyroxene forms rims on olivine. Olivine gabbros contain up to 60% subhedral plagioclase, 15–20% euhedral olivine, up to 10% magnetite oikocrysts, 10% clinopyroxene (rare oikocrysts), and <5% orthopyroxene.

The olivine gabbro and olivine gabbronorite in the upper part of the intrusion contain relatively abundant sulfides, in places >1 vol.%. These form the only commonly sulfide-bearing units within the layered mafic–ultramafic G1 Giles intrusions in Western Australia, and some have Cu concentrations up to 860 ppm (at 0.12 wt% SO_3). This is likely related to the magma's reaching sulfur saturation in response to protracted fractionation, analogous to, for example, the troctolitic Kiglapait intrusion in Labrador, where sulfur saturation is reached after 93% fractionation (Morse, 1981). Alternatively, the upper stratigraphic portions of the Jameson intrusion could have undergone incipient hydrothermal alteration and Cu–S addition, perhaps because of the voluminous volcanic activity that formed the Mount Palgrave Group, directly to the southwest. However, sulfur isotopic data for both of two troctolitic samples (GSWA 189475 and 189478) indicate $\delta^{34}S$ of +2.1 and +2.8, respectively, are broadly consistent with a magmatic origin. By contrast, rhyolites of the Mount Palgrave Group have a much wider sulfur isotopic range of $\delta^{34}S$, from +3.2 to +7.

We were able to sample several of the major magnetite seams. The seams appear separated by silicate intervals several hundreds of metres thick (Fig. 20). The major and trace element chemistry of the analysed magnetite layers is given in Table 2. All layers sampled are of massive iron oxide, containing <5% silicates, and have relatively coarse grain sizes (≤3 mm). These features possibly reflect sintering (Reynolds, 1985). The mineralogy of the seams is magnetite, granular ilmenite, fine ilmenite lamellae, abundant hematite replacement patches and lamellae (≤20 vol.%), and goethite. No layers markedly enriched in apatite were encountered, although this may reflect poor outcrop.

The most reliable observations and interpretations can be made on the basal magnetite seam. It dips about 20–30° to the southwest and strikes 100°. It has been traced along strike for about 19 km as an aeromagnetic anomaly with sporadic broken outcrop (Fig. 19c). It may reach a thickness of 50 m, and up to three subseams are developed locally. It is unclear whether this observed structure is due to primary magmatic processes or structural duplication. The contacts of the layer with its silicate host rocks are sharp. The immediate footwall and hangingwall consist of magnetite-bearing leucotroctolite and anorthosite, showing evidence of deformation. The broader footwall succession resembles pronounced interlayering between magnetite–gabbronorite and anorthosite. The mineralogy of the basal seam consists of magnetite and granular ilmenite, with relatively few ilmenite lamellae, although there is locally abundant hematite and goethite replacement (Fig. 21).

In the present study, we analysed three samples of the basal magnetite layer. Traka Resources Ltd sampled the layer along strike (39 samples in total) and along three traverses across the layer. Peak PGE concentrations are 2 ppm Pt+Pd+Au (Fig. 22), markedly higher than in the Bushveld Main Magnetite Layer (Fig. 23), although lower than in magnetite layers from, for example, the Stella intrusion in South Africa (Maier et al., 2003b). The metal concentration patterns show strong depletion in IPGE (Os–Ir–Ru) relative to PPGE (Rh–Pt–Pd), characteristic of evolved magmatic rocks (Fig. 23). The layer has relatively constant vanadium concentrations (up to 7400 ppm V, 1.35 wt% V_2O_5; Fig. 22), although PGE concentrations tend to be markedly enriched at the base. Sulfur concentrations are mostly 100–150 ppm, locally reaching 700 ppm. Sulfur concentrations do not correlate with either Cu or PGE (Fig. 22), suggesting some sulfur loss, possibly in response to equilibration of sulfide with magnetite (Naldrett and Lehmann, 1988), or in response to low-grade metamorphism. There is no correlation between concentrations of PPGE and IPGE, or between those of IPGE and vanadium or chromium; however, the average Pd/Ir ratio is 34, consistent with a magmatic origin of the PGE mineralization. The ratio Pt/Pd > 1, analogous to other examples of PGE mineralization in magnetites or magnetite gabbros (see Maier, 2005 and references therein). Phosphorous concentrations are mostly up to about 100 ppm, and iron concentrations reach 55 wt%.

Table 2. Compositional data for massive magnetite seams

Sample no.		*194652*	*194651*	*194648*	*194647*	*194646*	*194645*	*194653*	*194643*	*194642*	*194679*	*KPT-1*
Intrusion		Jameson	Jameson	Jameson	Jameson	Jameson	Jameson	Jameson	Jameson	Jameson	Blackstone	Standard
Layer		11	10	9	8	5	4	1	1	1	–	–
Easting		356003	356141	356665	356743	360042	360357	362197	360390	360390	435248	–
Northing		7140988	7141257	7141908	7142083	7142291	7142698	7147595	7144538	7144538	7119079	–
Fe_2O_3	wt%	60.90	60.99	60.07	63.24	59.51	61.71	54.31	52.00	56.44	60.36	12.48
TiO_2	wt%	13.34	14.96	15.00	8.16	15.98	2.00	18.67	20.93	17.06	14.99	0.72
Al_2O_3	wt%	1.49	1.98	2.25	2.57	1.39	4.25	2.79	2.56	2.30	2.27	12.07
MnO	wt%	0.21	0.28	0.32	0.19	0.14	0.03	0.21	0.12	0.20	0.26	0.12
MgO	wt%	1.05	1.36	1.39	0.42	0.86	0.09	1.30	1.00	1.55	1.68	3.28
CaO	wt%	0.02	<0.01	<0.01	0.19	0.03	0.24	0.05	0.11	<0.01	<0.01	7.59
As	ppm	0.04	0.08	0.64	0.60	<0.02	0.13	0.32	<0.02	<0.02	<0.02	2.61
Ba	ppm	251	259	116	171	221	86	51	32	–5	–3	452
Ce	ppm	94	97	104	99	93	97	83	80	88	95	57
Co	ppm	122	118	114	119	74	38	133	62	145	188	82
Cr	ppm	3267	4130	4879	2442	4635	36	396	286	341	6086	153
Eu	ppm	0.05	0.02	0.38	0.33	0.03	1.07	0.06	0.04	0.03	<0.01	1
Hf	ppm	1.66	29.53	48.41	19.28	30.36	20.04	44.00	28.42	25.09	52.70	4
La	ppm	0.63	0.20	5.81	0.97	0.52	2.11	0.86	0.19	0.36	0.26	27
Lu	ppm	<0.01	0.02	0.05	0.25	<0.01	0.20	0.03	<0.01	<0.01	<0.01	0
Ni	ppm	307	221	196	181	114	119	212	108	352	894	1228
Sc	ppm	18	23	25	19	19	9	27	31	26	22	26
Sm	ppm	0.18	0.08	1.31	0.62	0.05	1.12	0.17	0.02	0.07	0.05	5
Ta	ppm	0.15	0.22	0.31	-0.01	0.39	0.21	0.77	1.04	0.70	0.46	1
Tb	ppm	<0.01	0.04	0.28	0.02	0.05	0.28	<0.01	<0.01	<0.01	<0.01	1
Yb	ppm	0.11	0.04	0.49	1.70	0.04	1.28	0.11	0.06	0.07	<0.01	3
Dy	ppm	0.66	<0.04	0.89	0.95	<0.02	1.87	<0.02	<0.08	<0.13	0.79	3
In	ppm	0.05	0.13	0.13	0.08	0.08	0.01	0.14	0.14	0.10	0.08	0
Sr	ppm	116	<6	<18	<34	<2	<23	54	<28	<20	191	285
V	ppm	3246	3299	2832	2338	3042	249	5856	5609	5054	8592	176
Cu	ppm	144	204	192	139	90	659	368	642	513	249	881
Os	ppb	0.21	0.10	<0.065	0.11	0.28	0.15	0.33	0.47	0.45	3.14	–
Ir	ppb	0.68	0.14	0.05	0.05	0.26	0.04	5.34	6.08	5.98	3.61	–
Ru	ppb	0.58	0.23	0.17	<0.12	0.64	<0.12	0.17	<0.12	<0.12	6.16	–
Rh	ppb	1.37	0.30	0.09	<0.082	0.22	<0.082	12.40	8.24	9.84	5.90	–
Pt	ppb	28	5.16	1.22	1.18	2.32	2.40	657	987	866	3.19	–
Pd	ppb	28	6.81	1.44	1.90	3.12	1.84	343	70	227	0.79	–
Au	ppb	0.54	1.29	<0.5	<0.5	1.50	1.78	56	9.88	151	1.45	–

NOTES: * All elements were determined by instrumental neutron activation analysis (INAA), except for platinum group elements, which were determined by inductively coupled plasma–mass spectrometry (ICP-MS) after Ni sulfide fire assay.
– not applicable or not determined

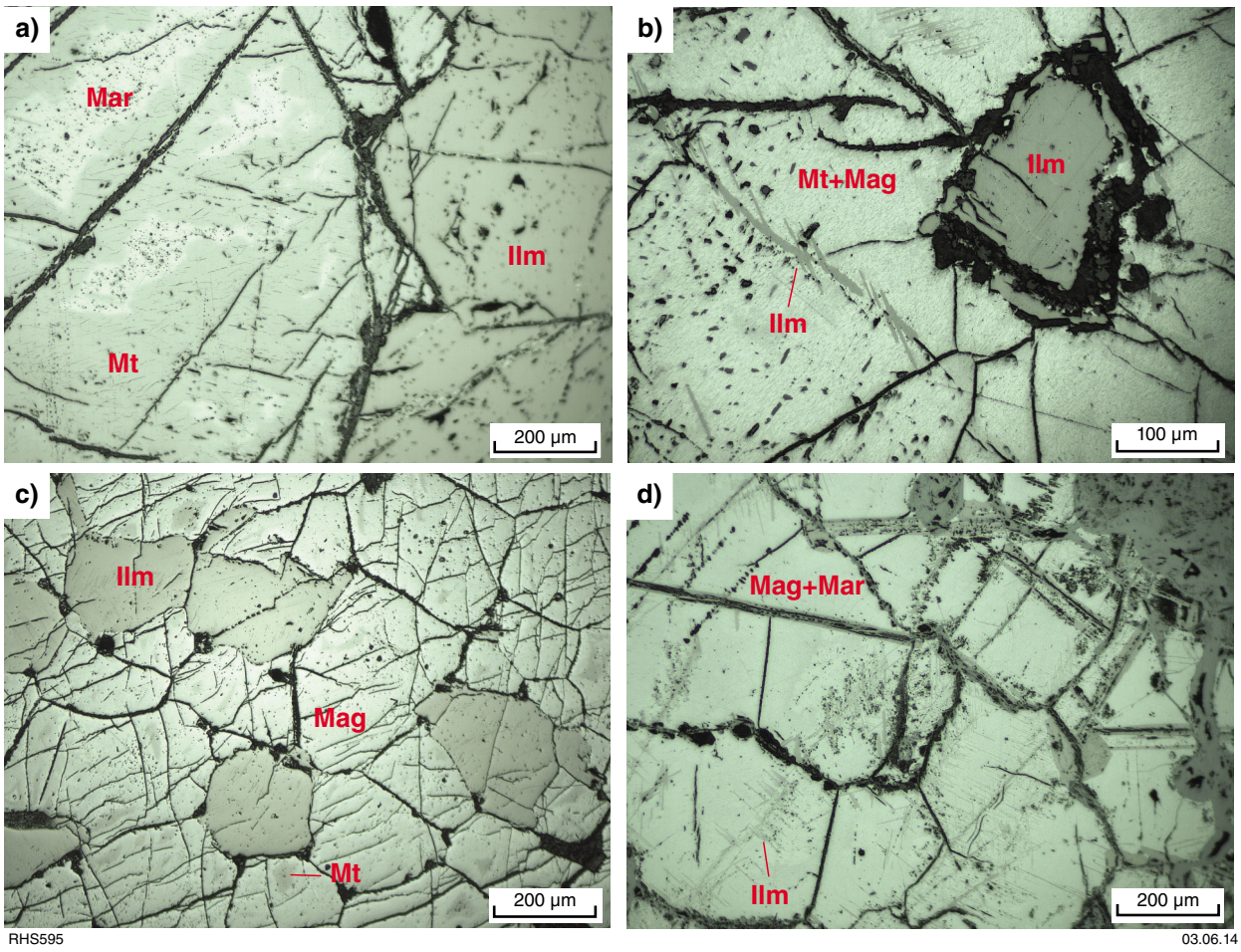

Figure 21. **Reflected-light microphotographs of Jameson Range magnetite seams: a) replacement patches of martite (pale material containing fine black specks) and maghemite within magnetite (basal magnetite layer, GSWA 194642); b) granular ilmenite and ilmenite (grey) exsolutions along fractures and cleavage planes within magnetite pervasively replaced by maghemite and martite (basal magnetite layer, GSWA 194653); c) granular ilmenite (grey) in magnetite pervasively replaced by maghemite and martite (magnetite layer 9, GSWA 194648); d) magnetite largely replaced by maghemite and martite; note fine ilmenite exsolution lamellae (grey) nucleating at fractures (magnetite layer 8, GSWA 194647).**

Magnetite layers 2 and 3 are not exposed, although their presence is suggested by prominent magnetic anomalies parallel to layer 1 (Fig. 20). Layers 4 and 5 are poorly exposed, consisting essentially of magnetite rubble. Layer 4 is pervasively replaced by goethite and hematite, although it also contains abundant granular ilmenite. In layer 5, ilmenite is predominantly granular, although it is pervasively hematized. Layers 6 and 7 are not exposed, although their presence is indicated by magnetic anomalies (Fig. 20). Layer 8 is also poorly exposed and may be a plug-like body. It contains abundant ilmenite exsolution lamellae and goethite replacement. Layer 9 is very poorly exposed, consisting essentially of magnetite rubble. The rock contains moderate amounts of ilmenite lamellae, although is pervasively replaced by hematite. Layer 10 contains abundant granular and lamellar ilmenite plus ilmenite replacement patches. Layer 11 is partly exposed and forms a massive, well-layered, possibly rotated layer. It dips about 30° to the southwest and contains some granular ilmenite in addition to numerous ilmenite lamellae. The compositional variation through the seams remains somewhat poorly defined, although it is evident that the concentrations of vanadium and chalcophile elements (PGE, Cu, Au) decrease sharply in the upper seams, whereas iron, chromium, and phosphorus concentrations increase (Table 2, Fig. 24).

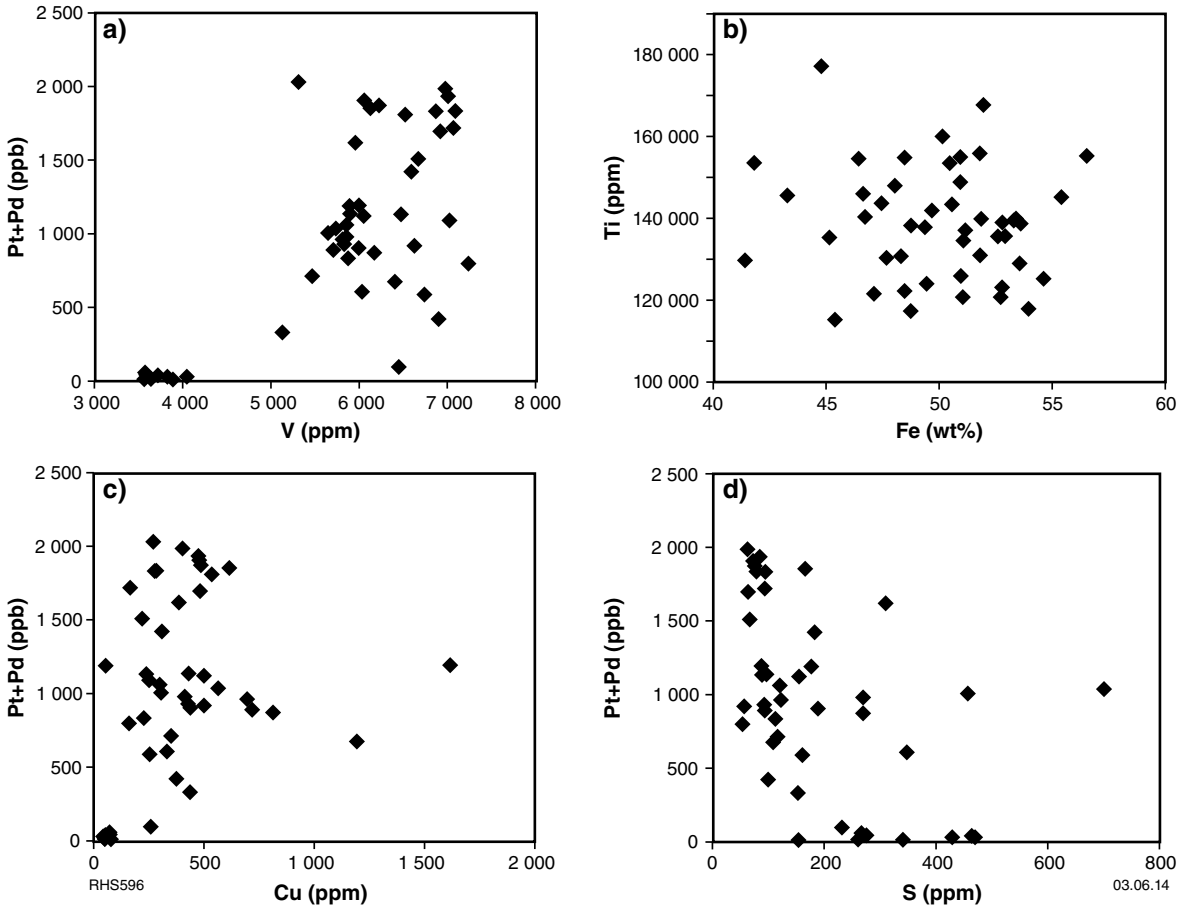

Figure 22. Composition of basal magnetite layer within the Jameson intrusion, based on 32 samples collected along strike by Traka Resources (Traka Resources Ltd, 2011, written comm., 21 October): a) Pt+Pd vs V; b) Ti vs Fe; c) Pt+Pd vs Cu; d) Pt+Pd vs S

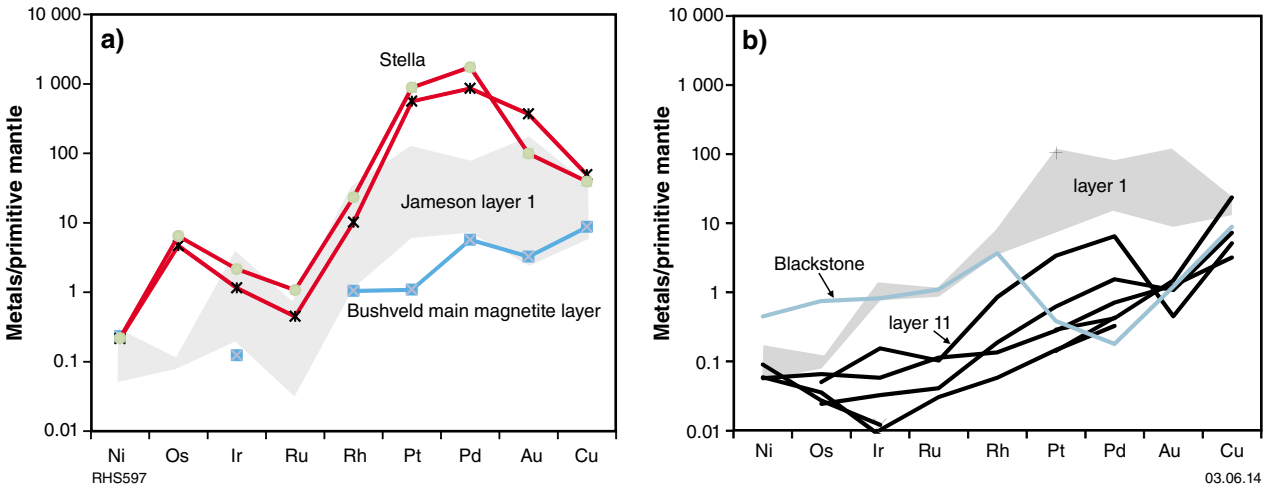

Figure 23. a) Metal patterns of the basal magnetite layer of the Jameson intrusion (shaded field), compared to basal magnetite layer in Upper Zone of Bushveld Complex (blue line) and PGE-rich magnetite layers of Stella intrusion, South Africa (red lines); (b) comparison of metal patterns in Jameson magnetite layers (black lines and shaded field) with Blackstone magnetite layer (blue line)

Table 3. Sulfur isotope data of samples from the mafic–ultramafic rocks of the Giles Event

Sample no.	*Rock type*	*Suite/Supergroup*	*Intrusion*	*Map sheet*	*Easting*	*Northing*	$\delta^{34}S$	*Standard deviation*	*Method*	*Analytical laboratory*
194635	Dacite	Bentley Supergroup	–	Mt Eveline	342816	7116524	2.1	0.1	Whole rock	NZ isotope centre
194615	Dacite	Bentley Supergroup	–	Mt Eveline	345651	7115042	1.8	0.4	Whole rock	NZ isotope centre
189598	Dacite	Bentley Supergroup	–	Mt Eveline	347144	7121042	2.4	0.3	Whole rock	NZ isotope centre
189576	Dacite	Bentley Supergroup	–	Mt Eveline	345933	7122902	3.7	0.1	Whole rock	NZ isotope centre
187074	Dacite	Bentley Supergroup	–	Mt Eveline	337457	7108507	5.3	0.4	Whole rock	NZ isotope centre
187060	Dacite	Bentley Supergroup	–	Mt Eveline	344119	7110049	3.2	0.2	Whole rock	NZ isotope centre
187056	Dacite	Bentley Supergroup	–	Mt Eveline	342204	7110741	6.8	0.4	Whole rock	NZ isotope centre
187053	Dacite	Bentley Supergroup	–	Mt Eveline	343084	7113287	6.9	0.4	Whole rock	NZ isotope centre
187078	Dacite	Bentley Supergroup	–	Mt Eveline	334880	7105348	4.7	0.1	Whole rock	NZ isotope centre
189587	Granite	Winburn Granite	–	Mt Eveline	344446	7120393	7.4	0.3	Whole rock	NZ isotope centre
194607	Granite	Winburn Granite	–	Mt Eveline	349087	7120373	3.5	0.9	Whole rock	NZ isotope centre
195127	Dacite	Bentley Supergroup	–	Bentley	341341	7137092	20.9	1	Whole rock	NZ isotope centre
185520	Rhyolite	Bentley Supergroup	–	Blackstone	436358	7113750	6.3	0.4	Whole rock	NZ isotope centre
189475	Troctolite	Giles intrusion (G1)	Jameson	Finlayson	360438	7144028	2.1	0.2	Whole rock	NZ isotope centre
189478	Troctolite	Giles intrusion (G1)	Jameson	Finlayson	359407	7141486	2.8	0	Whole rock	NZ isotope centre
187121	Gabbro	Giles intrusion (G2)	Murray Range	Holt	440546	7153023	0	0	Whole rock	NZ isotope centre
185587	Gabbro	Alcurra suite	–	Blackstone	401693	7112874	1.7	0.1	Whole rock	NZ isotope centre
174593	Gabbro	Alcurra suite	–	Bates	452221	7136057	0.8	0	Whole rock	NZ isotope centre
189495	Dolerite	Alcurra suite	–	Finlayson	363916	7129494	1.3	0	Whole rock	NZ isotope centre
183849	Mafic dyke	Kullal dyke	–	Bell Rock	486726	7116122	1.1	0	Whole rock	NZ isotope centre
Woo144	Olivine-gabbronorite	Alcurra suite	Halleys	Blackstone	–	–	–0.8	0.16 (2σ error)	In situ laser ICP-MS	GTK, Espoo
Bsc002 74-75	Peridotite	Alcurra suite	Halleys	Blackstone	–	–	–0.9	0.12 (2σ error)	In situ laser ICP-MS	GTK, Espoo

NOTES: – not applicable
ICP-MS inductively coupled plasma—mass spectrometry

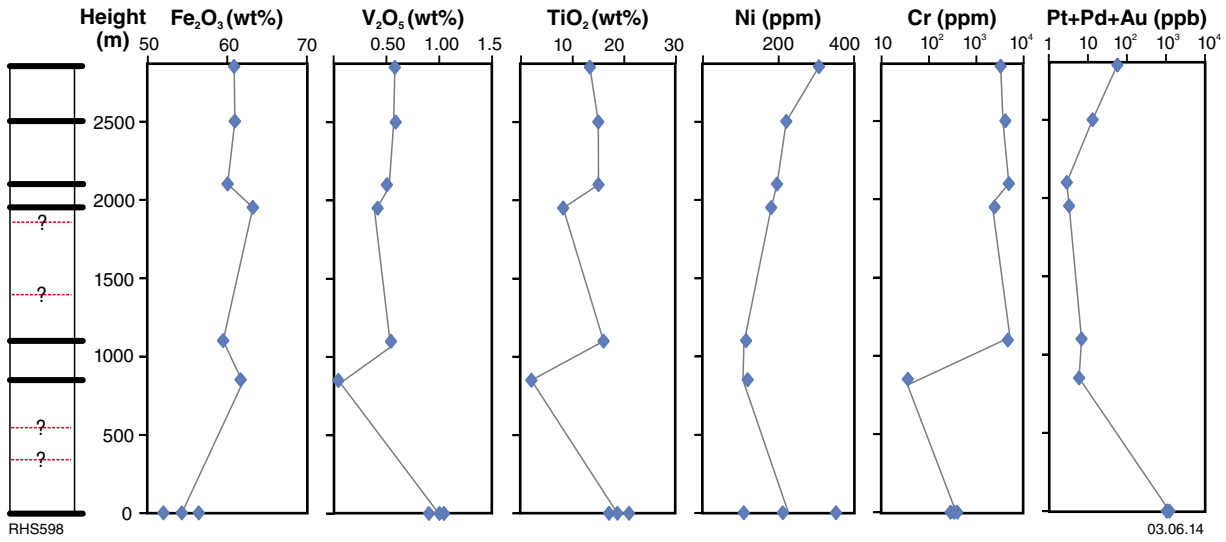

Figure 24. Composition of magnetite seams in the upper portion of the Jameson intrusion. Red lines indicate position of putative additional magnetite layers suggested by geophysical anomalies.

Bell Rock intrusion

This intrusion extends for about 50 km along a strike of about 120°. The exposed width is about 5–6 km, and the rocks dip at 70° to the southwest. Field exposures of graded layers and cross-bedding, and compositional data, discussed below, indicate younging to the southwest. We collected only 14 samples from this intrusion, partly because a detailed compositional study of the Bell Rock intrusion was previously conducted by Ballhaus and Glikson (1995), from which some of the following information is taken.

The exposed stratigraphic thickness is about 3800 m, although because most contacts are unexposed, this is a minimum estimate. The top of the intrusion is interpreted as in contact with volcanic rocks of the Bentley Supergroup; thus, either the intrusion has been deeply eroded after emplacement or the top contact is a fault. At the base of the intrusion are medium- to coarse-grained troctolites and gabbros. These rocks are overlain by magnetite-bearing troctolite in the centre and at the top of the intrusion, containing some centimetre- to tens of centimetre-thick magnetite seams, dunitic layers, numerous microgabbro sills, and a few anorthosite layers. Modal cyclicity occurs on a centimetre to metre scale. A recently completed drillhole at the western edge of the Latitude Hill intrusion (MDDH0001, drilled by Anglo American Exploration (Australia) Pty Ltd as part of the Department of Mines and Petroleum's Exploration Incentive Scheme co-funded drilling scheme), dipping 70° toward the southwest intersected highly deformed magnetite-rich troctolites interpreted to belong to the Bell Rock intrusion (Pascoe, 2012). Thus, magnetite seams might be present below cover.

Our most primitive samples are olivine gabbronorites and troctolites from the northern edge of the intrusion (Mg# ≤ 0.8, Cr/V = 7), consistent with field data indicating that the stratigraphic base of the intrusion is to the north. These rocks also tend to have the highest MgO and PGE concentrations (≤60 ppb Pt+Pd+Au). By contrast, many of the most leucocratic samples, commonly with relatively low Mg# (0.5 – 0.6) and Cr/V ratios (<1), were collected at the southern edge of the intrusion.

Ballhaus and Glikson (1995) found a broadly symmetrical compositional pattern across the body, with the marginal rocks relatively more evolved than those in the centre (Fo of 55–60 vs Fo of 67, Mg# of orthopyroxene 0.62 vs 0.71). Seubert et al. (2011) reported a slight enrichment in Cu and PGE toward the base and top of the intrusion. If the elevated metal concentrations and low Mg/Fe ratios reflect relatively high trapped liquid contents, the exposed southern and northern contact rocks may be the original marginal facies of the intrusion. The relatively unevolved composition of the centre of the intrusion could reflect inflation of the intrusion by several pulses of sulfide-undersaturated, primitive magma (Ballhaus and Glikson, 1995).

Blackstone intrusion

This intrusion forms an elongate body, about 50 km long, with a strike of about 90° and a width of up to 5 km (Appendix 6). Layering dips mostly at between 70 and 80° to the south, and is not overturned. The exposed true stratigraphic thickness of the body is about 4 km. The rocks are relatively undeformed and unaltered. Layering is locally pronounced and may be defined by thin (centimetre-scale) magnetite layers, or minor changes in modal proportions of pyroxene, olivine, and magnetite visible on weathered surfaces, and variations in grain size (Fig. 25). The rocks are mostly (olivine) gabbronorites and troctolites, each constituting approximately 50% of the total mass of the intrusion. The body is interpreted as the exposed northern limb of an upright west-trending

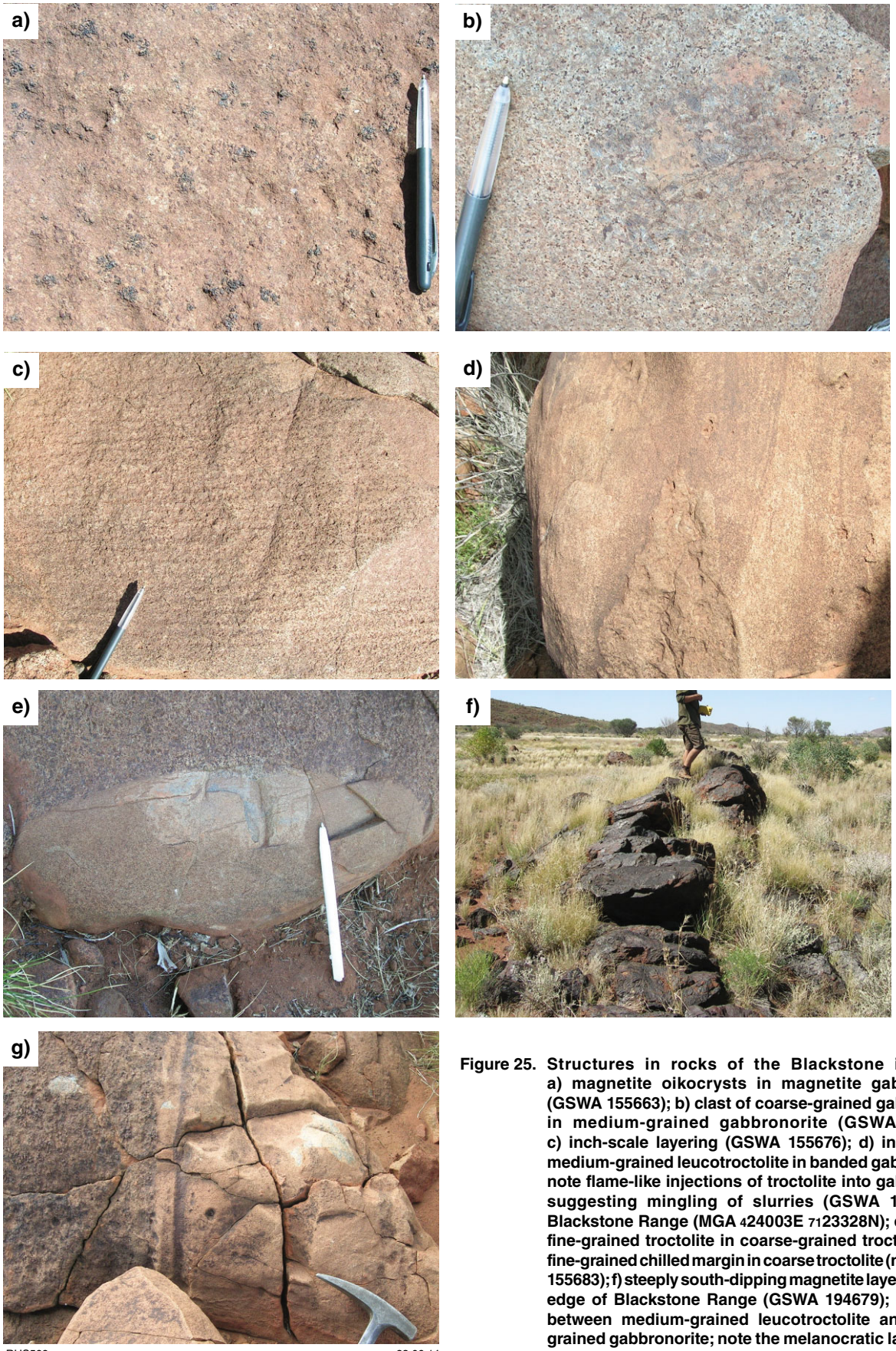

Figure 25. Structures in rocks of the Blackstone intrusion: a) magnetite oikocrysts in magnetite gabbronorite (GSWA 155663); b) clast of coarse-grained gabbronorite in medium-grained gabbronorite (GSWA 155675); c) inch-scale layering (GSWA 155676); d) inclusion of medium-grained leucotroctolite in banded gabbronorite; note flame-like injections of troctolite into gabbronorite suggesting mingling of slurries (GSWA 155655) at Blackstone Range (MGA $_{4}$24003E $_{71}$23328N); e) block of fine-grained troctolite in coarse-grained troctolite; note fine-grained chilled margin in coarse troctolite (near GSWA 155683); f) steeply south-dipping magnetite layer, southern edge of Blackstone Range (GSWA 194679); g) contact between medium-grained leucotroctolite and coarse-grained gabbronorite; note the melanocratic layer within the troctolite shows normal modal grading to the right, possibly indicating younging direction (GSWA 155313).

structural syncline (the Blackstone Syncline) with relics of the southern, northward-dipping limb sporadically exposed 20 km to the south, directly north of the Cavenagh intrusion. Thus, the body is about 1400 km^2. The intrusion is conformably overlain by felsic volcanic rocks of the Tollu Group (Bentley Supergroup) and several basal contact exposures indicate that intrusion was into the lower basaltic portions of the Kunmarnara Group (Bentley Supergroup). In terms of lithostratigraphy, the body bears strong similarities to the Bell Rock intrusion, although with an additional, more-fractionated, portion at its top.

Near the base of the succession fine- to medium-grained olivine gabbronorite is present. As this portion of the intrusion is adjacent to a fault along its northern margin, the rocks show signs of deformation, including kink bands and warped twin lamellae in plagioclase, and undulose extinction. Exsolution lamellae and blebs of clinopyroxene within orthopyroxene are common, as is exsolved magnetite within pyroxene (Fig. 26). The olivine gabbronorites are interlayered with relatively leucocratic variants of the same rock type. Approximately 250 m stratigraphically above the exposed base of the intrusion is a 150 m-thick layer of medium-grained magnetite–olivine-gabbronorite containing magnetite oikocrysts commonly 2 cm in diameter (Fig. 25a). Also present at this level is a laterally traceable fine-grained troctolite (GSWA 155655, Fig. 25d).

However, most of the troctolitic rocks in the Blackstone intrusion occupy the central and southern portions of the intrusion. These rocks contain less than 20% olivine although there are two layers of more olivine-rich troctolite (40% olivine, 100–150 m thickness) that are traceable through much of the length of the Blackstone intrusion, one in the central section of the Blackstone Range (sample GSWA 155669) and another near the southern edge of the Blackstone Range (GSWA 155681; note that this sample contains 10% pyroxene and is thus not a troctolite sensu stricto). The layers are also present in the Bell Rock intrusion where they contain up to 80% olivine, consistent with a model whereby the Blackstone and Bell Rock intrusions are the dismembered fragments of an originally contiguous intrusion (Nesbitt and Talbot, 1966; Glikson, 1995). In the upper part of the Blackstone intrusion exist discontinuous magnetite seams several millimetres thick within a coarse-grained troctolite. At the southern margin of the intrusion (MGA 435248E 7119079N) is an approximately 1 m-thick magnetite layer (Fig. 25f) that is relatively V rich (1.5% V_2O_5), although PGE poor (5 ppb Pt+Pd+Au). Copper concentrations are 250 ppm, suggesting the presence of minor sulfides, common to all magnetite-rich rocks in the upper portions of the Blackstone intrusion. It is uncertain whether this layer can be correlated to magnetite layer 1 in the Jameson–Finlayson intrusion, as the latter is PGE rich.

In compositional terms, the Blackstone intrusion is among the most fractionated of the Giles intrusions, with olivine Fo values of 40–65, plagioclase An values of 55–75, orthopyroxene Mg# of 0.5 – 0.7, and whole-rock Cr/V ratios mostly <1 (Table 1; see also Ballhaus and Glikson, 1995).

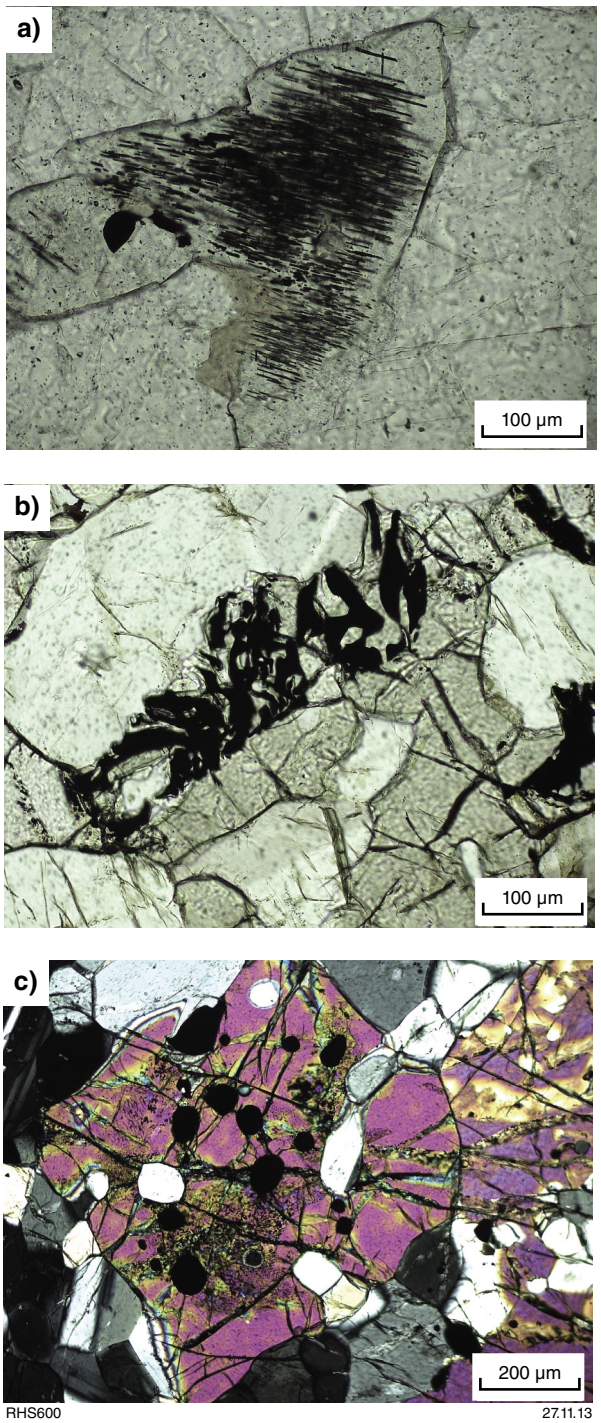

Figure 26. Metamorphic textures in rocks of the Giles intrusions: a) spinel exsolution lamellae within clinopyroxene (Bell Rock intrusion, GSWA 174625); b) exsolution of bleb-like magnetite from pyroxene (Cavenagh intrusion, GSWA 183651); c) exsolution of anhedral and subhedral magnetite from olivine (Cavenagh intrusion, GSWA 183651).

Alcurra Dolerite suite

The Alcurra Dolerite suite includes the dolerite dykes and sills that form the majority of the regional Warakurna Large Igneous Province, formed between c. 1078 and 1073 Ma (Wingate et al., 2004). Within the west Musgrave Province, rocks compositionally similar to the dolerite dykes also form small basic and intermediate bodies, and dykes typically emplaced near the margins of, or peripheral to, older G1 layered mafic intrusions, G2 massive gabbro, and comingled gabbro–granite. These rocks have also been included within the Alcurra Dolerite suite (Howard et al., 2009). The Alcurra Dolerite suite is recognized on the Blackstone, Holt, Finlayson, and Cooper map sheets. Contact relationships from the west Musgrave Province broadly constrain the emplacement dates of these rocks to <1078 Ma, and direct dating of some of the more evolved intrusions indicates magmatism continued to at least c. 1067 Ma (Howard et al., 2009).

Geochemical data from the west Musgrave Province now indicate that mafic compositions typical of the Alcurra Dolerite suite were likely formed over a much longer period, forming lavas throughout the Bentley Supergroup until at least 1047 Ma (Howard et al., 2009, 2011a; Smithies et al., 2013). Thus, the Alcurra Dolerite suite reflects reasonably long-lived melting of mantle rather than a specific melting event (Smithies et al., 2013).

The c. 1076 Ma mafic to intermediate bodies included here within the Alcurra Dolerite suite typically include fine- to medium-grained olivine gabbro, olivine norite, ferronorite, and ferrodiorite. They are commonly characterized by a 'dual texture', comprising a porous framework of coarse-grained crystals (mainly euhedral to acicular plagioclase), enclosing mineralogically identical (except for the presence in some rocks of accessory quartz in granophyric intergrowths) and locally granophyric-textured fine-grained assemblages in interstitial pockets and veins (interstitial liquid). In places, fine-grained rocks containing euhedral plagioclase phenocrysts are found. These rocks were crystallized from the interstitial liquid that was more-or-less free of the components that formed the coarse-grained crystal framework. The latter rocks are typified by evolved and Fe-rich tholeiitic compositions, resulting in a strong aeromagnetic signature and high specific gravity.

In the Blackstone Syncline, basic to intermediate intrusions of the Alcurra Dolerite suite have intruded into the G1 Blackstone intrusion and also the volcanic, volcaniclastic, and clastic rocks of the Kunmarnara and Tollu Groups of the Bentley Supergroup. To the west-northwest, on Finlayson, the marginal zones of the G1 Jameson intrusion have also been intruded by sills and northeast-trending dykes of Alcurra ferronorite. On Holt and Finlayson, these late intrusions form small bodies and dykes typically emplaced near the margins of, or peripheral to, the older G1 intrusions, presumably using contacts between layers and the intrusion and its country rocks as planes of weakness. The series of northeast-trending, coarse-grained ferrogabbro dykes that crosscut the G1 Jameson intrusion, and which also occur throughout the northern parts of Cooper, used fractures and faults related to the earlier Musgrave Orogeny.

The Alcurra Dolerite suite shows considerable compositional variation. Most rocks are relatively evolved, with low Mg# and Cr/V ratios and elevated incompatible trace element concentrations; however, the Alcurra Dolerite also contains more primitive samples that have Mg# ≤ 0.6, Cr/V ≤ 3, and MgO concentrations up to 9 wt%. Most samples are depleted in noble metals, with low Pt and Pd concentrations (<10 ppb Pt+Pd) and Cu/Pd ratios above primitive mantle levels. Sulfur concentrations are up to 2000 ppm, and $\delta^{34}S$ is in the mantle range, at +0.8 to +1.7. Notably, ratios of PGE to Au in rocks of the Alcurra Dolerite suite are markedly lower than in other Giles intrusive rocks (G1 and G2), in part due to elevated Au concentrations in the Alcurra Dolerites.

Saturn intrusion

The Saturn intrusion is delineated by an elliptical aeromagnetic anomaly about 10 km in diameter, between the Cavenagh and Blackstone intrusions (Figs 1, 4, and 27). A direct date of 1072 ± 8 Ma (U–Pb on baddeleyite in olivine gabbro) obtained for the intrusion (Redstone Resources Ltd, 2007, written comm., August) is within error of the c. 1078 to 1075 Ma date range for both the G1 and G2 phases of mafic magmatism related to the Giles Event. However, a younger date of the Saturn intrusion relative to the Blackstone intrusion is indicated because the intrusion cuts the layering of the Blackstone intrusion.

The concentric magnetic pattern indicates zones of magnetite enrichment, possibly including massive magnetite layers. None have been found on the surface, although outcrop is very poor. The only exposed rocks consist of scattered massive, medium-grained, leucocratic olivine gabbros, typically containing biotite and magnetite oikocrysts up to 1 cm wide that form up to 5% of the rock. Samples collected along the Phoebe traverse (Fig. 27) contain up to 6.7% TiO_2 and 800 ppm V, comparable to magnetite gabbros from the Jameson and Blackstone intrusions. The rocks in the centre of the intrusion are somewhat more primitive than those at the margin, having higher Mg# and lower Ti concentrations (Fig. 28), consistent with a dome-like structure.

The rocks are massive to weakly flow-banded, locally containing schlieren of fine-grained gabbronorite (for example, at the 'Camp' site, Fig. 27). Within the oikocrysts, magnetite forms a semicontinuous interstitial network between plagioclase crystals and is itself commonly partially rimmed by biotite. Plagioclase forms 65–75% of the rock, whereas ferromagnesian minerals form 20–30% of the rock. Olivine (typically <8 vol.%) occurs as rounded inclusions, commonly within orthopyroxene. Clinopyroxene forms either discrete anhedral crystals locally rimming orthopyroxene, or exsolution lamellae in orthopyroxene. The modal proportion of clinopyroxene exceeds that of orthopyroxene, and the rocks range from olivine gabbro to olivine gabbronorite. By contrast to most other mafic intrusions related to the Giles Event, biotite constitutes up to 5% of the rock, and there are abundant sulfides (pyrrhotite and chalcopyrite), reaching >1 vol.% (sample GSWA 185579).

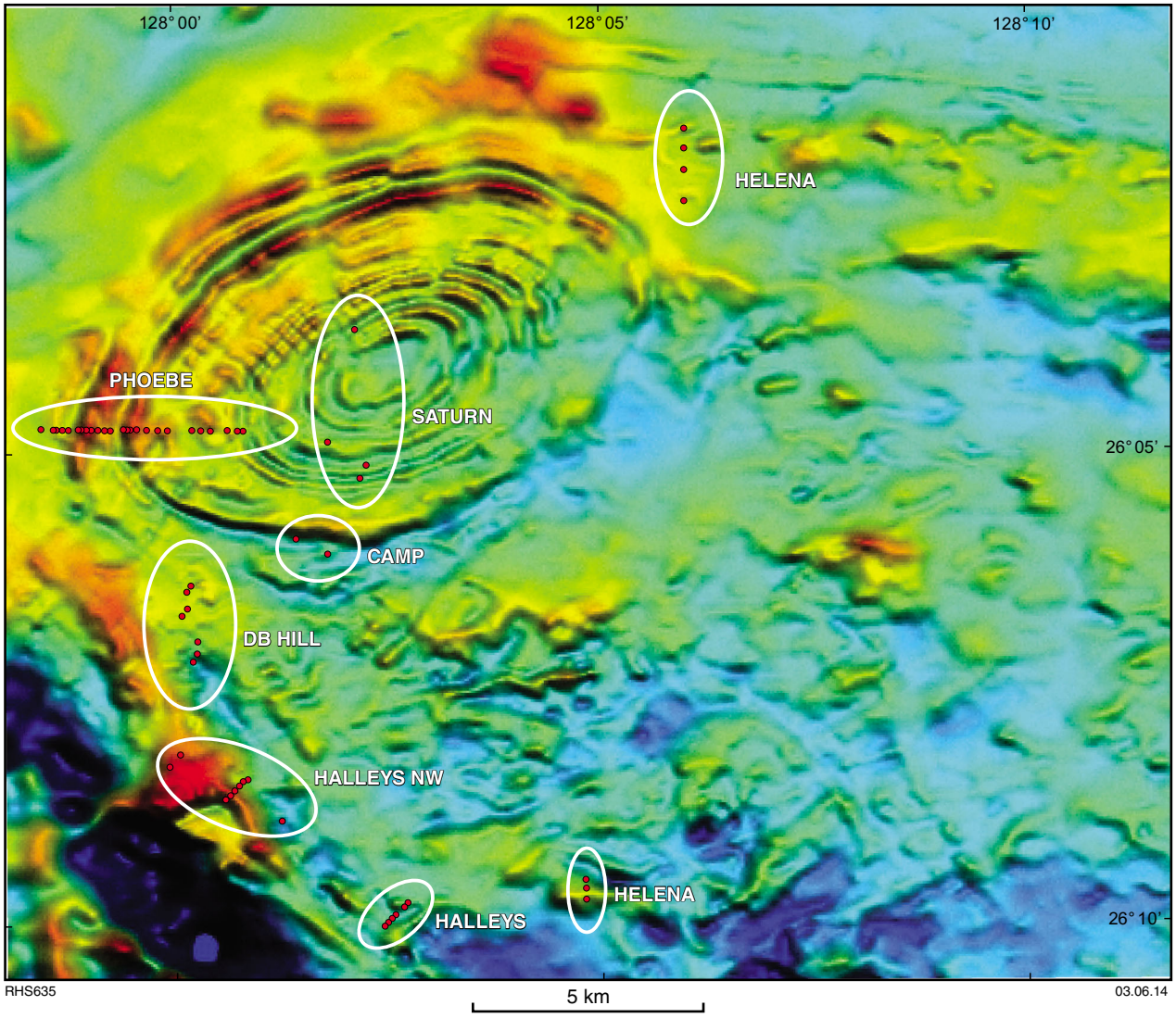

Figure 27. Aeromagnetic image of the Saturn intrusion, between the Cavenagh intrusion (lower left) and the Blackstone intrusion (to the north of the image). Red circles are sampling points for various transverses (named and enclosed in ellipses). Note the concentric pattern defining the Saturn intrusion.

The geochemistry of the rocks indicates relatively evolved compositions with Mg# ≤ 0.65 and Cr/V < 1. Platinum group element and Cu concentrations are typically low (Fig. 29), although they show a distinct increase approximately halfway up the magmatic stratigraphy (Fig. 28). Based on its age, the crosscutting relationships with rocks in the Blackstone Syncline, and the enrichment in mica and sulfide, the intrusion may be transitional between the G1/G2 intrusive phase and the Alcurra Dolerite suite.

Intrusions in the Halleys – Helena – DB Hill area

Mafic rocks outcropping to the northeast and south of the Saturn intrusion have been explored at the Halleys, Halleys NW, Helena, and DB Hill prospects (Redstone Resources, 2008b; Fig. 27). The intrusion(s) can be distinguished from the Cavenagh intrusion, because the latter has a strong remanent magnetic signature not seen in the former intrusions. Although contacts are not exposed, the crosscutting magnetic patterns suggest that these bodies intruded into the G1 intrusions, and also the volcanic, volcaniclastic, and clastic rocks of the Kunmarnara and lower Tollu Groups.

The rocks are mostly medium-grained, leucocratic, pyroxene-rich magnetite ferrogabbros or ferronorites. They have up to 60% clinopyroxene and orthopyroxene (Mg# of 0.65 – 0.7 for orthopyroxene; Mg# of 0.68 – 0.8 for clinopyroxene), 1–2% plagioclase (An 55–83), up to 20% intercumulus or oikocrystic magnetite, up to 5% biotite, and several percent of sulfide minerals. The rocks are typically massive, or show a weak, west-trending magmatic foliation. Oikocrysts of clinopyroxene

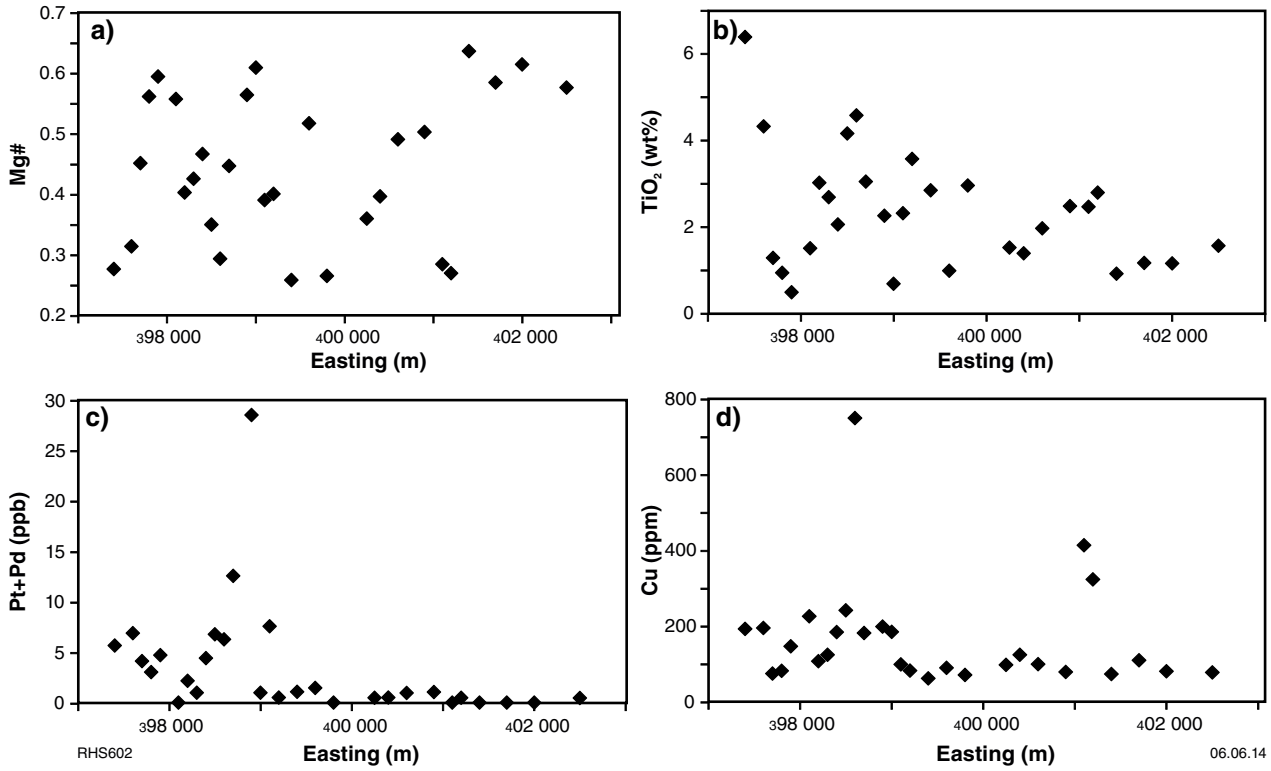

Figure 28. Compositional traverse (west to east) across the Saturn intrusion at Phoebe (see Fig. 27 for sample localities). Note increase in PGE and Cu concentrations approximately halfway along the traverse. Plots of: a) Mg#; b) TiO_2; c) Pt+Pd; d) Cu vs eastings.

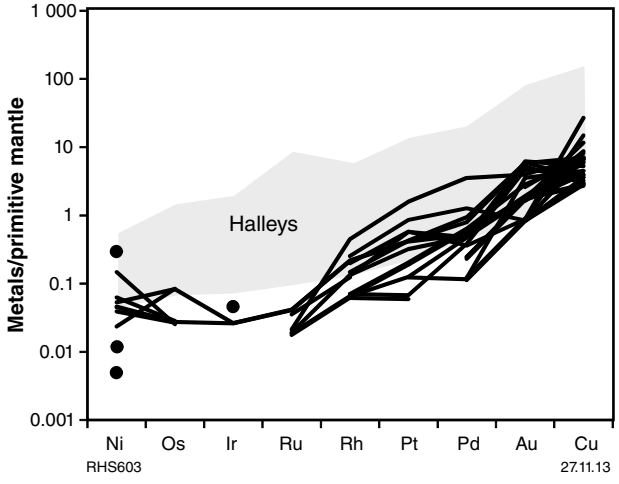

Figure 29. Mantle-normalized multi-element diagram of chalcophile elements for samples from the Saturn intrusion (black lines). Grey field shows platinum group element analyses from Halleys for comparison. Normalization factors from Barnes and Maier (1999). Black circles indicate Ni and Ir values for samples that have Os and/or Ru below the detection limit.

or magnetite can be up to 1 cm. The whole-rock compositions are relatively differentiated, showing lower Mg# (mostly <0.6), and higher V (≤3000 ppm) and Cu (≤4000 ppm) concentrations than in the upper portions of the Blackstone or Cavenagh intrusions. However, Cr/V ratios are locally elevated (≤7) due to chromium enrichment (≤1.6 wt%), mainly within magnetite. The highest chromium concentrations occur in near-massive magnetite, which has higher chromium concentrations than magnetite within magnetite layers of the Upper Zone of the Bushveld Complex (Klemm et al. 1985).

Of further note is that the rocks have locally high concentrations of Cu+Au+PGE. A pipe-like body has been delineated by drilling, with the best intersections containing 0.33 wt% Cu and 0.24 ppm PGE at >74 m depth, and 0.5 wt% Cu and 0.53 ppm PGE over >16 m (Redstone Resources, 2008, comm. at Annual General Meeting, 27 November). The chalcophile multi-element patterns show a progressive increase from Ni through the IPGE to the PPGE and Cu, indicative of a magmatic origin for the metals (Fig. 30). Notably, the patterns are different from the magnetite seams of the Bushveld Complex or the Stella, Jameson, and Saturn intrusions (Figs 23 and 29) in that they have lower PPGE/IPGE ratios. We considered whether the rocks could comprise the uppermost portions of the Cavenagh or Blackstone intrusions, although the latter has markedly lower mica

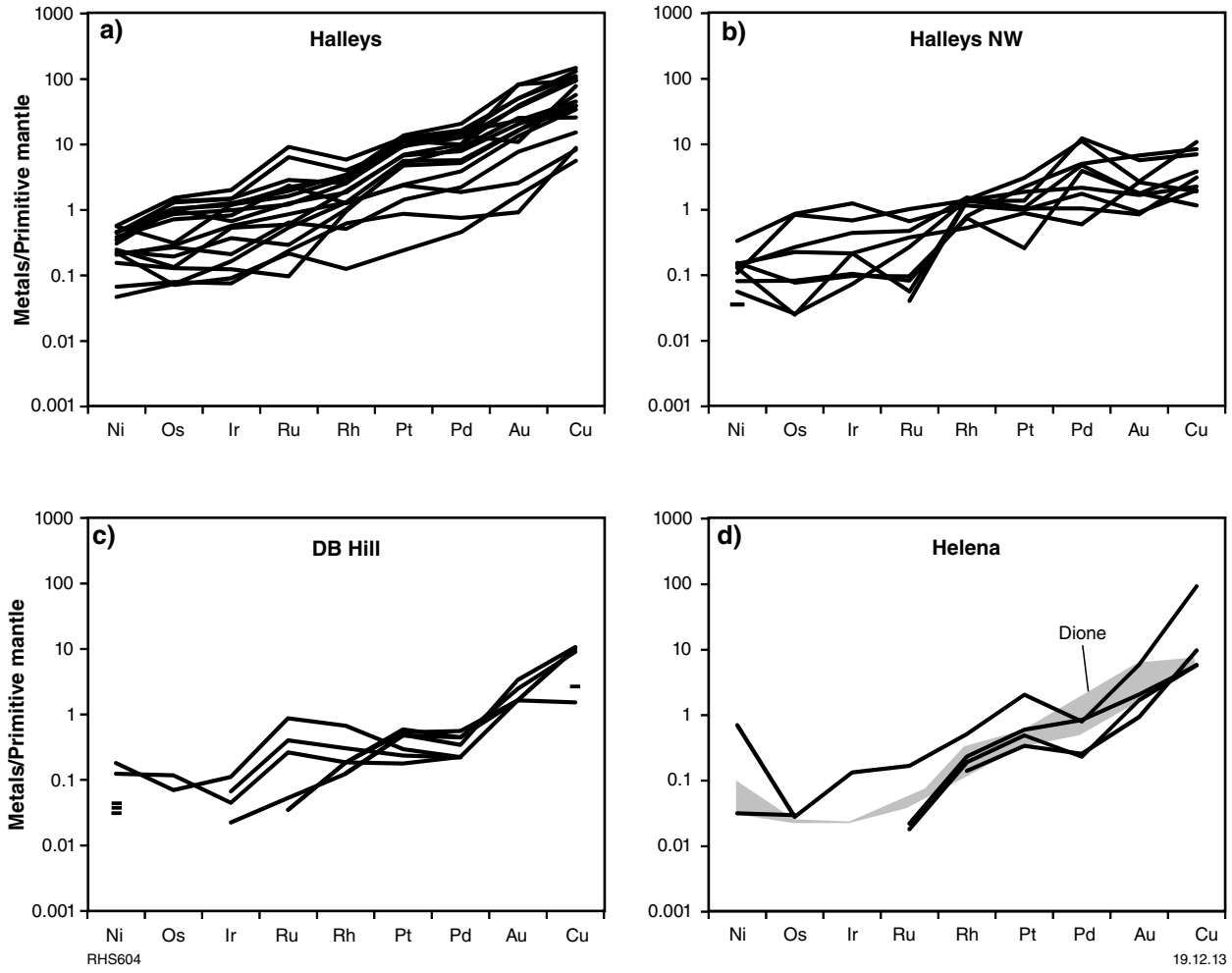

Figure 30. Mantle-normalized multi-element patterns of chalcophile elements for Halleys prospect (shaded area) and adjacent prospects (black lines; see Fig. 27, for localities): a) Halleys; b) Halleys NW; c) DB Hill; d) Helena; normalization factors are from Barnes and Maier (1999).

and sulfide concentrations, lower incompatible trace element concentrations, lower Cr/V ratios, and much lower Au/PGE ratios. Instead, the Halleys rocks have more chemical and petrographic affinities with the Alcurra Dolerite suite.

Nebo–Babel intrusion

The Nebo–Babel intrusion is about 25 km south of Jameson Community (Fig. 4). A detailed study of the Nebo–Babel Ni–Cu–PGE deposit was carried out by Seat et al. (2007, 2009) and Seat (2008), and the following section has been compiled mostly from this work.

The intrusion has been dated at 1068 ± 4 Ma (using U–Pb sensitive high-resolution ion microprobe [SHRIMP] on zircon; Seat, 2008). The intrusion has a tubular ('chonolithic') shape trending approximately north-northeast to east, and can be traced for about 5 km. The cross-section measures 1 km wide x 0.5 km high. The chonolith has a gentle west-southwest plunge of less than 10° and dips to the south at about 15°. It is offset by the Jameson Fault, which effectively divides it into the Nebo section in the east and the Babel section in the west. Based on geochemistry, the body is interpreted to be overturned. Where contacts are observed, it appears that it was emplaced in felsic orthogneiss of the Pitjantjatjara Supersuite, although our mapping of the area shows that paragneisses belonging to the Wirku Metamorphics are a more common older basement component in the region. The stratigraphy of the intrusion is characterized by a basal breccia zone (MBZ), overlain by a chilled margin (7–9% MgO), variably textured leucogabbronorite (VLGN), melagabbronorite (mela-GN), mineralized gabbronorite (MGN, present only in the Babel sector), and barren gabbronorite (BGN), which in the Nebo sector is associated with oxide–apatite gabbronorite (OAGN).

A massive and coarse-grained troctolite unit, about 15 m thick, is present only at Babel where it is located between VLGN and BGN in the upper part of the intrusion. Rhythmic layering is confined to the upper parts of the Babel sector and consists of 5–15 cm-thick

layers of plagioclase-rich pyroxenite grading upward into gabbronorite. The OAGN constitutes about 20–30% of the intrusion and is characterized by oxide-rich layers that are 5–30 cm thick, with gradational bases and sharp upper contacts.

In April 2002, Western Mining Corporation announced a drill intersection of 26 m containing 2.45% Ni, 1.78% Cu, and 0.09% Co at the Nebo–Babel prospect, one of the most significant nickel sulfide discoveries since Voisey's Bay in 1994. The Nebo–Babel deposit was discovered by conventional deflation lag geochemical sampling (Baker and Waugh, 2004). Resource estimates, obtained from 90 drillholes, are 392 Mt at 0.30% Ni and 0.33% Cu (Seat et al., 2007). The mineralized gabbronorite has a uniform grain size (5–20 mm) and consists of 55–65 vol.% plagioclase, 15–25 vol.% orthopyroxene, and 5–10 vol.% clinopyroxene. Other minerals include ilmenite, magnetite, biotite, and apatite. Sulfides are monoclinic pyrrhotite, pentlandite, chalcopyrite, and pyrite. The sulfide mineralization exhibits two styles: massive ores with associated sulfide breccias and stringers, and disseminated ores, typically forming interstitial blebs in the gabbronorite unit (MGN). Sulfur isotopic data show a remarkably narrow range of $\delta^{34}S$ values from 0 to +0.8‰. The metal tenors of the sulfides are mostly 5–6% Ni and 2–8% Cu (Cu/Ni ~ 1), and up to several parts per million each of Pt and Pd (Seat et al., 2009). The metal patterns of the chilled margins and the medium-grained rocks are fractionated, with a progressive increase from Ir to Cu. Notably, although the chilled margins have PGE concentrations typical of basaltic magmas (~10–20 ppb Pt and Pd each), Cu/Pd > 10 000, markedly above primitive mantle (Fig. 31). This chemistry could suggest a mantle source with unusually high Cu/Pd ratios. Equally, all medium-grained rocks show Cu/Pd ratios above primitive mantle values. The massive sulfides underwent fractional crystallization of a sulfide liquid, producing a cumulate of monosulfide solid solution relatively enriched in Os, Ir, Ru, and Rh and depleted in Pt, Pd, and Au.

Seat et al. (2007) suggested that the intrusion is a magma conduit (Fig. 32). The initial magma was proposed to have intruded along a shear zone or fault, more-or-less parallel to the regional foliation. During the first stage, chilled margins and then the VLGN units were emplaced. This order of emplacement is consistent with the progressive coarsening of the chilled margins toward the VLGN and the presence of chilled margin xenoliths within the VLGN rocks. Both chilled margin and VLGN units carry sulfides, interpreted by Seat et al. (2007) to indicate that some of the magmas entrained sulfides. However, other samples of chilled margin (Godel et al., 2011) contain about 1000 ppm S, and 10–20 ppb Pt and Pd each (i.e. levels similar to fertile basaltic magmas), suggesting that some of the initial magmas intruded in a sulfur-undersaturated state. The emplacement of the VLGN was followed by the MGN unit (Stage 2), which was intruded into the hot VLGN core zone, resulting in the splitting of the VLGN unit and further inflation of the conduit. The MGN magma was also proposed to be sulfide-oversaturated, based on the occurrence of disseminated sulfide blebs. Stage 3 comprises a new pulse of more-fractionated magma that was intruded between VLGN and MGN, forming the BGN unit. The flow of MGN magma is assumed to have been from the southwest, because the unit thins toward the northeast and at the same time becomes progressively more fractionated.

Nebo–Babel resembles the Uitkomst intrusion of South Africa in terms of its shape and size and its sulfide ore deposit (Gauert et al., 1995; Seat et al., 2007). Both intrusions have trough-like shapes, with cross-sections of about 1 km^2, some massive sulfides possibly representing a monosulfide solution (MSS) cumulate, and large amounts of disseminated sulfides. Both intrusions underwent protracted fractionation, have upper and lower chill zones, abundant xenoliths, and sill-like extensions, and are fault-controlled. Both are spatially and temporally associated with large layered intrusions. However, the Uitkomst magma was more primitive (12–15% MgO), resulting in a thick ultramafic portion.

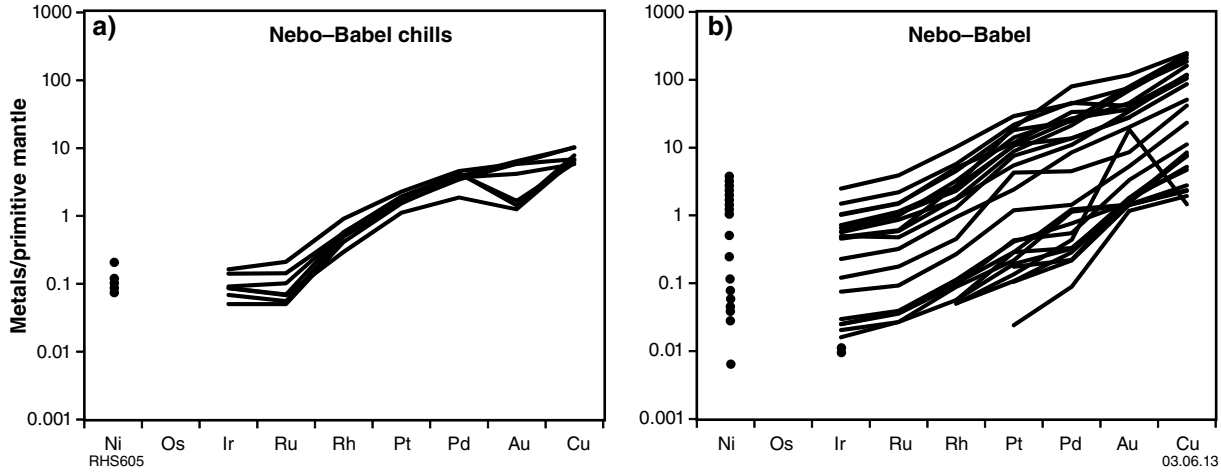

Figure 31. Mantle-normalized multi-element patterns of chalcophile elements in rocks from Nebo–Babel: a) chill zones; and b) intrusion, based on data of Seat et al. (2009); normalization factors are from Barnes and Maier (1999).

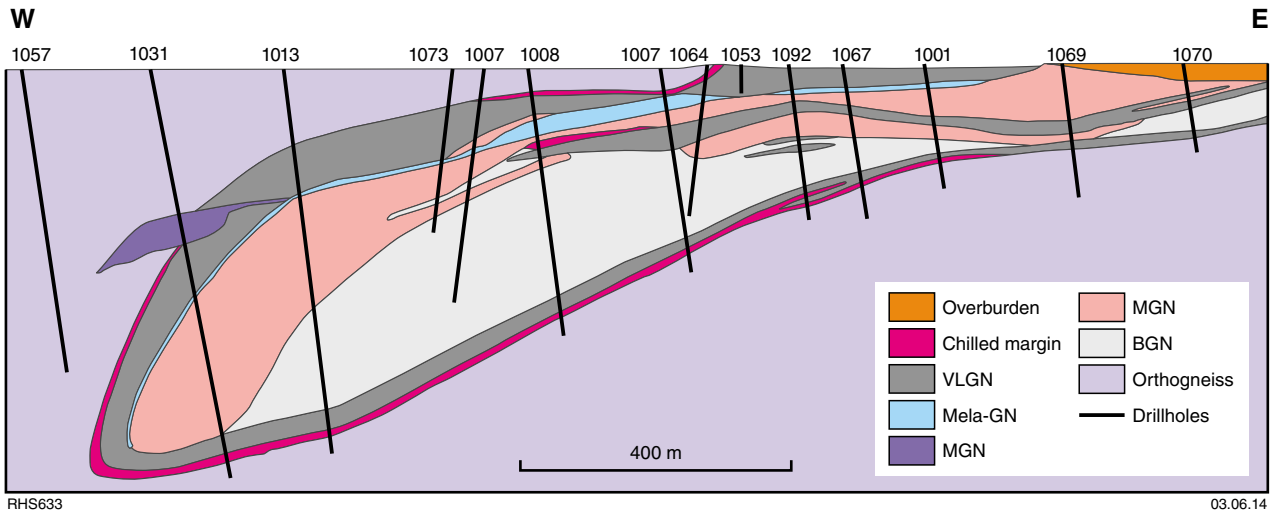

Figure 32. Longitudinal section of Babel segment of Nebo–Babel intrusion showing location of boreholes (redrawn from Seat et al., 2007). BGN = barren gabbronorite, mela-GN = melagabbronorite, MGN = mineralized gabbronorite, OAGN = oxide–apatite gabbronorite, VLGN = variably textured leucogabbronorite, FG MGN = fine-grained melagabbronorite; borehole numbers are across the top of the section.

Dykes related to the Giles Event and younger events

Studies of the dyke suites in the west Musgrave Province commenced with the work of Nesbitt et al. (1970), Zhao et al., (1994), Clarke et al. (1995b), Glikson et al. (1996), and Scrimgeour and Close (1999). Howard et al. (2006b) identified seven suites of dykes. The oldest dykes (c. 1170 Ma, ~8% MgO) belong to the Pitjantjatjara Supersuite and are the only pre-Giles Event mafic dykes recognized. During the Giles Event, magmatism associated with the emplacement of the Warakurna Large Igneous Province (Wingate et al., 2004) formed the Alcurra Dolerite suite (6–9% MgO; Zhao et al., 1994; Edgoose et al., 2004). Unnamed plagioclase-rich dolerite dykes (~8% MgO) clearly post-date the G1 intrusions; however, their timing with respect to other mafic intrusions of the Giles Event is unclear, and some outcrops suggest they are synchronous with G2 intrusions. Dolerite intrusions that post-date the Giles Event include unnamed olivine- and plagioclase-porphyritic dolerite dykes at c. 1000 Ma (~8% MgO), 825 Ma quartz dolerite dykes of the Gairdner Dyke Swarm (~8% MgO), and c. 800 Ma dykes of the Amata Dolerite (Zhao et al., 1994; Glikson et al., 1996; Wingate et al., 1998). A further suite of dykes with about 9.5% MgO and trace element-depleted characteristics may be of similar age or younger than the Gairdner Dyke Swarm.

Godel et al. (2011) identified five distinct dyke suites (NB1–5) in the Nebo–Babel area and investigated these as possible parental magmas to intrusions related to the Giles Event. Types NB1–3 are low-Ti basalts with 5–20% MgO, probably derived from the subcontinental lithospheric mantle (SCLM), whereas types NB4 and NB5 are high-Ti basalts with 5–14% MgO interpreted to be derived from a plume source. The NB1 type is broadly equivalent to the plagioclase-phyric dykes of Howard et al. (2006b) and is a potential candidate for a parental liquid to the G1 intrusions, containing about 10–13% MgO. NB4 was proposed as equivalent to the Alcurra Dolerite suite, consistent with low PGE concentrations in both suites. The other dyke suites studied by Godel et al. (2011), NB2–3 and 5, are not good candidates for parental magmas to the Giles intrusions. These dykes are either too coarse-grained and MgO-rich (NB2), or too young (NB5). NB3 dykes have intermediate compositions between NB1 and NB4 and thus may be hybrids of NB1 and the Alcurra Dolerite suite (Godel et al., 2011).

Analytical methods

Samples were prepared for analysis at GSWA using a jaw crusher followed by milling in a tungsten carbide mill. The mill was tested for possible contaminants, with only cobalt being significant (≤157 ppm in grinding tests). Major elements were determined by wavelength-dispersive X-ray fluorescence spectrometry (XRF) on fused disks using methods similar to those of Norrish and Hutton (1969). Precision is better than 1% of the reported values. Concentrations of Ba, Cr, Cu, Ni, Sc, V, Zn, and Zr were determined by wavelength-dispersive XRF on pressed pellets using methods similar to those of Norrish and Chappell (1977), whereas Cs, Ga, Nb, Pb, Rb, Sr, Ta, Th, U, Y, and REE were analysed by inductively coupled plasma–mass spectrometry (ICP-MS) using methods similar to those of Eggins et al. (1997), on solutions obtained by dissolution of fused glass disks. Precision for trace elements is better than 10% of the reported values. All whole-rock major and trace element data for the silicate rocks are listed in Table 1. All analyses and analytical details can be obtained from the WACHEM database (at <http://geochem.dmp.wa.gov.au/geochem/>).

Selected major and trace elements for the massive magnetite seams were determined by instrumental neutron activation analysis (INAA) at The University of Québec at Chicoutimi, Canada (Table 2).

Platinum, Pd, and Au were analysed by lead collection fire assay of 40 g of sample, followed by ICP quantitation. The detection limit was 1 ppb for each element. For selected samples, complete PGE spectra were obtained by ICP-MS at The University of Québec. Analytical details are given in Barnes et al. (2010). Platinum group element data are shown with the bulk of the lithophile element data in Table 1.

Sulfur isotopes were analysed by Rafter GNS Sciences at the New Zealand National Isotope Centre at Lower Hutt, New Zealand. Samples were measured in duplicate in tin capsules with equal amounts of V_2O_5 on a EuroVector elemental analyser connected to a GVI IsoPrime mass spectrometer. All results are averages and standard deviations of duplicates are reported with respect to the Vienna Canyon Diablo Troilite (VCDT) standard, normalized to internal standards R18742, R2268, and R2298 with accepted $\delta^{34}S$ values of –32‰, +3.3‰, and +8.6‰, respectively. The external precision for this instrument is better than 0.3 for $\delta^{34}S$. All data are listed in Table 3.

Strontium isotopes were analysed by laser ablation ICP-MS at GTK, Espoo, Finland. Analytical details are given in Yang et al. (2013), and the data are listed in Table 4.

For most samples, Sm–Nd isotopic analyses were determined by isotope dilution at the VIEPS Radiogenic Isotope Laboratory, Department of Earth Sciences, La Trobe University, Victoria. Analytical techniques follow those of Waight et al. (2000). All quoted ε_{Nd} values are initial values calculated at the time of igneous crystallization. For some samples, Nd isotopes were determined at GTK Espoo. Analytical details are given in Maier et al. (2013a). All Sm–Nd isotope data are listed in Table 5.

The composition of olivine, pyroxenes, plagioclase, and chromite were determined at The University of Oulu, Finland, using a JEOL JXA-8200 electron microprobe at an accelerating voltage of 15 kV and a beam current of 30 nA, which allowed an approximately 150 ppm detection limit for nickel. The accuracy of analyses was monitored using reference material of similar compositions. Compositional data are listed in Tables 6–9.

Comparative geochemistry of the intrusions

Lithophile element and Nd–Sr–S isotopic signatures

The major element composition of the G1 Giles intrusions is mainly controlled by variation in the modal proportions of olivine, orthopyroxene, clinopyroxene, plagioclase, and magnetite. Most of the ultramafic rocks exposed in the Wingellina Hills, Pirntirri Mulari, The Wart, and Morgan Range intrusions are wehrlites, websterites, or

Table 4. Strontium isotope data from intrusions of the Giles Event

Sample no.	*Intrusion*	*n*	$^{87}Rb/^{86}Sr$	$^{87}Sr/^{86}Sr$	$(^{87}Sr/^{86}Sr)_i$	2σ	*Age (Ga)*
189342	Morgan	9	0.001	0.70664	0.70663	0.00035	1.078
189348	Morgan	6	0.002	0.70736	0.70733	0.00030	1.078
189375	Pirntirri Mulari	9	0.011	0.70658	0.70642	0.00029	1.078
189354	Pirntirri Mulari	4	0.001	0.70880	0.70870	0.00110	1.078
189311	Lehman Hills	9	0.004	0.70726	0.70719	0.00041	1.078
189485	Jameson	9	0.023	0.70459	0.70425	0.00021	1.078
189471	Jameson	8	0.011	0.70449	0.70431	0.00019	1.078
189486	Jameson	9	0.010	0.70454	0.70439	0.00015	1.078
155659	Blackstone	9	0.003	0.70413	0.70408	0.00012	1.078
155656	Blackstone	8	0.003	0.70403	0.70399	0.00025	1.078
155670	Blackstone	8	0.005	0.70432	0.70424	0.00014	1.078
189447	Finlayson	8	0.011	0.70461	0.70445	0.00015	1.078
189456	Finlayson	9	0.014	0.70452	0.70432	0.00018	1.078
Woo144	Halleys	9	0.029	0.70500	0.70456	0.00017	1.068
BSC002	Halleys	4	0.020	0.70498	0.70468	0.00042	1.068
155643	Cavenagh	18	0.032	0.70665	0.70612	0.00017	1.078
155633	Cavenagh	6	0.005	0.70452	0.70566	0.00015	1.078
183611	Cavenagh	12	0.015	0.70588	0.70538	0.00013	1.078
183608	Cavenagh	9	0.001	0.70539	0.70445	0.00014	1.078

NOTE: *n* number of sample spots

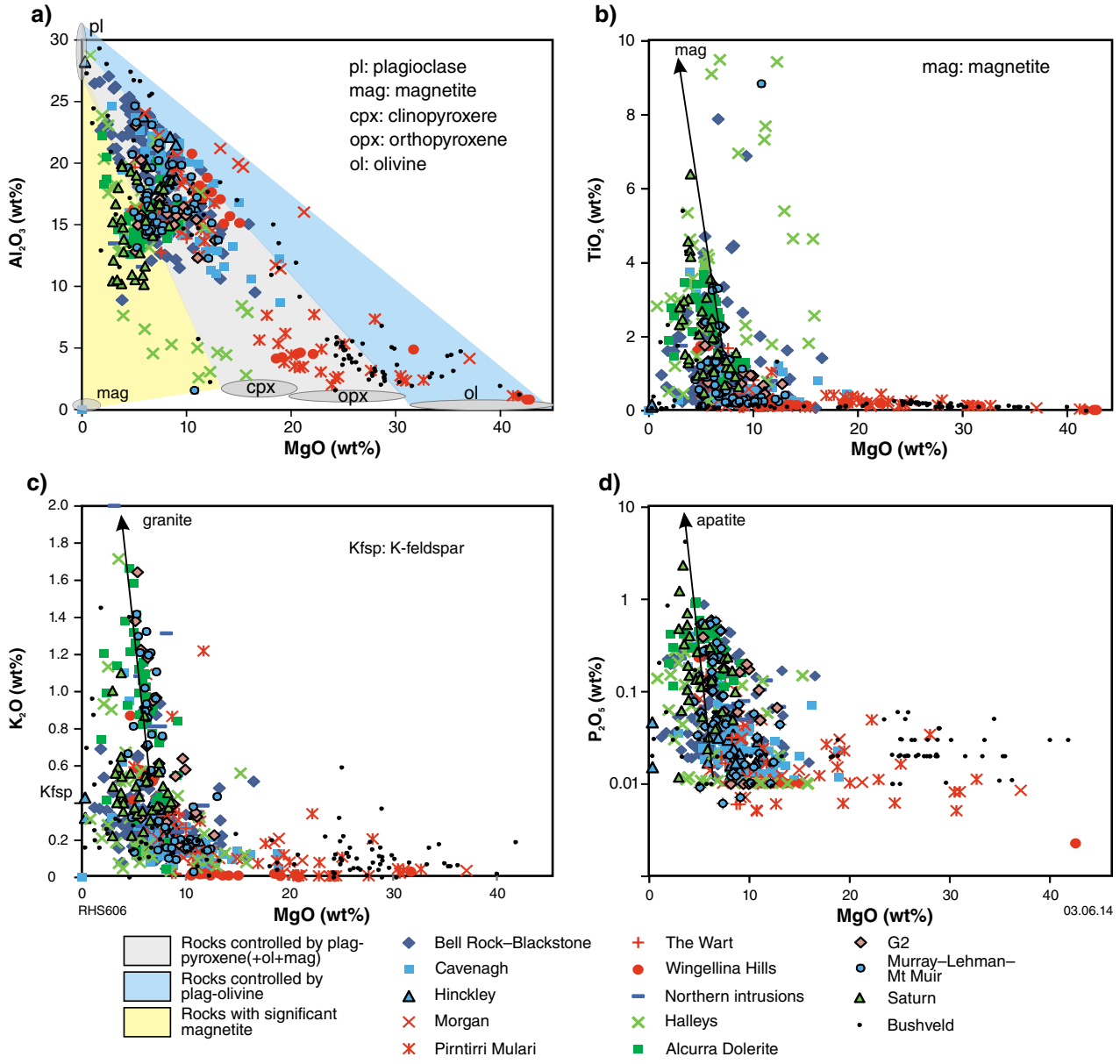

Figure 33. Binary variation diagrams vs MgO of selected major elements in the Giles intrusions: a) Al_2O_3; b) TiO_2; c) K_2O; d) P_2O_5. Coloured fields in (a) denote cumulates whose compositions are principally controlled by variation in modal proportions of plagioclase and olivine (blue) and plagioclase+pyroxene (grey). Yellow field indicates rocks that contain significant magnetite. Vectors in b)–d) indicate that some cumulates contain substantial magnetite, apatite, and granite components. 'Northern' intrusions include intrusive fragments to the north of Mt Muir and Hinckley Range.

harzburgites, with rare dunite. The modal proportion of plagioclase in these rocks is mostly <10%. The rocks are thus relatively enriched in MgO and depleted in Al_2O_3 (Fig. 33a). The bulk of the remaining samples are gabbronorites, containing <15% MgO and >10% Al_2O_3. Troctolites are relatively common in the Morgan Range, Cavenagh, and Mantamaru intrusions.

Based on the lever rule, it can be estimated that the modal proportion of plagioclase in the gabbroic–troctolitic rocks is mostly >50%, with the Cavenagh intrusion the most mafic (Fig. 33a,b). Titanomagnetite is an important phase in the Bell Rock–Blackstone–Jameson, Halleys, and Saturn intrusions, as indicated by their low MgO and Al_2O_3 concentrations and high TiO_2 concentrations (Fig. 33b). Elevated K_2O concentrations in the Hinckley Range and Murray Range intrusions attest to higher crustal contamination (Fig. 33c), whereas the high K_2O in the Halleys intrusion likely results from advanced fractionation, in view of the typically evolved nature of these rocks and that the country rocks are K-poor mafic intrusive rocks. The presence of apatite in the Halleys, Saturn, Jameson, and Blackstone intrusions is indicated by relatively elevated P_2O_5 concentrations (Fig. 33d).

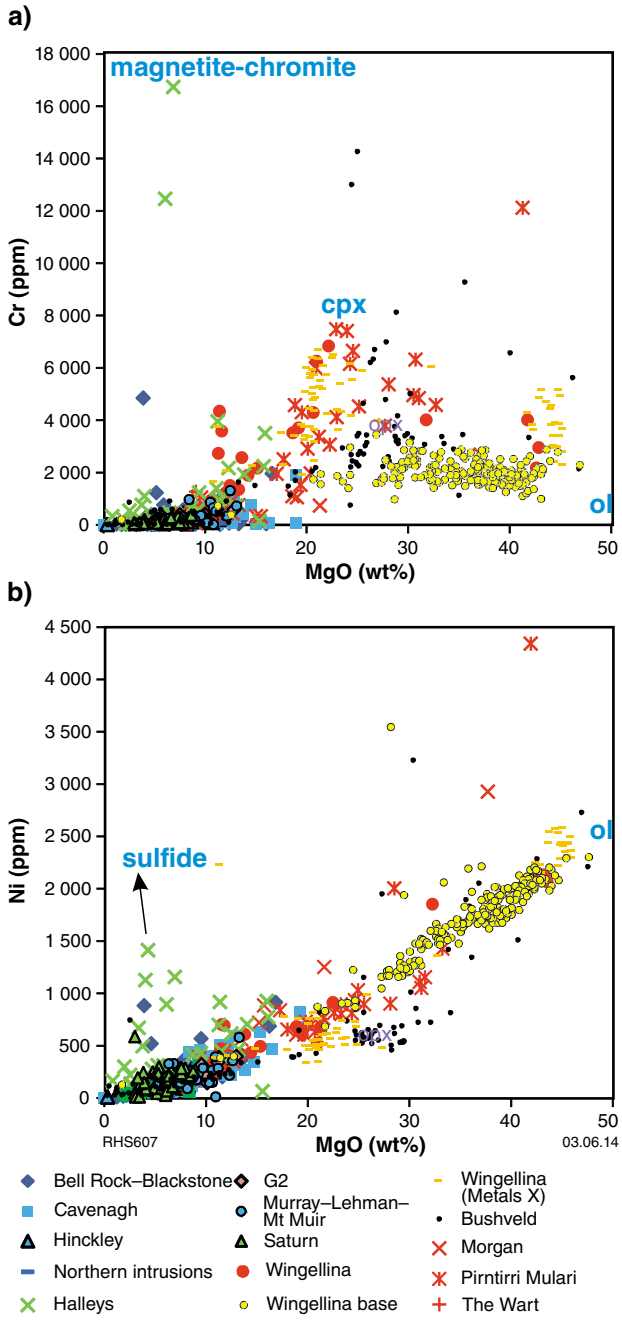

Figure 34. Rocks of the Giles intrusions plotted into binary variation diagrams vs MgO of: a) Cr; and b) Ni. Approximate compositions of selected silicate and oxide minerals are shown in blue lettering. Mineral abbreviations as for Figure 33.

In the ultramafic intrusions, the concentration of compatible trace elements (Cr and Ni) is controlled mainly by modal variation in olivine, clinopyroxene, and orthopyroxene (Fig. 34). Many samples from the Wingellina Hills intrusion, but only one from Pirntirri Mulari, contain more Cr than can be hosted in pyroxene, indicating the presence of cumulus chromite. Most gabbroic intrusions are relatively Cr-poor, containing <1000 ppm Cr, although gabbros from the Wingellina Hills and Halleys intrusions are relatively enriched in Cr. In the case of the Halleys intrusion, the high Cr concentrations are the result of abundant Cr-bearing magnetite, whereas the elevated Cr concentrations in the gabbros of the Wingellina Hills intrusion are due to the presence of unevolved Cr-rich clinopyroxene.

Nickel shows a strong positive correlation with MgO in most intrusions (Fig. 34b). In general, the olivine and pyroxene-rich rocks are more Ni-rich than plagioclase-rich rocks, due to high partition coefficient (D-values) of Ni (D_{Ni}) with regard to olivine (5–15, depending on pressure; Li and Ripley, 2010) and pyroxene (1–3; Green, 1994). Samples with significant amounts of olivine are largely confined to the Wingellina Hills intrusion, as indicated by whole-rock MgO > 30 wt% and Ni > 1000 ppm. The Wingellina Hills samples define a Ni–MgO trend that can be extrapolated to a Ni concentration in olivine of about 2500–3000 ppm, broadly overlapping with measured Ni concentrations in olivine from the Pirntirri Mulari intrusion (~3000 ppm). Two ultramafic samples from Pirntirri Mulari and one from the Morgan Range intrusion have markedly higher Ni concentrations than the remaining ultramafic samples. This is unlikely to reflect the presence of trace sulfides because the rocks do not have elevated Cu, S, or PGE concentrations. Instead, the elevated Ni concentrations are likely due to alteration, consistent with the analysed high loss-on-ignition (LOI) values of the samples. Sulfide and magnetite control could explain the slightly elevated Ni concentrations in the Halleys and Blackstone intrusions (up to ~1500 ppm Ni), relative to the other gabbroic–troctolitic intrusions, which mostly contain <500 ppm Ni.

Vanadium and scandium concentrations are largely controlled by the modal proportions of magnetite and clinopyroxene (Fig. 35), with clinopyroxene containing about 300 ppm V and about 70 ppm Sc. The highest vanadium concentrations occur in the relatively evolved Mantamaru, Halleys, and Saturn intrusions, and in rocks of the Alcurra Dolerite suite, due to the presence of cumulus magnetite.

Most G1 intrusions have broadly similar concentrations of Zr (~5–30 ppm) (Fig. 36) and other incompatible trace elements. Rocks of the Alcurra Dolerite suite, the Halleys and Saturn intrusions, G2 massive gabbros, and the Hinckley Range and Murray Range intrusions show markedly higher Zr concentrations. The elevated values in the Hinckley Range and Murray Range intrusions are likely due to contamination with granite or G2 gabbro, consistent with field evidence discussed earlier. The high Zr concentrations in the Alcurra Dolerite suite and in fine-grained G2 samples are partly because these rocks contain an important liquid component. The high Zr values

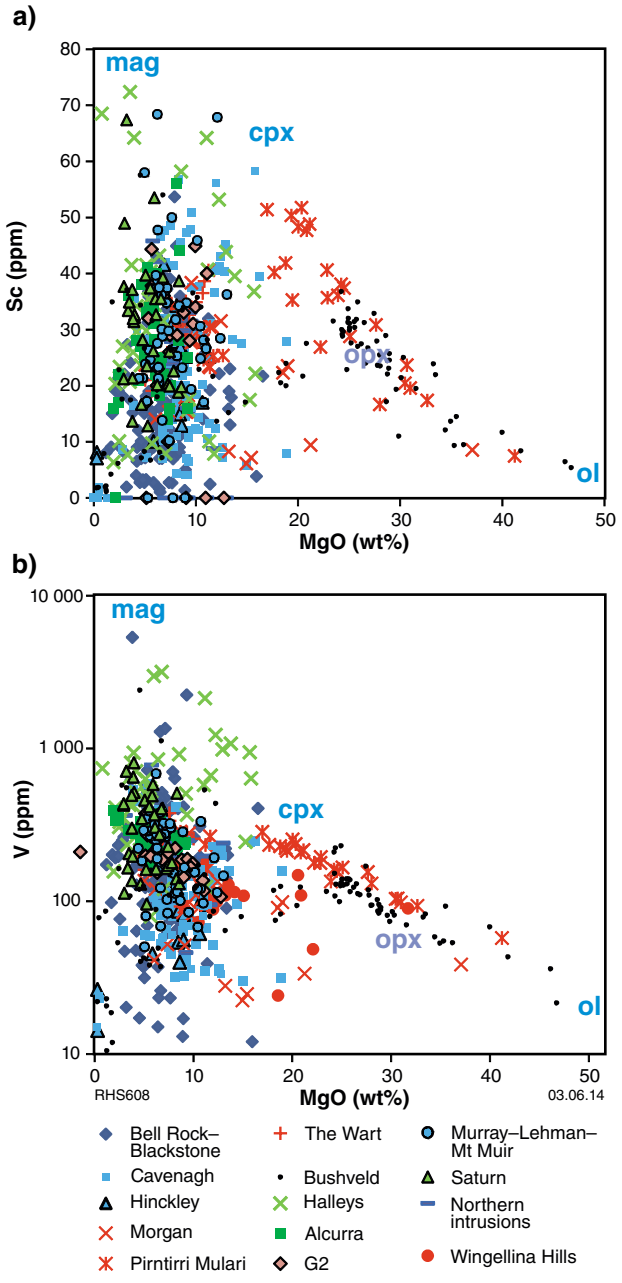

Figure 35. Binary variation diagrams vs MgO of: a) Sc; and b) V. mag = magnetite, cpx = clinopyroxene, opx = orthopyroxene, ol = olivine. 'Northern' intrusions include intrusive fragments to the north of Mt Muir and Hinckley Range. Cavenagh data include samples from Staubmann (2010). Mineral abbreviations as for Figure 33. Symbols as in Figure 34, with the addition of solid green squares for Alcurra Dolerite samples.

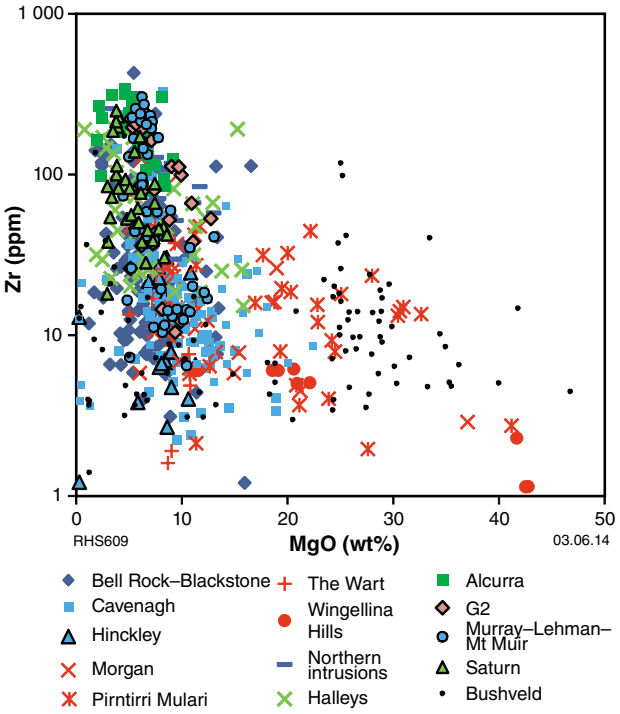

Figure 36. Binary variation diagram of Zr vs MgO. 'Northern' intrusions include intrusive fragments to the north of Mt Muir and Hinckley Range. Cavenagh data include samples from Staubmann (2010). Symbols as in Figure 34.

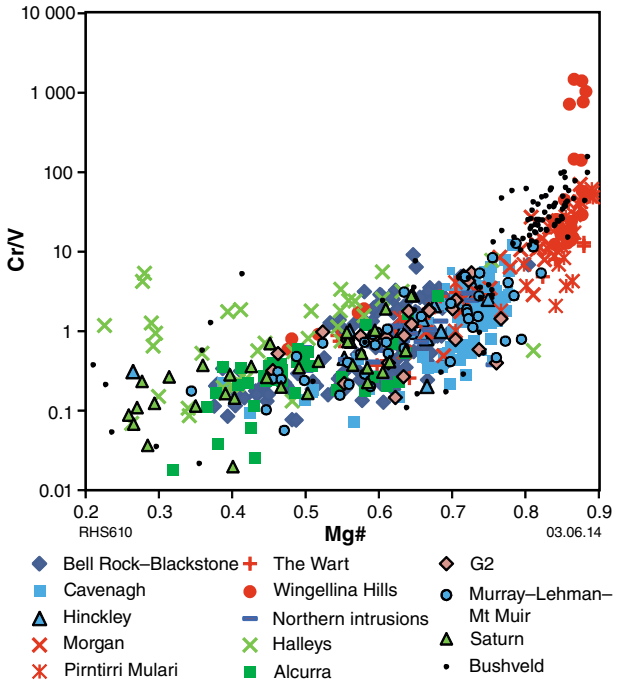

Figure 37. Binary variation diagram of Cr/V vs Mg# for the Giles intrusions. Bushveld data are from Maier et al. (2013b). 'Northern' intrusions include intrusive fragments north of Mt Muir and the Hinckley Range. Cavenagh data include samples from Staubmann (2010).

at Halleys and in the Saturn intrusion (up to 250 ppm Zr) are in part due to protracted fractionation, consistent with their typically evolved compositions (e.g. low Mg# and Cr/V ratios).

The state of differentiation of the various intrusions can be compared in a plot of Cr/V ratio vs Mg# (Fig. 37). The least evolved intrusions are Wingellina Hills, Pirntirri Mulari, The Wart, and Morgan Range. These intrusions show some overlap with the Ewarara intrusion in South Australia and the Lower Zone of the Bushveld Complex, South Africa, except that the latter has higher Cr/V ratios due to higher chromite abundance. Intrusions showing intermediate composition are Cavenagh, Murray Range, and Hinckley Range, and the intrusive fragments to the north of Mt Muir and Hinckley Range ('North' and 'Northeast' in Table 1). Relatively evolved intrusions include Mantamaru, Saturn, and Halleys, and dykes belonging to the Alcurra Dolerite suite.

The lithophile multi-element (spider) patterns of the mafic intrusions are fractionated, showing enrichment in the most incompatible elements and negative Nb anomalies (Fig. 38). Most samples have pronounced positive Sr and Eu anomalies, except for the Murray Range, the 'North' and 'Northeast' intrusive fragments, and gabbroic rocks from Wingellina Hills. Positive Ti anomalies are shown in the Mantamaru (Bell Rock, Blackstone and Jameson), Halleys, and Lehman Hills intrusions and in many samples from the Saturn intrusion (not evident in the average composition plotted in Fig. 38), indicating the presence of magnetite. The Saturn and Halleys intrusions have markedly higher incompatible trace element concentrations than most other intrusions, including the adjacent Cavenagh and Blackstone intrusions, consistent with a distinct magmatic lineage of Cavenagh. Michael Hills and the 'North' and 'Northeast' intrusive fragments also show elevated trace element concentrations. These patterns could reflect a lower cumulate component or more-fractionated compositions. Gabbro from the Wingellina Hills intrusion has the lowest trace element concentrations among the gabbroic rocks, and distinct negative Ti anomalies, reflecting the relatively unevolved nature of the Wingellina Hills magma.

The ultramafic rocks from the Pirntirri Mulari, Wingellina Hills, The Wart, and Morgan Range intrusions (pyroxenites, wehrlites, harzburgites, and rare dunite) share negative Nb anomalies with the gabbroic intrusions, although the former have less-fractionated multi-element patterns, reflecting their less-evolved character. The patterns are also more 'spiky', possibly reflecting element concentrations approaching the limit of analytical detection for many elements, and possibly alteration. Pyroxenites from the Wingellina Hills and Pirntirri Mulari intrusions have similar compositions, except for negative Zr anomalies at Wingellina Hills. The patterns of pyroxenites and gabbros from the Wingellina Hills intrusion are identical, indicating crystallization from magmas of broadly similar composition. Dunites from the Wingellina Hills, Pirntirri Mulari, and Morgan Range intrusions have the lowest trace element concentrations; many elements are below the analytical limit of detection. This likely reflects the low trapped liquid content of the rocks and the unevolved nature of the magma.

Data from suites that may represent liquids (i.e. that carry fewer cumulate components) are plotted in Fig. 39. The patterns of the Alcurra Dolerite suite (Fig. 39a), the G2 gabbros (Fig. 39b), the NB1 dykes, and the fine-grained chilled margins of the Nebo–Babel intrusion show similarities including pronounced negative Nb and Ta anomalies. The patterns of the G2 and Nebo–Babel chilled margins are particularly similar and also share negative Ti anomalies. Although the incompatible trace element concentrations of the rocks are higher than those in most, although not all (see Fig. 39c), G1 intrusions, it is clear that the shapes of the multi-element patterns for all mafic intrusions are remarkably similar, except that the rocks enriched in a liquid component lack positive Sr anomalies.

Microgabbros from the Cavenagh intrusion share positive Sr and Ti anomalies with many of the G1 cumulates (Fig. 39d). However, the patterns are much less fractionated and more 'spiky' than those of the other mafic rocks. This is a reflection of the high cumulate component and very low incompatible trace element concentrations in most microgabbros.

The relative effects of fractionation and contamination can be assessed by considering trace element ratios. The Mantamaru and Halleys intrusions, and the dykes of the Alcurra Dolerite suite, tend to show higher Nb/Ce ratios than most other intrusions, broadly overlapping with the primitive mantle range (Nb/Ce = 0.4; Fig. 40). The Hinckley Range intrusion presents some of the lowest Nb/Ce ratios, likely reflecting crustal contamination, consistent with the field evidence presented earlier.

The G2 samples and most ultramafic rocks have low Nb/Ce ratios, which can be modelled by contamination with the Pitjantjatjara Supersuite granites formed during the earlier Musgrave Orogeny (Fig. 40). The low Nb/Ce ratios of many of the highly differentiated samples from the Saturn intrusion probably reflect the presence of apatite, consistent with high P contents of up to 2.1% P_2O_5, whereas the high Nb/Ce ratios of some samples from the Halleys and Mantamaru intrusions are likely due to the presence of ilmenite.

The high Th/TiO_2 ratios of the G2 intrusions, Alcurra Dolerite suite, Cavenagh intrusion, and many ultramafic samples from the Wingellina Hills, Pirntirri Mulari, and The Wart likely result from contamination, whereas the Mantamaru intrusion samples with low Th/TiO_2 and high Ce/Sm ratios are interpreted to reflect accumulation of ilmenite and apatite (Fig. 41). The Nd isotopic composition of the intrusions is plotted vs Ce/Nb ratio in Figure 42. The Mantamaru intrusion has systematically more-radiogenic Nd isotopic compositions (ε_{Nd} = 0 to +2) and lower Ce/Nb ratios (mostly 2–7) than the other intrusions. The least radiogenic Nd isotope compositions are found in the G2 gabbros and the G1 Cavanagh and Morgan Range intrusions (ε_{Nd} = –1 to –4, Ce/Nb = 3–13). Similarly low ε_{Nd} values are found at Kalka in South Australia (Wade, 2012). Rocks of the Alcurra Dolerite suite plot at an intermediate position (ε_{Nd} = –1 to +2, Ce/Nb ~ 3–5). Nebo–Babel overlaps with the Alcurra Dolerite suite (ε_{Nd} = –1.7 to 0.3, Ce/Nb = 5–7, except for the contaminated Nebo–Babel marginal rocks, which have ε_{Nd} as low as –3). Basement rocks in the Nebo–Babel area

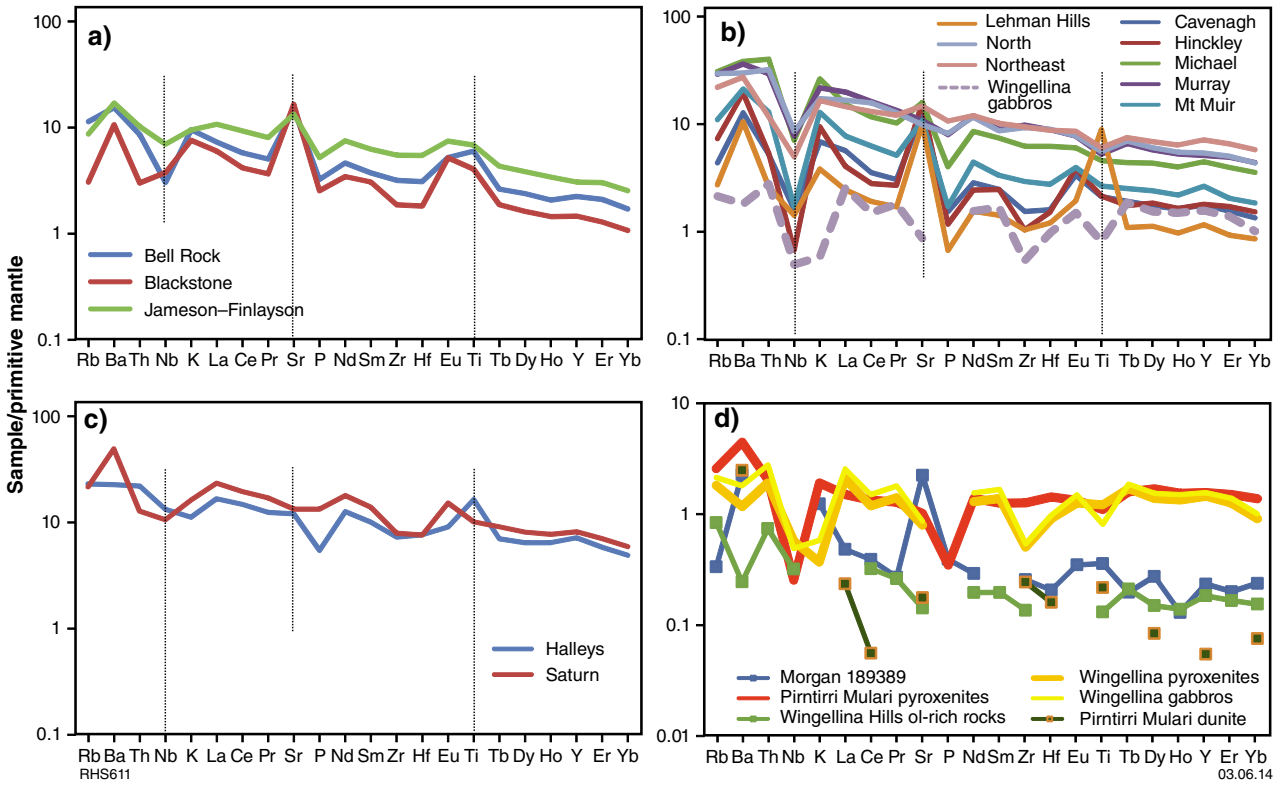

Figure 38. Primitive mantle-normalized multi-element variation diagrams of Giles intrusions: a) Evolved troctolitic intrusions; b) G1 gabbroic intrusions; c) late intrusions; d) ultramafic intrusions (ultramafic rocks only). Normalization factors from Sun and McDonough (1989). In b) 'North' and 'Northeast' refer to intrusions and intrusive fragments north of Mt Muir and Hinckley Range, respectively (see text for further explanation).

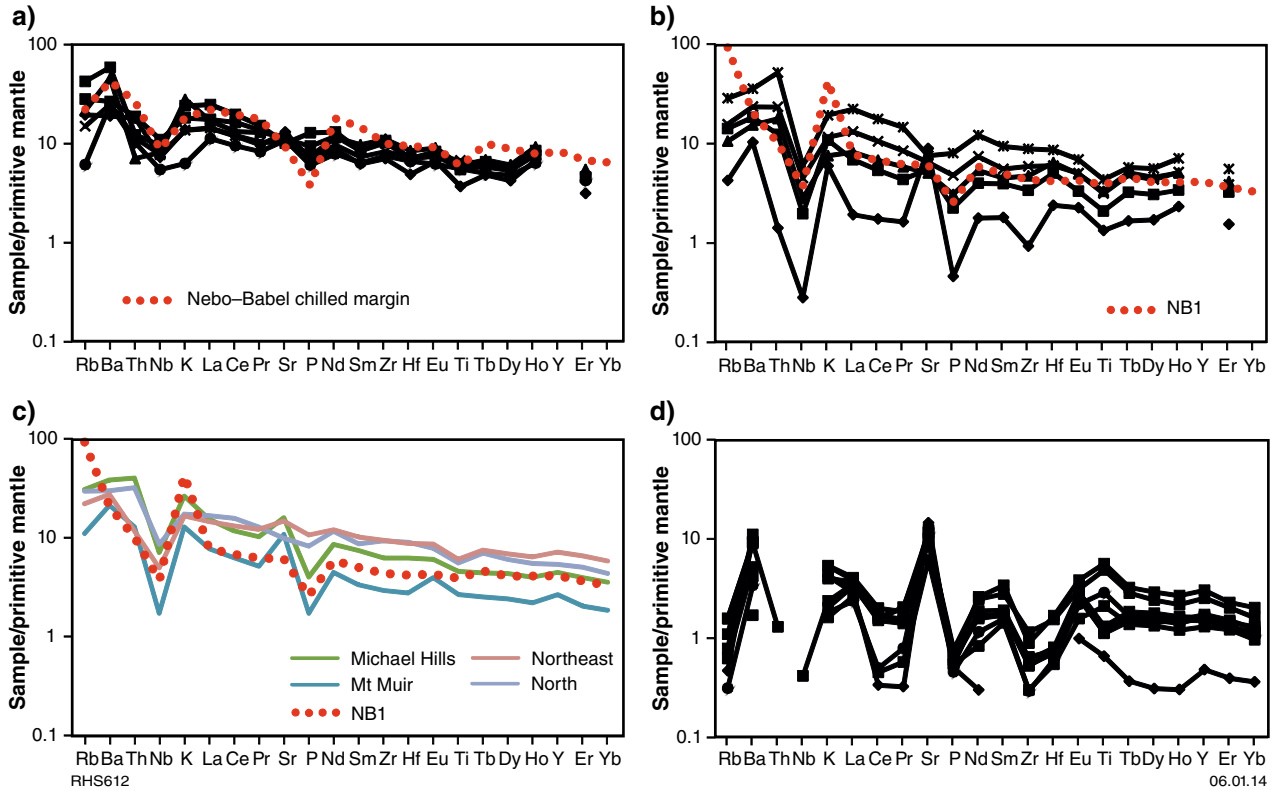

Figure 39. Primitive mantle-normalized multi-element variation diagrams for rocks of the Giles Event that may be liquids, including: a) unevolved samples of the Alcurra Dolerite suite; b) unevolved samples of the G2 gabbros; c) G1 gabbros enriched in incompatible trace elements; and d) Cavenagh microgabbros. Normalization factors are from Sun and McDonough (1989).

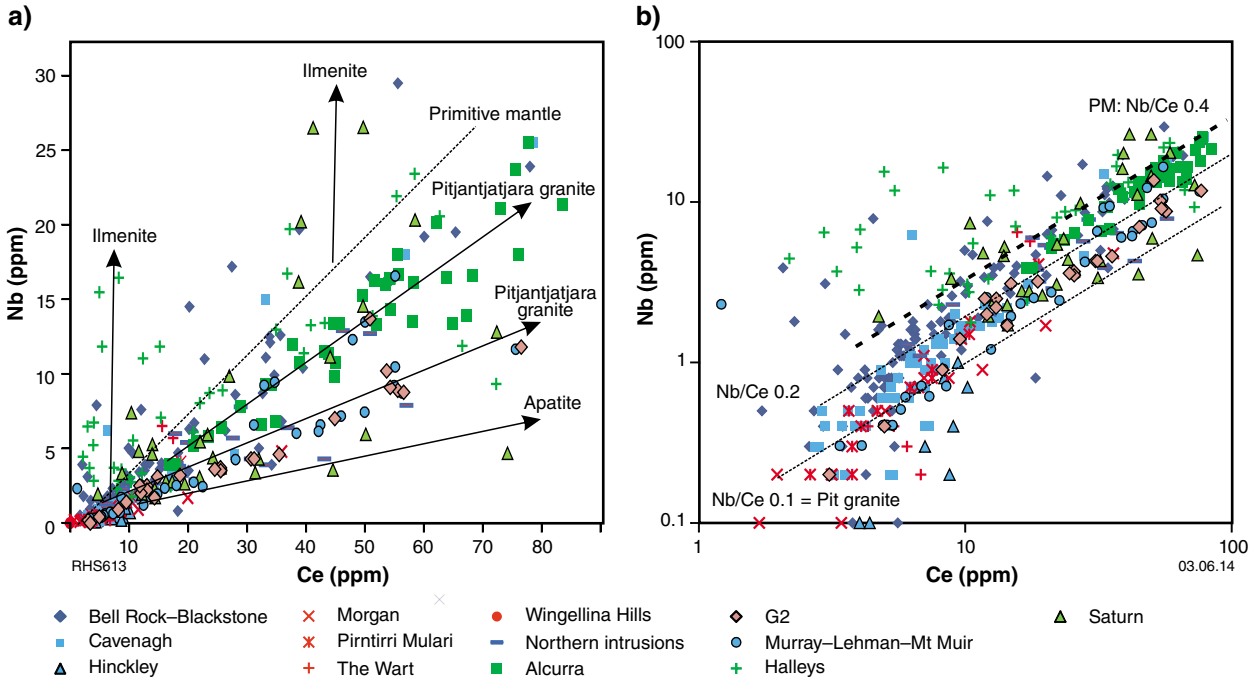

Figure 40. Binary variation diagrams of Nb vs Ce: a) vectors pointing to cumulus phases that may cause fractionation of Nb/Ce ratios, and potential contaminants in the rocks; and b) data plotted on a logarithmic scale to improve resolution between cumulate samples that have low trace element concentrations. Most of the troctolitic intrusions (Mantamaru), the Alcurra Dolerite suite, and the Halleys and Saturn intrusions have primitive mantle-like Nb/Ce ratios, whereas many of the other intrusions (notably Cavenagh, Hinckley Range, Murray Range, and the ultramafic intrusions) contain a crustal component, possibly of Pitjantatjara granite (Pit granite). 'Northern' intrusions include intrusive fragments to the north of Mt Muir and Hinckley Range.

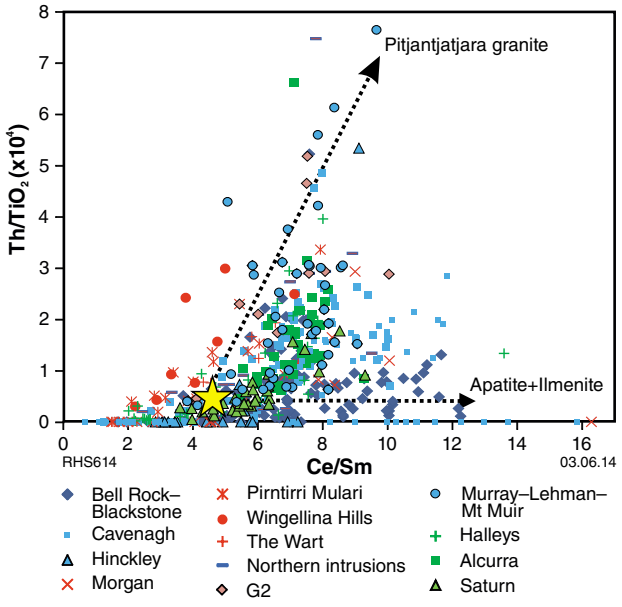

Figure 41. Binary variation diagram of Th/TiO_2 vs Ce/Sm for the Giles intrusions. Vectors point to potential contaminant (Pitjantjatjara granite) and cumulus apatite or ilmenite, which could shift the composition of the rocks to high Th/TiO_2 or Ce/Sm ratios, respectively. Yellow star denotes primitive mantle. 'Northern' intrusions include intrusive fragments to the north of Mt Muir and the Hinckley Range. Cavenagh data include samples from Staubmann (2010).

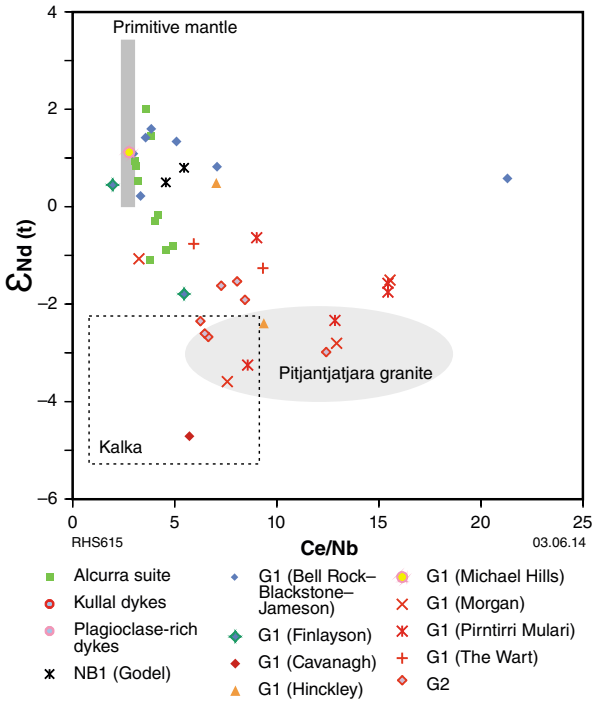

Figure 42. Plot of ε_{Nd} vs Ce/Nb for the Giles intrusions. Note that troctolitic G1 intrusions and the Alcurra Dolerite suite plot near the mantle range, whereas the other intrusions contain an enriched component. The compositional field of Pitjantjatjara granite contains the 10th–90th percentile of Ce/Nb data. Data for Kalka intrusion are from Wade (2006).

have ε_{Nd} values of –4.5 to –5 and Ce/Nb ratios of 9 (Seat et al., 2011), whereas the regional Pitjantjatjara granite suite has ε_{Nd} of –2 to –4 and highly variable Ce/Nb (5 to >20).

In situ Sr isotope analyses on plagioclase, determined by laser ICP-MS, are broadly consistent with the Nd isotope data. The least radiogenic Sr isotopic values are found in the Mantamaru and Halleys intrusions, with more-radiogenic values at Morgan Range, Lehman Hills, and Cavenagh. The Mantamaru and Halleys intrusions also show much less internal variation than the other intrusions (Fig. 43–45). Somewhat counter-intuitively, the wehrlite in the Pirntirri Mulari intrusion has the most radiogenic Sr isotopic value, and it is distinctly more radiogenic than the Pirntirri Mulari gabbronorite. The data are relatively homogenous and are thus unlikely to have been affected by alteration. The Halleys data overlap with those from Nebo–Babel (for which only whole-rock Sr data are available; Seat et al., 2011). Microgabbros from the Cavenagh intrusion have lower initial Sr isotope ratios (I_{Sr} = ($^{87}Sr/^{86}Sr)_i$ = 0.7042 – 0.7057) than Cavenagh medium-grained gabbros (I_{Sr} = 0.7052 – 0.7068) (Fig. 45). Furthermore, the medium-grained samples show greater isotopic variation (Fig. 45). Possibly, the relatively late-stage microgabbro magma was shielded from contamination due to lining of the feeder conduits by earlier mafic material.

A plot of initial Sr isotope ratio vs Ce/Nb ratio (Fig. 46) illustrates the relatively large crustal component in the Pirntirri Mulari, Morgan Range, and Lehman Hills intrusions, consistent with the ε_{Nd} vs Ce/Nb plot (Fig. 42). Notably, the Sr isotope data from the analysed intrusions broadly overlaps those from the different zones of the Kalka intrusion (Gray and Goode, 1989). Thus, almost the entire spread in Sr isotopic values seen within the suite of mafic–ultramafic intrusions from the west Musgrave Province can also be found within the single Kalka intrusion. In both cases, the ultramafic rocks contain the largest crustal component, with the anorthosites, leucogabbros, and troctolites having more mantle-like compositions.

Whole-rock sulfur isotope data are available for rocks of the Jameson intrusion, Nebo–Babel (Seat et al., 2009), the G2 gabbros, and the Alcurra Dolerite suite (Table 3, Fig. 47). We also collected data for sulfide-bearing rhyolites from the Bentley Supergroup in the Palgrave area (Figs 1 and 4). In situ (laser ablation ICP-MS) sulfur isotope data were collected from Halleys.

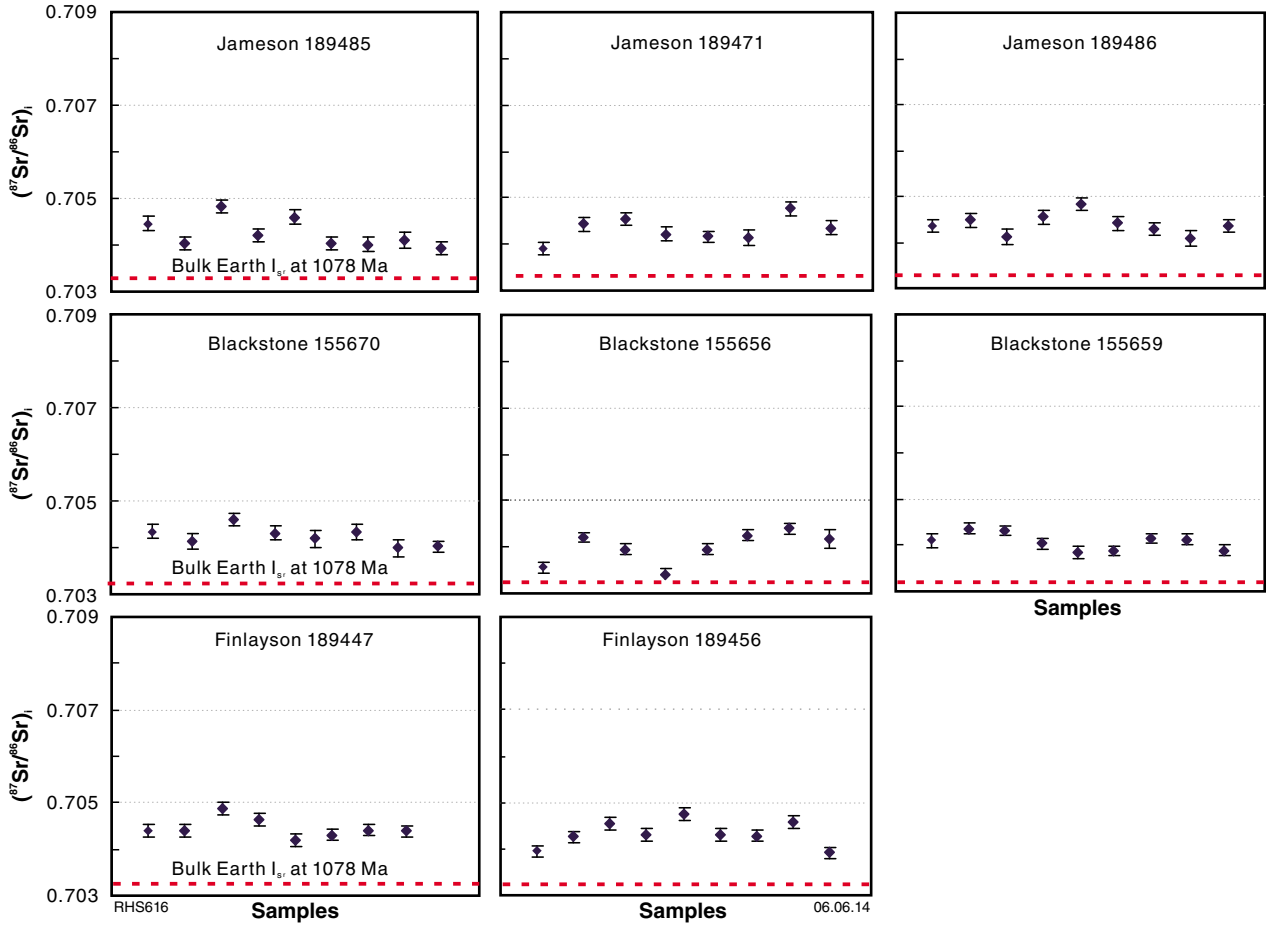

Figure 43. In situ Sr isotope data for the Mantamaru intrusion. Note that values in all three major outcrops of this intrusion overlap, are internally relatively homogenous, and plot relatively close to the bulk Earth Sr isotope value at 1078 Ma. Numbers refer to GSWA sample numbers.

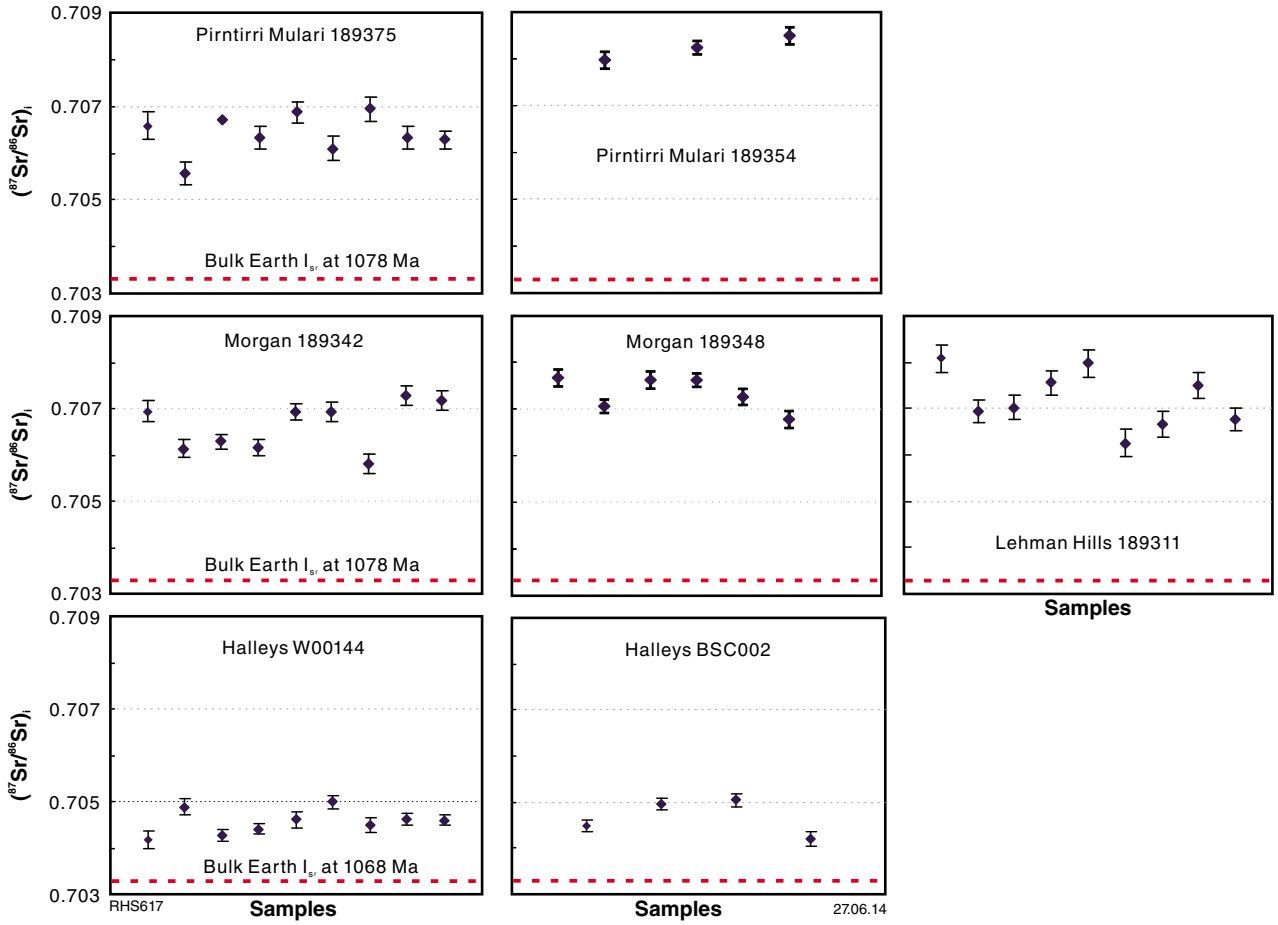

Figure 44. In situ Sr isotope data for Pirntirri Mulari, Morgan Range, Lehman Hills, and Halleys intrusions. Note relatively radiogenic values for Pirntirri Mulari, Morgan Range, and Lehman Hills, but less-radiogenic values for Halleys. Halleys also shows less intra-sample variation than the other intrusions. Numbers refer to GSWA sample numbers.

All mafic intrusions plot near the mantle range, suggesting that the sulfides are of mantle derivation, or that any crustal sulfides were juvenile or underwent no sulfur isotopic fractionation, or that the assimilated crustal sulfides equilibrated at high R-factors (mass ratio of silicate melt to sulfide melt; Campbell and Naldrett, 1979; Lesher and Burnham, 2001).

Sulfur and chalcophile elements

Sulfur concentrations of the intrusions of the Giles Event are mostly relatively low, at <200 ppm (Fig. 48a). Higher sulfur concentrations are present in the Wingellina Hills, The Wart, Saturn, Murray Range, Hinckley Range, 'North' and 'Northeast' intrusive fragments, the magnetite-rich samples of the Jameson–Blackstone intrusion, some of the G2 massive gabbros, and the Alcurra Dolerite suite. No sulfur data are available for the Halleys intrusion, although based on Cu concentrations >4000 ppm and petrographic observations, we estimate that the Halleys intrusion contains up to several percent sulfides. Sulfide-rich mafic intrusive rocks were also intersected at the Manchego Prospect (Phosphate Australia, 2014). The highest sulfide concentrations among the Giles intrusions are found at Nebo–Babel, where drilling intersected thick (several tens of metres) intervals containing several percent disseminated sulfides and massive sulfide lenses (up to 27 m thick) near the stratigraphic base of the intrusion (Seat et al., 2007).

Most mafic–ultramafic intrusions that formed during the Giles Event are relatively Cu poor (<200 ppm Cu, Fig. 48b), and there is a clear trend to higher Cu concentrations from the relatively unevolved (ultramafic) to the evolved (mafic) rocks, consistent with the incompatible nature of Cu in fractionating sulfur-undersaturated magma. The highest Cu concentrations occur in the Halleys and Nebo–Babel intrusions, in some samples from the Saturn intrusion, and the uppermost portions of the Jameson intrusion, including the massive magnetite layers which contain up to 700 ppm Cu. Elevated Cu concentrations are also found in the pyroxenites hosting the PGE reefs of the Wingellina Hills intrusion (≤500 ppm Cu), and in a sulfide-bearing (?reef) pyroxenitic sample from the Pirntirri Mulari intrusion (350 ppm Cu). However, in most mafic–ultramafic intrusions formed during the Giles Event, elevated Cu (and S) concentrations are the exception.

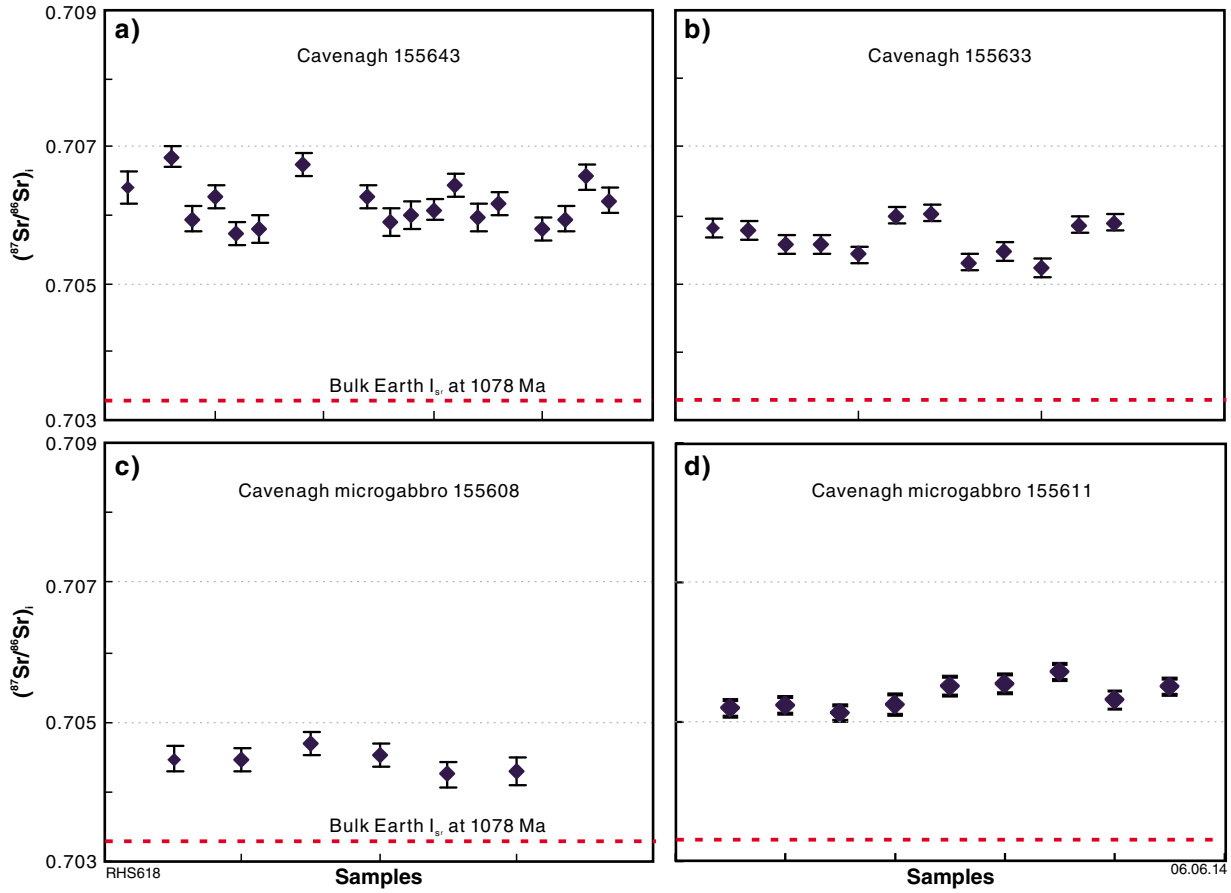

Figure 45. In situ Sr isotope analyses for the Cavenagh intrusion. Note that fine-grained microgabbros have less-radiogenic values than the medium-grained Cavenagh samples, and show less internal variation between grains. Numbers refer to GSWA sample numbers.

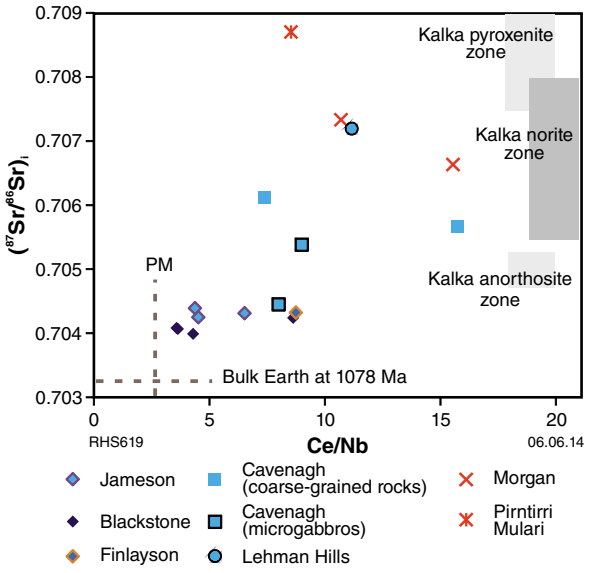

Figure 46. Variation diagram of initial Sr isotope ratio vs Ce/Nb ratio (primitive mantle value for Ce/Nb from Sun and McDonough, 1989; bulk Earth value from De Paolo and Wasserburg, 1976). Data for Kalka are from Gray and Goode (1989). Note that the Kalka intrusion shows almost the entire spread of Sr isotope values seen in the Giles intrusions in the west Musgrave Province. PM = primitive mantle

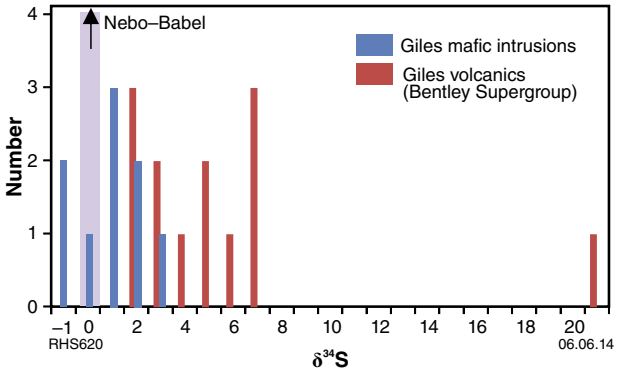

Figure 47. Sulfur isotope data for mafic and felsic magmatic rocks of the west Musgrave Province. Nebo–Babel data (shaded bar) are from Seat et al. (2009).

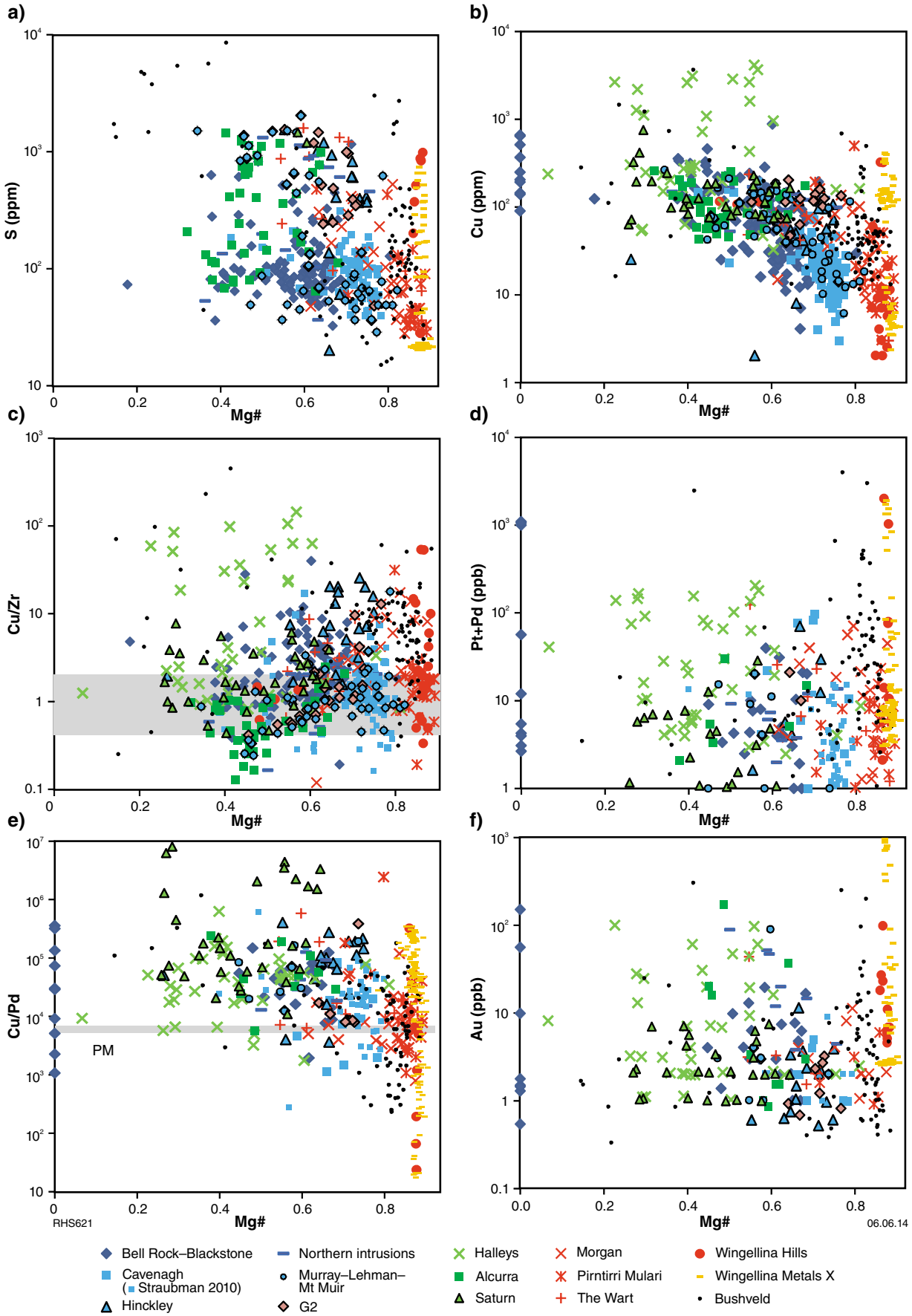

Figure 48. Binary variation diagrams vs Mg# of: a) S; b) Cu; c) Cu/Zr; d) Pt+Pd; e) Cu/Pd; and f) Au. Shaded bar in c) denotes range in Cu/Zr ratio in Southern African continental flood basalts (from Maier et al., 2003a). Primitive mantle value in e) is from Barnes and Maier (1999).

The Cu/Zr ratios of many of the rocks (Fig. 48c) plot between 0.5 and 2, in the range of many sulfur-undersaturated basalts globally (e.g. southern African flood basalts; Maier et al., 2003a). These data are consistent with the relative paucity of sulfides in many intrusions formed during the Giles Event. In view of the PGE depletion of most intrusions (discussed below), indicating that the Giles magmas reached sulfur saturation relatively early, the low Cu/Zr ratios are noteworthy. Possibly, Cu/Zr ratios are not affected by the equilibration of sulfide at the high R-factors that likely applied to the large Giles intrusions. Elevated Cu/Zr ratios, indicating the presence of cumulus sulfide, are largely confined to the most differentiated or contaminated intrusions (Mantamaru, Halleys, Saturn, Hinckley Range), although they also occur at Morgan Range and Nebo–Babel, and in the websterite-hosted PGE reefs of the Wingellina Hills intrusion. In the latter two intrusions, sulfides have clearly been concentrated more efficiently than in the other intrusions, for reasons discussed later.

Most of the intrusions contain <30 ppb Pt+Pd (Fig. 48d). Notable exceptions are the pyroxenite-hosted PGE reefs of the Wingellina Hills intrusion, containing up to several parts per million PGE, the sulfide-bearing pyroxenitic sample from the Pirntirri Mulari intrusion (200 ppb PGE, not shown in Fig. 48d due to lack of major element data), and the samples from the pipe-like body in the Halleys intrusion (up to 200 ppb PGE). Other PGE-rich sulfides not plotted include those from Nebo–Babel and Manchego. The upper magnetite-enriched portions of the Jameson intrusion have up to about 2 ppm PGE. Scattered PGE enrichment, not necessarily accompanied by sulfide enrichment, has also been found in a few samples from the Morgan Range (≤80 ppb), The Wart (one sample with 120 ppb), and Cavenagh (three samples with 75–100 ppb) intrusions. We considered whether these elevated PGE concentrations could be the result of hydrothermal metal mobility, but most of these rocks are unaltered, are enriched in both Pt and Pd, and have low LOI values, whereas most hydrothermal PGE enrichments resemble highly variable Pt/Pd ratios.

Most samples from the Giles intrusions have Cu/Pd ratios above primitive mantle values (~7000); thus, they are PGE depleted relative to the primitive mantle (Fig. 48e). Cu/Pd ratios progressively increase with decreasing Mg#, consistent with sulfide saturation reached at a relatively early stage of magmatic fractionation. Platinum group element – rich samples (Cu/Pd < primitive mantle) are mostly confined to the Wingellina Hills, Pirntirri Mulari, Morgan Range, and Cavenagh intrusions; that is, rocks with Mg# mostly >60. The greatest spread of Cu/Pd ratios, with both fertile and depleted samples, is found in the Wingellina Hills intrusion. The Halleys and Saturn intrusions have Cu/Pd ratios mostly above primitive mantle values, despite the enrichment in PGE. This finding could suggest that the magma was already PGE depleted when sulfide saturation occurred, that it assimilated Cu-rich crust, or that the mantle source was relatively enriched in Cu. Magnetite layer 1 from the Jameson intrusion also has low Cu/Pd ratios (lower than primitive mantle), suggesting that this intrusion did not previously reach sulfur saturation or that its upper portion crystallized from a new fertile magma batch replenishing a PGE-depleted resident magma.

Gold concentrations show a broadly similar distribution to PGE concentrations (Fig. 48f), with relatively high values in the Wingellina Hills and Halleys intrusions, and the upper portions of the Mantamaru intrusion. Most other intrusions show low Au concentrations. Notable exceptions are some of the northern intrusive fragments (to the north of Mt Muir and Hinckley Range), which contain up to 90 ppb Au, without concomitant PGE enrichment. These samples are also relatively sulfur rich, possibly suggesting hydrothermal origin for the Au, or contamination with Au–S-rich crustal rocks.

Most samples that contain significant liquid components (NB1 dykes, the Alcurra Dolerite suite, and Nebo–Babel chilled margins) are PGE depleted, having Cu/Pd ratios above mantle values (>10 000). The main exceptions are the primitive G2 gabbros, many of which contain 10–15 ppb Pt and Pd each, and Cu/Pd ratios broadly at mantle levels. Gold concentrations are relatively low in the NB1 dykes, the G2 gabbros, and the Nebo–Babel chilled margins (mostly 1–3 ppb Au), although they are markedly higher in the Alcurra Dolerite suite, of which several samples contain >10 ppb Au.

Mineral chemistry

In the present study we determined the compositions of olivine, orthopyroxene, clinopyroxene, and plagioclase in more than 50 rock samples from the intrusions formed during the Giles Event (although not in rocks of the Alcurra Dolerite suite or the G2 massive gabbros).

Olivine has between 40 and 87 mol.% Fo (Fig. 49). Variation within individual intrusions is pronounced, possibly reflecting multiple magma replenishment or variable contamination, consistent with considerable variation in in situ Sr isotope ratios of plagioclase, such as within the Cavenagh intrusion (Fig. 45). In general, olivine from parts of the Cavenagh and Blackstone intrusions show the lowest Fo values, whereas the highest values in olivine are shown in the Wingellina Hills, Pirntirri Mulari, The Wart, and Morgan Range intrusions. Samples from the Jameson, Saturn, Hinckley Range, Murray Range, Nebo–Babel, Lehman Hills, and Latitude Hill intrusions contain olivine with intermediate Fo contents. The lack of an olivine gap in the G1 intrusions, analogous to that seen in olivine from the Bushveld Complex (Eales and Cawthorn, 1996), may reflect derivation of the magmas from a common deeper staging chamber(s) (Ballhaus and Glikson, 1995). We proposed that at high pressure, olivine was a liquidus phase that crystallized cotectically with pyroxene.

The Ni concentration of olivine from the mafic and mafic–ultramafic intrusions related to the Giles Event reaches up to 3500 ppm (Fig. 49a), showing a positive correlation with Fo content. These Ni concentrations are higher, at comparable Fo contents, than in olivines from most basic magmas globally, although a similar pattern of relatively high Ni concentrations is found in many

other layered intrusions, including the Bushveld Complex and the Stillwater intrusion (Fig. 49b). The highest Ni concentrations in olivine identified so far in magmatic rocks are found in the Kevitsa intrusion of Finland (up to 1.5 wt% Ni; Yang et al., 2013).

The origin of the Ni enrichment in the layered intrusions remains poorly understood. Several models may be considered, none of which is entirely satisfactory.

1. Equilibration of olivine with trapped melt lowering the Fo content without affecting Ni concentrations — This process should result in the decoupling of Fo from Ni concentrations in olivine, and from the An contents of comagmatic plagioclase, as at Cavenagh and Hinckley Range (Fig. 50a). This model was preferred by Staubmann (2010), who conducted a detailed study of olivines in part of the Cavenagh intrusion. However, Ni enrichment has also been identified in olivines from fine-grained dykes related to the G1 intrusions (NB1 suite of Godel et al., 2011), which should not be affected by trapped melt percolation. The high Ni concentrations are thus at least in part an early magmatic phenomenon.

2. Equilibration of olivine with percolating sulfide liquid — This model is considered unlikely, as most intrusive rocks related to the Giles Event are relatively sulfide poor.

3. Assimilation of Ni-rich sulfide by the magmas before final emplacement — Presently this model is also considered unlikely due to the paucity of magmatic Ni sulfides in the west Musgrave Province crust.

4. Magma derivation from a pyroxenitic–eclogitic mantle source (Sobolev et al., 2011) — This model implies that most layered intrusions globally are derived from pyroxenitic mantle sources, for which there is presently no evidence.

5. Reduction of the magma (for example, due to contamination), resulting in relatively low Fo contents — The oxygen fugacity of the Giles layered intrusions is thought to be around a quartz–fayalite–magnetite (QFM) buffer (Staubman, 2010), similar to most other mafic–ultramafic crustal rocks.

6. Polybaric magmatic fractionation, with initial crystallization of pyroxene at depth depleting the magma in MgO relative to Ni, followed by magma ascent and final emplacement at lower pressure, under which conditions olivine may become stable — The high Ni concentration of the magma and the relatively high D_{Ni} at low pressure (Li and Ripley, 2010) would result in elevated Ni in olivine. This model has been applied to Ni-rich olivines in the Kunene Complex, Namibia (Maier et al., 2013a). An early, high-pressure, stage of (clino)pyroxene crystallization would be consistent with distinctly lower Cr/Al ratios of pyroxenes in the Giles intrusions relative to the Bushveld Complex (Fig. 51b), although the model leaves the elevated Ni concentrations of olivine in other intrusions (e.g. the Bushveld Complex) unexplained.

Plagioclase from intrusions related to the Giles Event studied here contains between 48 and 87 mol.% An (Fig. 50). The highest An contents occur in gabbros from The Wart intrusion (An 69–87). Slightly lower An contents (mostly between 75 and 80 mol.%, with several samples with An as low as 65) are present in gabbronorites from the Morgan Range intrusion. The lowest An contents in cumulus plagioclase occur in the Blackstone and Saturn intrusions. Intercumulus plagioclase in ultramafic rocks typically has lower An contents than cumulus plagioclase in mafic rocks; plagioclase in pyroxenites from The Wart intrusion have An 62–74, whereas those in ultramafic rocks from the Pirntirri Mulari intrusion have the lowest An contents of all intrusions, at <66 mol.%. Notably, gabbros of the Pirntirri Mulari intrusion also have lower An (<70) than gabbroic rocks from The Wart intrusion. Iron concentrations of plagioclase show no correlation with An contents, analogous to, for example, the Bushveld Complex (Maier and Eales, 1997). Most plagioclase analysed here has <0.3% FeO, although those in the Cavenagh and Latitude Hill intrusions form exceptions, in that they have markedly higher Fe concentrations, up to 0.8% FeO.

Anorthite contents of plagioclase show a positive correlation with Fo in olivine (Fig. 50), with the exception of some samples from the Hinckley and Cavenagh Ranges, some Ewarara samples (not shown), and one sample from the Pirntirri Mulari intrusion. The latter intrusion has much lower An contents than the other intrusions with similar Fo contents (see also Ballhaus and Glikson, 1995). The variation in anorthite content at relatively constant Fo in the Hinckley Range and Cavenagh intrusions may be due to reaction of olivine with percolating residual Fe-rich melt. The An–Fo compositional trend overlaps with that of the Bushveld Complex, although the latter has an olivine gap at Fo 60–80 because the peritectic reaction of olivine to pyroxene temporarily destabilizes olivine. Ballhaus and Glikson (1995) proposed that the lack of an olivine gap in the Giles intrusions is due to polybaric fractionation, as discussed above.

In the rocks studied here, orthopyroxene Mg# is 0.6 – 0.89 (Fig. 51a). The ultramafic intrusions show the highest values, notably at Pirntirri Mulari and The Wart, whereas orthopyroxene in the Blackstone intrusion shows the lowest Mg# values. The Cr_2O_3 concentration in orthopyroxene is up to 0.9 wt%, decreasing rapidly with decreasing Mg#. The highest Cr concentrations occur in Pirntirri Mulari and The Wart orthopyroxenes, with Morgan Range orthopyroxenes having slightly lower Cr concentrations. The remaining intrusions contain <1000 ppm Cr in orthopyroxene.

In a plot of Cr_2O_3 vs Al_2O_3 (Fig. 51b), two sample populations can be distinguished for the Pirntirri Mulari intrusion: one shows relatively high Cr/Al ratios and the other relatively low Cr/Al ratios. The orthopyroxenes analysed here have broadly similar Cr concentrations to orthopyroxenes from the Bushveld Complex, although markedly higher Al concentrations. The high Al concentrations in the intrusions related to the Giles Event could reflect a higher pressure of crystallization (Ballhaus and Glikson, 1995; Goode and Moore, 1975), although

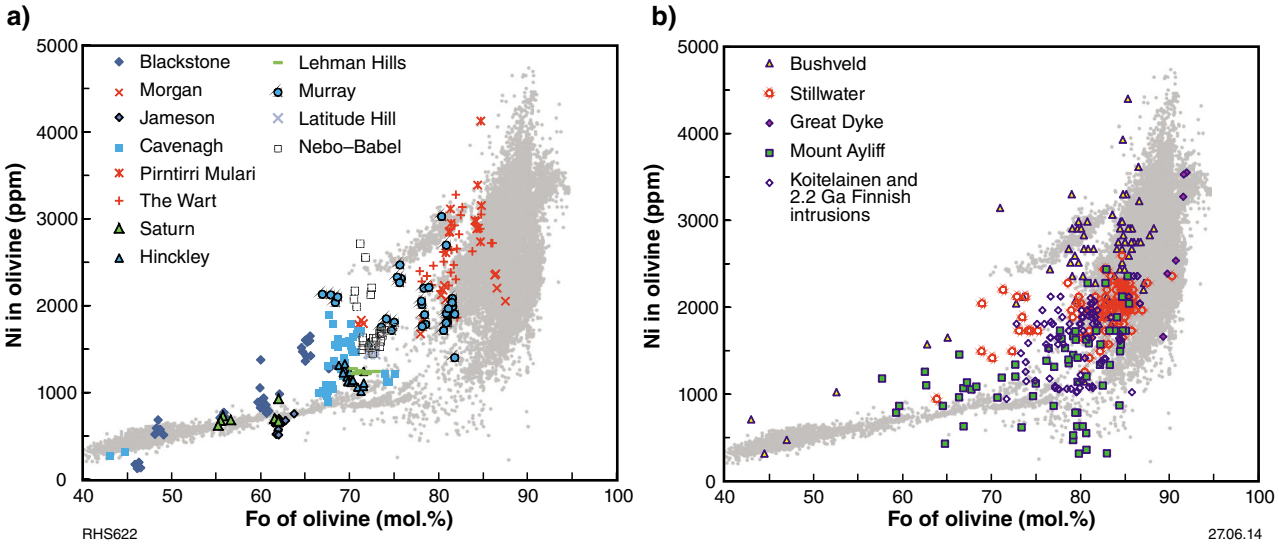

Figure 49. Plot of Ni vs Fo in olivine: a) data from the west Musgrave Province; b) global data of layered intrusions (data compiled from Teigler and Eales, 1996; Maier and Eales, 1997; Lightfoot and Naldrett, 1983; Raedeke, 1982; E Hanski, unpublished data). Grey shading is background data, from Sobolev et al. (2011).

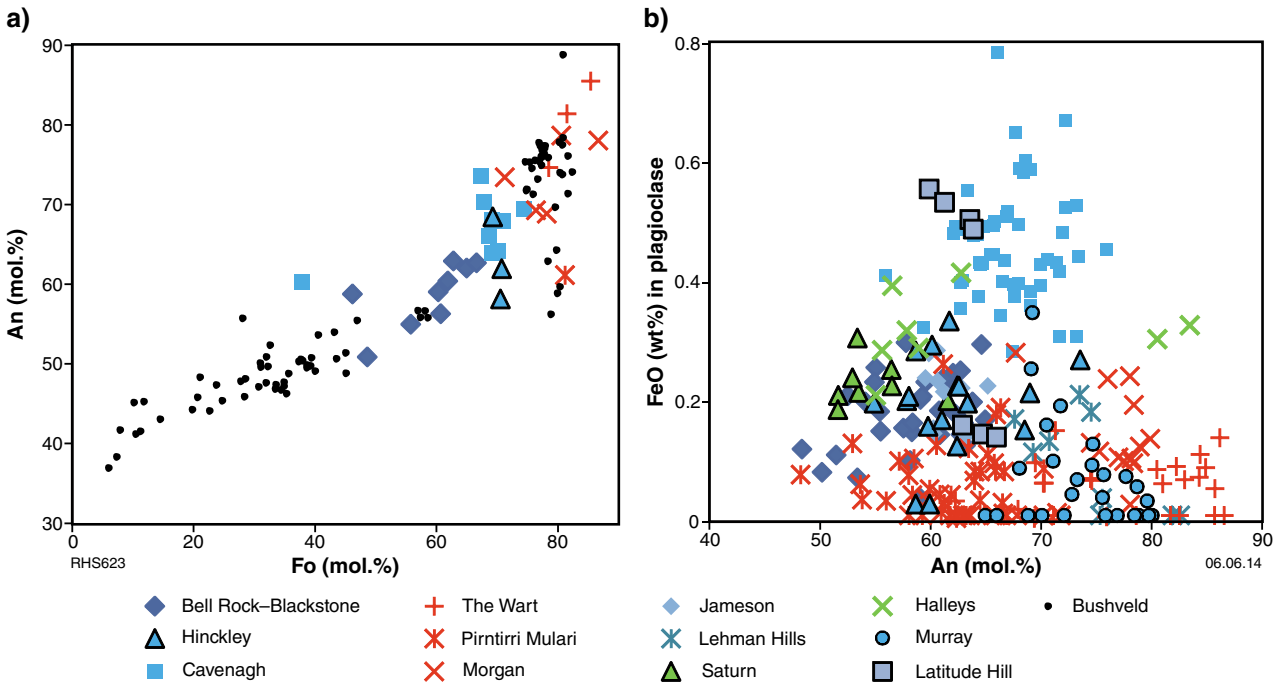

Figure 50. Composition of plagioclase in the Giles intrusions: a) anorthite content vs Fo content; and b) FeO vs anorthite content. Note lack of olivine gap, such as found, for example, in the Bushveld Complex. Bushveld data are from Teigler and Eales (1996) and Maier and Eales (1997).

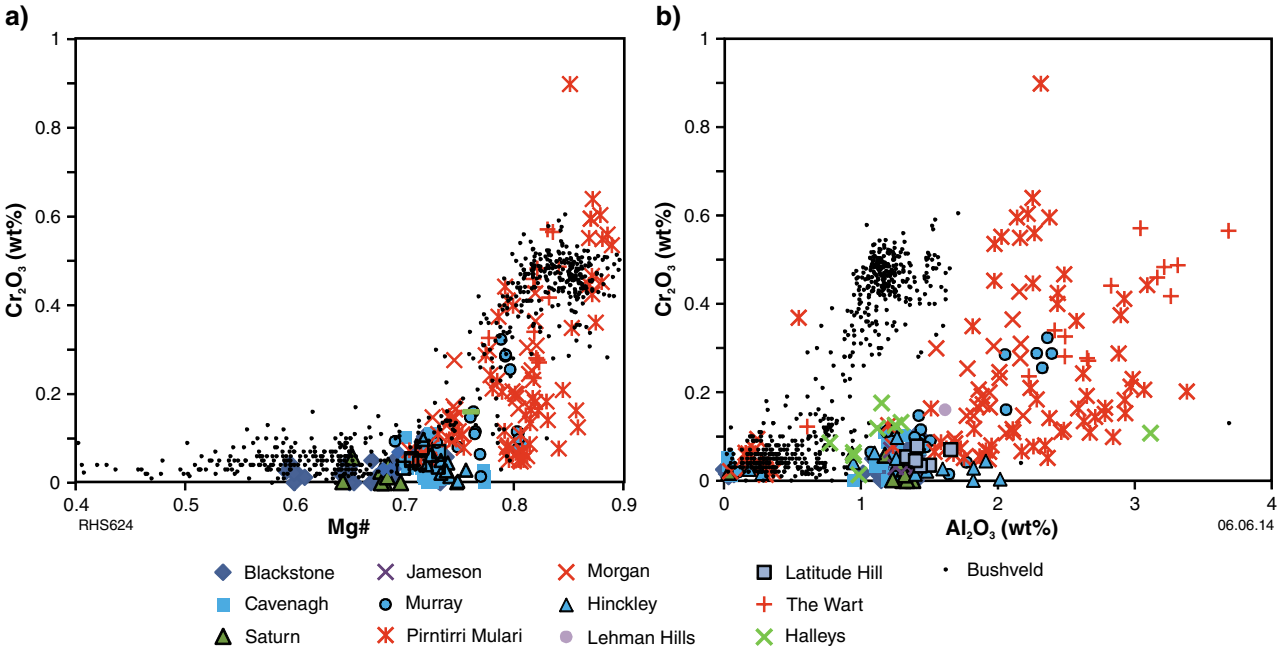

Figure 51. Composition of orthopyroxene in the Giles intrusions: a) Cr_2O_3 vs Mg#; b) Cr_2O_3 vs Al_2O_3. Note that Giles orthopyroxenes have distinctly higher Cr_2O_3/Al_2O_3 ratios than Bushveld orthopyroxene. Bushveld data are from Teigler and Eales (1996) and Maier and Eales (1997).

it remains unclear why this would not have resulted in simultaneous Cr enrichment, because Cr substitutes for Al in the orthopyroxene lattice. Alternatively or additionally, the Giles Event magmas may have assimilated plagioclase-rich lower crust. Nickel concentrations of orthopyroxene reach up to 1000 ppm (not shown), in the same range as orthopyroxene in the Bushveld Complex (Teigler and Eales, 1996). The highest Ni concentrations are found in the Pirntirri Mulari intrusion, followed by The Wart and Cavenagh intrusions. The latter intrusion shows the most significant variation in Ni concentrations of orthopyroxene.

The composition of clinopyroxene is plotted in Figure 52. Aluminium concentrations show a weak positive correlation with Cr concentrations. Clinopyroxene from the Pirntirri Mulari, The Wart, and Wingellina Hills intrusions is relatively Al and Cr rich (with up to 5% Al_2O_3 and 1.5% Cr). Clinopyroxenes from the other intrusions have <0.6 wt% Cr_2O_3 and <3.5 wt% Al_2O_3. Clinopyroxene from the Hinckley Range intrusion shows higher Al/Cr ratios than the other intrusions, possibly reflecting contamination of the Hinckley Range magma with granite (Fig. 52). In a Cr vs Mg# plot (Fig. 52b), clinopyroxene shows good overlap with the Bushveld Complex, although in a Cr_2O_3 vs Al_2O_3 plot it is evident that clinopyroxene in the intrusions related to the Giles Event has significantly lower Cr/Al ratios than clinopyroxene in the Bushveld Complex, analogous to orthopyroxene.

In the present study, chromite has only been analysed in one sample from the Pirntirri Mulari intrusion, although our data can be compared with the large database on Wingellina Hills chromite published by Ballhaus and Glikson (1989). Chromite in the Giles intrusions tends to be more Al-rich (Cr/Al < 1) than many other layered intrusions such as the Bushveld Complex (Teigler and Eales, 1993) and the Great Dyke (Wilson, 1982). Chromite from the Pirntirri Mulari intrusion has a Cr/Al ratio of 0.25, and Cr_2O_3 concentrations reach 27 wt%, somewhat lower than that of the Wingellina Hills intrusion (34 wt% Cr_2O_3), whereas chromite from the Bushveld Complex contains >40 wt% Cr_2O_3. Spinel inclusions in olivine have less Cr than do spinel within clinopyroxene, as has been found at Jimberlana (Roeder and Campbell, 1985), possibly because olivine is more permeable for diffusional exchange (Ballhaus and Glikson, 1989).

Notably, chromite in wehrlite from the Pirntirri Mulari intrusion is present mostly within clinopyroxene and plagioclase, although it may also form inclusions in olivine. This suggests that the magma reached chromite saturation before or during olivine crystallization. Ballhaus and Glikson (1989) argued that the Wingellina Hills magma was chromite-undersaturated and chromite was only temporarily stabilized during the formation of wehrlites in response to supercooling. However, PELE modelling (Boudreau, 1999) of an NB1 dyke composition that is a potential parent melt to the ultramafic Giles intrusions indicates a crystallization sequence of chromite–olivine–clinopyroxene–plagioclase–orthopyroxene at pressures of 1–5 kbar and an oxygen fugacity between QFM and QFM-1. Olivine–chromite cumulates would thus not be unexpected in the Giles intrusions. We suggest that the chromite-poor websterites could have formed due to destabilization of chromite after pyroxene appeared on the liquidus. Sorting of chromite-bearing protocumulates may also have played a role, analogous to the model of Maier et al (2013b) for the Bushveld Complex.

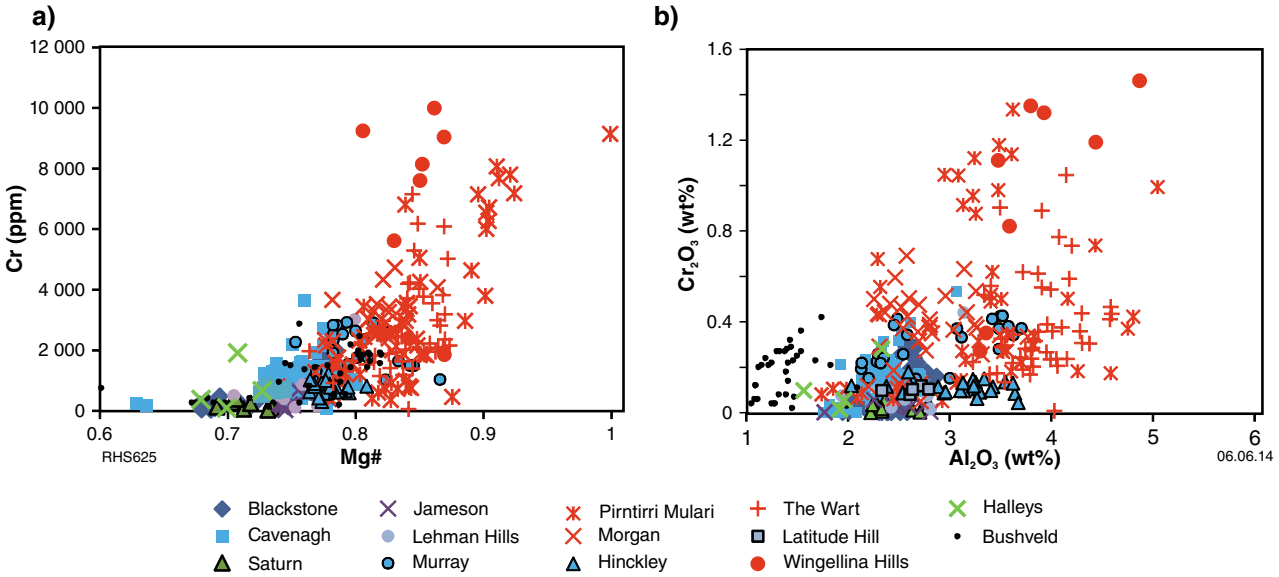

Figure 52. Composition of clinopyroxene in the Giles intrusions: a) Cr_2O_3 vs Mg#; b) Cr_2O_3 vs Al_2O_3. Bushveld data are from Mitchell (1986), Teigler and Eales (1996), and Maier and Eales (1997).

Discussion

Parental magmas to intrusions related to the Giles Event

The identification of the parental magma to an intrusion is of great interest to petrologists and economic geologists because this provides information on the nature of the mantle source, potential interaction of the magma with crust, the crystallization history of the intrusion, and the prospectivity of an igneous suite to host magmatic mineral deposits. The composition of parental magmas may be estimated using various methods. One of the most common approaches is the study of the chilled margins of intrusions. Potential chilled margins have been described from Ewarara and Kalka (Goode, 1970) and Nebo–Babel (Seat et al., 2007). The latter have been well characterized, and contain 7–9 wt% MgO. However, chilled margins of intrusions are commonly contaminated and thus not necessarily representative of the primary magma.

Another approach could be to consider microgabbroic rocks that are present within some of the Giles intrusions, including the Cavenagh, Murray Range, and Pirntirri Mulari intrusions. The mineral compositions in the microgabbros overlap with those in their medium-grained host rocks, suggesting the microgabbros are cogenetic with the parental liquids to the intrusions. However, many of the microgabbros are cumulates, as indicated by their low incompatible element concentrations, notwithstanding their apparent high cooling rate and the presence of quench textures. The average composition of 29 microgabbro samples from the Cavenagh intrusion (data of Staubmann, 2010; present data) is 11.9 wt% MgO and 9.48 wt% FeO_T, with 511 ppm Cr, 318 ppm Ni, and 10 ppm Zr. The microgabbros thus provide restricted further insight to the composition of the magma.

A method that has been used with success in the Bushveld Complex is the examination of fine-grained sills or dykes in the footwall of an intrusion (Sharpe, 1981; Godel et al., 2011). Therefore, considerable effort has been made to characterize the dyke suites in the west Musgrave Province (Howard et al., 2006b; Godel et al., 2011). For the ultramafic portions of the G1 intrusions, the fine-grained low-Ti tholeiitic 'plagioclase-rich dykes' first described from the Bell Rock Range area (Howard et al., 2007), and which are equivalent to the NB1 dyke type of Godel et al. (2011), provide a suitable parent.

A further potential parental magma type could be the primitive members of the G2 massive gabbros. These contain about 10–13 wt% MgO, 12 wt% FeO_T, 350 ppm Ni, up to 700 ppm Cr, and 10–15 ppb each of Pt and Pd. This composition is broadly consistent with the original estimation of Ballhaus and Glikson (1989) for the parental magma of the Wingellina Hills intrusion. Based on the composition of olivine, these authors suggested that the magma was a tholeiitic basalt with approximately 12 wt% MgO and 200 ppm Ni (assuming olivine with an Fe/Mg ratio 0.3 times that of a coexisting melt and D_{Ni} olivine–melt = 10). Li and Ripley (2010) suggest that for a magma with 12 wt% MgO the D-values of Ni into olivine are probably about 8; thus the magma probably contained 300–400 ppm Ni. For the Cr concentration of the magma, Ballhaus and Glikson (1995) suggested a value of 150–200 ppm, based on clinopyroxene–melt partition coefficients of around 10.

Crystallization of the Wingellina Hills intrusion from NB1-type magma is consistent with whole-rock variation of Wingellina Hills harzburgites, which plot along the

tieline from primitive Wingellina Hills olivine to NB1 (Fig. 53). None of the other c. 1070 Ma dyke suites analysed by Godel et al. (2011) or Howard et al. (2006b) provides a suitable fit. Furthermore, Godel et al. (2011) modelled that NB1-like compositions would reach sulfur saturation after 30% crystallization, during the appearance of plagioclase on the liquidus, consistent with the position of the PGE reefs in the Wingellina Hills intrusion. Note that the Nd isotopic signature of NB1 is slightly more radiogenic than that of the ultramafic intrusions (Fig. 42). By contrast, the G2 gabbros have a less-radiogenic composition than the ultramafic intrusions. Thus, the parental magma must have been variably contaminated during or after emplacement, consistent with variable Nd isotopic signatures of all ultramafic intrusions.

Our modelling using the PELE software (Boudreau, 1999) indicates that NB1 has a crystallization order of chromite>olivine+chromite>olivine+chromite+clinopyroxene>chromite+clinopyroxene+plagioclase +orthopyroxene, broadly consistent with petrographic observations on the Pirntirri Mulari and Wingellina Hills intrusions. The modelled Fo content at 1–5 kb is 87 mol.%, similar to that in the intrusions. The chromite-poor websterites at Pirntirri Mulari, The Wart, and Wingellina Hills would be explained by contamination (destabilizing olivine), minor changes in pressure (changing phase equilibria to remove the magma from the clinopyroxene–olivine cotectic), or some sorting process to fractionate clinopyroxene from olivine and chromite. The basal succession at the Wingellina Hills and Kalka (South Australia) intrusions, and most of the central portions of Pirntirri Mulari, have a crystallization sequence olivine>orthopyroxene+olivine+chromite>orthopyrene+clinopyroxene, indicating that there exist at least two different liquid lines of descent in the intrusions related to the Giles Event. This situation is analogous to the Muskox intrusion, where the basal rocks show a crystallization sequence of olivine>clinopyroxene+olivine, whereas the upper units show olivine>olivine+orthopyroxene. Irvine (1970) suggested that the latter rocks formed from a liquid that was contaminated with partial melts of the roof. By contrast, Ballhaus and Glikson (1989) proposed that the orthopyroxene-rich rocks formed due to mixing of primitive magma with Si-rich (evolved) resident magma. However, this model is difficult to reconcile with the thick harzburgitic intervals found at the base of the Wingellina Hills intrusion.

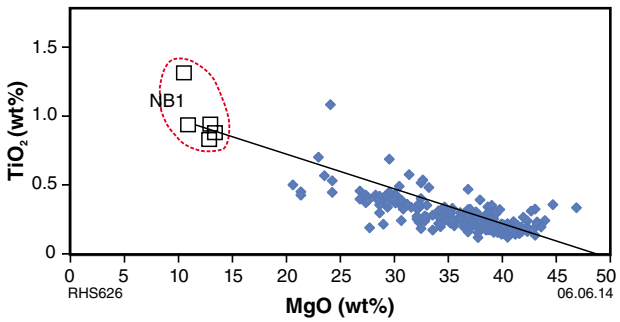

Figure 53. Whole-rock data (blue diamonds) from drillcore intersecting basal portion of Wingellina Hills intrusion (data normalized to volatile free assuming 10% loss-on-ignition). Note that the data plot near a tieline between Wingellina Hills olivine and NB1 (open square symbols), consistent with a model whereby the composition of Wingellina Hills rocks is controlled by olivine and NB1 liquid.

The Nebo–Babel chilled margin may be a good candidate for the parental magma to the gabbroic intrusions. This chilled margin is a basalt with 7–9 wt% MgO and Mg# of 51–61, broadly equivalent to the NB3 dykes of Godel et al. (2011) (a Ti-depleted basalt with 6–8 wt% MgO). However, Godel et al. (2011) suggested that this magma is itself a result of mixing of Mg-basaltic NB1 and the Alcurra Dolerite suite. The most primitive members of the Alcurra Dolerite suite have 8–9 wt% MgO and Cr/V ratios of 2–4 (Table 1). Based on similarities in incompatible trace element ratios and common enrichment in mica and sulfide, the Alcurra Dolerite suite provides a good candidate for the parental magma to the Halleys and Saturn intrusions (Howard et al., 2009). Godel et al. (2011) further proposed that the Alcurra Dolerite suite is equivalent in composition to the NB4 dykes. Both have broadly similar MgO contents and are PGE depleted. The combined data thus suggest that the parental magma to the gabbroic intrusions was of broadly basaltic composition, with <10 wt% MgO, possibly represented by NB3 or the Nebo–Babel chilled margin. The broad similarity in the trace element patterns for all mafic intrusions could suggest that all were derived from a similar source, although followed by variable differentiation and contamination.

Ballhaus and Glikson (1995) suggested that the magma parental to the gabbroic and troctolitic intrusions is a differentiated residue of the primitive magmas. This may be true, although in that case fractionation of the primary magma must have pre-dated contamination of the parental magma to the ultramafic bodies because our Nd isotope data indicate relatively unradiogenic (i.e. more crustally contaminated) Nd isotope compositions in the ultramafic intrusions, and relatively radiogenic (less contaminated) Nd isotope compositions in the troctolitic intrusions. It would be feasible that all magmas were derived from the same mantle source, followed by variable degrees of contamination. Potentially, the magmas could have ponded at the base of the crust and then drained through major lineaments or faults during the formation of the Ngaanyatjarra Rift. The troctolitic intrusions would have been least contaminated because they intruded either early into cold crust, or late into refractory crust. However, the ultramafic intrusions and the G2 magmas were contaminated relatively strongly (or the effects of contamination are more readily detected due to lower trace element concentrations in the magmas; see below), and the Alcurra Dolerite suite magma underwent intermediate degrees of contamination.

Source of magmas

Godel et al. (2011) showed that the NB1 magma type that is the potential parent to the ultramafic intrusions of

the Giles Event has low TiO_2 concentrations and middle REE to high REE (MREE/HREE) ratios (Fig. 39). Godel et al. (2011) suggested this would have required a source containing amphibole; that is, the subcontinental lithospheric mantle (SCLM). Other evidence used to suggest the presence of enriched SCLM beneath the Musgrave Province included model ages for basement rocks from c. 2010 to 1590 Ma, although we prefer to interpret these model ages as the date of the basement rather than SCLM. Furthermore, the relatively high sulfur concentrations of the NB1 magmas (~1000 ppm; Godel et al., 2011) would seem inconsistent with an SCLM source (cf. the low S contents in Bushveld B1 magmas; Barnes et al., 2010). The Pt/Pd ratios of the NB1 and the G2 gabbros (0.8 – 0.9), and of the reefs in the Wingellina Hills intrusion (Pt/Pd ~1) are also unlike SCLM magmas such as the GPII kimberlites or Bushveld Complex parent magma (Barnes et al., 2010; Maier et al., 2013c).

Finally, for the entire period between c. 1220 and c. 1120 Ma, the west Musgrave Province formed one of the world's largest and longest lived belts of mid-crustal UHT metamorphism (Kelsey et al., 2009). To achieve and maintain mid-crustal conditions of >1000°C at 7 kbar (Kelsey et al., 2009), Smithies et al. (2010) suggested that the regional SCLM must have been removed. A dramatic lowering in the pressure of crustal melting at the beginning of the Musgrave Orogeny (Smithies et al., 2011) supports the idea of a substantial crustal thinning event at that time. If there was SCLM at the beginning of the Giles Event, it must have formed after the Musgrave Orogeny. Because UHT metamorphism continued for almost 100 Ma, any SCLM present at the beginning of the Giles Event must have been still young, hot, and weak, and any metasomatism of the SCLM could not have resulted in the observed non-radiogenic Nd isotopic compositions of the NB1 dykes ($\varepsilon_{Nd} = -2$). Thus, we do not subscribe to the model of SCLM derivation of the NB1 magma. Instead, there is evidence that NB1 is derived from a depleted asthenospheric source, based on the mid-ocean ridge basalt (MORB)-like Yb–Ti–Zr–Nb concentrations. The composition of NB1 could be modelled by a small degree (<<5%) of contamination of asthenospheric high-Mg basalt with crust, particularly given that Musgrave crustal components are extremely HFSE-rich (Smithies et al., 2009; Kirkland et al., 2013).

The origin of the Alcurra Dolerite suite magma remains equally controversial. Godel et al. (2011) suggested that the NB4 dykes, which they considered analogues of the Alcurra Dolerite suite, were plume melts, based on their high Ti concentrations and relatively high MREE/HREE ratios, which may require residual garnet in a deep source. However, some of our Alcurra Dolerite suite samples have as little as about 1.2 wt% TiO_2 at Mg# about 60, and thus, the high Ti samples could simply reflect a tholeiitic trend. The Alcurra Dolerite suite-type rocks have La/Yb ratios between 5 and 9.7; these are not accompanied by depletions in Yb concentrations (average 3.34 ppm) with respect to MORB and are better explained through minor crustal contamination (<<1%) of HFSE-rich Musgrave crust. The high Pt/Pd and Au/PGE ratios of primitive Alcurra Dolerite suite dykes (and the related Halleys intrusion) would be consistent with a SCLM component, although the low PGE concentrations and high Cu/Pd ratios are not. The sulfur concentrations of Nebo–Babel chilled margins, NB4 dykes, and many Alcurra Dolerite suite samples are also much higher than in other basaltic magmas considered as derived from the SCLM (for example Bushveld Complex magmas; Barnes et al., 2010).

We considered whether the magmas represented by the Alcurra Dolerite suite (and NB4 dykes) could have formed through melting of mantle that contained old, subducted, mafic oceanic crust. This could explain the high Cu/Pd ratios of the Alcurra Dolerite suite relative to other fertile basalts with similar Mg#, and the relatively high Au/PGE ratios, although not the high Pt/Pd ratios. The mantle source for the Alcurra Dolerite suite possibly contained both delaminated crust and mantle lithosphere. More work is clearly required to constrain the source of the Alcurra Dolerite suite.

Contamination

The intrusions related to the Giles Event show ε_{Nd} values that range from +2 to –5 (Fig. 42 and Table 5). This range could be due to variable contamination in the crust, or melting of several compositionally diverse mantle sources, or both. The contrasting processes cannot be readily distinguished using isotope and trace element data (Lassiter and De Paolo, 1997). However, there is abundant field evidence for in situ contamination of the G2 gabbros and some layered G1 intrusions such as Hinckley Range (Fig. 15) and Kalka (Gray and Goode, 1989).

The Wingellina Hills intrusion (and Kalka) has a crystallization order of olivine>olivine+orthopyroxene> orthopyroxene+clinopyroxene in its basal sequence that is consistent with contamination from floor material. In addition, the broad correlation between ε_{Nd} values and Ce/Nb ratios also suggests that some of the G1 intrusions assimilated crust. Among the intrusions in the west Musgrave Province, Cavenagh shows the lowest ε_{Nd} values (ε_{Nd} as low as –5), overlapping with the basalts of the Mummawarrawarra and Glyde Formations of the Bentley Supergroup (and Warakurna Supersuite). Although the Musgrave crust at that stage only showed ε_{Nd} values ranging from –3 to –6, which would require very substantial contamination of the Cavenagh magma, available contaminants such as granites of the Pitjantjatjara Supersuite are extremely rich in HFSE, which may greatly reduce the required amounts of contamination (Kirkland et al., 2013).

More-radiogenic values occur in rocks of the Morgan Range ($\varepsilon_{Nd} = -3$), Hinckley Range ($\varepsilon_{Nd} = -2$), and Pirntirri Mulari ($\varepsilon_{Nd} = -1$) intrusions. We have no Nd isotope data for the Wingellina Hills intrusion, although whole-rock and mineral compositions are similar to those of the Pirntirri Mulari intrusion, as is the stratigraphic position of the PGE reefs, suggesting a broadly similar contamination history for both intrusions. In general, the Nd isotope data of the gabbroic and ultramafic Giles intrusions in Western Australia are in the same range as those of the Kalka intrusion in South Australia, with ε_{Nd} about –2 in anorthosites and as low as –5 in gabbronorites and basal ultramafic rocks (Gray et al., 1981; Wade, 2006).

The unevolved samples of the G2 gabbros show the highest MgO concentrations (≤12.7 wt%) and Mg# (≤73 and typically >60) of all the regional Giles Event mafic magmas, although they also show among the highest Ce/Nb ratios and lowest ε_{Nd}. The samples show MORB-like HFSE patterns, although the Th and LREE enrichments reflect crustal contamination (Fig. 39). The trends of decrease in ε_{Nd} values with decrease in Ce/Nb ratios for G2 rocks (Fig. 42) or SiO_2 (not shown), suggest that the proportion of crustal material increased as the magmas evolved.

Neodymium and Sr isotopic data for the troctolitic intrusions (Mantamaru) approximate chondritic uniform reservoir (CHUR) (ε_{Nd} mostly ranges from 0 to +2, I_{Sr} ~ 0.704) and are markedly more radiogenic (for Nd) or less radiogenic (for Sr) than any Musgrave crust present at the time. Together with trace element ratios (for example, Ce/Nb) these data indicate only little (<5%) crustal contamination in the troctolitic intrusions.

Rocks of the Alcurra Dolerite suite have slightly less-radiogenic values (ε_{Nd} of +1 to –1) than the Mantamaru intrusion, although similar Ce/Nb ratios, suggesting somewhat higher degrees of contamination than in Mantamaru. Again, Kirkland et al. (2013) pointed out that average known older crustal components of the west Musgrave Province are more highly enriched, particularly in HFSE, Th, and LREE, than global crustal averages. This means that extremely small degrees of contamination of a basaltic melt could greatly enrich incompatible trace element concentrations and produce marked changes in Nd and Hf isotopic compositions, particularly if assimilation is of low-degree partial melts of crust rather than bulk assimilation.

For example, Smithies et al. (2013) showed that less than 10% bulk contamination of average Pitjantjatjara Supersuite granite into the most primitive sample of the Alcurra Dolerite suite can explain the entire isotopic variation and much of the highly incompatible trace element variation within the Alcurra Dolerite suite. Assuming assimilation of a low-degree (20%) partial melt of an average Pitjantjatjara Supersuite granite rather than bulk assimilation, the required assimilation reduces to <4%. Factoring in enrichments attributable to the approximately 50% crystallization of the Alcurra Dolerite suite (modelling estimates in Smithies et al., 2013) with a fractionating assemblage of 30% olivine, 50% plagioclase, and 20% clinopyroxene, reduces the initial contamination (bulk or partial melt) required to explain enrichments in highly incompatible trace elements to <1%, far less than the value of 30% proposed by Godel et al. (2011).

If available crustal contaminants are systematically subtracted from the most primitive Alcurra Dolerite to achieve chondritic Ce/Nb ratios, Ce/Sm ratios still remain slightly above chondritic values. Major element models (Smithies et al., 2013) show that at this stage olivine is the only liquidus phase and so fractional crystallization will have little effect on incompatible trace element ratios. Such low amounts of contamination would produce slightly more-radiogenic Nd isotope values, and it would thus appear unlikely that the mantle source was markedly depleted. Thus, the primitive members of the Alcurra Dolerite suite-type magmas were most likely derived from relatively shallow melting (<80 km) of a slightly depleted mantle source and have undergone early and very minor (<4%) contamination with highly enriched crustal material, followed by closure of the continuously fractionating system to further contamination. This model can be applied to all magmas of the Giles Event, consistent with the broad similarity in Nd isotopic data within individual intrusions, although with variation in Ce/Nb and La/Sm ratios in the intrusions.

Emplacement and crystallization

It has been suggested that the Giles intrusions constitute a rare example of an intrusive suite emplaced at highly variable crustal depths, from the lower crust to the near surface (Glikson, 1995). Our work confirms that some of the troctolitic intrusions in the southwest were emplaced at relatively shallow levels (from subvolcanic depths to <12 km), whereas the exposure level deepens to the north and east.

Preserved county-rock inclusions and contacts indicate that the Mantamaru intrusion was emplaced at the stratigraphic level of the Mummawarrawarra Basalt (Kunmarnara Group). The low metamorphic grade (greenschist facies) of the basalts indicates an upper crustal and extensional environment for intrusion. Constraints on the crystallization age of these G1 intrusions are the minimum depositional date of the Kunmarnara Group (defined by granite intrusion at c. 1078 Ma; Sun et al., 1996; Howard et al., 2011b), and a direct U–Pb zircon date of 1076 ± 4 Ma (Kirkland et al., 2011) on a layered Giles intrusion gabbro (GSWA 194762).

Primarily in the eastern part of the west Musgrave region (Hinckley Range), massive gabbro (G2) cuts the layered G1 intrusions and typically shows abundant and widespread evidence of comingling with leucogranitic magmas. The leucogranite intrudes as dykes and also forms larger pluton-scale bodies in basement rocks (e.g. South Hill, Tollu pluton). The leucogranite typically includes quartz syenites, syenogranites, and lesser monzogranites. This bimodal magmatism was also accompanied by deformation (shearing and west-northwest folding adjacent to major shear zones); date constraints on magmatism and deformation lie between 1078 ± 3 and 1074 ± 3 Ma (Howard et al., 2011b). These date constraints are almost identical to those for the layered Giles (G1) intrusions; however, where temporal field relationships can be established, G2 intrusions always post-date G1.

South of Blackstone Community, in the Blackstone Sub-basin, rhyolites of the Smoke Hill Volcanics directly overlie the layered G1 Blackstone intrusion (a component of the Mantamaru intrusion) without an obvious intervening fault. Crystallization, or depositional, ages for the rhyolites (1071 ± 8 Ma [GSWA 191728; Coleman, 2009]; 1073 ± 7 Ma [GSWA 191706; Coleman, 2009], and 1073 ± 8 Ma [GSWA 189561; C Kirkland,

2014, written comm., 1 January]) are within analytical error of the emplacement date range of the G1 and G2 intrusions, and rhyolite compositions strongly resemble those of leucogranites associated with G2 intrusions. This requires extensive and rapid crustal uplift, erosion, and exhumation of the layered Giles G1 intrusions, immediately followed by felsic volcanism.

Some of the ultramafic intrusions were proposed to have been emplaced at a higher pressure (Goode and Moore, 1975; Ballhaus and Berry, 1991). Evidence interpreted to indicate high-pressure crystallization includes high Al concentrations of pyroxene, spinel exsolution in pyroxene and plagioclase, rutile exsolution in pyroxene, antiperthitic exsolution in plagioclase, and orthopyroxene–clinopyroxene–spinel–albite coronas between olivine and plagioclase (Goode and Moore, 1975; Ballhaus and Glikson, 1989). Goode and Moore (1975) suggested that the Ewarara intrusion was emplaced at 10–12 kbar. If the crust was only about 35 km thick at the end of the Musgrave Orogeny (e.g. Smithies et al., 2011), only 40 Ma before the Giles Event, emplacement of the Ewarara intrusion was then likely near the base of the crust. Ballhaus and Glikson (1989) proposed a somewhat shallower depth of emplacement for the Wingellina Hills and Pirntirri Mulari intrusions, at 6.5 kbar (~20 km). However, because the coeval gabbroic intrusions are up to 10 km thick, the original emplacement depth of the ultramafic bodies may have been as low as 10 km.

A relatively deep emplacement level of the ultramafic intrusions could explain why they are less abundant than the gabbroic and troctolitic bodies. If the ultramafic intrusions were typically emplaced at a deeper level than the mafic intrusions, there should be proportionally more ultramafic intrusions in South Australia because the crust there is exposed at a deeper level (Goode, 2002). This scenario appears valid. Also consistent with this model is that the ultramafic bodies tend to be exposed in the cores of regional folds (i.e. the anticline north of Blackstone Community hosts the Pirntirri Mulari and Morgan Range intrusions), or along faults. However, based on PELE modelling, the An contents of plagioclase in the Wingellina Hills and The Wart intrusions are too high for high-pressure crystallization and more consistent with a pressure of 1 kbar. By contrast, the low An contents of plagioclase in the Pirntirri Mulari intrusion would be consistent with deeper emplacement relative to Wingellina Hills and The Wart. Viewed solely from a stratigraphic perspective, this idea is inviting, as the Wingellina Hills intrusion is closer to the core of the anticline situated to the north of Blackstone Community.

Several lines of evidence suggest that the G1 intrusions were emplaced thorough sill inflation. First, the intrusions lack notable contact metamorphic zones. Second, at Pirntirri Mulari there is evidence for intrusion of pyroxenite into gabbro. Third, microgabbros in the Cavenagh intrusion commonly have sharp basal and top contacts, indicating magma intrusion into semiconsolidated cumulates. At the Kalka intrusion there are thick segments interpreted as recrystallized country rocks (N2 zone; Goode, 1970), suggesting that the intrusion was emplaced as several sills separated by rafts or screens of country rock. Sill inflation has previously been proposed for The Wart and Nebo–Babel intrusions (Ballhaus and Glikson, 1995; Seat et al., 2007), the Bushveld Complex (Maier and Barnes, 1998), and the Kunene Complex (Maier et al., 2013a).

The origin of the layering in the studied intrusions remains uncertain. The G1 intrusions contain layers and schlieren of magnetite, anorthosite, ultramafic rocks, and microgabbros (Figs 17 and 19), and abundant xenoliths and autoliths. Centimetre-scale layering has been observed in pyroxenite from the Ewarara and Wingellina Hills intrusions (Goode, 1970; Ballhaus and Glikson, 1989). Other features described include convoluted layering (Wingellina Hills; Ballhaus and Glikson, 1989), scour channels (Kalka; Goode, 1970), graded layers (overturned in places) and load casts (e.g. in the Olivine Gabbro and Anorthosite Zones of the Kalka intrusion; Goode, 1970), and strong alignment of plagioclase and pyroxene. These features are analogous to those described in the Bushveld Complex where they were explained by magma replenishment and cumulate slumping and sorting (Maier et al., 2013b). Goode and Krieg (1967) further described a suite of transgressive picrite plugs in the Ewarara intrusion. It is possible that these plugs are analogous to Bushveld dunite pipes.

Fragmentation of intrusions

Past authors speculated that some or all G1 intrusions are tectonically dismembered remnants of a larger intrusion (Sprigg and Wilson, 1959; Nesbitt and Talbot, 1966; Glikson, 1995; Smithies et al., 2009; Howard et al., 2011b; Aitken et al., 2013). This idea is partly based on the considerable deformation of the intrusions, particularly in the north and east, decreasing to the south and west. In the west Musgrave Province, the Cavenagh and Blackstone intrusions are least deformed (Glikson, 1995), whereas the Murray Range intrusion is among the most deformed. Significant deformation has also affected the Wingellina Hills, Pirntirri Mulari, Lehman Hills, and Jameson intrusions. In some cases, deformation is focused along the contacts of the intrusions, expressed by mylonite zones, for example, at the top of the Pirntirri Mulari intrusion. Deformation is greater along layer contacts such as magnetite layer 1 in the Jameson intrusion. The Latitude Hill and Blackstone intrusions, for example, have undergone large-scale folding.

A possible model of the original configuration of many of the Giles intrusion(s) could be the Kalka intrusion (Goode, 1970), a 6 km-thick body with a 450 m-thick ultramafic basal portion (basal orthopyroxenite, progressively changing to websterite with height) and a gabbroic–troctolitic–anorthositic upper portion. Peridotites are exposed at the nearby Gosse Pile intrusion, which has been interpreted as the tectonically dismembered lower portion of the Kalka intrusion (Moore, 1971). By contrast to the above model, Ballhaus and Glikson (1995) suggested that, except for the combined Blackstone–Bell Rock intrusions, most G1 intrusions are distinct intrusions.

The present work supports connecting some, but not all, of the bodies. Specifically, geophysical, lithological, and compositional data strongly indicate that the Jameson–Finlayson, Blackstone, and Bell Rock intrusions are fragments of an originally contiguous body (i.e. the Mantamaru intrusion). It has a minimum preserved size of 3400 km^2, making it one of the largest mafic–ultramafic intrusions on Earth, after the Bushveld Complex (60 000 km^2). It is in the same size range as the Great Dyke, Stillwater, Sept Iles, and Dufek intrusions (3000–5000 km^2). The Cavenagh intrusion may form the southern limb of the synclinal Blackstone intrusion (Nesbitt and Talbot, 1966; Aitken et al., 2013). This would add at least another 540 km^2 to the size of the Mantamaru intrusion.

However, there are some important compositional differences between the Blackstone and Cavenagh intrusions. The Blackstone intrusion is much more differentiated than the Cavenagh intrusion, and it has a massive magnetite layer, which appears absent from the Cavenagh intrusion. The Cavenagh intrusion has elevated PGE concentrations in its upper portion whereas the Blackstone intrusion is PGE depleted. Finally, the Blackstone intrusion has a distinctly more-radiogenic Nd isotopic signature than the Cavenagh intrusion. However, note that individual intrusions can have a wide range of trace element and isotopic compositions, as seen, for example, in the Bushveld and Kalka intrusions.

It is tantalizing to speculate that the Wingellina Hills, Pirntirri Mulari, The Wart, Morgan Range, Kalka, Gosse Pile, and Ewarara intrusions, all in the Tjuni Purlka Zone, may originally have formed a single body. This would imply a displacement of up to 50 km within the Tjuni Purlka Zone. Olivine and pyroxene compositions in these intrusions show considerable overlap, and the PGE reef in the Wingellina Hills intrusion is at a similar stratigraphic position as the Cu–PGE-rich horizon in the Pirntirri Mulari intrusion (equivalent horizons have not yet been examined in detail in the other intrusions). The Wingellina Hills intrusion contains much more olivine and chromite and has higher PGE concentrations than the other bodies; however, it is possible that the Wingellina Hills intrusion is the central portion of a large lopolith, analogous to the central portions of the Great Dyke and Jimberlana intrusions, and the other intrusions with important ultramafic portions are the peripheral segments. However, the composition of plagioclase in the Wingellina Hills and The Wart intrusions is much less sodic than plagioclase from Pirntirri Mulari, suggesting either emplacement at different depths (relatively shallow for Wingellina Hills and The Wart, deep for Pirntirri Mulari), or containing diverse crustal contaminants.

In summary, at present the only strong case for dismemberment of an originally contiguous body is the Mantamaru intrusion, consisting of the Jameson, Blackstone, and Bell Rock Ranges. However, future work may well show that other Giles intrusions are also fragments of larger precursor intrusions.

Comparison to other large layered intrusions

In order to evaluate the petrogenesis and mineralization potential of the intrusions emplaced during the Giles Event, it is useful to draw comparisons with the well-characterized and highly mineralized Bushveld Complex (Fig. 54). In compiling Figure 54, it was necessary to schematize the stratigraphic thickness of the Giles intrusions because their estimated thicknesses are commonly much greater than those of the Bushveld Complex or any other of the known layered intrusions. For example, the Jameson–Finlayson Range intrusion comprises >4 km of cumulates that are compositionally broadly equivalent to the 1.5 km-thick Upper Zone of the Bushveld Complex. The thickness of the Hinckley Range intrusion may be as much as 6 km, whereas the comparable Main Zone of the Bushveld Complex is 2–3 km thick. It is likely that faulting has locally caused some structural thickening of some intrusions, although there is no evidence for large-scale structural duplication of layering or for structural juxtaposition of compositionally distinctive layers. Thus, it appears that the unusual thickness of some of the Giles intrusions is more-or-less a primary feature.

The Pirntirri Mulari, Wingellina Hills, and The Wart intrusions are approximate stratigraphic equivalents of the Lower and Critical Zones of the Bushveld Complex. Both the Giles ultramafic intrusions and the Bushveld Lower Zone show basal reversals, thick ultramafic portions, and numerous ultramafic–mafic cyclic units. Bushveld-style PGE reefs have been identified in the Wingellina Hills intrusion, and there are indications a reef may exist in the Pirntirri Mulari intrusion. The prospective horizon of The Wart (and other Giles ultramafic intrusions) remains poorly studied, partly due to restricted access.

A major difference between the Giles ultramafic intrusions and the Bushveld Complex is that the former lack chromitite seams. The Wingellina Hills intrusion contains thin chromitite schlieren and lenses, but The Wart and Pirntirri Mulari intrusions are essentially barren of chromitite. This difference is possibly due to the different crystallization orders of these Giles intrusions. In the Pirntirri Mulari and The Wart intrusions, Cr-rich clinopyroxene crystallized early, which could have led to depletion of the residual magma in chromium. By contrast, the Wingellina Hills intrusion has a thick harzburgitic basal portion, possibly causing a lesser degree of chromium depletion of the fractionating magma. In addition, late magmatic concentration and sorting processes, as advocated by Maier et al. (2013b) for the Bushveld Complex, may have been relatively less efficient in the Pirntirri Mulari and The Wart intrusions.

The Morgan Range intrusion could be a stratigraphic equivalent to the Upper Critical Zone – Main Zone transition interval of the Bushveld Complex, as it contains some ultramafic rocks at its northern edge, although it is otherwise dominated by gabbronoritic rocks of moderately

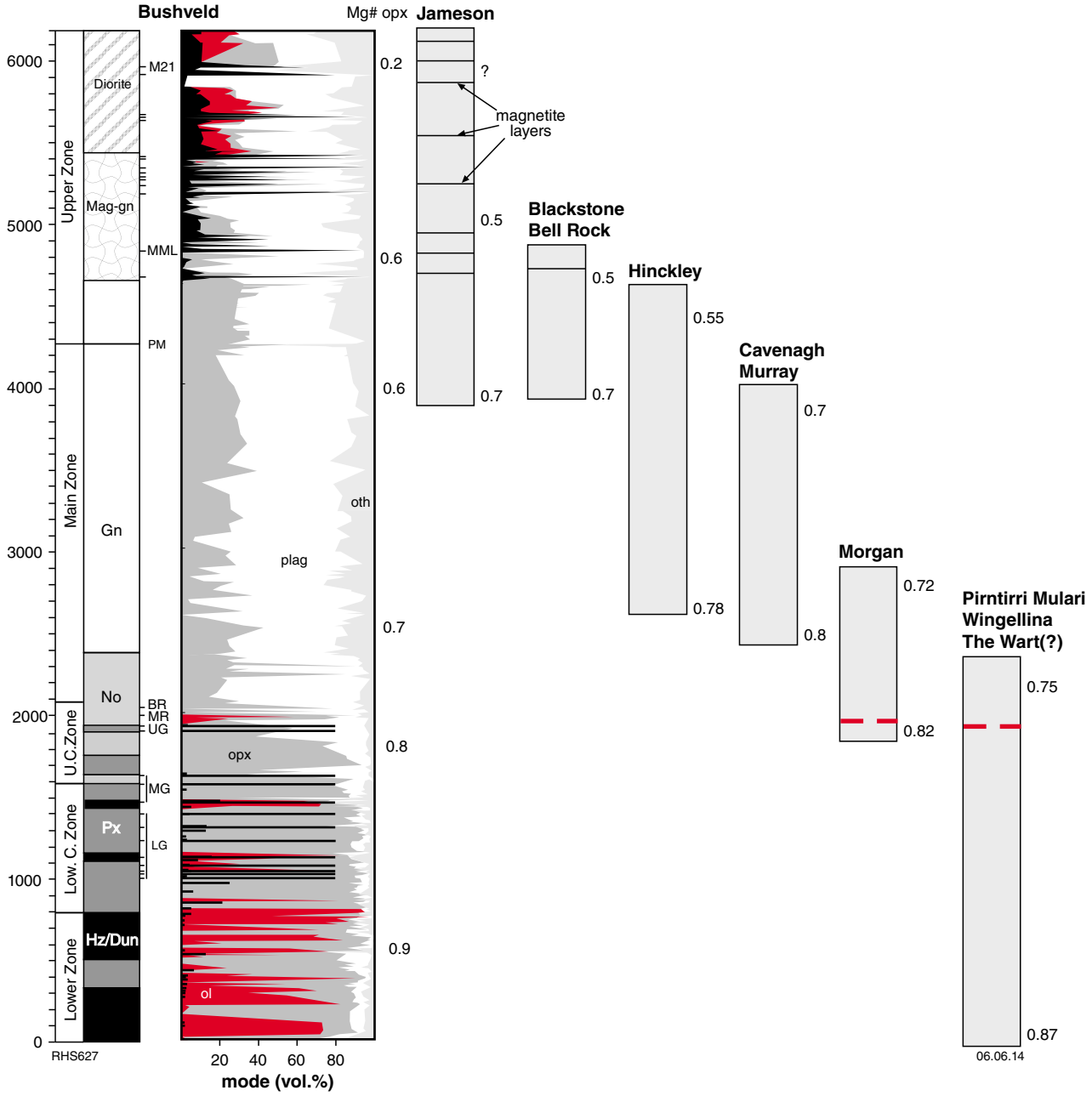

Figure 54. Stratigraphic comparison of Giles intrusions with Bushveld Complex. (Bushveld log and data from Maier et al., 2013b). Low.C. Zone = Lower Critical Zone. U.C. Zone = Upper Critical Zone

evolved composition. Whether Morgan Range contains a PGE reef analogous to that at Wingellina Hills remains unknown. The Cavenagh, Michael Hills, Latitude Hill, Hinckley Range, Murray Range, Lehman Hills, and Mt Muir intrusions could be stratigraphic equivalents of the Main Zone, as they have intermediate compositions and, in some cases, are relatively poorly layered.

The Mantamaru intrusion seems the approximate stratigraphic equivalent of the Bushveld Upper Zone. Specifically, the upper portion of the Jameson intrusion shares several similarities with the Bushveld Upper Zone. First, both contain several magnetite layers (~25 in the Bushveld, at least 11 at Jameson) that are between a few centimetres to more than 10 m thick (i.e. layer 1 at Jameson, magnetite layer 21 in Bushveld) and may contain anorthosite xenoliths. Second, most layers have sharp lower contacts, whereas the upper contacts may be gradational. Third, there is a trend of decreasing vanadium concentration with height from the basal to the upper layers (Fig. 24), and within individual layers. In the Bushveld Complex, the fourth layer from the base (in the eastern limb) constitutes the Main Magnetite Layer from which >50% of the world's vanadium production is derived (Crowson, 2001). It combines considerable thickness (up to ~3 m) with some of the highest vanadium concentrations found among Bushveld magnetitites (1.5–2% V_2O_3; Klemm et al. 1985).

However, there are also important differences between the Bushveld Complex and the upper portion of the Jameson intrusion. For example, the basal magnetite seam in the Jameson intrusion has higher PGE concentrations than the equivalent Bushveld magnetite layer(s). The low PGE concentrations of the Bushveld basal magnetite seams could be due to the formation of the world-class reefs, the Merensky and UG2 Reefs, at stratigraphically lower levels, effectively extracting the PGE from the magma. If this model is correct, the implication could be that the Mantamaru intrusion has a low potential to host PGE reefs at depth. Alternatively, the PGE depletion of the Bushveld basal magnetites could reflect their exposure at the margin of the Bushveld lopolith, with relatively PGE-rich seams possibly present in the centre of the Bushveld Complex.

Another difference between the Bushveld Complex and the upper portion of the Jameson intrusion is that the Bushveld Complex has an apatite-rich layer near the top, whereas no apatite-rich layers have yet been identified in the Jameson intrusion. However, there is a trend of P_2O_5 enrichment in some of the upper magnetite layers (Traka Resources, 2011), and up to 0.8 wt% P has been intersected by boreholes in magnetite to the south of the Bell Rock Range (P Polito, 2013, written comm., 29 July). A further difference between the two intrusions is that the vanadium concentrations in the basal magnetite layer of the Jameson intrusion are somewhat lower than in the Bushveld Complex, possibly due to lower R-factors (mass ratio of silicate melt to sulfide melt; Campbell and Naldrett, 1979) in the Jameson intrusion. This interpretation is possibly consistent with a weak positive correlation between the vanadium concentration of magnetite and the size of the host layered intrusion (Fig. 55). The scatter seen in the plot could be partly due to uncertainties related to intrusion size, in turn related to poor exposure, and other factors that may influence the vanadium concentration of magnetite layers, such as the cooling rate.

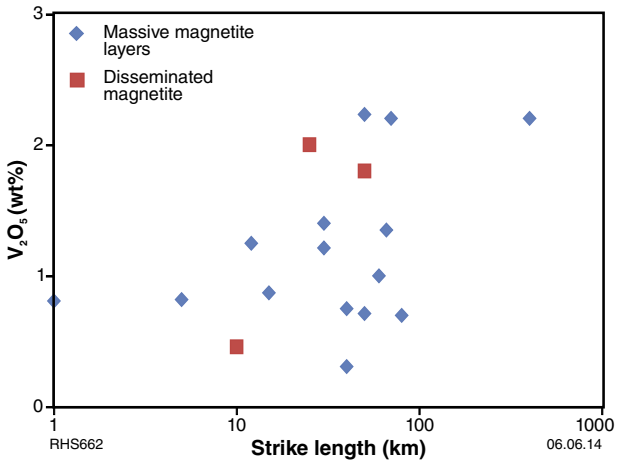

Figure 55. Correlation between intrusion strike length and vanadium concentration of magnetite in global magnetite-bearing intrusions (see Table 10 for data sources)

Tectonic setting

The Musgrave Province has been located between the thick lithospheric keels of the West Australian, South Australian, and North Australian Cratons since the Mesoproterozoic. Begg et al. (2009) proposed that mantle plumes might be channelled along cratonic keels, resulting in strong adiabatic mantle partial melting and mafic magmatism at the margins of cratons or within cratonic suture zones. However, the long time span of continuing mantle magmatism and UHT metamorphism in the Musgrave Province is inconsistent with a mantle plume model (Evins et al., 2010b; Smithies et al., 2013, 2014). Instead, Smithies et al. (2013, 2014) suggested that the Musgrave Province acted as a stationary zone of mantle upwelling for >200 Ma, resulting in a persisting hot zone characterized by mafic and felsic magmatism and UHT metamorphism. These features appear to point to a plate-driven trigger for magmatism. Mantle melting could have been caused by processes such as lithospheric delamination, volatile transfer from the SCLM or the crust to the asthenosphere, or mantle flow along an irregular base of the lithosphere (Silver et al., 2006). The resulting mantle magmas may have ponded at the base of the thinned lithosphere then periodically drained during collisional events, resulting in transpressional rupturing (Silver et al., 2006). A similar scenario was envisaged for the Ventersdorp, Great Dyke, Bushveld, and Soutpansberg continental magmatic events in southern Africa (Foulger, 2010).

In the case of the Musgrave region, events during and after the 1345–1293 Ma Mount West Orogeny likely resulted in crustal thickening, partial melting, and densification of lower crust. Evidence from the REE geochemistry of granites related to the subsequent, 1220–1150 Ma, Musgrave Orogeny is that this event began with a change from deep to shallow crustal melting that can be related to delamination of residual lower crust and the underlying lithospheric mantle. The ensuing UHT metamorphism from 1220 to 1120 Ma supports a sustained regime of highly thinned crust, with little or no remaining lithosphere. Throughout this period, magmatism was predominantly felsic because the lower crust was a melting, assimilation, storage, and homogenization (MASH) zone, preventing ascent of dense mafic magmas. The crustal thermal structure established during the Musgrave Orogeny strongly influenced conditions at the beginning of the Giles Event (Smithies et al., 2014). The Giles Event was triggered by far-field forces acting on the margins of the West Australian Craton (Evins et al., 2010b; Smithies et al., 2014). Initial subsidence and deposition of the Kunmarnara Group ensued, followed by draining of ponded subcrustal melts (G1, G2, Alcurra Dolerite suite). The relatively early G1 and G2 magmas underwent variable contamination during ascent into the crust (Fig. 56). Subsequent magmas (Alcurra Dolerite suite) were typically less contaminated because the crust had become more refractory. These magmas are more differentiated because the crust had become thicker, leading to more intra-crustal ponding and fractional crystallization. The composition of Alcurra magmas (including their low PGE concentrations, high Cu/Pd, Pt/Pd, and Au/PGE ratios) could be explained by

foundering of crust and new SCLM (Fig. 56a), lowering of the mantle solidus, and melting of a hybrid crust-rich mantle.

The formation of the large layered intrusions of the Giles Event can be explained within the context of a prevailing compressive regime, allowing the magma to form inflating sills rather than dykes. Importantly, the Musgrave Province demonstrates that large layered intrusions are not confined to cratons. What is required is a stable, broadly (at least locally and temporarily) compressive tectonic environment where magmas can ascend in locally extensional, possibly transpressional zones.

Origin of mineralization

PGE reefs within the Wingellina Hills layered intrusion

Layered intrusions host the bulk of the world's PGE resources in the form of stratiform layers or so-called reefs. Many layered intrusions host reefs (see summary in Maier, 2005), although economic examples are presently confined to the Bushveld Complex, Stillwater Complex, and Great Dyke. In all cases, the reefs consist of <1–3% disseminated sulfides within laterally extensive layers of ultramafic or mafic rocks. The host intrusions are exceedingly sulfur poor, suggesting that sulfide saturation of the magma was eventually reached due to fractionation.

Many authors consider addition of external sulfur, normally considered responsible for the formation of most Ni–Cu sulfide ores, of little importance. This interpretation is consistent with mantle-like sulfur isotopic signatures in most reefs (Liebenberg, 1970; Li et al., 2008). At least for the Bushveld Complex, mixing between compositionally different magmas was also probably not important in reef formation, because Bushveld magmas were highly sulfur undersaturated (Barnes et al., 2010). Sulfides likely concentrated during cumulate sorting in response to synmagmatic subsidence of the intrusions (Maier et al., 2013b).

The Wingellina Hills main PGE reef shows many similarities to the Great Dyke and Munni Munni PGE reefs, including the broadly stratiform nature, formation toward the top of the ultramafic portion of the intrusion (Fig. 57), and the offset patterns of the chalcophile elements. The total amount of PGE is also within the same range in both the Wingellina Hills reef and the Main Sulfide Zone of the Great Dyke. In both cases, there is no marked change in trace element ratios across the reef. The origin of the Wingellina Hills main reef can be modelled by a process of sulfide saturation in response to fractionation of an NB1-type magma. This type of magma has been shown to reach sulfur saturation after about 30% fractionation, near when plagioclase appears on the liquidus (Godel et al., 2011), and consistent with the position of the reef at the top of the ultramafic portion. Wingellina Hills has several additional zones of PGE enrichment above the main PGE reef. These zones could reflect new magma influxes. The metal concentrations of these additional reefs could be lower because the residual magma was PGE poor following the formation of the main reefs.

Important differences between the PGE reefs at Wingellina Hills and those in the Great Dyke and Bushveld Complex include the lower PGE grades and sulfide contents of the Wingellina Hills reefs. The low grade could reflect less-efficient metal concentration caused by faster cooling rates in a relatively small intrusion, whereas the paucity of sulfides could be due to metamorphic sulfur loss, consistent with subcotectic sulfide proportions in most Wingellina Hills rocks. Fluid flow might have lead to mobilization of Au and Cu, explaining the offset patterns. Alternatively, the offset patterns could be due to higher D-values of PGE relative to Cu and Au, and very high R-values of early sulfides (Barnes, 1993).

Cu–Ni–PGE–Au mineralization at Halleys

Platinum group element–Cu–Au reef-style mineralization is common to the upper portions of many layered intrusions (see Maier, 2005 for a summary). The enrichment of magnetite together with sulfide at the Halleys prospect could suggest that the Halleys body is the evolved top portion of a layered intrusion, perhaps a correlative of the magnetite-rich upper part of the Blackstone intrusion. However, Halleys has much higher gold and sulfur concentrations and mica contents than the Blackstone intrusion, and field relationships indicate that it crosscuts the southern segment of the Blackstone intrusion. Thus, if Halleys were the upper portion of a large intrusion, this intrusion would likely be a different body from the Blackstone or Cavenagh intrusions, and instead be related to the Alcurra Dolerite suite to which the Saturn intrusion also belongs. The relatively high Au/PGE ratio is a hallmark of Alcurra-type magma. However, a direct correlation between the Halleys and Saturn intrusions is inconsistent with the distinct magnetic signature of the intrusions.

An alternative model could be that the mineralization at Halleys is more akin to contact-style mineralization in many mafic–ultramafic intrusions, including the Platreef of the Bushveld Complex. Such deposits are considered to have formed through a combination of processes, including sulfide saturation in response to fractional crystallization, commonly accompanied by floor contamination. The proximity of the floor would have caused a high cooling rate of the magma, producing wide, disseminated mineralization rather than narrow sulfide reefs. Sulfides at Halleys have $\delta^{34}S$ of –0.9, providing little added constraints on the nature of the sulfur source. More work is clearly required to further constrain the petrogenesis of the intrusion and its mineralization.

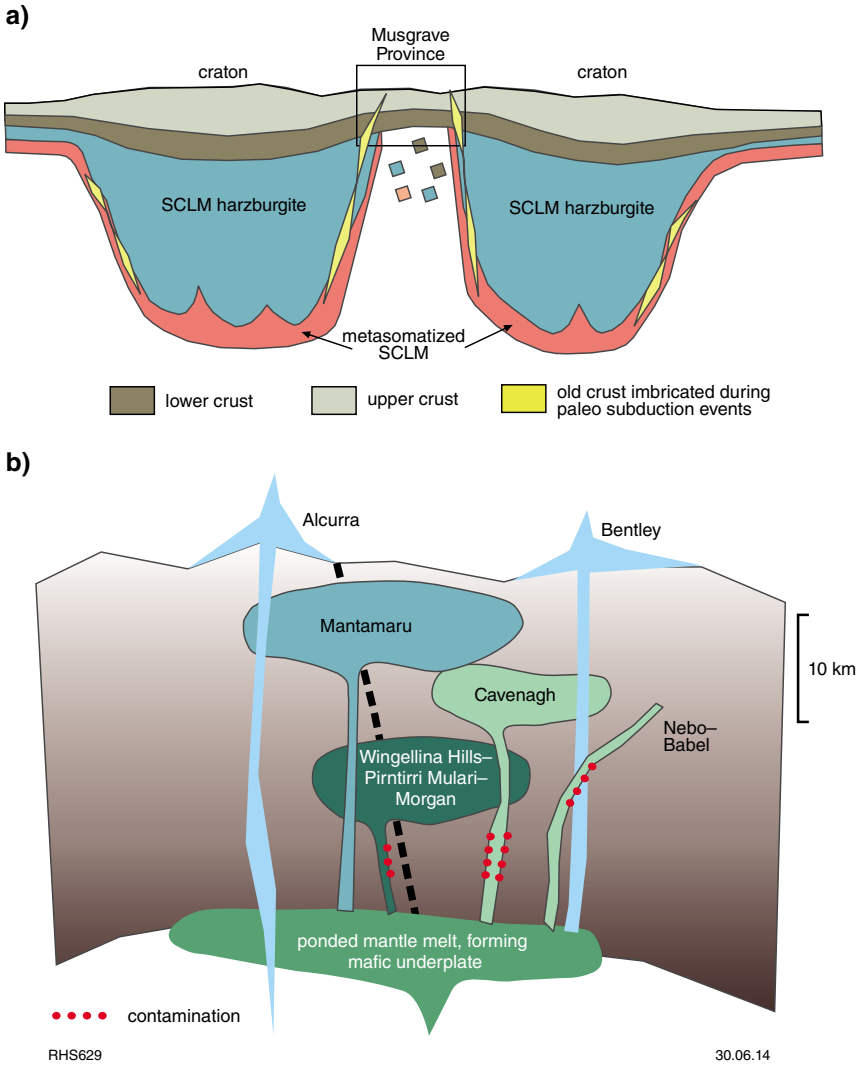

Figure 56. Schematic model of emplacement of the Giles intrusions: a) foundering of crust and new SCLM (shown as shapes between the SCLM harzburgite); b) ponding and ascent of mantle melts. See text for discussion. SCLM = subcontinental lithospheric mantle

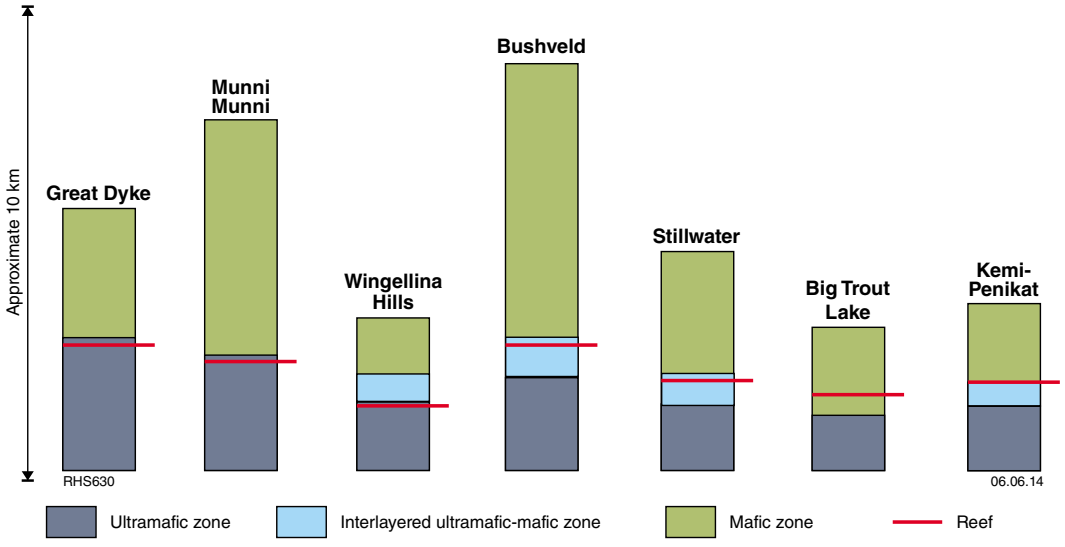

Figure 57. Comparison of the positions of the platinum group element reef in a number of well-characterized layered intrusions

Vanadium and PGE mineralization in magnetite seams of the Jameson intrusion

The petrogenesis of oxide seams in layered intrusions has been reviewed by Maier et al. (2013b). Fractional crystallization of basaltic magmas ultimately leads to cotectic crystallization of magnetite with silicates, forming magnetite-bearing gabbroic and dioritic rocks. To form massive oxide layers, magnetite must effectively fractionate from the magma, as the cotectic proportions of magnetite and silicates are between 5 and 30% (Toplis and Carroll, 1996). One main criticism of crystal fractionation models has been that the high yield strength of basaltic magmas prevents effective segregation of small magnetite crystals to form laterally extensive, massive oxide layers with sharp bottom and top contacts (McBirney and Noyes, 1979). Irvine et al. (1998) proposed that cumulate layers in the Skaergaard intrusion precipitated from density currents of crystal slurries that swept down the chamber walls. Maier et al. (2013b) rejected this model for oxide layers in the Bushveld Complex because density currents would not preserve the abundant, highly elongated to wispy, subhorizontally oriented anorthosite autoliths within chromitite and magnetitite layers. An alternative model invokes a shift in phase stability fields of oxides caused by changes in pressure (Cameron, 1980; Lipin, 1993) affecting the entire magma chamber simultaneously. Temporary supersaturation in magnetite could also be achieved by an increase in the oxygen fugacity of the magma, for example, by contamination (Ulmer, 1969), or a combination of magma mixing, pressure change, and oxidation in response to magma replenishment.

One of the most popular models for the formation of massive magnetite layers is saturation of the magma in an iron oxide liquid (Philpotts, 1967; Naslund, 1983; Zhou et al., 2005). Several experimental studies have produced immiscible iron oxide liquids from silicate liquids (Freestone, 1978; Roedder, 1978; Naslund, 1983). However, the experiments that produced iron oxide liquids started with silicate liquids with compositions that are very different from natural rocks. Toplis and Carrol (1995, 1996) and Tollari et al. (2006, 2008) showed that using compositions close to natural basalts and diorites, magnetite or ilmenite crystallize before the magmas become saturated with iron oxide liquid. Therefore, the experimental evidence presently does not support the immiscibility model. Textural evidence has also been cited in support of the immiscibility model, with a number of workers reporting the presence of Fe-rich and Fe-poor melt inclusions in apatites from layered intrusions (e.g. Jakobsen et al., 2005; Charlier et al., 2011). However, melt inclusions in general are not reliable indicators of overall melt composition due to boundary layer effects (London, 2008). Eales and Cawthorn (1996) rejected the liquid immiscibility model for the magnetite layers of the Bushveld Complex on the grounds that the iron oxide liquid would not have formed sharp planar contacts with the underlying cumulates, but percolated into the interstitial spaces in the cumulate. This criticism is equally valid for formation of seams in the intrusions related to the Giles Event.

Maier et al. (2013b) proposed that magnetite seams form through crystal sorting of oxide–silicate slurries that slump along the chamber floor during subsidence of large, slowly cooling magma chambers. The slurries could be injected into the semiconsolidated crystal pile, and locally form transgressive pipes. Evidence for cumulate deformation and slumping has been found in magnetite seams of other layered intrusions. Such features are also found in magnetite-rich rocks intersected by drillcore to the south of Bell Rock Range.

Magnetite layers in layered intrusions commonly contain PGE-rich sulfides (see Maier, 2005 for a summary of occurrences). The sulfides may have precipitated in response to a rapid depletion in iron of the magma, or magma reduction following crystallization of copious amounts of magnetite (Jugo et al., 2005). If the magma still contained PGE at this relatively advanced stage of differentiation, the sulfides would be PGE rich. In the magnetitites of the Bushveld Complex the sulfides are PGE poor, presumably because of the formation of the PGE reefs in the Critical Zone. In the Jameson intrusion, magnetites are relatively rich in PGE, possibly suggesting there is no PGE reef at depth.

Nebo–Babel Ni–Cu deposit

The Nebo–Babel Ni–Cu deposit bears a number of similarities to other magmatic Ni–Cu sulfide deposits. Of particular note are the tubular (chonolithic) shape and high abundance of sulfides relative to the size of the body. Seat et al. (2007, 2009) argued that the magma flow regime and dynamics would have played a major role in the precipitation and distribution of sulfides, analogous to the models applied to, for example, Noril'sk and Voisey's Bay. The distribution of sulfides would have been controlled by changes in magma velocity, in turn related to changes in the orientation of the conduit. However, by contrast to Noril'sk and Voisey's Bay, sulfide saturation at Nebo–Babel was interpreted to have been achieved largely by magma mixing of Alcurra-type magma with NB1-type magma, and orthogneiss contamination, without addition of external sulfur (Seat et al., 2007; Godel et al., 2011). The magma-mixing model is consistent with the considerable compositional overlap between NB3 dykes (interpreted as hybrid Alcurra–NB1 magma) and the Nebo–Babel chilled margins. Furthermore, Nebo–Babel appears to be at the boundary between two compositional crustal domains: to the east of Nebo–Babel the mafic rocks are of NB1 and Alcurra Dolerite lineage, whereas to the west, only the Alcurra Dolerite lineage appears present.

In terms of mass balance, the orthomagmatic model of sulfur derivation is certainly feasible: extracting 100 ppm S from 1 km^3 of magma can produce a massive sulfide lens 1 km long, 10 m high, and 20 m wide. However, in recent literature on magmatic Ni–Cu deposits, the prevalent trend has been to explain massive sulfide deposits in general by the addition of externally derived sulfur. One of the main reasons for this explanation is that the alternative (i.e. orthomagmatic derivation of the sulfur) would require an extremely effective concentration mechanism (Keays and Lightfoot, 2010), as the cotectic

proportion of sulfide precipitating from sulfur-saturated troctolitic–gabbronoritic magma is very small (perhaps as little as 0.1 wt%) due to the increase in iron concentration of fractionating plagioclase-saturated magma (Scoates and Mitchell, 2000). Quantitative modelling to resolve this question is needed, although field evidence provides some insight. Massive sulfides are extremely rare in layered intrusions, illustrating that concentrating cotectically precipitating sulfides from convecting magma is difficult. It seems doubtful that it would be easier in fast-flowing magmas within magma feeder systems.

The basis for the model of Seat et al. (2007) was that the sulfide ore and its gabbroic host rocks both have mantle-like sulfur isotopic compositions, and that the rocks of the Pitjantjatjara Supersuite, which forms the immediate country rock to the mineralized gabbro, are sulfur poor. However, the mantle-like isotopic composition of the Nebo–Babel mineralization, and of the host gabbro, do not exclude a country rock source of sulfur; they only require that the contaminant was isotopically juvenile and that R-factors were large (Lesher and Burnham, 2001).

Granites of the Pitjantjatjara Supersuite are only a very minor lithological component within this part of the Mamutjarra Zone. The main rock types within this area include rocks of the Wirku Metamorphics, Winburn Granite, and Bentley Supergroup. The Wirku Metamorphics comprise a range of pelitic and psammitic metasedimentary rocks and are highly unlikely to have mantle-like sulfur isotopic compositions. However, the Winburn Granite and volcanic and volcaniclastic rocks of the Bentley Supergroup are cogenetic (Smithies et al., 2013), and in the area around and to the west of Nebo–Babel itself (the Palgrave area) they typically contain visible sulfides (mostly pyrite) and are locally sulfide-rich. In addition, our bedrock geological interpretation of the area directly to the south of Nebo–Babel infers the presence of a deep graben structure filled by rocks of the Bentley Supergroup. Thus, there clearly exist several locally available potentially sulfur-rich country rocks.

Whereas much of the Bentley Supersuite was deposited after c.1065 Ma and could not have interacted with the Nebo–Babel gabbro, deposition of the lower portion (the Mount Palgrave Group and much of the Kaarnka Group), pre-dates intrusion of the Nebo–Babel gabbro (Smithies et al., 2013) and thus provides a potential contaminant. In addition, magmatism associated with the Bentley Supergroup is overwhelmingly dominated by mantle-derived tholeiitic mafic magmas and by their felsic derivatives. The felsic volcanic rocks and the Winburn Granite are dominantly strongly ferroan and alkaline-calcic (A-type) derived through fractionation of mantle-derived mafic magmas, rather than through partial melting of crustal sources (Smithies et al., 2013). The presently available sulfur isotopic data for the units of the Bentley Supergroup indicate a range of compositions, with those from the lower part having $\delta^{34}S$ between +1.8 and +7, potentially representing a suitable sulfur source for the Nebo–Babel deposit.

In summary, considering that there is compositional and lithological evidence for country rock contamination at Nebo–Babel, and because the basement contains lithologies that may have provided juvenile sulfur to the magma, we suggest that addition of external sulfur to the Nebo–Babel magma remains possible. External addition of juvenile volcanic rocks would be consistent with the relatively high Cu/Pd and Cu/Ni ratios (due to addition of crustal Cu) and high Au/Pd ratios (due to addition of crustal Au) at Nebo–Babel (see data of Seat et al., 2007).

Thoughts on prospectivity

Large magmatic events dominated by mafic–ultramafic magmas increase heat flux into the crust, triggering crustal melting, devolatization, and large-scale fluid flow. Deposit types favored by such regimes include magmatic PGE–Cr–Fe–P deposits in large layered intrusions, Ni–Cu sulfide ores formed through assimilation of sulfur-rich strata in magma feeder conduits or at the base of layered intrusions, and hydrothermal deposits of variable style, notably in the roof and sidewalls of the largest intrusions. Pirajno et al. (2006) drew analogies between the Giles Event and the Bushveld Complex of South Africa. Both are associated in space and time with bimodal volcanic rocks which, in the case of the Bushveld Complex, are well endowed with a wide range of hydrothermal ore deposits, ranging from greisen-style deposits, breccia pipes with Sn–W, to epithermal and mesothermal lode gold and iron oxide–copper–gold (IOCG) deposits. The Musgrave region too has a high potential for such deposits, as highlighted by the discovery of Cu–Au vein mineralization in the felsic volcanic rocks of the Tollu Group to the north of the Cavenagh Range (Abeysinghe, 2003). In the following section, we briefly examine the prospectivity for certain commodities and deposit styles.

Magmatic Ni–Cu

Most magmatic Ni–Cu deposits are thought to form where basic-ultrabasic magma interacts with crustal sulfide (Naldrett, 1997, and references therein). Due to the apparent paucity of sulfides in the exposed crustal rocks, including the Giles intrusions, the discovery of the Nebo–Babel deposit thus came as a surprise to many explorers and researchers. It is now known that there is a paucity of crustal sulfide mainly because of the poor exposure in the region, and underexploration. Specifically, volcanic rocks of the Bentley Supergroup locally contain significant amounts of sulfide. Furthermore, the Musgrave Province contains several translithospheric suture zones (e.g. Howard et al., 2011b; Aitken et al., 2012, 2013) that could be intracratonic collision zones, potentially hosting sulfur-bearing subducted crust. These structures could have been activated at various stages during the tectonic history of the province, potentially leading to multiple mineralization events.

Another positive factor for the Ni–Cu potential of the Musgrave Province is the craton margin setting (cf. Begg et al., 2009). Such settings host most world-class Ni–Cu deposits, including Noril'sk, Voisey's Bay, and Kambalda. The question arises as to why only one major Ni–Cu deposit has been found so far. Nickel–Cu and other mineral deposits tend to form clusters, suggesting there should be more deposits in the Musgrave

Province. However, exploration during the last decade has identified several low-grade deposits (Halleys, Manchego, and Succoth) suggesting the true potential of the west Musgrave province for Ni–Cu sulfide deposits remains unrealized.

Magmatic PGE

Economic PGE deposits globally are hosted by large layered intrusions (e.g. Bushveld, Great Dyke, and Stillwater). Among the four largest intrusions known, only the Dufek intrusion of Antarctica appears to lack economic PGE reefs, although this may be due to lack of exposure. The correlation between reef size and PGE potential has been explained by a model where high-grade PGE reefs form through cumulate sorting during subsidence of the intrusion (Maier et al., 2013b). The largest intrusions undergo more subsidence and have a lower cooling rate, resulting in stronger slumping and sorting.

Furthermore, the economically viable intrusions need to have crystallized from fertile, PGE-rich mantle magma, formed through high degrees of partial melting, and undergoing relatively little contamination with sulfidic crust. Finally, a stable, far-field compressional tectonic regime is favorable to allow the formation of large sill-like bodies. A cratonic setting and a metasomatized SCLM mantle source do not seem required to form PGE reefs, although all presently economic intrusions lie within Archean cratons.

Based on the above considerations, the PGE prospectivity of the Giles intrusions has to be considered high. The magmas related to the Giles Event (notably the G2 gabbros) are fertile in terms of PGE. Some of the intrusions (notably Mantamaru) are among the largest on Earth, and field and compositional evidence for contamination or sulfur addition is restricted. The PGE reefs discovered so far are relatively rich; the basal magnetite in the Jameson intrusion has a much higher grade than the Bushveld magnetitites. The grade of the Wingellina Hills PGE reefs is lower than that of the Bushveld reefs, although the total amount of PGE in individual intersections of the reef package is comparable to the Upper Critical Zone of the Bushveld Complex (i.e. the PGE at Wingellina Hills are less concentrated). Whether this concentration pattern is due to the relatively small size of the intrusion remains unresolved. Future exploration could concentrate on two targets: PGE reefs in the mafic–ultramafic transition interval, and PGE in magnetite seams in the upper portions of mafic intrusions.

PGE reefs in the mafic–ultramafic transition interval

Because all ultramafic Giles intrusions have similar lithologies (websterite, harzburgite, olivine orthopyroxenite), it is possible, if not likely, that they underwent similar crystallization and sulfur saturation histories, and thus, more PGE reefs exist in addition to the Wingellina Hills reef. However, the key sections in the interlayered mafic–ultramafic zones of The Wart, Pirntirri Mulari, Morgan Range, and the intrusions in South Australia (for example, the interlayered peridotite–norite zone, the norite zone, and the N2 zone at Kalka), remain poorly studied.

The Pirntirri Mulari Cu and PGE-rich zone lies at a similar stratigraphic level as Wingellina Hills, although Pirntirri Mulari remains very poorly sampled. By analogy with Wingellina Hills, the main target is the sulfur-poor succession stratigraphically below the exposed sulfide-bearing rocks. In all cases, PGE reefs in the Giles intrusions may be less sulfur rich than reefs elsewhere, due to later (Petermann) metamorphism. This low sulfur content might render the reefs invisible to the naked eye. The wide spread in Cu/Pd ratios at Wingellina Hills (Fig. 48) is a good prospectivity indicator, interpreted to reflect that the magma reached sulfide saturation during final emplacement.

Another factor to note is that Wingellina Hills may be the remnants of an originally much larger body, potentially including the Pirntirri Mulari, The Wart, Kalka, Gosse Pile, and Ewarara intrusions. Such a model was initially considered by Nesbitt and Talbot (1966) and would be consistent with the observation that all these intrusions are in the Tjuni Purlka Zone. The model would also help to explain the relatively large amount of PGE in the Wingellina reefs, unusual for an intrusion of such a relatively small size. According to the model of Maier et al. (2013b), the best reefs would be expected in the central domain of such a composite intrusion. Even if the intrusions were not linked, there may be several additional, unexposed blocks.

PGE in magnetite seams in the upper portions of mafic intrusions

The prospectivity of the upper portions of layered intrusions has been summarized by Maier (2005). Low-grade Pd–Au reefs are present, for example, in the 2435 Ma Koitelainen intrusion of northern Finland (Mutanen, 1997), the 55 Ma Skaergaard intrusion of Greenland (Andersen et al., 1998), the 2640 Ma Rio Jacaré Complex of northeast Brazil (Sá et al., 2005), at Birch Lake in the 1107 Ma Duluth Complex of Minnesota (Miller et al., 2002), the 992 Ma Rincon del Tigre intrusion of Bolivia (Prendergast et al., 1998), the 1096 Ma Sonju Lake intrusion within the Duluth Complex (Miller et al., 2002), and the 1108 Ma Coldwell Complex of Ontario (Barrie et al., 2002). In all these cases, the mineralization is uneconomic because of low PGE grades (0.5 – 5.5 ppm peak values) and, partly, to low Pt/Pd ratios.

By contrast, the Stella intrusion of South Africa contains potentially economic PGE-rich reefs, where an approximately 1 m-thick, laterally persistent magnetitite layer contains 10–15 ppm PGE (Maier et al., 2003b). The implication is that the upper parts of layered intrusions are interesting targets for PGE reefs, consistent with the discovery of laterally persistent PGE enrichment in the basal magnetite layer of the Jameson intrusion. Whether the Blackstone and Bell Rock intrusions contain similar PGE-rich magnetite layers remains uncertain, due to lack of exposure. The exposed massive magnetite layer in the

Table 10. Vanadium contents in magnetite within layered intrusions globally

Intrusion	*Maximum strike (approx. km)*	*Stratigraphic thickness (approx. km)*	*Size (approx. km²)*	*Age (Ga)*	*V_2O_5 (wt%)*	*Occurrence*	*Reference*
Bushveld	400	8	60 000	2.05	2.20	S, P	Klemm et al. (1985)
Duluth	30		5 000	1.1	1.21	P	Nabil (2003)
Dufek	50	8–9	6 000	0.184	2.23	S	R Hanemann, 2012, written comm., 21 December
Jameson	66	10	>1 000	1.07	1.35	S	This study
Rio Jacaré	70	1	–	2.64	2.20	S	Sá et al. (2005)
Stella	12	1.5	–	3.01	1.25	S	Maier et al. (2003b)
Trompsburg[(a)]	50	2.5	2 500	1.9	0.71	S	Reynolds (1979)
Rooiwater	30	7.5	600	2.961	1.40	S	Reynolds (1979)
Mambula[(a)]	5	–	–	1.145	0.82	S	Reynolds (1979)
Kaffirskraal[(a)]	1	–	2	2.055	0.81	S	Reynolds (1979)
Usushwana[(a)]	40	1	800	3	0.31	S	Reynolds (1979)
Dore Lake	40	4.5	600	2.7	0.75	S	Allard (1976)
Windimurra	60	11.5	2 300	2.81	1.00	S	Habteselassie et al. (1996)
Panzihua	15	2	–	0.26	0.87	S	Zhou et al. (2005)
Sept Iles	80	6	5 000	0.544	0.70	S	Cimon (1998)
Koitelainen	25	3.2	600	2.45	2.00	D	Mutanen (1997)
Koillismaa	50	2.5	500	2.45	1.80	D	Karinen and Hanski, in prep. (2014), WD Maier, 2014, written comm., 23 February
Otanmäki	10	2	150	2.05	0.46	D	Otanmäki, at <http://www.otanmaki.fi>
Akanvaara	10	3.3	70	2.45	0.71	D	Mutanen (1997)

NOTES: (a) average values
S seam
P plug
D disseminated
– size unknown either because the steep dip of layering only exposes a profile, or because of limited data

Blackstone intrusion is PGE poor, as are the magnetite-rich drillcore intersections to the south of Bell Rock. Magnetite-rich zones in other intrusions (for example, Kalka) remain unstudied for PGE. Possible additional targets include Saturn, where Cu concentrations show a marked increase halfway through the exposed intrusion (Fig. 28), the poorly known Halleys intrusion that contains up to 200 ppb PGE+Au, and the Manchego Prospect where PGE concentrations reach 1 ppm.

Notably, the Giles Event shows that Ni and PGE deposits can coexist within a mafic magmatic province. This is relatively rare globally, probably because the formation of PGE reefs is hindered by the presence of sulfur-rich crust. In the Musgrave Province, the key may be the presence of late, large-volume, felsic, sulfur-bearing magmatism providing an external sulfur source for the formation of Ni–Cu deposits, although not affecting the formation of the early PGE reefs. This hypothesis needs to be explored with more detailed geochronology.

V–Ti–Fe–P–Cr-rich oxide seams

The global correlation between size of intrusions and vanadium concentration of magnetite (Fig. 55, Table 10) is less strong than that between intrusion size and PGE grade of reefs. Even relatively small intrusions can contain thick magnetite seams enriched in vanadium (e.g. Stella and Mambula intrusions; Reynolds, 1979; Maier et al., 2003b). The Giles intrusions have high prospectivity for iron oxide, as suggested by the thick magnetite seams in the Jameson and Blackstone intrusions, and disseminated magnetite-rich zones south of the Bell Rock intrusion and in the Halleys intrusion. However, only the Jameson and Blackstone seams are vanadium rich.

In theory, the titanium concentration of the seams should increase with height, as observed in the Bushveld Complex (Klemm et al., 1985). Whether this effect also applies to the Jameson intrusion is unclear. Some of the ilmenite in the lower seams is in the form of fine exsolution lamellae

that can be difficult and uneconomic to extract, although reconnaissance work suggests that in many cases ilmenite is in granular form. The iron potential of the seams could also be considerable, particularly layer 1, which can be up to 50 m thick. The Kalka anorthosite zone contains between 5 and 10 % oxides throughout, and a 3 m-thick olivine–magnetite layer that remains little studied. In addition, there may be pipe-like oxide bodies in the upper portion of some intrusions (for example, layer 8 of the Jameson intrusion). Two transgressive iron oxide bodies (100 m long, 20–50 m wide, 1.3% V_2O_5) have been identified in the N2 subzone at Kalka (Goode, 1970). The bodies were interpreted to have formed by ductile flow of iron oxides during the Petermann Orogeny.

The potential for apatite deposits remains unknown. Most of the samples analysed here are apatite free, although Traka Resources (2013) found somewhat elevated phosphorus concentrations (up to 250 ppm P) in layer 5 of the Jameson intrusion. Anglo American intersected elevated phosphorus concentrations (up to 8000 ppm P) in magnetite-rich rocks to the south of the Bell Rock intrusion, suggesting there could be apatite potential in unexposed or unstudied upper magnetite seams. Minor amounts of apatite were also described from Kalka (Goode, 2002). Based on analogy with the Bushveld Complex, potential apatite-rich layers may exist towards the top of the intrusions; in the Bushveld Complex, nelsonite forms the uppermost of the magnetite seams.

By contrast, the potential for chromite seams in the intrusions of the Giles Event is low, as suggested by the lack of any notable chromite enrichment in the studied intrusions, possibly due to the early crystallization of clinopyroxene in many intrusions, leading to early depletion in chromium (Ballhaus and Glikson, 1989).

Hydrothermal deposits

The prospectivity of the west Musgrave Province for hydrothermal deposits has been assessed by Pirajno et al. (2006), from which the following section is summarized. The bimodal character of the Giles Event constitutes a highly prospective setting for hydrothermal (and magmatic) mineral systems, comprising subvolcanic intrusions, high silica, and H_2O-poor rhyolitic rocks (lavas and pyroclastic flows) that typically form calderas and domes, shield volcanoes, and rift structures. Potential hydrothermal mineral systems include low-sulfidation epithermal precious metal deposits, IOCG deposits, uranium and reduced Mo–Sn–W porphyry systems, and stratabound Au–Ag deposits, and are typically associated with potassic, fluorite, and carbonate alteration.

Vein systems and stratabound Cu, Pb, Ag, Zn, Au, and fluorite occur in felsic volcanic and volcaniclastic rocks such as the Smoke Hill Volcanics and the rocks around Skirmish Hill. The veins are structurally controlled (e.g. Tollu intrusion), possibly suggesting that some of them may be the distal parts of larger mineral systems, such as IOCG, epithermal, or intracontinental-type porphyry Mo deposits. Notably, Olympic Dam-style deposits and epithermal and porphyry systems are associated in time and space with A-type granitic intrusions in intraplate rift settings, such as in central Asia, where a large number of mineral deposits are in rift structures and temporally linked with large igneous provinces (Borisenko et al., 2006).

Laterite

Limonitic ochre material is best developed at the world-class Wingellina Hills deposit (187 Mt at about 1% Ni and 0.08% Co; >167 Mt is classified as probable mining reserve; Metals X Ltd, 2013). Limonitic ochre is also present at Claude Hills (4.5 Mt at 1.5% Ni; Goode, 2002), in the Pirntirri Mulari intrusion, and in the southeastern part of the Bell Rock intrusion where excavations exposed laterite, ochre, and chalcedonic veins above a zone of saprolite (Howard et al., 2011b). The ochres formed by selective leaching of SiO_2 and MgO, which is especially pronounced along shear zones, and the resulting passive concentration of residual alumina, iron oxides, and Ni. Potential for further deposits exists at other ultramafic intrusions. The lateritic material is locally cut by semiprecious, pale green chrysoprase mined artisanally since the 1960s, particularly in the Kalka area (Goode, 2002).

The lateritic profiles may also have some potential for scandium deposits, particularly where the parent rock was clinopyroxenite. To our knowledge, no relevant investigations have so far been conducted.

Conclusions

The west Musgrave Province is between the West Australian, South Australian, and North Australian Cratons. The area was the focus of long-lived mantle upwelling producing large volumes of magnesian basaltic to tholeiitic magma and their felsic derivatives. Magmatism led to crustal melting, lithospheric delamination, and a high crustal heat flux over >200 Ma The broadly compressive regime with localized extension favored the formation of several large mafic–ultramafic layered intrusions. Due to the large size of the bodies, cooling rates were relatively slow. Crustal loading may have led to subsidence and sagging prior to complete solidification. The cumulates unmixed and formed lenses and layers of peridotite and magnetitite that are locally enriched in PGE. Syn- to post-magmatic tectonism led to fragmentation of many of the intrusions. The degree of crustal contamination was mostly relatively minor (<5%), although locally, basaltic magmas mingled with coeval granitic magmas. The mineralization potential of the Musgrave Province is considerable. The mafic–ultramafic intrusions host significant vanadium, PGE and Ni–Cu deposits, with high potential for iron, titanium, and apatite. The heat flux generated by the large mantle melting event likely led to widespread crustal fluid flux that may have formed hydrothermal mineral deposits of variable style.

References

Abeysinghe, PB 2003, Mineral occurrences and exploration activities in the Arunta-Musgrave area: Geological Survey of Western Australia, Record 2002/9, 33p.

Aitken, AR, Dentith, MC, Evans, SF, Gallardo, LA, Joly, A, Thiel, S, Smithies, RH and Tyler, IM 2013, Imaging crustal structure in the west Musgrave Province from magnetotelluric and potential field data: Geological Survey of Western Australia, Report 114, 81p.

Aitken, ARA, Smithies, RH, Dentith, MC, Joly, A, Evans, S and Howard, HM 2012, Magmatism-dominated intracontinental rifting in the Mesoproterozoic: the Ngaanyatjarra Rift, central Australia: Gondwana Research, doi.org/10.1016/j.gr.2012.10.003.

Allard, GO 1976, The Dore Lake Complex and its importance to Chibougamau geology and metallogeny: Ministère des Richesses Naturelles, Direction Générale des Mines, Qébec, Canada, DP368.

Andersen, JCØ, Rasmussen, H, Nielsen, TFD and Ronsbo JG 1998, The Triple Group and the Platinova Au and Pd reefs in the Skaergaard Intrusion: stratigraphic and petrographic relations: Economic Geology, v. 93, p. 485–509.

Baker, PM and Waugh, RS 2004, Surface geochemistry and the discovery of the Babel and Nebo magmatic Ni-Cu-PGE deposits: Australian Institute of Geoscientists; Nickel Symposium, Perth, 12 November 2004.

Ballhaus, C and Berry, RF 1991, Crystallization pressure and cooling history of the Giles Layered Igneous Complex, central Australia: Journal of Petrology, v. 32, p. 1–28.

Ballhaus, C and Glikson, AY 1989, Magma mixing and intraplutonic quenching in the Wingellina Hills intrusion, Giles Complex, central Australia: Journal of Petrology, v. 30, p. 1443–1469.

Ballhaus, C and Glikson, AY 1995, The petrology of layered mafic–ultramafic intrusions in the Giles Complex, western Musgrave block, central Australia: AGSO Journal, v. 16, p. 69–89.

Barnes, S-J 1993, Partitioning of the PGE and gold between silicate and sulphide magmas in the Munni Munni Complex, Western Australia: Geochimica et Cosmochimica Acta, v. 57, p. 1277–1290.

Barnes, S-J and Maier, WD 1999, The fractionation of Ni, Cu and the noble metals in silicate and sulphide liquids, *in* Dynamic processes in magmatic ore deposits and their application to mineral exploration *edited by* RR Keays, CM Lesher, PC Lightfoot, and CEG Farrow: Geological Association of Canada; Short Course Notes 13, p. 69–106.

Barnes, S-J, Maier, WD and Curl, E 2010, Composition of the marginal rocks and sills of the Rustenburg Layered Suite, Bushveld Complex, South Africa: implications for the formation of the PGE deposits: Economic Geology, v. 105, p. 1491–1511.

Barrie, CT, MacTavish, AD, Walford, PC, Chataway, R and Middaugh, R 2002, Contact-type and magnetitite reef-type Pd-Cu mineralization in ferroan olivine gabbros of the Coldwell Complex, Ontario, *in* The geology, geochemistry, mineralogy and mineral beneficiation of platinum-group elements *edited by* LJ Cabri: Canadian Institute of Mining, Metallurgy and Petroleum, Special Volume 54, p. 321–338.

Becker, H, Horan, MF, Walker, RJ, Gao, S, Lorand J-P and Rudnick, RL 2006, Highly siderophile element composition of the Earth's primitive mantle: constraints from new data on peridotite massifs and xenoliths: Geochimica et Cosmochimica Acta, v. 70, p. 4528–4550.

Begg, GC, Griffin, WL, Natapov, LM, O'Reilly, SY, Grand, SP, O'Neill, CJ, Hronsky, JMA, Poudjom Djomani, Y, Swain, CJ, Deen, T and Bowden, P 2009, The lithospheric architecture of Africa: seismic tomography, mantle petrology, and tectonic evolution: Geosphere, v. 5, p. 23–50.

Berg, JH 1980, Snowflake troctolite in the Hettasch intrusion, Labrador: evidence for magma-mixing and supercooling in a plutonic environment: Contributions to Mineralogy and Petrology, v. 72, p. 339–352.

Betts, PG and Giles, D 2006, The 1800–1100 Ma tectonic evolution of Australia: Precambrian Research, v. 144, p. 92–125.

Bodorkos, S and Wingate, MTD 2008, 174589: quartz syenite dyke, Amy Giles Hill; Geochronology Record 715: Geological Survey of Western Australia, 4p.

Bodorkos, S, Wingate, MTD and Kirkland, CL 2008a, 174538: metamonzogranite, Mount Daisy Bates; Geochronology Record 712: Geological Survey of Western Australia, 4p.

Bodorkos, S, Wingate, MTD and Kirkland, CL 2008b, 174558: metamorphosed quartz diorite, Mount Fanny; Geochronology Record 713: Geological Survey of Western Australia, 4p.

Bodorkos, S, Wingate, MTD and Kirkland, CL 2008c, 174736: granofelsic metasyenogranite, Mount Fanny; Geochronology Record 717: Geological Survey of Western Australia, 4p.

Bodorkos, S, Wingate, MTD and Kirkland, CL 2008d, 174737: foliated metamonzogranite, Mount Fanny; Geochronology Record 718: Geological Survey of Western Australia, 5p.

Bodorkos, S, Wingate, MTD and Kirkland, CL 2008e, 174747: metagabbro, Mount Fanny; Geochronology Record 719: Geological Survey of Western Australia, 4p.

Borisenko, AS, Sotnikov, VI, Izokh, AE, Polyakov, GV and Obolensky, AA 2006, Permo–Triassic mineralization in Asia and its relation to plume magmatism: Russian Geology and Geophysics, v. 47, p. 166–182.

Boudreau, AE 1999, PELE–a version of the MELTS software programme for the PC platform: Computers and Geosciences, v. 25, p. 201–203.

Camacho, A 1989, The Woodroffe Thrust, eastern Musgrave Block, NT: A problem of large scale melting during thrusting: Geological Society of Australia, Abstracts 24, p. 14–15.

Camacho, A 1997, An isotopic study of deep crustal orogenic processes: Musgrave Block, Central Australia: The Australian National University, Canberra, PhD thesis (unpublished).

Camacho, A, Compston, W, McCulloch, M and McDougall, I 1997, Timing and exhumation of eclogite facies shear zones, Musgrave Block, central Australia: Journal of Metamorphic Geology, v. 15, p. 735–751.

Cameron, EN 1980, Evolution of the Lower Critical Zone, central sector, eastern Bushveld Complex: Economic Geology, v. 75, p. 845–871.

Campbell, IH and Naldrett, AJ 1979, The influence of silicate: sulfide ratios on the geochemistry of magmatic sulfides: Economic Geology, v. 74, p. 1503–1505.

Charlier, B, Namur, O, Toplis, MJ, Schiano, P, Cluzel N, Higgins, MD and Vander Auwera, J 2011, Large-scale silicate liquid immiscibility during differentiation of tholeiitic basalt to granite and the origin of the Daly gap: Geology, v. 39, p. 907–910.

Cimon, J 1998, Le Complexe de Sept Iles, L'unité à apatite de rivière des rapides, Complexe de Sept Îles, Localisation stratigraphique et facteurs à l'origine de sa formation: Ministère des Ressources Naturelles, Québec, ET97-05, 41p.

Clarke, GL, Buick, IS, Glikson, AY and Stewart, AJ 1995b, Structural and pressure-temperature evolution of host rocks of the Giles Complex, western Musgrave Block, central Australia: evidence for multiple high-pressure events: AGSO Journal of Australian Geology and Geophysics, v. 16, p 127–146.

Clarke, GL, Sun, S-S and White, RW 1995a, Grenville age belts and associated older terranes in Australia and Antarctica: AGSO Journal of Australian Geology and Geophysics, v. 16, p. 25–39.

Coleman, P 2009, Intracontinental orogenesis in the heart of Australia: structure, provenance and tectonic significance of the Bentley Supergroup, western Musgrave Block, Western Australia: Geological Survey of Western Australia, Record 2009/23, 48p.

Collins, WJ and Teyssier, C 1989, Crustal scale ductile fault systems in the Arunta Inlier, central Australia: Tectonophysics, v. 158, p. 49–66.

Crowson, P 2001, Mineral handbook 2000–2001: Mining Journal Books, Kent Edenbridge, 486p.

De Paolo, DJ and Wasserburg, GJ 1976, Inferences about magma sources and mantle structure from variations of $^{143}Nd/^{144}Nd$: Geophysical Research Letters, v. 3, p. 743–746.

Daniels, JL 1974, The Geology of the Blackstone region, Western Australia: Geological Survey of Western Australia, Bulletin 123, 257p.

Eales, HV and Cawthorn, RG 1996, The Bushveld Complex, *in* Layered intrusions *edited by* RG Cawthorn: Elsevier, Amsterdam, 181–229.

Edgoose, CJ, Scrimgeour, IR and Close, DF 2004, Geology of the Musgrave Block, Northern Territory: Northern Territory Geological Survey, Report 15, 48p.

Eggins, SM, Woodhead, JD, Kinsley, LPJ, Mortimer, GE, Sylvester, P, McCulloch, MT, Hergt, JM and Handler, MR 1997, A simple method for the precise determination of >40 trace elements in geological samples by ICPMS using enriched isotope internal standardisation: Chemical Geology, v. 134, p. 311–326.

Evins, PM, Smithies, RH, Howard, HM, Kirkland, CL, Wingate, MTD and Bodorkos, S 2010a, Redefining the Giles Event within the setting of the 1120–1020 Ma Ngaanyatjarra Rift, west Musgrave Province, Central Australia: Geological Survey of Western Australia, Record 2010/6, 36p.

Evins, PM, Smithies, RH, Howard, HM, Kirkland, CL, Wingate, MTD and Bodorkos, S 2010b, Devil in the detail: the 1150–1000 Ma magmatic and structural evolution of the Ngaanyatjarra Rift, west Musgrave Province, Central Australia: Precambrian Research, v. 183, p. 572–588.

Evins, PM, Smithies, RH, Howard, HM and Maier, WD 2009, Holt, WA Sheet 4546: Geological Survey of Western Australia, 1:100 000 Geological Series.

Flöttmann, T and Hand, M 1999, Folded basement-cored tectonic wedges along the northern edge of the Amadeus Basin, central Australia; evaluation of orogenic shortening: Journal of Structural Geology, v. 21, p. 399–412.

Foulger, GR 2010, Plates vs plumes: Wiley-Blackwell, Chichester, 328p.

Freestone, IC 1978, Liquid immiscibility in alkali-rich magmas: Chemical Geology, v. 23, p. 116–123.

Gauert, CDK, de Waal, SA and Wallmach, T 1995, Geology of the ultrabasic to basic Uitkomst Complex, eastern Transvaal, South Africa: an overview: Journal of African Earth Sciences, v. 21, p. 553–570.

Giles, D, Betts, PG and Lister, GS 2004, 1.8 – 1.5-Ga links between the North and South Australian Cratons and the Early–Middle Proterozoic configuration of Australia: Tectonophysics, v. 380, p. 27–41.

Glikson, AY (editor) 1995, The Giles mafic–ultramafic complex and environs, western Musgrave Block, central Australia: Thematic issue: AGSO Journal of Geology and Geophysics, v. 16, no. 1–2, 193p.

Glikson, AY, Stewart, AT, Ballhaus, GL, Clarke, GL, Feeken, EHT, Level, JH, Sheraton, JW and Sun, S-S 1996, Geology of the western Musgrave Block, central Australia, with reference to the mafic–ultramafic Giles Complex: Australian Geological Survey Organisation, Bulletin 239, 206p.

Godel, B, Seat, Z, Maier, WD and Barnes, S-J 2011, The Nebo–Babel Ni-Cu-PGE sulfide deposit (West Musgrave Block, Australia): part 2 — constraints on parental magma and processes, with implications for mineral exploration: Economic Geology, v. 106, p. 557–584.

Goode, ADT 1970, The petrology and structure of the Kalka and Ewarara layered basic intrusions, Giles Complex, central Australia: The University of Adelaide, Adelaide, PhD thesis (unpublished).

Goode, ADT 1976a, Small scale primary cumulus igneous layering in the Kalka layered intrusion, Giles Complex, central Australia: Journal of Petrology, v. 17, p. 379–397.

Goode, ADT 1976b, Sedimentary structures and magma current velocities in the Kalka layered intrusion, central Australia: Journal of Petrology, v. 17, p. 546–558.

Goode, ADT 1977a, Vertical igneous layering in the Ewarara layered intrusion, central Australia: Geological Magazine, v. 114, p. 215–218.

Goode, ADT 1977b, Flotation and remelting of plagioclase in the Kalka Intrusion, central Australia: petrological implications for anorthosite genesis: Earth and Planetary Science Letters, v. 34, p. 375–380.

Goode, ADT 1977c, Intercumulus igneous layering in the Kalka layered intrusion, central Australia: Geological Magazine, v. 114, p. 215–218.

Goode, ADT 1978, High temperature, high strain rate deformation in the lower crustal Kalka Intrusion, central Australia: Contributions to Mineralogy and Petrology, v. 66, p. 137–148.

Goode, ADT 2002, The Western Musgrave Block – Australia: Data Metallogenica, District Overview, 42p.

Goode, ADT and Krieg, GW 1967, The geology of Ewarara Intrusion, Giles Complex, central Australia: Journal of the Geological Society of Australia, v. 14, p. 185–194.

Goode, ADT and Moore, AC 1975, High pressure crystallisation of the Ewarara, Kalka and Gosse Pile intrusions, Giles Complex, central Australia: Contributions to Mineralogy and Petrology, v. 51, p. 77–97.

Gray, CM 1971, Strontium isotope studies on granulites: The Australian National University, Canberra, PhD thesis (unpublished), 242p.

Gray, CM 1967, The geology, petrology and geochemistry of the Teizi metanorthosite: The University of Adelaide, Adelaide, Honours thesis (unpublished).

Gray, CM, Cliff, RA and Goode, ADT, 1981, Neodymium–strontium isotopic evidence for extreme contamination in a layered basic intrusion: Earth and Planetary Science Letters, v. 56, p. 189–198.

Gray, CM and Goode, ADT 1989, The Kalka layered intrusion, central Australia: a strontium isotopic history of contamination and magma dynamics: Contributions to Mineralogy and Petrology, v. 103, p. 35–43.

Green, TH 1994, Experimental studies of trace-element partitioning applicable to igneous petrogenesis — Sedona 16 years later: Chemical Geology, v. 117, p. 1–36.

Habteselassie, MM, Mathison, CI and Gilkes, RJ 1996, Vanadium in magnetite gabbros and its behaviour during lateritic weathering, Windimurra Complex, Western Australia: Australian Journal of Earth Sciences, v. 43, p. 555–566.

Haines, PW, Hand, M and Sandiford, M 2001, Palaeozoic syn-orogenic sedimentation in central and northern Australia: a review of distribution and timing of intracontinental orogens: Australian Journal of Earth Science, v. 48, no. 6, p. 911–928.

Howard, HM, Smithies, RH, Kirkland, CL, Evins, PM and Wingate, MTD 2009, Age and geochemistry of the Alcurra Suite in the west Musgrave Province and implications for orthomagmatic Ni-Cu-PGE mineralization during the Giles Event: Geological Survey of Western Australia, Record 2009/16, 16p.

Howard, HM, Smithies, RH and Pirajno, F 2006b, Geochemical and Nd isotopic signatures of mafic dykes in the western Musgrave Complex: Geological Survey of Western Australia Annual Review 2005–06, p. 64–71.

Howard, HM, Smithies, RH, Pirajno, F and Skwarnecki, MS 2006a, Bates, WA Sheet 4646: Geological Survey of Western Australia, 1:100 000 Geological Series.

Howard, HM, Smithies, RH, Pirajno, F and Skwarnecki, MS 2007, Bell Rock, WA Sheet 4645: Geological Survey of Western Australia, 1:100 000 Geological Series.

Howard, HM, Smithies, RH, Werner, M, Kirkland, CL and Wingate, MTD 2011a, Geochemical characteristics of the Alcurra Dolerite (Giles Event) and its extrusive equivalents in the Bentley Supergroup: Geological Survey of Western Australia, Record 2011/2, p. 27–30.

Howard, HM, Werner, M, Smithies, RH, Kirkland, CL, Kelsey, DL, Hand, M, Collins, A, Pirajno, F, Wingate, MTD, Maier, WD and Raimondo, T 2011b, The geology of the west Musgrave Province and the Bentley Supergroup — a field guide: Geological Survey of Western Australia, Record 2011/4, 119p.

Iljina, MJ and Lee, CA 2005, PGE deposits in the marginal series of layered intrusions, *in* Exploration for platinum group element deposits *edited by* JE Mungall: Mineralogical Association of Canada, Short Course Series 35, p. 75–96.

Irvine, TN 1970, Crystallization sequences in magmas of the Muskox intrusion and some other layered intrusions: Geological Society of South Africa, Special Publication 1, p. 441–476.

Irvine, TN, Andersen, JCO and Brooks, CK 1998, Included blocks (and blocks within blocks) in the Skaergaard intrusion: geological relations and the origins of rhythmic modally graded layers: Geological Society of America, Bulletin 110, p. 1398–1447.

Jakobsen, JK, Veksler, IV, Tegner, C and Brooks, CK 2005, Immiscible iron- and silica-rich melts in basalt petrogenesis documented in the Skaergaard intrusion: Geology, v. 33, p. 885–888.

Jugo, PJ, Luth, RW and Richards, JP 2005, An experimental study of the sulfur content in basaltic melts saturated with immiscible sulfide or sulfate liquids at 1300°C and 1.0 GPa: Journal of Petrology, v. 46, p. 783–798.

Keays, RR and Lightfoot, PC 2010, Crustal sulfur is required to form magmatic Ni–Cu sulfide deposits: evidence from chalcophile element signatures of Siberian and Deccan Trap basalts: Mineralium Deposita, v. 45, p. 241–257.

Kelsey, DE, Hand, M, Evins, P, Clark, C and Smithies, H 2009, High temperature, high geothermal gradient metamorphism in the Musgrave Province, central Australia: potential constraints on tectonic setting, *in* Biennial conference of the Specialist Group for Geochemistry, Mineralogy and Petrology, Kangaroo Island, November 2009 *edited by* NE Timms, J Foden, K Evans and C Clark: Geological Society of Australia Abstracts No. 96, p. 28.

Kelsey, DE, Hand, M, Smithies, H, Evins, P, Clark, C and Kirkland, CL 2010, What is the tectonic setting of long-lived Grenvillian-aged ultrahigh temperature, high geothermal gradient metamorphism in the Musgrave Province, central Australia?: Geological Society of America, Abstracts with Programs, 42(5), p. 516.

King, RJ 2008, Using calculated pseudosections in the system NCKFMASHTO and SHRIMP II U–Pb zircon dating to constrain the metamorphic evolution of paragneisses in the Latitude Hills, West Musgrave Province, Western Australia: Geological Survey of Western Australia, Record 2009/15, 67p.

Kirkland, CL, Wingate, MTD and Bodorkos, S 2008a, 183496: orthogneiss, Mount West; Geochronology Record 747: Geological Survey of Western Australia, 5p.

Kirkland, CL, Wingate, MTD and Bodorkos, S 2008b, 183459: charnockite, Latitude Hill, Geochronology Record 722: Geological Survey of Western Australia, 5p.

Kirkland, CL, Wingate, MTD and Bodorkos, S 2008c, 183509: leucogranite dyke, Mount West; Geochronology Record 724: Geological Survey of Western Australia, 4p.

Kirkland, CL, Wingate, MTD and Bodorkos, S 2008d, 193850: leucogranite dyke, Mount Fanny; Geochronology Record 748: Geological Survey of Western Australia, 4p.

Kirkland, CL, Wingate, MTD and Bodorkos, S 2008e, 174761: porphyritic granite dyke, Bell Rock; Geochronology Record 721: Geological Survey of Western Australia, 4p.

Kirkland, CL, Wingate, MTD and Bodorkos, S 2008f, 185509: leucogranite, Mount Aloysius; Geochronology Record 725: Geological Survey of Western Australia, 4p.

Kirkland, CL, Wingate, MTD and Smithies, RH 2011, 194762: leucogabbro, Mount Finlayson; Geochronology Record 966: Geological Survey of Western Australia, 4p.

Kirkland, CL, Smithies, RH, Woodhouse, AJ, Howard, HM, Wingate, MTD, Belousova, EA, Cliff, JB, Murphy, RC and Spaggiari, CV 2013, Constraints and deception in the isotopic record; the crustal evolution of the west Musgrave Province, central Australia: Gondwana Research, v. 23, p. 759–781.

Klemm, DD, Henckel, J, Dehm, R and von Gruenewaldt, G 1985, The geochemistry of titanomagnetite in magnetite layers and their host rocks of the eastern Bushveld Complex: Economic Geology, v. 80, p. 1075–1088.

Kouchi, A, Tsuchiyama, A and Sunagawa, I 1986, Effect of stirring on crystallisation kinetics of basalt: texture and element partitioning: Contributions to Mineralogy and Petrology, v. 93, p. 429–438.

Kruger, FJ 2005, Filling the Bushveld Complex magma chamber: lateral expansion, roof and floor interaction, magmatic unconformities, and the formation of giant chromitite, PGE, and Ti–V magnetitite deposits: Mineralium Deposita, v. 40, p. 451–472.

Lassiter, JC and De Paolo, DJ 1997, Plume/lithosphere interaction in the generation of continental and oceanic flood basalts: chemical and isotopic constraints, *in* Large igneous provinces *edited by* JJ Mahoney and MF Coffin: American Geophysical Union, Geophysical Monographs v. 100, p. 335–356.

Latypov, R 2003, The origin of marginal compositional reversals in basic-ultrabasic sills and layered intrusions by Soret fractionation: Journal of Petrology, v. 44, p. 1579–1618.

Lesher, CM and Burnham, OM 2001, Multicomponent elemental and isotopic mixing in Ni–Cu–(PGE) ores at Kambalda, Western Australia: Canadian Mineralogist, v. 39, p. 421–446.

Li, C and Ripley, EM 2010, The relative effects of composition and temperature on olivine-liquid partitioning: statistical deconvolution and implications for petrologic modelling: Chemical Geology, v. 275, p. 95–104.

Li, C, Ripley, EM, Oberthür, T, Miller, JD Jr and Joslin, GD 2008, Textural, mineralogical and stable isotope studies of hydrothermal alteration in the main sulfide zone of the Great Dyke, Zimbabwe and the precious metals zone of the Sonju Lake Intrusion, Minnesota, USA: Mineralium Deposita, v. 43, p. 97–110.

Liebenberg, L 1970, The sulfides in the layered sequence of the Bushveld igneous Complex: Geological Society of South Africa, Special Publication, v. 1, p. 108–208.

Lightfoot, PC and Naldrett, AJ 1983, The geology of the Tabankulu section of the Insizwa Complex, Transkei, Southern Africa, with reference to the nickel sulphide potential: Transactions of the Geological Society of South Africa, v. 86, p. 169–187.

Lipin, BR 1993, Pressure increases, the formation of chromite seams, and the development of the Ultramafic series in the Stillwater Complex, Montana: Journal of Petrology, v. 34, p. 955–976.

London, D 2008, Pegmatites: Canadian Mineralogist, Special

Publication, v. 10, 374p.

Maier, WD 2005, Platinum-group element (PGE) deposits and occurrences: mineralization styles, genetic concepts and exploration criteria: Journal of African Earth Sciences, v. 41, p. 165–191.

Maier, WD and Barnes, S-J 1998, Concentrations of rare earth elements in silicate rocks of the Lower, Critical and Main Zones of the Bushveld Complex: Chemical Geology, v. 150, p. 85–103.

Maier, WD, Barnes, S-J, Gartz, V and Andrews, G 2003b, Pt–Pd reefs in magnetitites of the Stella layered intrusion, South Africa: a world of new exploration opportunities for platinum group elements: Geology, v. 31, p. 885–888.

Maier, WD, Barnes, S-J and Groves, DI 2013b, The Bushveld Complex, South Africa: formation of platinum–palladium, chrome and vanadium- rich layers via hydrodynamic sorting of a mobilized cumulate slurry in a large, relatively slowly cooling, subsiding magma chamber: Mineralium Deposita, v. 48, p. 1–56.

Maier, WD, Barnes, S-J and Marsh, JS 2003a, The concentrations of the noble metals in southern African flood-type basalts and MORB: implications for petrogenesis and magmatic sulphide exploration: Contributions to Mineralogy and Petrology, v. 146, p. 44–61.

Maier, WD and Eales, HV 1997, Correlation within the UG2 – Merensky Reef interval of the Western Bushveld Complex, based on geochemical, mineralogical and petrological data: Geological Survey of South Africa, Bulletin 120, 56p.

Maier, WD, McDonald, I and Le Roex, A 2013c, PGE contents in kimberlites: constraints on mantle sources, *in* Mineral deposit research for a high-tech world *edited by* E Jonsson et al.: SGA, 12th biennial SGA meeting, Uppsala, Sweden, 12–15 August 2013, proceedings, p. 1044–1046.

Maier, WD, Rasmussen, B, Li, C, Barnes, S-J and Huhma, H 2013a, The Kunene anorthosite complex, Namibia, and its satellite bodies: geochemistry, geochronology and economic potential: Economic Geology, v. 108, p. 953–986.

McBirney, AR and Noyes, RM 1979, Crystallization and layering of the Skaergaard intrusion: Journal of Petrology, v. 20, p. 487–554.

Metals X Ltd 2013, Globally significant nickel project, viewed 8 April 2014, <http://www.metalsx.com.au/system/assets/26/original/Nickel_Division.pdf>.

Miller, JD, Green, JC, Severson, MJ, Chandler, VW, Hauck, SA, Peterson, DM and Wahl, TE 2002, Geology and mineral potential of the Duluth Complex and related rocks of northeastern Minnesota: Minnesota Geological Survey Report, v. 58, 207p.

Mitchell, AA 1986, The petrology, mineralogy and geochemistry of the Main Zone of the Bushveld Complex at Rustenburg Platinum Mine, Union Section: Rhodes University, Grahamstown, PhD thesis (unpublished).

Moore, AC 1971, Some aspects of the geology of the Gosse Pile ultramafic intrusion, central Australia: Journal of the Geological Society of Australia, v. 18, p. 69–80.

Morris, PA and Pirajno, F 2005, Geology, geochemistry, and mineralization potential of Mesoproterozoic sill complexes of the Bangemall Supergroup, Western Australia: Geological Survey of Western Australia, Report 99, 72p.

Morse, SA 1981, Kiglapait geochemistry IV: the major elements: Geochimica et Cosmochimica Acta, v. 45, p. 461–479.

Mutanen, T 1997, Geology and petrology of the Akanvaara and Koitelainen mafic layered intrusions and Keivitsa–Satovaara layered complex, northern Finland: Geological Survey of Finland, Bulletin 395, 233p.

Nabil, H 2003, Genèse des dépots de Fe–Ti–P associés aux intrusions litées (exemples: l'intrusion mafique de Sept Îles au Québec; Complexe de Duluth aux États Unis): The University of Quebec, Chicoutimi, PhD thesis (unpublished).

Naldrett, AJ 1997, Key factors in the genesis of Noril'sk, Sudbury, Jinchuan, Voisey's Bay and other world-class Ni–Cu–PGE deposits: implications for exploration. Australian Journal of Earth Sciences, v. 44, p. 283–315.

Naldrett, AJ and Lehmann, J 1988, Spinel nonstoichiometry as the explanation for Ni-, Cu-, and PGE-enriched sulphides in chromitites, *in* Geo–Platinum 87 *edited by* HM Prichard et al.: Elsevier, Barking, p. 93–109.

Naslund, HR 1983, The effect of oxygen fugacity on liquid immiscibility in iron-bearing silicate melts: American Journal of Science, v. 283, p. 1034–1059.

Nesbitt, RW, Goode, ADT, Moore, AC and Hopwood, TP 1970, The Giles Complex, central Australia: a stratified sequence of mafic and ultramafic intrusions: Special Publications of the Geological Society of South Africa, v. 1, p. 547–564.

Nesbitt, RW and Talbot, JL 1966, The layered basic and ultrabasic intrusives of the Giles Complex, central Australia: Contributions to Mineralogy and Petrology, v. 13, p. 1–11.

Norrish, K and Chappell, BW 1977, X-ray fluorescence spectrometry, *in* Physical Methods in Determinative Mineralogy, 2nd Edition *edited by* J Zussman: Academic Press, London, p. 201–272.

Norrish, K and Hutton, JT 1969, An accurate X-ray spectrographic method for the analysis of a wide range of geological samples: Geochemica et Cosmochimica Acta, v. 33, p. 431–453.

Parsons, I and Becker, S 1987, Layering, compaction and postmagmatic processes in the Klokken Intrusion, *in* Origins of igneous layering *edited by* I Parsons: Reidel, Dordrecht, p. 29–92.

Pascoe, A 2012, The geochemistry and petrogenesis of the mafic and ultramafic Giles intrusions at Latitude Hill, west Musgrave Province, Western Australia: The University of Tasmania, Hobart, BSc Honours thesis (unpublished).

Philpotts, AR 1967, Origin of certain iron–titanium oxide and apatite rocks: Economic Geology, v. 62, p. 303–315.

Phosphate Australia Ltd 2014, Manchego Prospect: Musgrave Project, Western Australia, viewed 6 May 2014, <http://www.asx.com.au/asxpdf/20140103/pdf/42lz643zrngqwx.pdf>.

Pirajno, F, Smithies, HR and Howard, HM 2006, Mineralisation associated with the 1076 Ma Giles mafic–ultramafic intrusions, Musgrave Complex, central Australia: a review: SGA News, v. 20, p. 1–20.

Prendergast, M, Bennett, M and Henicke, G 1998, Platinum exploration in the Rincon del Tigre Complex, eastern Bolivia: Transactions of the Institute of Mining and Metallurgy, v. 107, p. B39–47.

Raedeke, LD 1982, Petrogenesis of the Stillwater Complex: The University of Washington, Seattle, PhD thesis (unpublished).

Raimondo, T, Collins, AS, Hand, M, Walker-Hallam, A, Smithies, RH, Evins, PM and Howard, HM 2009, Ediacaran intracontinental channel flow: Geology, v. 37, p. 291–294.

Raimondo, T, Collins, AS, Hand, M, Walker-Hallam, A, Smithies, RH, Evins, PM and Howard, HM 2010, The anatomy of a deep intracontinental orogen: Tectonics, v. 29, TC4024, doi:10.1029/2009TC002504, 2010.

Redstone Resources Ltd 2008a, Quarterly report for the period ending June 30th 2008, viewed 6 May 2014, <http://www.redstone.com.au/investor_centre_asx_announcements_files/2008_07_31_01.pdf>.

Redstone Resources Ltd 2008b, Report of the Annual General Meeting, viewed 8 April 2014, <http://www.asx.com.au/asxpdf/20081127/pdf/31dvzvjbkp7f5b.pdf>.

Reynolds, IM 1979, Vanadium-bearing titaniferous iron ores from the Rooiwater, Usushwana, Mambula, Kaffirskraal and Trompsburg Igneous Complexes, Randburg: Natal Institute of Metallurgy, Report 2017, 61p.

Reynolds, IM 1985, The nature and origin of titaniferous magnetite-rich layers in the Upper Zone of the Bushveld Complex: a review and synthesis: Economic Geology, v. 80, p. 1089–1108.

Roedder, E 1978, Silicate liquid immiscibility in magmas and in the system K_2O-FeO-Al_2O_3-SiO_2: an example of serendipity: Geochimica et Cosmochimica Acta, v. 42, p.1597–1617.

Roeder, PL and Campbell, IH 1985, The effect of postcumulus reactions on composition of chrome-spinels from the Jimberlana Intrusion: Journal of Petrology, v. 26, p. 763–786.

Sá, HS, Barnes, S-J, Prichard, HM and Fisher, PC 2005, The distribution of base metals and platinum-group elements in magnetitites and their host rocks in the Rio Jacaré Intrusion, Northeastern Brazil: Economic Geology, v. 100, p. 333–348.

Scoates, JS, and Mitchell, JN 2000, The evolution of troctolitic and high-Al basaltic magmas in Proterozoic anorthosite plutonic suites and implications for the Voisey's Bay massive Ni–Cu sulfide deposit: Economic Geology, v. 95, p. 677–701.

Scrimgeour, IR and Close, DF 1999, Regional high pressure metamorphism during intracratonic deformation: the Petermann orogeny, central Australia: Journal of Metamorphic Geology, v. 17, p. 557–572.

Seat, Z 2008, Geology, petrology, mineral and whole-rock chemistry, stable and radiogenic isotope systematics and Ni–Cu–PGE mineralisation of the Nebo–Babel intrusion, west Musgrave, Western Australia: The University of Western Australia, Perth, PhD thesis (unpublished).

Seat, Z, Beresford, SW, Grguric, BA, Gee, MA and Grassineau, NV 2009, Reevaluation of the role of external sulfur addition in the genesis of Ni–Cu–PGE deposits: evidence from the Nebo–Babel Ni–Cu–PGE deposit: West Musgrave, Western Australia: Economic Geology, v. 104, p. 521–538.

Seat, Z, Beresford, SW, Grguric, BA, Waugh, RS, Hronsky, JMA, Gee, MMA, Groves, DI and Mathison, CI 2007, Architecture and emplacement of the Nebo–Babel gabbro-norite-hosted magmatic Ni–Cu–PGE sulfide deposit, West Musgrave, Western Australia: Mineralium Deposita, v. 42, p. 551–582.

Seat, Z, Gee, MA, Grguric, BA, Beresford, SW and Grassineau, NV 2011, The Nebo–Babel Ni–Cu–PGE sulfide deposit (West Musgrave, Australia): Part 1. U/Pb Zircon Ages, whole-rock and mineral chemistry, and O–Sr–Nd isotope compositions of the intrusion, with constraints on petrogenesis: Economic Geology, v. 106, p. 527–556.

Seubert, REB, Keays, RR and Jowitt, SM 2011, Petrogenesis and Ni–Cu–PGE sulfide potential of the Bell Rock Range, Giles Complex, central Australia, *in* Society for Geology applied to mineral deposits, (SGA) Meeting, Townsville, Qld, Proceedings.

Sharpe, MR 1981, The chronology of magma influxes to the eastern compartment of the Bushveld Complex, as exemplified by its marginal border group: Journal of the Geological Society of London, v. 138, p. 307–326.

Sheraton, JW and Sun, S-s 1995, Geochemistry and origin of felsic igneous rocks of the western Musgrave Block: AGSO Journal, v. 16, p. 107–125.

Silver, PG, Behn, MD, Kelley, K, Schmitz, M and Savage, B 2006, Understanding cratonic flood basalts: Earth and Planetary Science Letters, v. 245, p. 190–201.

Smithies, RH, Howard, HM, Evins, PM, Kirkland, CL, Bodorkos, S and Wingate, MTD 2009, The west Musgrave Complex — some new geological insights from recent mapping, geochronology, and geochemical studies: Geological Survey of Western Australia, Record 2008/19, 20p.

Smithies, RH, Howard, HM, Evins, PM, Kirkland, CL, Kelsey, DE, Hand, M, Wingate, MTD, Collins, AS, Belousova, E and Allchurch, S 2010, Geochemistry, geochronology and petrogenesis of Mesoproterozoic felsic rocks in the western Musgrave Province of central Australia, and implication for the Mesoproterozoic tectonic evolution of the region: Geological Survey of Western Australia, Report 106, 73p.

Smithies, RH, Howard, HM, Evins, PM, Kirkland, CL, Kelsey, DE, Hand, M, Wingate, MTD, Collins, AS and Belousova, E 2011, Mesoproterozoic high temperature granite magmatism, crust–mantle interaction and the intracontinental evolution of the Musgrave Province: Journal of Petrology, doi:10.1093/petrology/egr010.

Smithies, RH, Howard, HM, Kirkland, CL, Werner, M, Medlin, CC, Wingate, MTD and Cliff, JB 2013, Geochemical evolution of rhyolites of the Talbot Sub-basin and associated felsic units of the Warakurna Supersuite: Geological Survey of Western Australia, Report 118, 74p.

Smithies, RH, Kirkland, CL, Korhonen, FJ, Aitken, ARA, Howard, HM, Maier, WD, Wingate, MTD, Quentin de Gromard, R and Gessner, K 2014, The Mesoproterozoic thermal evolution of the Musgrave Province in central Australia – Plume vs. the geological record: Gondwana Research, http://dx.doi.org?10.1016/j.gr.2013.12.014.

Sobolev, SV, Sobolev, AV, Kuzmin, DV, Krivolutskaya, NA, Petrunin, AG, Arndt, NT, Radko, VA and Vasiliev, YR 2011, Linking mantle plumes, large igneous provinces and environmental catastrophes: Nature, v. 477, p. 312–316.

Sprigg, RC and Wilson, RB 1959, The Musgrave mountain belt in South Australia: Geologische Rundschau, v. 47, p. 531–542.

Staubmann, M 2010, The petrogenesis and economic potential of the Southern Cavenagh Range Intrusion (West Musgraves), Western Australia: The University of Tasmania, Hobart, BSc Honours thesis (unpublished).

Stewart, AJ 1995, Resolution of conflicting structures and deformation history of the Mount Aloysius granulite massif, western Musgrave Block, central Australia: AGSO Journal of Australian Geology and Geophysics, v. 16, p. 91–105.

Sun, S-s, and McDonough, WF 1989, Chemical and isotopic systematics of oceanic basalts: implications for mantle composition and processes, *in* Magmatism in the ocean basins *edited by* AD Saunders and MJ Norry: Geological Society Special Publication, 42, p. 313–345.

Sun, S-S, Sheraton, JW, Glikson, AY and Stewart, AJ 1996, A major magmatic event during 1050–1080 Ma in central Australia, and an emplacement age for the Giles Complex: AGSO Journal of Australian Geology and Geophysics, 24, p. 13–15.

Tegner, C, Wilson, JR and Brooks, CK 1993, Intraplutonic quench zones in the Kap Edvard Holm layered gabbro complex, east Greenland: Journal of Petrology, v. 34, p. 681–710.

Teigler, B and Eales, HV 1993, Correlation between chromite composition and PGE mineralization in the Critical Zone of the western Bushveld Complex: Mineralium Deposita, v. 28, p. 291–302.

Teigler, B and Eales, HV 1996, The Lower and Critical Zones of the western limb of the Bushveld Complex, as indicated by the Nooitgedacht boreholes: Geological Survey of South Africa, Bulletin 111, 126p.

Tollari, N, Baker, D and Barnes, S-J 2008, Experimental effects of pressure and fluorine on apatite saturation in mafic magmas, with reference to layered intrusions and massif anorthosites: Contributions to Mineralogy and Petrology, v. 156, p. 161–175.

Tollari, N, Toplis, MJ and Barnes, S-J 2006, Predicting phosphate saturation in silicate magmas: an experimental study of the effects of melt composition and temperature: Geochimica et Cosmochimica Acta, v. 70, p. 1518–1536.

Toplis, MJ and Carroll, MR 1995, An experimental-study of the influence of oxygen fugacity on Fe–Ti oxide stability, phase-relations, and mineral–melt equilibria in ferro-basaltic systems: Journal of Petrology, v. 36, p. 1137–1170.

Toplis, MJ and Carroll, MR 1996, Differentiation of ferro-basaltic magmas under conditions open and closed to oxygen: implications for the Skaergaard intrusion and other natural systems: Journal of Petrology, v. 37, p. 837–858.

Traka Resources Ltd 2011, Quarterly Activities Report for the three months ended 30 June 2011.

Traka Resources Ltd 2013, Musgrave Project, viewed 29 August 2013, <http://www.trakaresources.com.au>.

Ulmer, GC 1969, Experimental investigation of chromite spinels: Economic Geology, Monograph 4, p 114–131.

Wade, BP 2006, Unravelling the tectonic framework of the Musgrave Province, central Australia: The University of Adelaide, Adelaide, PhD thesis (unpubished).

Wade, BP 2012, Unravelling the tectonic framework of the Musgrave Province, Central Australia: The University of Adelaide, PhD, 219p.

Wade, BP, Kelsey, DE, Hand, M and Barovich, KM 2008, The Musgrave Province: stitching north, west and south Australia: Precambrian Research, v. 166, p. 370–386.

Wadsworth, WJ 1988, Silicate mineralogy of the middle zone cumulates and associated gabbroic rocks from the Insch Intrusion, NE Scotland: Mineral Magazine, v. 52, p. 309–322.

Waight, TE, Maas, R and Nicholls, IA 2000, Fingerprinting feldspar phenocrysts using crystal isotopic composition stratigraphy: implications for crystal transfer and magma mingling in S-type granites: Contributions to Mineralogy and Petrology, v. 139, p. 227–239.

White, RW, Clarke, GL and Nelson, DR 1999, SHRIMP U–Pb zircon dating of Grenville-age events in the western part of the Musgrave Block, central Australia: Journal of Metamorphic Geology, v. 17, p. 465–481.

Wilson, AH, 1982, The Geology of the Great 'Dyke', Zimbabwe: the ultramafic rocks: Journal of Petrology, v. 23, p. 240–292.

Wilson, AH, Naldrett, AJ and Tredoux, M 1989, Distribution and controls of platinum group element and base metal mineralization in the Darwendale subchamber of the Great Dyke, Zimbabwe: Geology, v. 17, p. 649–652.

Wingate, MTD, Campbell, IH, Compston, W and Gibson, GM 1998, Ion microprobe U–Pb ages for Neoproterozoic basaltic magmatism in south-central Australia and implications for the breakup of Rodinia: Precambrian Research, v. 87, p. 135–159.

Wingate, MTD, Pirajno, F and Morris, PA 2004, Warakurna large igneous province: a new Mesoproterozoic large igneous province in west-central Australia: Geology, v. 32, p. 105–108.

Yang, S, Maier, WD, Hanski, E, Lappalainen, M, Santaguida, F and Määttä, S 2013, Origin of ultra-nickeliferous olivine in the Kevitsa Ni–Cu–PGE mineralized intrusion, Lapland, Finland: Contributions to Mineralogy and Petrology, v. 166, p. 81–95.

Zhao, J-X, McCulloch, MT and Korsch, RJ 1994, Characterisation of a plume-related ~800 Ma magmatic event and its implications for basin formation in central-southern Australia: Earth and Planetary Science Letters, v. 121, p. 349–367.

Zhou, M-F, Robinson, PT, Lesher, CM, Keays, RR, Zhang, C-J and Malpas, J 2005, Geochemistry, petrogenesis and metallogenesis of the Panzhihua gabbroic layered intrusion and associated Fe–Ti–V oxide deposits, Sichuan Province, SW China: Journal of Petrology, v. 46, p. 2253–2280.

Appendix 1

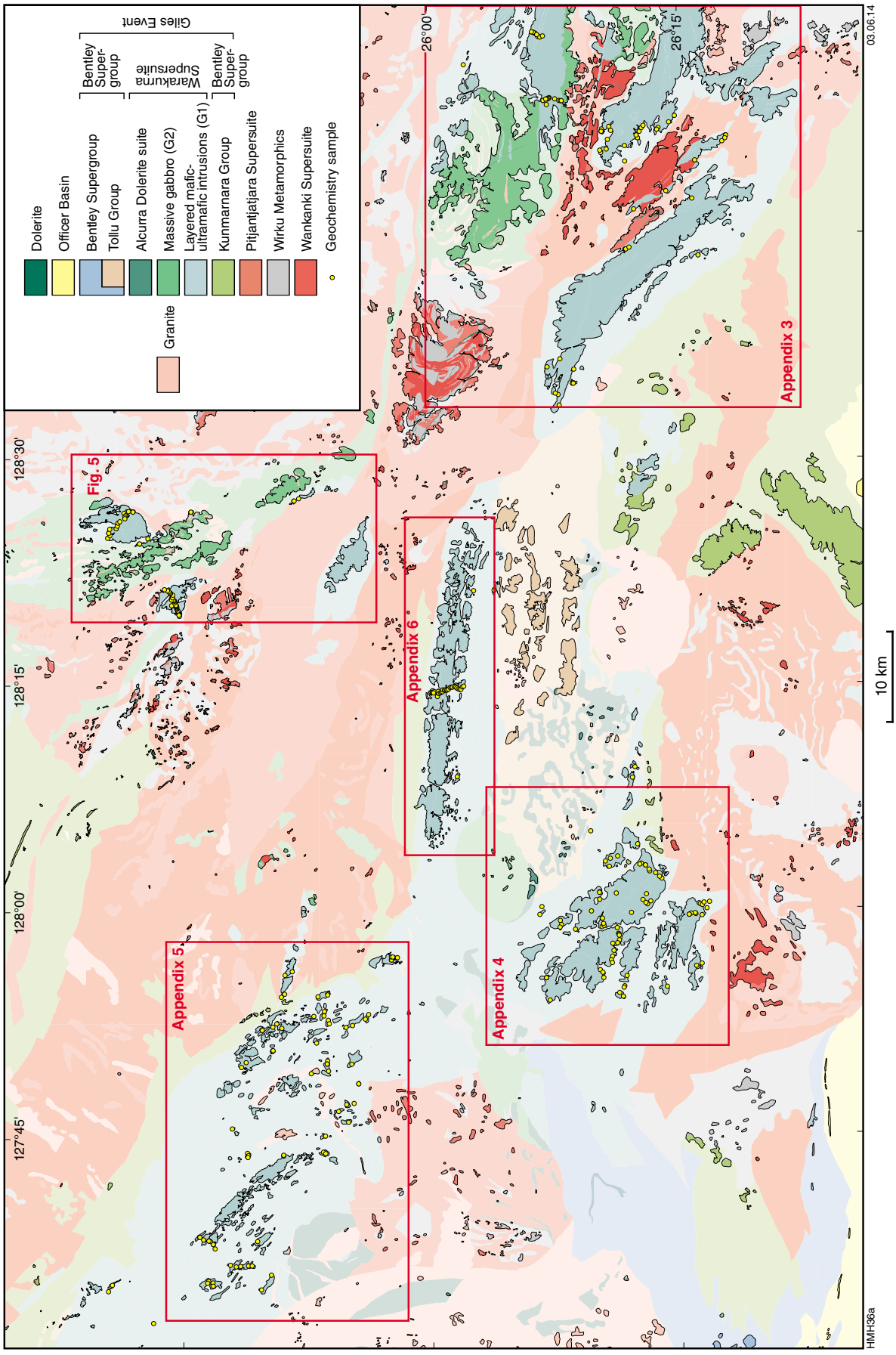

Simplified solid geological map of the west Musgrave Province. Light shaded areas indicate regions of regolith cover.

Appendix 2

Legend to Appendices 1, and 3–6

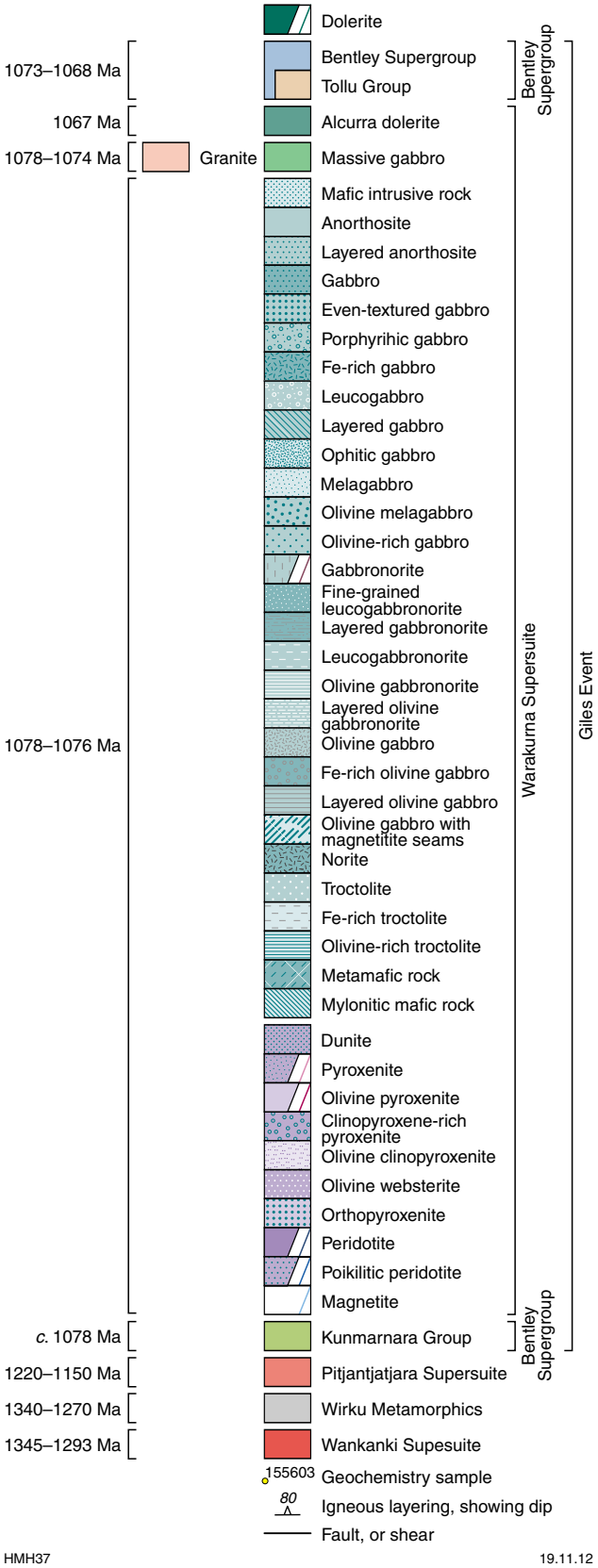

Appendix 3

Interpreted bedrock geological map of the Bell Rock – Wingellina area, showing sample localities. Light shaded areas indicate regions of regolith cover.

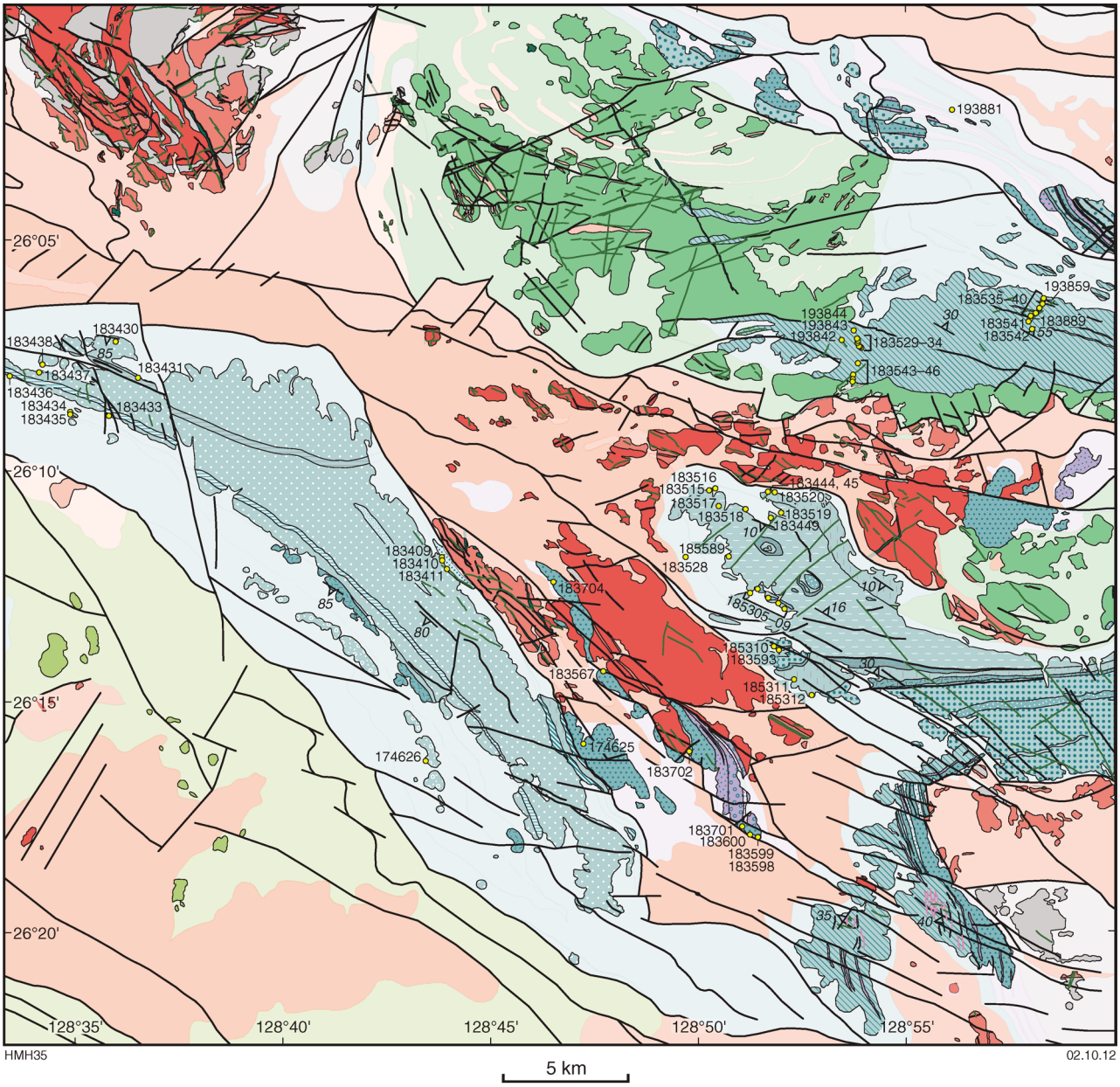

Appendix 4

Interpreted bedrock geological map of the Cavenagh Range area, showing sample localities. Light shaded areas indicate regions of regolith cover.

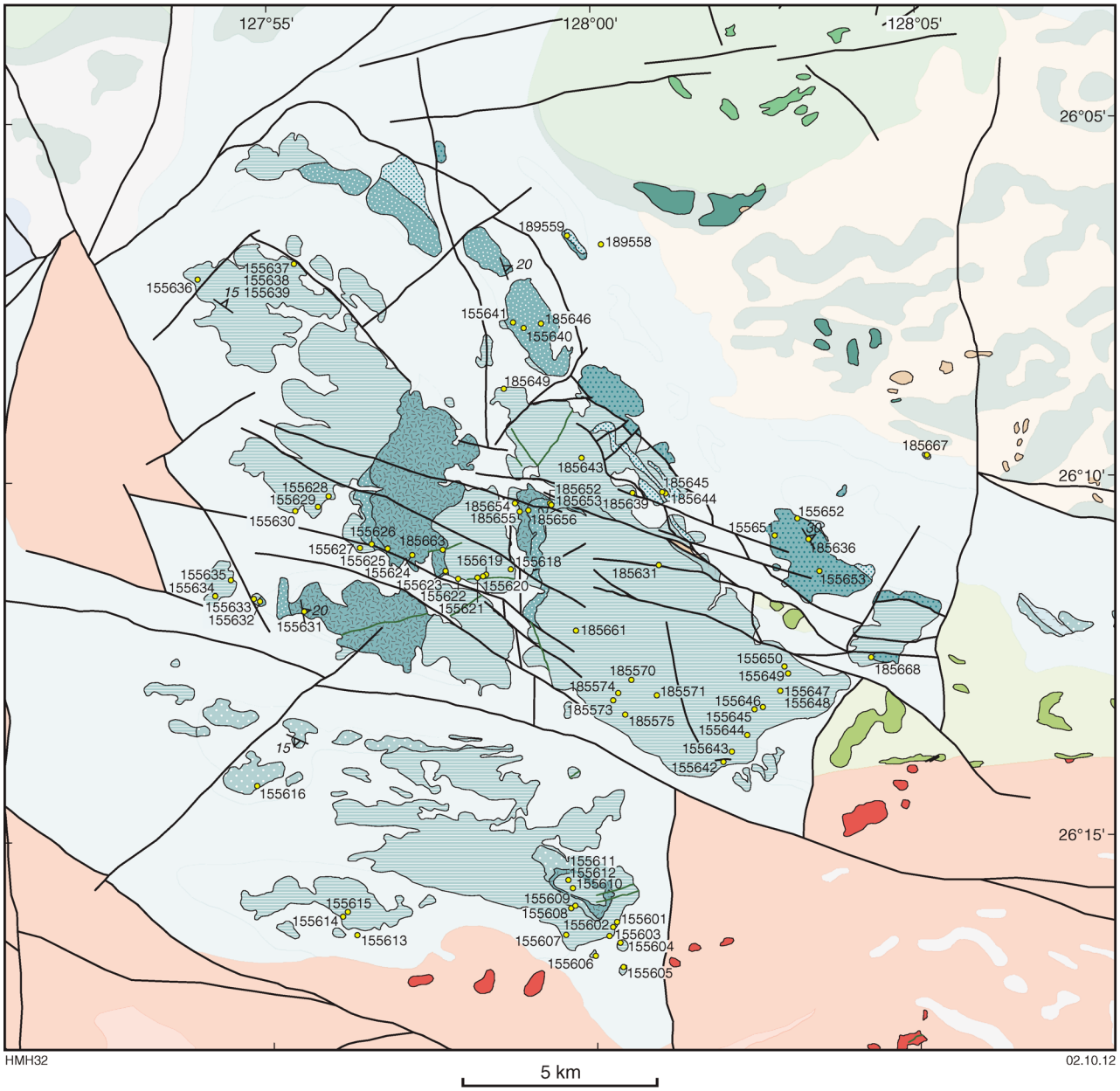

Appendix 5

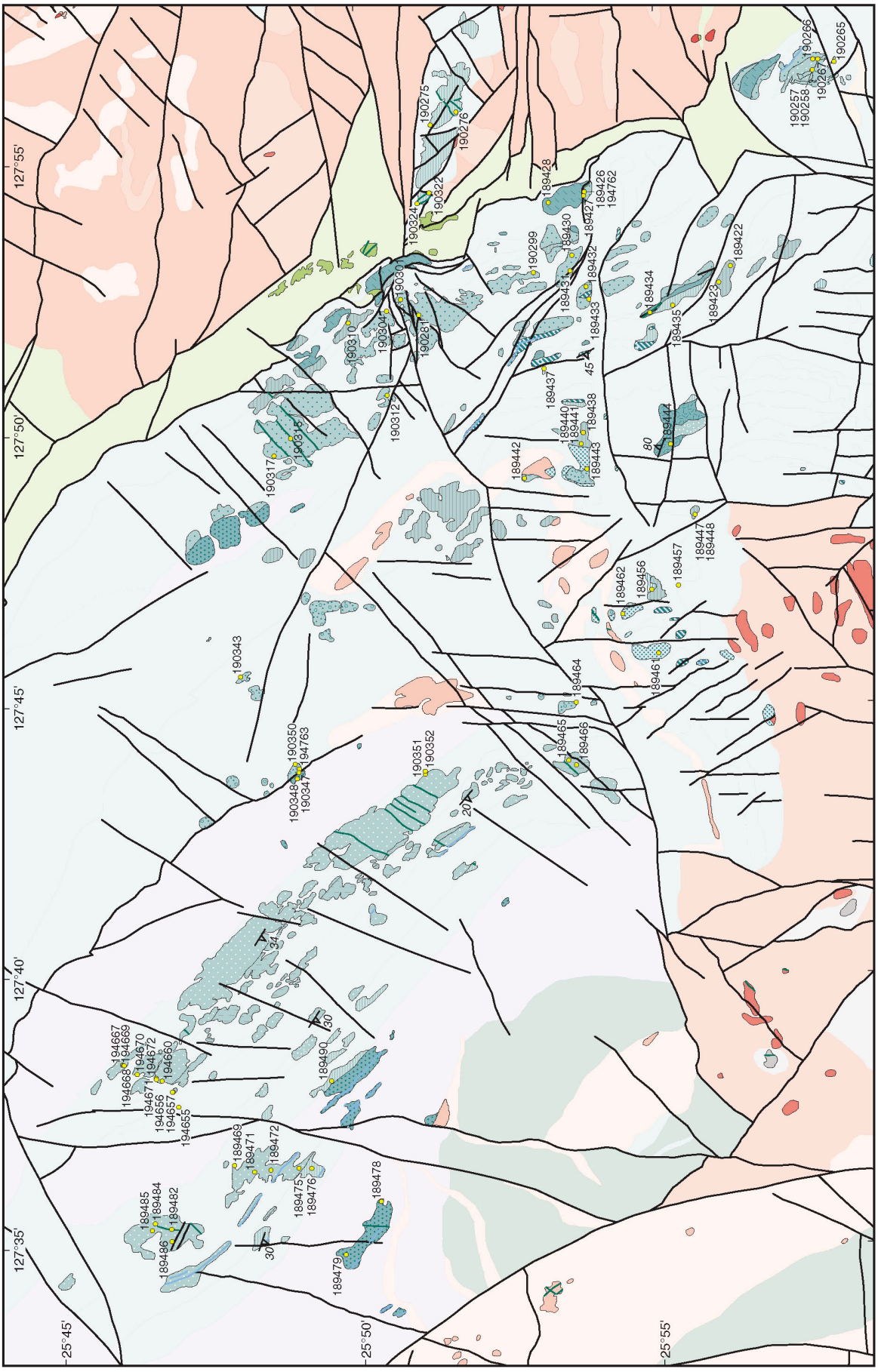

Interpreted bedrock geological map of the Jameson area, showing sample localities. Light shaded areas indicate regions of regolith cover.

Appendix 6

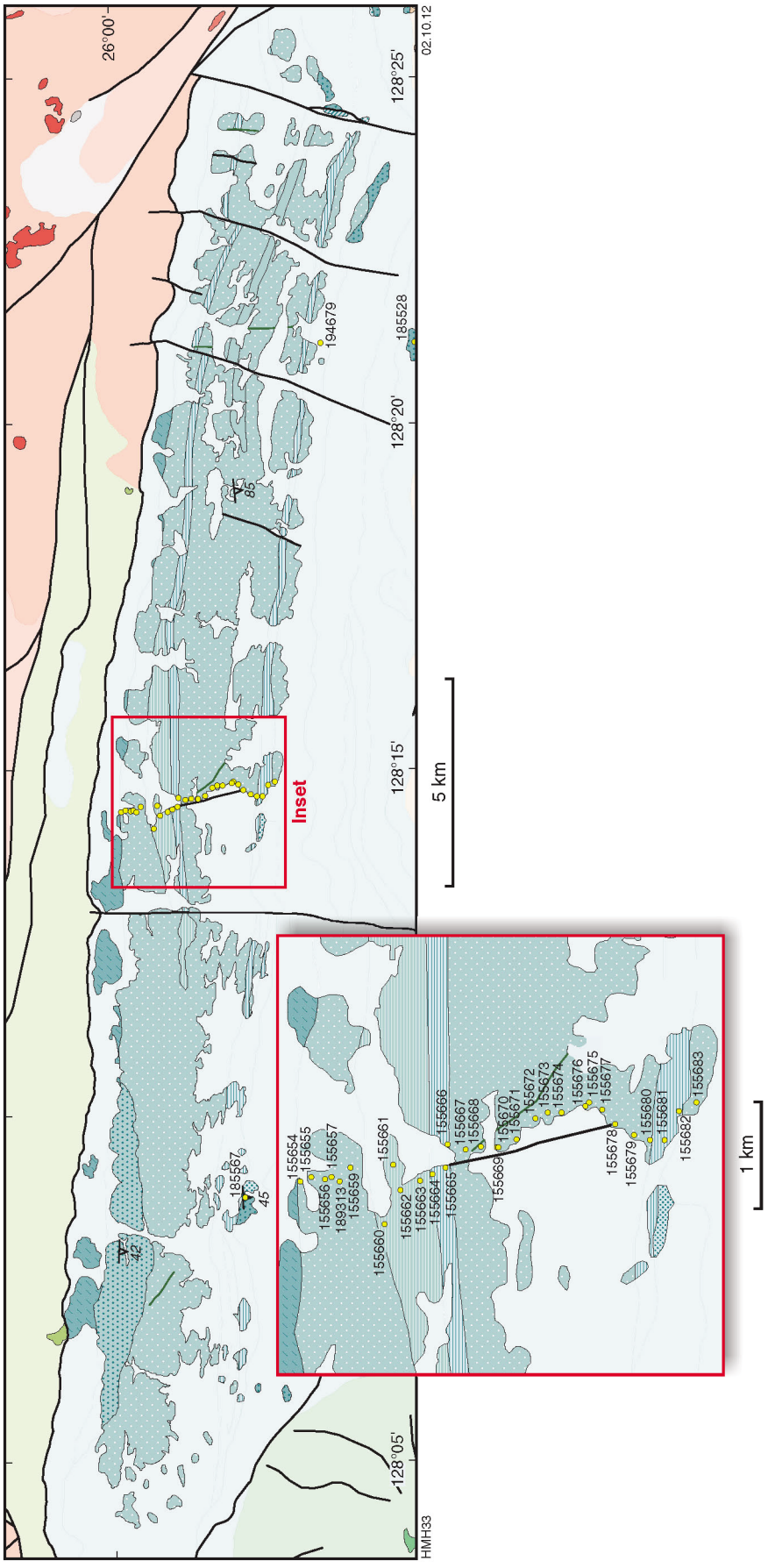

Interpreted bedrock geological map of the Blackstone area, showing sample localities. Light shaded areas indicate regions of regolith cover.

This Report outlines the geology, petrogenesis and prospectivity for magmatic (PGE–Ni–Cu–V–Ti–P–Fe) mineral deposits of more than a dozen mafic-ultramafic layered intrusions belonging to the Giles Event. The intrusions were emplaced into the Musgrave Province, a complex Proterozoic terrane located at the intersection between the West Australian, North Australian and South Australian Cratons. Intrusions studied include Wingellina Hills, Pirntirri Mulari, The Wart, Hinckley Range, Michael Hills, Murray Range, Morgan Range, Cavenagh, Bell Rock, Blackstone, and Jameson-Finlayson. The last three are tectonically dismembered portions of an originally contiguous body, here named the Mantamaru intrusion that had a strike length of >170 km and a width of at least 20 km, making it one of the world's largest layered intrusions.

Further details of geological products and maps produced by the Geological Survey of Western Australia are available from:

Information Centre
Department of Mines and Petroleum
100 Plain Street
EAST PERTH WA 6004
Phone: (08) 9222 3459 Fax: (08) 9222 3444

www.dmp.wa.gov.au/GSWApublications

MAIER et al.

MAFIC-ULTRAMAFIC INTRUSIONS OF THE GILES EVENT, WESTERN AUSTRALIA: PETROGENESIS AND PROSPECTIVITY FOR MAGMATIC ORE DEPOSITS

REPORT 134